Swansea University
Prifysgol Abertawe

The Role of Adipocytes in the Ovarian Cancer Metastatic Niche

Michael Ellis Williams; BSc, MSc

Submitted to Swansea University in the fulfilment of the requirements for the Degree of Doctor of Philosophy

Swansea University

2023

Summary

Ovarian cancer is characterised by metastasis to the adipocyte-rich omentum and the development of resistance to chemotherapy. Adipocytes within the omentum may play an important role in promoting ovarian cancer growth and metastasis. The ovarian cancer metastatic microenvironment is highly inflamed, and an inflammatory environment is associated with aggressive disease and poor outcomes. *In vitro* models which incorporate multiple elements of the tumour microenvironment can be used to explore interactions between cancer cells and non-malignant cells within the metastatic niche and understand the contribution of inflammatory signalling to cancer progression.

Methodology

Three-dimensional models were generated incorporating ovarian tumour spheroids and adipocytes or adipose-derived signalling factors. The role of adipocytes on ovarian cancer growth, invasion and response to therapy was explored. The impact of inflammation of adipocytes on the response of ovarian cancer cell lines was explored in co-culture systems.

Results

Adipose-derived factors and adipocyte co-culture promoted ovarian cancer growth. Adipose-derived exosomes induced an invasive, chemoresistant phenotype in ovarian cancer cells through microRNA transfer. Inflammation of adipocytes induced a pro-cancer phenotype, inducing the release of fatty acids which are sequestered by proliferating cancer cells. Adipocyte-derived interleukin-6 signalling activates signal transducer and activator of transcription-3 (STAT3), regulating ovarian cancer response to cisplatin therapy.

Conclusions

Adipocytes play an important role in the progression of epithelial ovarian cancer. Adipocyte-derived signalling drives clinically important aspects of ovarian cancer activity including tumour growth, metastasis, and response to therapy. Adipocyte-derived signalling may be a target for therapy to overcome chemoresistance in advanced stage ovarian cancer.

Declarations

This work has not previously been accepted in substance for any degree and is not currently submitted in candidature for any other degree.

Signed 

Date: 21st May 2025

This thesis is the result of my own investigations, except where otherwise stated. Where correction services have been used, the extent and nature of the correction is clearly marked in a footnote(s). Other sources are acknowledged by footnotes giving explicit references. A bibliography is appended.

Signed 

Date: 21st May 2025

I hereby give consent for my thesis, if accepted, to be available for electronic sharing after expiry of a bar on access approved by the Swansea University

Signed 

Date: 21st May 2025

The University's ethical procedures have been followed and, where appropriate, that ethical approval has been granted.

Signed 

Date: 21st May 2025

Contents

Acknowledgements

First and foremost, I would like to acknowledge my two wonderful supervisors Prof. Deya Gonzalez and Dr Francesca Taraballi for all their guidance over the course of my PhD. Thanks to Deya for her incredible support during the uncertainty of the pandemic, and to Francesca for welcoming me into a new country and new lab with open arms.

Thanks to everyone at RBGO past and present for their help and training. Also, to all my friends and colleagues at Swansea for keeping me sane and entertained. Special thanks to Alex Bulpitt for his air mattress and hundreds of hours of amusement.

Grazie mille to everyone at the Methodist in the Taraballi lab and beyond including, but not limited to, Chiara Mancino, Federica Giordano, Stefano Serpelloni, April Ewing, Stefania Lenna, Emelia Morris, Sara Rota, Will May and Dr Matt Hogan.

A huge thanks to my Mum for a lifetime of support and love, and for giving us a home during the pandemic. Thanks to Mum, Richard and Charlotte (and Aster) for bringing a little bit of Wales into the apartment every Sunday morning.

Most importantly thank you to my incredible wife Liz, without whom I would never even have started a PhD let alone finished one. Thank you for your support, love, and incredible patience and for following me halfway across the world on an amazing adventure.

Abbreviations

ACC	Acetyl-CoA carboxylase
ADSC	Adipose-derived stem cells
Akt	Protein kinase B
AMP	Adenosine monophosphate
AMPK	AMP-activated protein kinase
APN	Adiponectin
ATCC	American Type Culture Collection
ATGL	Adipose triglyceride lipase
ATP	Adenosine triphosphate
BMI	Body mass index
BRCA	Breast cancer gene
BSA	Bovine serum albumin
CAF	Cancer-associated fibroblast
CA125	Cancer antigen 125
CPT	Carnitine palmitoyltransferase
CSC	Cancer stem cell
CM	Conditioned medium
CLSM	Confocal laser scanning microscopy
Cq	Quantification cycle
cDNA	Complementary DNA
DAG	Diacylglycerol
DAPI	4′,6-diamidino-2-phenylindole
DNA	Deoxyribonucleic acid
DNMT1	DNA methyltransferase 1
DMEM	Dulbecco's Modified Eagle Medium
DMSO	Dimethyl sulfoxide
dsDNA	Double-stranded DNA
ECM	Extracellular matrix
EDTA	Ethylenediaminetetraacetic acid

EGFR	Epidermal growth factor receptor
ELISA	Enzyme-linked immunosorbent assay
EMT	Epithelial-to-mesenchymal transition
EOC	Epithelial Ovarian Cancer
EPIC	European Prospective Investigation in Cancer and Nutrition
EV	Extracellular vesicle
FABP4	Fatty acid-binding protein 4
FACS	Fluorescence-activated cell sorting
FAK	Focal adhesion kinase
FBS	Fetal bovine serum
FFA	Free fatty acid
FGF	Fibroblast growth factor
GAPDH	Glyceraldehyde-3-phosphate dehydrogenase
HBSS	Hanks' Balanced Salt Solution
HE4	Human epididymis protein 4
HGSOC	High-grade serous ovarian carcinoma
HIF-1	Hypoxia-inducible factor 1
HRT	Hormone replacement therapy
HSL	Hormone-sensitive lipase
IFN	Interferon
IL-x	Interleukin - x
IL-6R	Interleukin-6 receptor
IP	Intraperitoneal
IV	Intravenous
JAK	Janus kinase
LD	Lipid droplet
LGSOC	Low-grade serous ovarian carcinoma
LOT	Liquid overlay technique
M-CSF	Macrophage colony-stimulating factor
MAG	Monoacylglyceride

MIF	Macrophage migration inhibitory factor
MMP	Matrix metalloproteinase
MVB	Multivesicular body
mTOR	Mammalian target of rapamycin
mRNA	Messenger RNA
miRNA	MicroRNA
MSC	Mesenchymal stem cell
NF-kB	Nuclear factor-kappa B
NK Cell	Natural killer cell
NTA	Nanoparticle tracking analysis
OT-CM	Omental tissue-conditioned medium
P13K	Phosphoinositide 3-kinase
P13K/Akt/mTOR	Phosphoinositide 3-kinase / Protein kinase B /mammalian target of rapamycin signalling pathway
PARP	Poly(ADP-ribose) polymerase
PBS	Phosphate-buffered saline
PCR	Polymerase chain reaction
PDI	Polydispersity index
PDX	Patient-derived xenograft
PLIN	Perilipin
polyHEMA	Poly(2-hydroxyethyl methacrylate)
PPARγ	Peroxisome proliferator-activated receptor gamma
PVDF	Polyvinylidene fluoride
Q-RT-PCR	Quantitative real-time polymerase chain reaction
RFU	Relative fluorescence units
RIPA buffer	Radioimmunoprecipitation assay buffer
RNA	Ribonucleic acid
ROS	Reactive oxygen species
RPL19	Ribosomal protein L19
RXR	Retinoid X receptor
SCD1	Stearoyl-CoA desaturase 1

siRNA	Small interfering RNA
SKOV-3/LUC	SKOV-3 ovarian cancer cells engineered to express luciferase
SNP	Single nucleotide polymorphism
SPARC	Secreted protein, acidic and rich in cysteine
STAT	Signal transducer and activator of transcription
STIC	Serous tubal intraepithelial carcinoma
SVF	Stromal vascular fraction
TAK1	Transforming growth factor beta-activated kinase 1
TBS	Tris-buffered saline
TBS/T	TBS with Tween 20
TGF	Transforming growth factor
TNF	Tumor necrosis factor
UCP1	Uncoupling protein 1
ULA	Ultra-low attachment
UMI	Unique molecular identifier
UV	Ultraviolet
VCAM-1	Vascular cell adhesion molecule 1
VCAN	Versican
VEGF	Vascular endothelial growth factor
WAT	White adipose tissue

List of Figures

List of Tables

Chapter 1. Introduction

1.1 Ovarian Cancer

Ovarian cancer is the deadliest gynaecological malignancy, contributing approximately 314 new cases and 207 deaths per 100,000 people every year globally (1). Ovarian cancer is the 5th most common cause of cancer death in women in the USA, leading to around 12,810 deaths in 2021 (2) and predicted to have caused 26,500 deaths in the EU and 4,000 deaths in the United Kingdom in 2022 (3). Once considered a single disease, ovarian cancer is now understood to comprise a heterogenous range of subtypes with distinct origins, molecular characteristics, clinical presentations, treatment and prognosis (4). Epithelial ovarian cancer (EOC) accounts for ~90% of cases and the majority of deaths and is the focus of this study. Non-epithelial ovarian cancers include subtypes such as germ cell tumors, sex cord-stromal tumors, and small cell ovarian cancer. Germ cell tumors primarily affect younger women and are often curable, with high survival rates, especially when diagnosed at an early stage (5). Sex cord-stromal tumors are rare and their prognosis varies depending on the specific subtype and stage at diagnosis (6). Small cell ovarian cancer is an aggressive subtype that accounts for a small percentage of cases and is often diagnosed at an advanced stage, leading to a challenging treatment landscape (7).

1.2 Epithelial Ovarian Cancer

Epithelial ovarian cancers are classified based on their epithelial site of origin or predominant epithelial cell type, and comprise multiple subtypes including serous, endometrioid, clear cell, and mucinous ovarian cancers (4, 8). High grade serous ovarian carcinoma (HGSOC) is most commonly diagnosed and accounts for 70-80% of all ovarian cancer deaths (9, 10) and is therefore the most commonly studied malignancy. Conversely, low-grade serous ovarian carcinoma (LGSOC) is less common and is characterized by slow growth and improved outcomes. Over the past decade, a model which characterises EOC based on manner of carcinogenesis, originally proposed by Kurman and Shih in 2004, has been widely accepted (11, 12). Within this classification system, type I tumours, including LGSOC, endometrioid, clear cell and mucinous, develop in a step-wise progression from epithelial neoplasms and are relatively slow growing, leading to earlier diagnosis and improved outcomes (13). Type I neoplasms are relatively genomically stable, in contrast to Type II tumours in which *TP53* mutations are common (~80% of tumours), leading to genetic instability and rapid evolution (13). Rapid development of Type II ovarian cancers, predominantly HGSOC, can result in late diagnosis of disease and these cancers are responsible for the majority of ovarian cancer deaths (9).

Late diagnosis is a major contributing factor in high mortality rates observed for EOC, alongside common development of resistance to therapy. EOC is commonly staged according to the FIGO (International Federation of Gynecology and Obstetrics) system which classifies cancer based on tumour size and extent of spread to lymph nodes and distant organs (14). HGSOC is most commonly diagnosed at FIGO stage III (51%) and stage IV (29%) (10), indicating metastasis of sites outside the pelvis. Given the 5-

year survival rates for patients diagnosed at stages I-IV are 89%, 71%, 41%, and 20% respectively (10), the contribution of late-stage diagnoses to overall ovarian cancer mortality is clear.

1.3 Ovarian Cancer Diagnosis and Treatment

There are currently no effective screening strategies for detection of ovarian cancer. Carbohydrate antigen 125 (CA125) was identified in 1981 as a potential marker for ovarian cancer (15), however, CA125 screening has poor predictive power and a high rate of false positive can generate anxiety and distress, as well as unnecessary follow-up testing, in patients (16). CA125 screening in the general population has been shown to have no impact on overall ovarian cancer mortality (17), though can be useful in testing patients presenting with symptoms to detect more aggressive forms of EOC. (18). Testing for multiple biomarkers, including Human Epididymis Protein 4 (HE4) and mesothelin alongside CA125, in combination has been proposed to improve accuracy and limit false positives (19, 20).

Ovarian cancer patients present in the clinic with a range of non-specific symptoms including abdominal bloating and distension, nausea, change in bowel and urinary function, back pain, fatigue and weight loss (21). Following diagnosis, treatment for advanced stage ovarian cancer typically consists of surgery combined with chemotherapy (8). Cytoreductive or debulking surgery consists of removal of as much tumour as is possible as well as surrounding tissues and in many cases a bilateral salpingo-oophorectomy (removal of ovaries and fallopian tubes) and hysterectomy (removal of uterus). Stage I EOC is typically initially treated by debulking surgery alone

(22). Chemotherapy normally consists of at least 6 rounds of treatment with combination of platinum-based drug (cisplatin or carboplatin) and taxane (paclitaxel or decotaxel), ordinarily delivered after surgery but in some cases 3 doses are administered prior to surgery, for example to reduce tumour burden prior to surgery in cases of advanced stage disease, or for patients who are not healthy enough for optimal debulking surgery (22). Intraperitoneal (IP) administration of chemotherapy, or IP in combination with intravenous (IV) has been shown to be more effective than IV alone (23, 24, 25).

More targeted approaches can be effective in some circumstances. In patients with *BRCA1/BRCA2* mutations, where DNA repair mechanisms are impaired, poly-adenosine diphosphate ribose polymerase (PARP) inhibitors have been shown to improve outcomes by inducing synthetic lethality through targeting of alternate mechanisms of DNA repair (26). Clinical trials indicate that PARP inhibitors, including olaparib, niraparib and rucaparib, are most effective as maintenance therapy to extend remission in patients sensitive to platinum therapy (27, 28, 29, 30). Anti-angiogenic drugs, in particular bevacuzimab which targets vascular endothelial growth factor (VEGF) signalling, have been approved for use alongside standard chemotherapy (31). Bevacuzimab, as well as anti-angiogenic tyrosine kinase inhibitor pazopanib, has modest impact on patient survival and seems to be most effective in *BRCA*-negative patients with high risk disease (32).

While PARP inhibitors and anti-angiogenic drugs have been approved for use in ovarian cancer patients in the last 10 years, they have not had a drastic impact on patient survival (3). Similarly, liposomal doxorubicin (doxil) has been shown to reduce off site toxicity and side effects, however patients receiving doxil face similar rates of disease relapse (33). As such, despite the development of new drugs, standard care

for patients with advanced stage epithelial ovarian cancer has not significantly changed over the past ~40 years. Given the poor 5-year survival rates for patients with stage III and IV epithelial ovarian cancer, new treatment options for patients are urgently needed.

1.4 Ovarian Cancer Risk

Several factors have been identified which may impact the risk of ovarian cancer development. The most significant genetic risk factor is germline mutations of *BRCA1* and *BRCA2*, commonly associated with breast cancer risk. Either *BRCA1* or *BRCA2* are mutated in up to 13-17% of ovarian cancer patients, increasing to over 25% in patients with HGSOC (34, 35, 36). Both *BRCA1* and *BRCA*2 encode proteins with roles in DNA damage repair (BReast CAncer gene 1 and 2), enabling the accumulation of mutations necessary for malignant transformation. Germline mutations of other genes related to DNA damage repair are related to ovarian cancer patients, including *RAD51C* and *RAD51D*, as well as *PALB2* and *BARD1* which encode proteins in the Fanconi anaemia– BRCA pathway (37). Women with germline mutations in both *BRCA1* and *BRCA2* may undergo risk-reducing salpingo-oophorectomies.

The most significant risk factor for ovarian cancer is age, and the probability of developing ovarian cancer increases every decade of a woman's life until 70, where risk peaks at 1 in 283 (0.4%) in the US (10). Age-related risk is common in many cancers, as somatic mutations accumulate over time. However, ovarian cancer risk has also been associated with other age-related aspects of female reproductive health (38, 39). The number of ovulation cycles of a woman's lifetime is correlated with higher

ovarian cancer risk, while use of the contraceptive pill and pregnancy, which interrupt ovulation, can reduce risk (40, 41). This has led to the development of the 'incessant ovulation' hypothesis which posits that each ovulation event can cause minor damage to the ovarian surface epithelium, resulting in repeated damage and repair, increasing the likelihood of mutation and transformation. Alternatively, the 'gonadotropin hypothesis' attributes the impact of reproductive factors on ovarian cancer risk to levels of gonadotropins (42). Hormone replacement therapy (HRT) has been shown to increase ovarian cancer risk, potentially through increased estrogen-induced proliferation in the ovaries (43, 44).

1.5 Obesity and Adiposity as Risk Factors for Ovarian Cancer

Obesity is a risk factor for a number of cancers, in particular hormone-related cancers such as endometrial cancer and postmenopausal breast cancer (45, 46). A 2007 meta-analysis of 28 studies found 24 that reported a positive correlation between obesity and ovarian cancer risk and found that this correlation was consistent across subtypes (47). The same group performed a follow-up analysis in 2013 which sought to evaluate the risk of obesity on the prevalence of ovarian cancer subtypes and found that high (>30) body mass index (BMI) was associated with increased risk of endometrioid, mucinous and LGSOC, but not HGSOC (48). They found that the association was strongest amongst pre-menopausal women, while a report from the European Prospective Investigation in Cancer and Nutrition (EPIC) cohort found the association was strongest in post-menopausal women. As such, the role of obesity and increased BMI in risk of ovarian cancer is still not clear. Importantly, meta-analyses have found a negative correlation between obesity and ovarian cancer survival, including in

patients with HGSOC (49, 50), indicating that obesity and adiposity may play a role in disease progression and metastasis as well as carcinogenesis.

1.6 Ovarian Cancer Development

Due to its prevalence and impact, HGSOC has been the focus of the majority of research into epithelial ovarian cancer origin and carcinogenesis. Multiple sites of origin have been proposed for HGSOC, most prominently the ovaries and fallopian tubes. As noted above, the incessant ovulation hypothesis suggests that damage and repair at the ovarian surface epithelium results in accumulation of mutations leading to carcinogenesis. However, no pre-cancerous ovarian lesions have been identified as potential sites of ovarian cancer origin (8). Growing evidence suggests that the fallopian tube epithelium represents the most common site of origin for HGSOC, including the presence of pre-cancerous lesions known as serous tubal intraepithelial carcinoma (STIC), identified in women with *BRCA1* mutations undergoing risk-reducing salpingo-oophorectomies (51). Transgenic deletion of HGSOC-associated genes (*Brca1* and *2*, *Tp53*, *Pten*) in the fallopian tube in mouse can induce the development of HGSOC-like malignancies (52), while deletion of such genes in ovarian surface epithelium results in histologically distinct neoplasm (53). It has been suggested that incessant cyclical ovulation may generate a state of chronic inflammation, leading to neoplastic transformation in neighbouring fallopian tube epithelum (54). Given the heterogeneity apparent in EOC, it is likely multiple, distinct sites of origin exist.

High levels of inter- and intra-tumoral heterogeneity have been demonstrated in HGSOC, though *TP53* is mutated in most tumours at all stages (55, 56, 57). HGSOC

are characterized by their widespread genomic instability, including defective homologous recombination, leading to a varied mutational landscape including widespread copy number gain and loss (8, 58). Conversely, Type I cancers such as LGSOC progress in a slower, step-wise fashion as tumorigenic mutations accumulate (4, 8).

1.7 Ovarian Cancer Metastasis

1.7.1 Ovarian Cancer Metastasis Overview

Following transformation of epithelium in the ovaries or fallopian tubes, the development of secondary metastases is a multistep process typically requiring: 1) shedding of cells from the primary tumour; 2) intra-peritoneal dissemination of tumour cells; 3) attachment at the peritoneal mesothelium and 4) invasion at a secondary site within the peritoneal cavity (Figure 1.1) (8). Transformed ovarian epithelial cells rarely disseminate through the vasculature and the peritoneal cavity is the primary region of EOC metastasis. Detachment of transformed epithelial cells is associated with the epithelial to mesenchymal transition (EMT), whereby cells shift to a motile, invasive, mesenchymal-like phenotype (59). EMT is characterized by a ‘cadherin switch’: expression of the epithelial adhesion protein E-cadherin is decreased while expression of mesenchymal-associated N-Cadherin is increased, alongside other mesenchymal-associated membrane proteins such as vimentin and fibronectin (60). EMT is regulated by a suite of transcription factors, most notably Snail, Slug, Twist and Zeb1/2 (61, 62). Notably, EMT is also associated with resistance to chemotherapy in EOC (61).

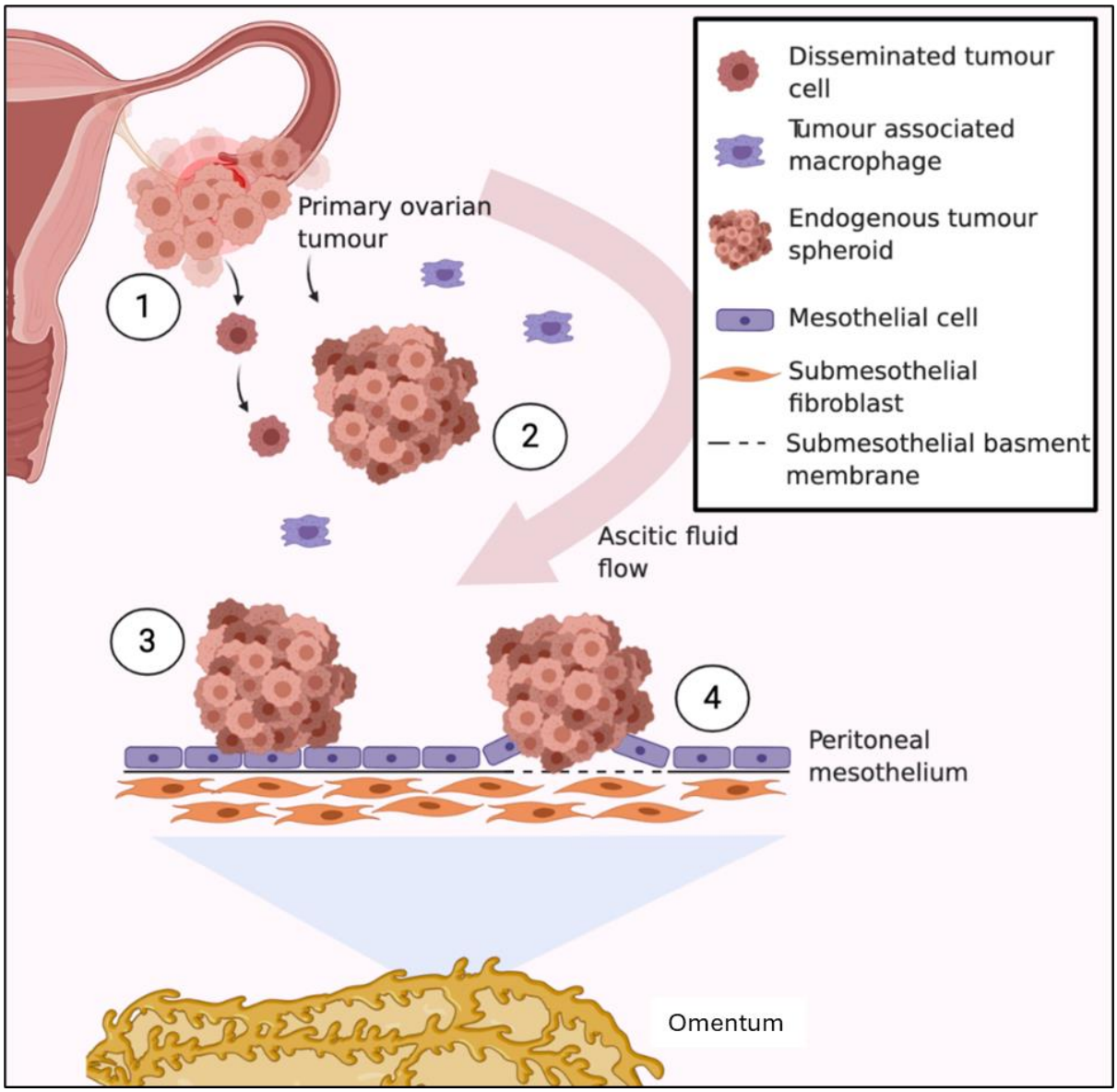

Figure 1.1 Epithelial Ovarian Cancer Metastasis. *Metastasis of EOC cells within the peritoneum requires 1) shedding of cells from the primary tumour via EMT, 2) dissemination of tumour cells within the peritoneal cavity as single cells or cells clusters (tumour spheroids), enabled and promoted by fluid flow within the inflamed ascites, 3) attachments of tumour cells at a secondary site within the peritoneal mesothelium and 4) invasion through the mesothelial membrane via matrix remodelling. Created with BioRender.com.*

Following EMT, EOC cells disseminate through the peritoneum as single cells or clusters of cells (endogenous tumour spheroids) (63, 64). Although it is as yet unclear whether cells more commonly detach from a primary ovarian tumour as a multi-cell aggregate, or if detached single cells aggregate in ascites fluid, a survival advantage for clusters of cells over single cells has been reported (65), while the formation of endogenous spheroids in ascites is associated with poor disease prognosis (66, 67). Disseminating tumour aggregates may also incorporate non-malignant cell types, including mesothelial cells, fibroblasts and macrophages (66, 68, 69)

Disseminating EOC cells within the peritoneal cavity is associated with the development of ascites, accumulation of fluid in the abdominal cavity caused by imbalance in fluid production and reabsorption and characterized by a highly inflamed environment (70). Ascites is associated with poor prognosis, and the inflammatory microenvironment within the peritoneal cavity promotes cancer cell proliferation and metastasis (71, 72). The inflammatory nature of the ascites microenvironment is discussed in detail below. Tumour cells within the peritoneal cavity are also subject to specific physical conditions which can have a significant impact on their activity and viability. In particular, fluid flow within malignant ascites exerts shear and tensile stress on tumour cell aggregates, as well as directing colonizing cells along routes to distant metastatic targets (73, 74, 75).

Endogenous tumour spheroids represent discrete metastatic units capable of seeding secondary metastases in the peritoneal cavity (63, 66). As hypothesised by Steven Paget in 1899, the “seed” of ascites tumour spheroids, as well as individual tumour spheroids, will preferentially colonize vulnerable microenvironments within the

peritoneal cavity, the “soil” of intraperitoneal metastasis (76, 77). These common sites of colonization include the peritoneum and peritoneal organs, notably the omentum, which are lined by a mesothelial monolayer on top of a basement membrane and stromal tissue (8). The generation of a secondary tumour requires 1) adherence of tumour cells to the mesothelial cell layer; 2) invasion through the submesothelial basal membrane and 3) extensive remodelling of extracellular matrix components and tissue architecture. Vascular cell adhesion molecule-1 (VCAM-1), present on mesothelial cells, binds β1-integrin on ovarian cancer cells, enabling attachment (78, 79). The submesothelial matrix is rich in collagens type I and III, as well as fibronectin and laminin, and ovarian cancer activity in the submesothelial layer increases collagen production in cancer-associated fibroblasts (80, 81). Matrix components exert physical forces and induce transcriptional changes in cancer cells through integrin-mediated binding, while cancer cells remodel extracellular matrix (ECM) through proteolytic matrix metalloprotease (MMP) activity (82).

1.7.2 Inflammation in the Peritoneal Metastatic Microenvironment

Ascites is an inflammatory condition and the malignant ascites associated with ovarian cancer development is characterized by abundance of inflammatory cytokines (83, 84). Inflammatory cytokines, alongside other inflammatory mediators such as reactive oxygen species (ROS), are secreted by disseminating tumour cells, inducing the recruitment of immune components such as tumours associated macrophages (TAMs), natural killer (NK) cells, dendritic cells and T regulatory cells, which in turn further contribute to peritoneal inflammation through inflammatory signalling (Figure 1.2) (85). EOC cells produce macrophage colony-stimulating factor (M-CSF),

attracting macrophages and other monocytes to the tumour microenvironment (TME), while bi-directional tumour necrosis factor- α (TNFα) signalling promotes macrophage infiltration and the generation of an inflamed microenvironment (86, 87, 88). Depletion of macrophages in peritoneum can inhibit metastasis in mouse, and immune cells in the omentum are a source of pro-cancer chemoattractant signalling (89, 90, 91).

Inflammatory mediators act on EOC cells, inducing proliferation and metastasis (92, 93, 94), as well as other components of TME such as cancer associated fibroblasts (CAFs) to induce matrix remodelling and aid invasion (Figure 1.2) (95). Cells in the TME promote tumour metastasis by disrupting signalling pathways, such as Phosphoinositide 3-kinase/Protein kinase B (PI3/Akt) and Ras/Extracellular signal-regulated kinase (Ras/ERK), which govern migration and invasion. Downstream signalling, including Rho family GTPases, extracellular proteases, integrins, matrix-associated proteins like focal adhesion kinases (FAK), and transcription factors like ETS2 and AP-1, are influenced by these pathways (85, 96). Fibroblasts within the TME can be reprogrammed via tumour- and immune derived signalling (notably interleukin-6 and TNFα) to a cancer activated fibroblast (CAF) phenotype, inducing ECM remodelling via veriscan (VCAN) regulated MMP expression (95, 97). CAFs can also suppress anti-tumour immunity via *CXCL12* expression (98). Potential roles for inflammatory mediators are discussed below.

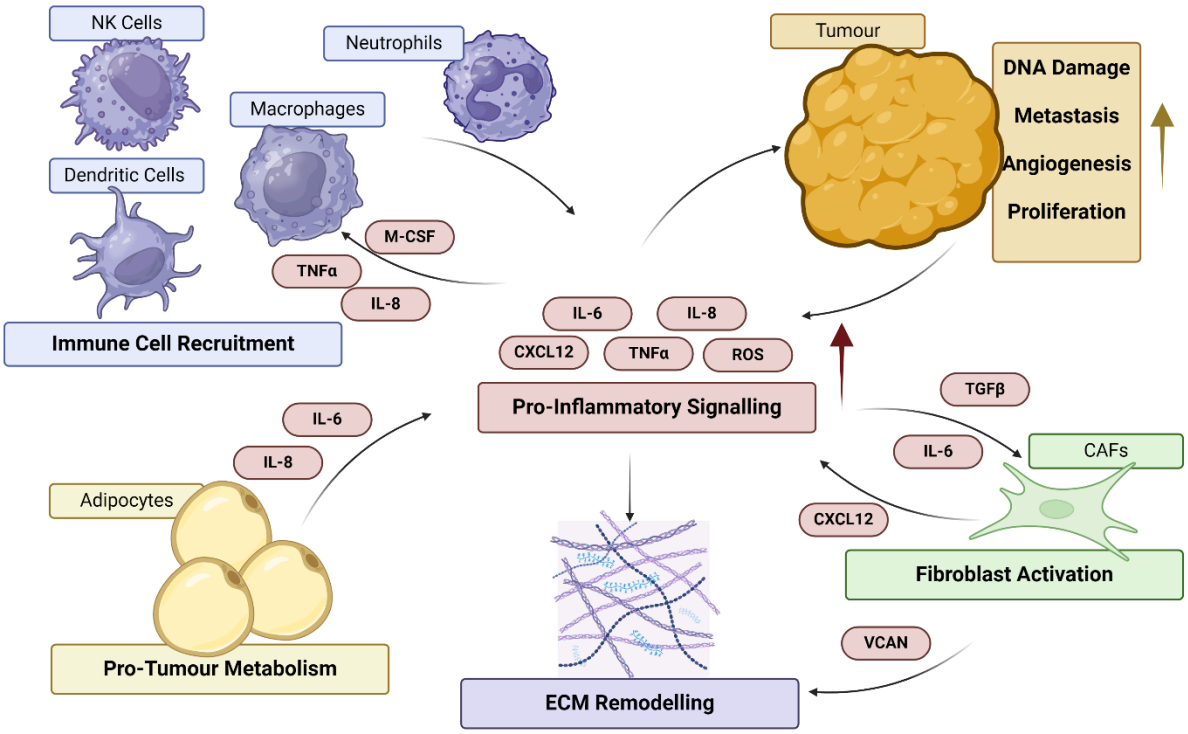

Figure 1.2 The Inflammatory Tumour Microenvironment in Ovarian Cancer Metastasis. *Signalling between tumour cells and non-malignant cells within the TME generates an inflammatory environment via accumulation of pro-inflammatory cytokines and other inflammatory mediators. An inflammatory environment promotes EOC metastasis via 1) recruitment of immune cells, 2) induction of pro-tumour metabolism, 3) remodelling ECM to enable invasion and 4) activation of CAFs. An inflammatory TME induces increased DNA damage, angiogenesis, tumour cell proliferation and metastasis in cancer cells. Created with BioRender.com.*

1.7.2.1 Interluekin-6

The role of interleukin-6 (IL-6) has been the most thoroughly explored of inflammatory cytokines acting in the EOC inflammatory tumour microenvironment (TME). Ovarian cancer cells and TAMs have been shown to produce IL-6 (99) and IL-6 concentration is high in ascites and has been proposed as a prognostic factor for EOC (71, 100, 101, 102). IL-6 signalling acts through binding its receptor IL-6R, initiating a signalling

cascade whereby two heterotrimers consisting of IL-6, IL-6R, and gp130 combine to create a hexameric complex. Within this complex, members of the cytoplasmic Janus kinase (JAK) family of tyrosine kinases bind to gp130, initiating the phosphorylation of downstream targets including signal transducers and activator of transcription (STAT) transcription factors. Once phosphorylated, activated STATs migrate to the nucleus, where they induce widespread gene transcription (83, 103).

In mouse, blocking of IL-6 signalling reduced ascites formation, indicating a role for IL-6 in the initiation of acute inflammation (102). Paracrine signalling of tumour-derived IL-6 can enhance EOC proliferation and induce MMP secretion (104, 105), promoting adhesion and invasion through JAK/STAT signalling (106). Importantly, IL-6 can also suppress anti-cancer immune response by downregulation of interleukin-2 (IL-2), while TAMs can secrete IL-6, inducing STAT3 activation in IL-6 EOC cell proliferation (94). Adipocytes have been identified as a source of IL-6 in the TME and adipocyte-derived IL-6 signalling can promote EOC proliferation and invasion (107, 108).

1.7.2.2 Interluekin-8

Similarly to IL-6, Interleukin-8 (IL-8) has been shown to be abundant in ascites of EOC patients and is associated with poor prognosis (109). IL-8 binds multiple membrane protein, most prominently G protein-coupled receptors CXCR1 and CXCR2 and *in vitro* IL-8 treatment can stimulate EOC growth by upregulation of cyclins B2 and D1 via Akt phosphorylation (110), however *in vivo* IL-8 may indirectly inhibit tumour growth through the recruitment of neutrophils (86, 111). In metastasis, IL-8 has been shown

to promote peritoneal invasion through transforming growth factor beta-activated kinase 1/ nuclear factor-kappa B (TAK1/NFkB) signalling via CXCR2 binding (112).

1.7.2.3 Tumour Necrosis Factor-α

TNFα plays an important role in promoting inflammation and regulating immune response to ovarian cancer. TNFα is secreted by inflammatory macrophages, though TNFα release by tumour cells has been reported (113, 114). EOC-derived TNFα can promote TAM recruitment and inflammatory macrophages are abundant in ascites fluid (87). Macrophages are typically polarised to either M1, pro-inflammatory phenotype or M2, anti-inflammatory phenotype (115). The anti-inflammatory capacity of M2 macrophages in the EOC metastatic environment may be important in inhibiting anti-cancer immunity and increased presence of M2 macrophages is related to increased survival (116). However, M1 macrophages have been demonstrated to play an important role in the development of an inflamed ascites and peritoneal TME and have been shown to promote metastasis through TNFα-mediated NF-kB activation (89, 117). In a positive feedback loop, EOC cells secrete further TNFα, increasing local inflammation as well as stimulating transforming growth factor-α (TGFα) in cancer associated fibroblasts, promoting metastasis through epidermal growth factor receptor (EGFR) signalling (118).

1.7.2.4 Reactive Oxygen Species

Reactive oxygen species (ROS) include oxygen ions and peroxides and are naturally produced in cells during various cellular processes, including metabolism and immune responses. Uncontrolled ROS production can lead to oxidative stress, which can contribute to inflammation and disease, including cancer. ROS may play an important role in generation of an inflamed microenvironment in response to tissue damage, leading to initial transformation as per the incessant ovulation hypothesis (85). In relation to EOC metastasis, ROS leads to activation of lysyl oxidase, which is inversely correlated with E-Cadherin expression, suggesting a role for ROS in EOC dissemination (119).

1.7.3 Exosome Signalling in the EOC Metastasis

Research into signalling within the TME has focussed on cytokine signalling between tumour and various non-malignant cell types within the peritoneal metastatic environment. Extracellular vesicles, in particular exosomes, have been also implicated in the generation of metastatic microenvironments in a number of malignancies (120). Exosomes are 30-150nm vesicles and can carry of cargo proteins, lipids, metabolites, RNA and DNA, enabling signalling at a distance through a diverse range of mechanisms and pathways (Figure 1.3). Exosome biogenesis is via the endocytic pathway through invagination of endosomal membrane which leads to generation of multivesicular bodies (MVBs). Formation of exosomes relies on coordination of endosomal sorting complexes required for transport (ESCRTs), tetraspanins, Rab GTPases and lipid modifying enzymes, all of which can interact with cargo to enable loading into putative exosomes. MVBs fuse with the plasma membrane, resulting in the release of exosomes, along with their cargo, into extracellular space (121). In most

cases, exosomes are taken up through caveolin- or clathrin mediated endocytosis (122). Exosome signalling to specific target cells is regulated by a diverse range of exosomal membrane proteins, including tetraspanins and integrins, lipid composition of exosomes and surface receptors at the target site (122). Exosomes typically express marker surface proteins including CD9, CD63, CD81, CD82 which aid in cell penetration (123).

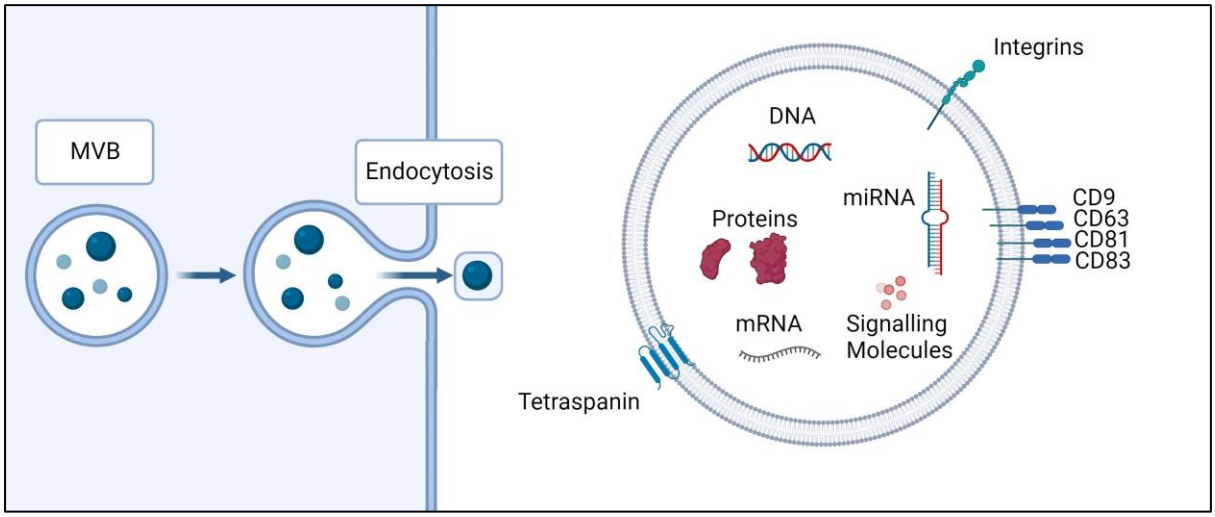

Figure 1.3 Exosome Signalling. *Exosomes are generated via endocytosis following budding of multivesicular bodies from the endosomal membrane. Exosome signalling to specific target cells is achieved through the incorporation of specific membrane proteins as well as through lipid composition of the exosome membrane. Exosomes can carry a range of cargo including genomic elements, proteins, and signalling molecules such as cytokines and growth factors. Created with BioRender.com.*

Due to their relative stability and capacity for specific receptor-regulated transport, exosomes have been implicated in signalling at distance, including in the generation of the pre-metastatic niche in a number of malignancies (120). For example, in pancreatic cancer, tumour-derived exosomes induce expression of fibronectin in hepatic stellate cells in the liver, generating a fibrotic microenvironment more amenable to metastasis (124). Blockade of exosome synthesis and release by

inhibition of Rab GTPases can also decrease lung metastasis in breast cancer and bone metastasis in melanoma in mouse models (125, 126).

In ovarian cancer, *in vitro* models have demonstrated the capacity for EOC-derived exosomes to induce CD44 expression in mesothelial cells, resulting in increased MMP expression which can act to destabilize the mesothelial ECM and enable EOC invasion (127). A separate study similarly demonstrated that EOC-derived exosomes can induce ECM reconstruction through MMP expression, however this work showed direct transfer of MMP1 mRNA as exosome cargo (128). Elsewhere, EOC exosomes have been shown to generate a pro-cancer environment through activation of fibroblasts to cancer associated fibroblasts and differentiation of adipose-derived stem cells to a tumour-associated myofibroblast phenotype (129, 130).

Exosome-derived microRNAs (miRNAs) have an impact on ovarian cancer development and progression, as well as resistance to therapy (131). One study found miR-99a-5p is relatively abundant in EOC patient serum, and EOC cell line-derived exosomes and exosomal miR-99a-5p can promote vimentin and fibronectin expression in peritoneal mesothelial cells (as seen previously) to generate a pro-metastatic environment. EOC exosome-derived miRNAs have been implicated in pro-cancer immune regulation in two studies from the same group, specifically via miR-940 regulated macrophage M2 polarization (132, 133).

1.7.4 Omental Metastatic Niche

The omentum is invaded in the majority of cases of metastatic EOC, with omental metastases present in >60% of cases and >80% of HGSOC (107, 134, 135). The

omentum is a large, soft pad of visceral adipose tissue, approximately 20 x 15 x 2cm, covering the abdominal cavity and connected to the spleen, stomach, pancreas and colon. The omentum has functions in energy storage, insulation, angiogenesis and metabolism, as well as diverse immune regulatory capacity including tissue repair and regeneration (136). Alongside abundant adipocytes, the omentum is composed of fibroblasts, multipotent stem cells and a mesothelial lining, as well as immune component. The omentum has been referred to as 'the policeman of the abdomen' due to its healing capacity (137), and so called 'milky spots' of the omentum are aggregates of B cells, T cells, macrophages and dendritic cells which act to promote wound healing and protect against infection (136).

Adipose tissue in the omentum is metabolically active and can have systemic effects on metabolism and inflammation through secretion of hormones and cytokines (136). The omentum is thought to contribute significantly to metabolic dysfunction in obesity, and contributes to increased serum triacylglycerides (TAG) and fatty acid levels (138, 139, 140), as well as increased levels of leptin and resistin leading to obesity-associated insulin resistance (141). Obesity can generate a state of chronic, low grade inflammation in adipose tissue, and abundant macrophages in omentum adipose tissue may contribute to inflammation via secretion of pro-inflammatory mediators (142). Adipose tissue is remodelled and dysregulated during metastatic invasion of the omentum (80), which may further promote inflammation by inhibition of normal immune and metabolic regulatory function.

The omentum represents a major source of energy for metastasizing tumour cells, largely in the form in lipids such as free fatty acids secreted from omental adipocytes. A number of studies have highlighted the importance of bi-directional changes in metabolism in omental adipocytes and EOC cells in ovarian cancer metastasis (107,

143, 144, 145, 146). Changes in metabolism in cancer cells and cancer-associated adipocytes, and how these drive ovarian cancer progression, are now discussed.

1.8 Metabolism in Adipocytes and Tumour Cells in Ovarian Cancer Progression

1.8.1 Cancer Metabolism Overview

The first prominent report of altered metabolism in cancer cells came from Otto Warburg in the 1920s, who recognised a preference for anaerobic metabolism of glucose to lactate, even in the presence of oxygen, termed ‘aerobic glycolysis’ (147). This preference for glycolysis is in contrast to most healthy cells, where oxidative phosphorylation in the mitochondria generates adenosine triphosphate (ATP) in the presence of oxygen, a considerably more efficient process for energy generation. Changes in cellular metabolism are now recognised as a ‘hallmark of cancer’ (148) and cancer-specific metabolism is a potential target for therapy (149). Given the enormous diversity in how cancers develop and spread, the spectrum of cancer-specific metabolic alterations is wide. Broadly, cancer metabolism is reprogrammed to enable survival in hypoxic and stressful conditions and to promote rapid growth and proliferation (150).

1.8.2 Glucose Metabolism in Cancer

Glucose is a major source of cellular energy, and the rate of glucose metabolism (glycolytic flux) is closely regulated systemically by glucagon and insulin. In oxidative

phosphorylation, glucose is metabolized to pyruvate via glycolysis, which is then imported to the mitochondria via mitochondrial pyruvate carriers. The classical example of metabolic reprogramming is the Warburg effect, as detailed above, whereby glucose metabolism in normoxic conditions is dysregulated. Glycolytic flux is regulated, via hypoxia inducible factor-1 (HIF-1) by the phosphatidylinositol 3-kinase – Protein Kinase B – mammalian target of rapamycin (P13K/AKT/mTOR) pathway, which in normal cells is activated in response to growth factor signalling (151). However, mutations in components of the P13K/AKT/mTOR pathway, common in cancers, lead to dysregulation of energy metabolism allowing unrestrained growth in the absence of extracellular signalling (152). Dysregulation and mutation of the P13K/Akt/mTOR pathway is common in ovarian cancer and inhibitors of the pathway have shown significant anti-cancer effects preclinically (153, 154). Solid tumours often generate hypoxic conditions due to rapid cell proliferation and hypoxia-associated HIF-1, a regulator of glycolytic flux downstream of P13K/AKT/mTOR, is a target for anti-cancer therapy in EOC (119, 155).

1.8.3 Fatty Acid Metabolism in Cancer

Energy homeostasis is regulated by control of glucose, amino acid and lipid metabolism and cancer cells upregulate anabolic metabolism, i.e. synthesis and utilization of proteins, lipids and nucleotides (150). Lipid metabolism, also regulated in part by P13K/AKT/mTOR, is the focus of research into cancer-specific metabolism in ovarian cancer (156, 157). Lipids, primarily free fatty acids, are taken up via fatty acid chaperone proteins such as Fatty Acid Binding protein 4 (FABP4) and CD36. Fatty acids are stored in lipids droplets, most commonly as triacylglycerides, or transported

to the mitochondria for oxidation (Figure 1.4) (158). β-oxidation of fatty acids is a rich source of cellular energy: oxidation of one 16-carbon fatty acid molecule can generate 129 ATP molecules compared to 38 generated by mitochondrial metabolism of one glucose molecule. For fatty acid β oxidation, fatty acids are converted to Acyl-CoA by Acyl-CoA synthetase. In order for Acyl-CoA to enter the nucleus, it is converted to Acyl-carnitine by carnitine palmitoyltransferase I (CPT1), before being reconverted to Acyl-CoA in the mitochondria by CPT2. Acyl-CoA can then enter the citric acid cycle for energy production via a series of oxidation steps (159). Fatty acids are also synthesised de novo from Acyl-CoA through fatty acid synthase (FASN), via an intermediate step of malonyl-CoA catalysed by acetyl-CoA carboxylase (ACC) (149). (Figure 1.4) Alongside their role as a source of cellular ATP, fatty acids also form the building blocks of multiple lipid species, including phospholipid components of the cell membrane.

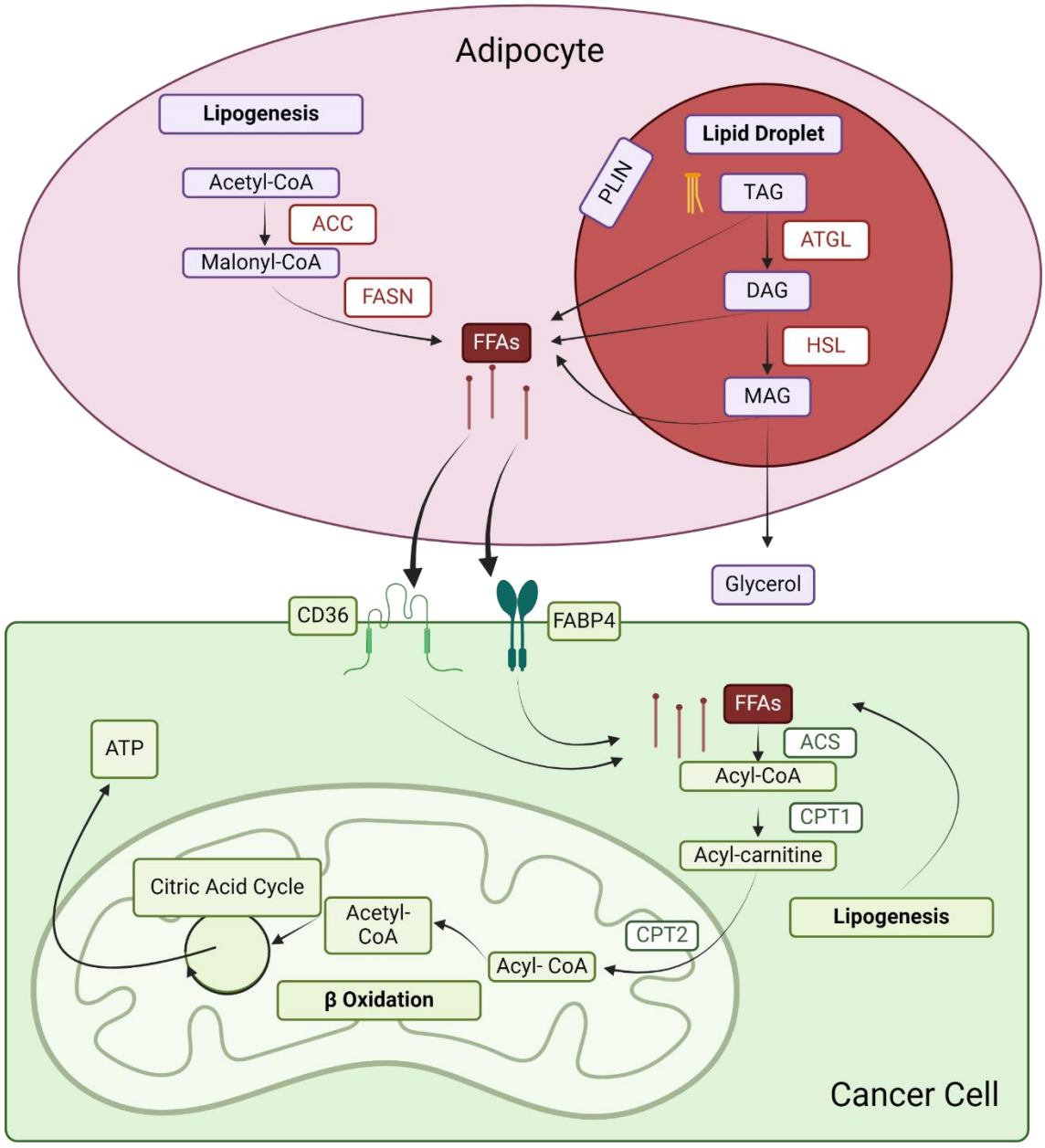

Figure 1.4 Fatty Acid Metabolism in Adipocytes and Cancer Cells. *Adipocyte-derived fatty acids are a source of energy in many tumours. De novo fatty acid synthesis occurs via first carboxylation of acetyl-CoA to malonyl Co-A by acetyl-CoA carboxylase (ACC). Formation of fatty acids from malonyl CoA is catalysed by fatty acid synthase (FASN). In adipocytes, and during dysregulated lipid metabolism in cancer, fatty acids and other lipid species are converted to triacylglycerides (TAGs) for storage in lipid droplets. Fatty acids are released from storage as TAGs via sequential lipolysis to diacylglycerides (DAG)s and monoacylglycerides (MAGs) by adipose triglyceride lipase (ATGL) and hormone sensitive lipase (HSL). Free fatty acids (FFAs) can be released from adipocytes passively before uptake into cancer cells via fatty acid chaperone proteins CD36 and fatty acid binding protein 4*

(FABP4). Energy is generated from fatty acids in cancer cells via β oxidation in the mitochondria. In order for transfer into the mitochondria, FFAs are converted into acyl-CoA by acyl-CoA synthetase (ACC) and then into acyl-carnitine by carnitine palmitoyltransferase I (CPT1). Following entry into mitochondria, CPT2 catalyses conversion back to acyl-CoA, which can then enter the citric acid cycle and enable adenosine triphosphate (ATP) production. Created with BioRender.com

Cancer is characterized by lipid remodelling: widescale alterations in fatty acid uptake, de novo fatty acids synthesis, rates of β oxidation and synthesis of other lipid species (159). Fatty acid uptake is often upregulated and expression of fatty acid chaperone proteins, including FABP4, CD36 and the fatty acid transport protein (FATP) family, is increased (159, 160). In ovarian cancer, knockdown of *CD36* and *FABP4* can reduce metastasis and increase survival in mouse and uptake of fatty acids from adipocytes results in increased CPT1 activation and acyl-CoA activation (107, 143). Increased uptake of fatty acids also results in the accumulation of lipid droplets in cancer cells, providing a source of energy during metabolic stress such as hypoxia, as regulated by HIF-1 (161). Fatty acid uptake is increased under hypoxic conditions, and increases in FABP4, a target of HIF-1α, may be indicative of a fatty acid scavenging phenotype in ovarian cancer (162).

Alongside increased uptake of fatty acids, de novo fatty acid synthesis, normally only apparent in adipocytes and hepatocytes, is often increased in cancer cells and FASN is associated with aggressiveness and poor prognosis in EOC (163, 164). *FASN* can be considered an oncogene and inhibition of FASN in ovarian tumours can reduce tumour growth through perturbation of upregulated P13K/AKT/mTOR signalling (165, 166). Stearoyl-CoA desaturase-1 (SCD1) converts mono-unsaturated fatty acids into saturated fatty acids, altering the composition of fatty acids. In ovarian cancer, SCD1 expression is elevated, particularly in cancer stem cells, while inhibiting SCD1 has been shown to suppress the growth of ovarian cancer stem cells in mouse models (167). SCD-1 is a target of the transcription factor NF-kB which is known to play a role in inflammation-mediated metastasis and is upregulate by TNFα and IL-8 (112, 117). Increased fatty acid synthesis and diversification of lipid synthesis machinery provides

metabolic flexibility in cancer cells that enables them to proliferate and spread under stressful conditions (159).

1.8.4 Adipocyte Metabolism in Cancer

The primary function of adipose tissue is energy storage, though there are important role for adipocytes and adipose tissue in temperature regulation, immunity and systemic endocrine regulation. Alongside adipocyte, adipose tissue incorporates populations of stem cells and pre-adipocytes, immune cells (including macrophages, T cells, B cells and NK cells), fibroblasts, endothelial cells and pericytes (168). There also exists significant diversity among adipocytes: white adipocytes function primarily in energy storage while brown adipocytes are thermogenic and regulate body temperature (169, 170). Beige adipocytes also play a role in thermogenesis but have distinct gene expression profiles from brown adipocytes: they lack basal expression of mitochondrial uncoupling protein 1 (UCP1), a source of heat generation in mitochondria-rich brown fat, but can upregulate UCP1 in response to extracellular signalling (171). Within these adipocyte phenotypes there is significant differences in gene expression profiles between different tissues and organs (172). Omental adipocytes, for example, is composed primarily of white adipocytes expressing higher levels of proteins involved in lipid metabolism compared to subcutaneous adipocytes (173).

Lipid droplets form the most recognisable aspect of adipocyte physiology and are formed of mostly of triacylglycerides (TAGs) alongside cholesterol and a suite of regulatory proteins. Lipid droplets are contained within a phospholipid monolayer

containing lipid metabolism regulating proteins including perilipin (PLIN), adipose triglyceride lipase (ATGL) and hormone sensitive lipase (HSL) (174). White adipocytes are unilocular, typically containing one large lipid droplet, while brown adipocytes are multilocular. Fatty acids are released from lipid droplets via lipolysis, usually in response to hormone signalling. ATGL and HSL are activated by protein kinase A phosphorylation and catalyse hydrolysis of TAGs to diacylglycerides (DAGs) and DAGs to free fatty acids and glycerol. Free fatty acids generated by lipolysis are released from adipocytes into blood and surrounding tissues (Figure 1.4) (174, 175).

Lipid metabolism is regularly dysregulated in cancer and changes in adipocyte lipid secretion impacts cancer-specific metabolism in tumours (108, 156, 157, 176). Direct transfer of lipid from adipocytes to prostate cancer cells has been demonstrated in vitro using Fourier transform infrared (177), linking adipocyte-derived lipids to prostate cancer preference for generation of energy via β oxidation (178). Adipocytes in co-culture with breast cancer cells increase fatty acid secretion and undergo ‘delipidation’ resulting in loss of adipocyte phenotype and activity, a phenomenon validated in tumour-adjacent adipose tissue from breast cancer patients (179). Invasion of adipose tissue is often accompanied by such changes in tissue composition: adipocytes undergo delipidation and are replaced by tumour-supporting fibroblasts and cancer cells (108). Analysis of omental tissue in ovarian cancer patients by immunohistochemistry and flow cytometry revealed a decrease in adipocytes and increase in SMA-expressing fibroblasts correlated with severity of disease (80). Breast cancer cells can induce MMP-11 expression in adipocytes in co-culture, as well as TGF-β and TNF-α secretion, resulting in dedifferentiation into a fibroblast-like phenotype and potentiating invasion through matrix remodelling (180)

1.8.5 Adipocytes in the Omental Metastatic Niche

Signalling pathways and mechanisms regulating omentum tropism in EOC were first elucidated in work by Nieman and colleagues in 2011 (107). In the study, fluorescently labelled EOC cells were injected intraperitoneally into mouse and were found to home preferentially to the omentum. IL-6 and IL-8 were expressed in human primary omental adipocytes, while inhibition of IL-6 and IL-8 signalling with inhibitory antibodies significantly reduced omentum homing of EOC cells in mouse. Using co-culture models incorporating human primary adipocytes and EOC cell lines, they demonstrated an increase in lipids in EOC cells following co-culture, as well as an increase in fatty acid β oxidation. FABP4 was upregulated in EOC cells following co-culture and inhibition of FABP4 in mouse decreased tumour volume and number of metastases. This study suggested a model in which omentum-derived cytokine signalling induces EOC metastasis to the omentum, and omental adipocytes provide energy for ovarian cancer growth through provision of free fatty acids (FFAs). Importantly, this work centred omental adipocytes as important regulators of EOC metastasis and demonstrated how targeting of adipocyte-tumour interactions could act to inhibit metastasis.

In a follow up study, the same group demonstrated a role for another fatty acid chaperon protein, CD36, in adipocyte-enhanced ovarian cancer cell growth (143). Furthermore, co-culture with omental adipocytes significantly altered EOC cell metabolism, shifting cells from reliance on glucose oxidation to uptake and metabolism of fatty acids. Inhibition of *CD36* with silencing RNA (siRNA) or inhibitory antibody decreased tumour number and weight in mouse. More recently, they demonstrated that inhibition of *FABP4* expression can sensitize ovarian tumours to carboplatin

treatment in mouse (144) and adipocytes promote metastasis by regulating synthesis of glycerophospholipids which may be necessary for membrane alterations required for attachment and invasion (145). Elsewhere, it has also been reported that knockdown of siRNA-mediated knockdown of *FABP4* in endothelial cells can prevent tumour-associated angiogenesis, decreasing metastasis in mouse (181). Targeting fatty acid oxidation by inhibiting CPT1, the enzyme responsible for fatty acid uptake into mitochondria, with etomoxir reduced metastasis and disease progression in mouse (182).

Multiple studies have demonstrated that adipocytes can promote ovarian cancer cell proliferation (107, 143, 144, 183, 184) and several other regulatory mechanisms have been proposed for the pro-cancer effects of omental adipocytes. Salt-inducible kinase 2 (SIK2) is an adenosine monophosphate (AMP)-activated protein kinase (AMPK) and has roles in energy homeostasis and lipid metabolism (185). *SIK2* was demonstrated to be upregulated in omental metastases relative to primary ovarian lesions and *SIK2* inhibition can prevent omental metastasis in mouse (146). Miranda and colleagues propose SIK2 as a master-regulator of ovarian cancer response to adipocytes due its capacity to activate, via phosphorylation, acetyl-CoA carboxylase and phosphoinositide 3-kinases (PI3Ks) and therefore regulate fatty acid oxidation (through CPT1 activation) and cancer cell proliferation (146). Metformin, which has been shown to sensitize EOC cells to chemotherapy, may act by regulating AMPK activity (184). Secreted protein acidic and rich in cysteine (SPARC), a non-structural subunit of extracellular matrix, is overexpressed in a wide range of pathologies including obesity, inflammation and cancer (186) and its role in adipocyte – EOC interactions has been explored (183). Inhibition of SPARC in mice and cancer cells in adipocyte co-culture increased EOC proliferation and omentum homing, suggesting

SPARC acts as a tumour suppressor and may play an anti-inflammatory role (187). Notably, in adipocyte – EOC co-culture SPARC inhibited increased lipolysis and decreased fatty acid release in adipocytes (183).

Alongside omental adipocytes, stem cell populations present in omentum may play a role in facilitating EOC metastasis. Omental adipose-derived mesenchymal stem cells (MSCs) support tumour growth by promoting vascularization through the increased expression of growth factors like VEGF, fibroblast growth factor (FGF), and Stromal cell-derived factor 1- α SDF1-α (188). Additionally, these MSCs help ovarian cancer cells by enhancing glycolysis and reducing oxidative stress through the regulation of nitric oxide levels in the omental metastatic niche (189). Adipose stem cells may also promote omental metastasis through upregulation of MMPs in ovarian cancer cells resulting in remodelling of the omental ECM required for attachment and invasion (190).

1.8.5 Obesity and Cancer

Numerous cancers have been linked to obesity, including breast, endometrial, colorectal, oesophageal, kidney, gallbladder, uterine, pancreatic, and liver cancer (191, 192), as well as ovarian cancer, as discussed in Section 1.5. Obesity, broadly defined as a BMI >30, is characterized by excess energy surplus, resulting in TAG accumulation in lipid droplets, adipocyte hypertrophy and hyperplasia and ultimately dysregulation of adipose tissue metabolism and function. Adipose tissue is an important source of hormone signalling and dysregulation leads to systemic effects on endocrine signalling via increased secretion of adipokines such as leptin. Expansion

and hypertrophy of white adipose tissue results in cell death, immune infiltration and the development of chronic low-grade inflammation (193). Immune cell infiltration is drastically increased, and macrophage number can increase 10-20 fold in adipose tissue in obese patients (194). Within this inflamed adipose environment fatty acid secretion is increased, resulting in hyperlipemia of the blood (195).

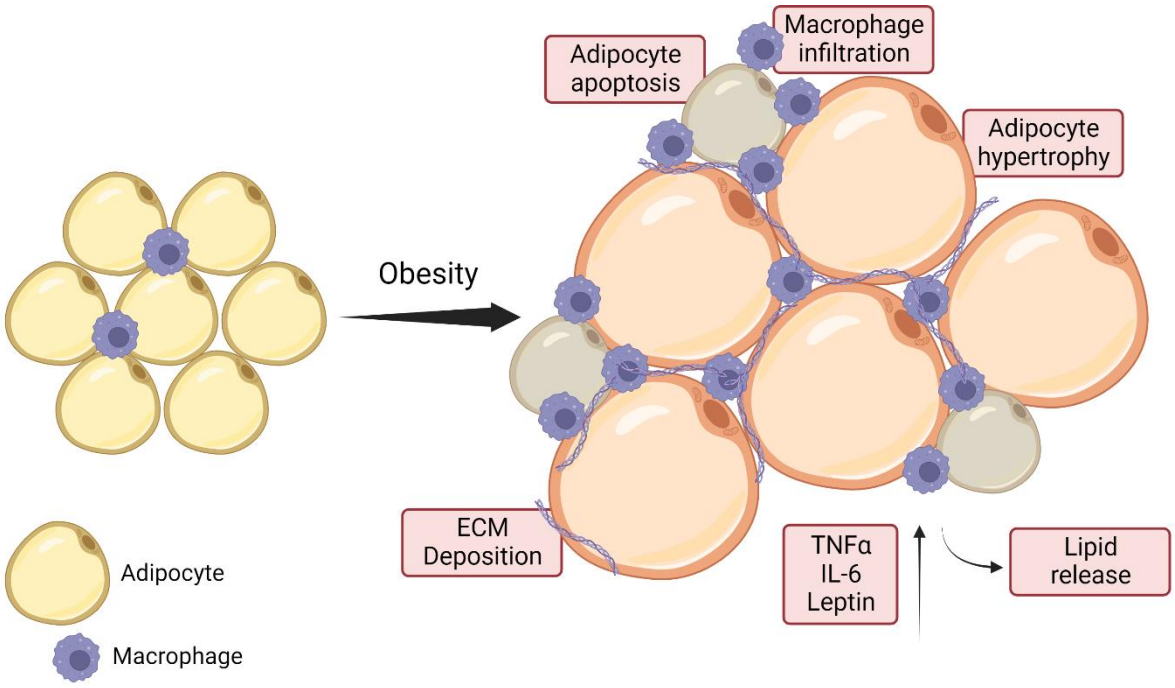

Figure 1.5 Obesity in Adipose Tissue. *Excess of cellular energy for storage in adipocyte leads to adipocyte enlargement (hypertrophy) and cell death via apoptosis. Adipocyte apoptosis and hypertrophy results in recruitment of inflammatory macrophages and the release of inflammatory cytokines, generating a state of chronic, low-grade inflammation. Adipose inflammation leads to increased ECM deposition and ultimately tissue fibrosis, as well as increased secretion of lipids from adipocytes, leading to hyperlipidaemia. Created with BioRender.com.*

As noted previously, an inflamed environment promotes EOC and fatty metabolism is upregulated in ovarian cancer cells, indicating potential roles for obesity in EOC metastasis. In a high fat diet-induced obesity mouse model, pancreatic cancer cells

displayed increased fatty acid β-oxidation and mice showed higher levels of TNF-α and IL-6 (196). Obesity induced increases in tumour growth could be inhibited by knockdown of TNF-α receptor, suggesting an inflammation-mediated mechanism. Similarly in hepatocellular carcinoma, obese mice demonstrated increased tumour burden which was precluded by genetic knockdown of *TNFα* and *IL6* (197). Adipocyte-derived leptin may also play an important role in obesity-associated cancer mortality (192) and can activate the JAK/STAT pathway (198, 199). In ovarian cancer, leptin receptor overexpression has been related to mortality (200), and leptin treatment in vitro can inhibit apoptosis in EOC cells via PI3K/Akt activation (201).

1.9 Mechanisms of Chemoresistance in Ovarian Cancer

The development of resistance to chemotherapy in major obstacle to effective treatment of EOC in the clinic. Conventional chemotherapy consists of platinum-based drugs like cisplatin and taxanes such as paclitaxel (22). Cisplatin binds nuclear DNA, inhibiting transcription through binding purine residues and leading to DNA damage and ultimately apoptosis (202). Paclitaxel binds and stabilizes microtubules, preventing formation and the mitotic spindle resulting in mitotic arrest and apoptosis (203). Both of these drugs are not cancer cell specific and therefore have severe off target effects.

As most patients respond to therapy at first before remission, ovarian cancer therapeutic resistance can largely be considered acquired, and may therefore evolve over the course of treatment from a small population of resistant stem cells (204). The existence of bona fide cancer stem cells (CSCs) in ovarian cancer is debated, however

markers for stemness have been described, including CD44 which is linked to chemoresistance through its activation of STAT3 (205). In a xenograft mouse model, small molecule inhibition of STAT3 can sensitize resistant ovarian tumours to cisplatin therapy (206). Tumour heterogeneity may play a role in the generation of resistant populations of cells as a diverse mutational background enables multiple routes to survival during therapy-induced cytotoxicity. HGSOC, characterized by the development of resistance following remission, often displays high intra-tumoral heterogeneity (56, 58). Acquired resistance can occur through dysregulation of apoptotic signalling or increased tolerance of DNA damage, inhibiting the pro-apoptotic mechanisms of action of cisplatin and paclitaxel (207).

Populations of stem-like cells, as well as phenotypic heterogeneity, enable changes in phenotype through populations of cells such as those apparent during EMT. EMT is associated with chemoresistance in EOC (208, 209) and Notch-3-induced activation of EMT in EOC cells acts to protect them from carboplatin therapy. Blocking endothelin A receptor has been shown to regulate Snail activity, upregulated in post-EMT cells, resulting in reversal of the cadherin switch and sensitization of cancer cells to therapy in a xenograft model (210). In HGSOC, exosomes have been shown to transmit platinum resistance through DNA methyltransferase I (DNMT1), impacting regulation of DNA damage responses in tumour cells.

1.10 Models of Ovarian Cancer

Given the complex nature of EOC development and progression outlined above, models which are able to recapitulate some aspects of ovarian cancer native environment are able to provide insights into disease pathology and explore therapies

which seek to overcome metastasis and resistance to therapy. Traditional homotypic two dimensional (2D) monolayer cell cultures cannot recreate the complex three-dimensional (3D) environment in which cancer cells exist in vivo, and do not recapitulate the network of cell-cell signals and microenvironmental cues which guide tumour cell activity and response (211, 212). Mouse models, including the gold-standard patient-derived xenograft (PDX) models, remain time-consuming and expensive, while evaluating the relevance of data from the murine tumour environment to clinical outcomes remains challenging. In light of these experimental limitations, complex, three-dimensional in vitro models of EOC which incorporate multiple cell types, matrix components and physical stimuli have become more prominent, and the development of such models has been identified as a priority for the progression of EOC research (9).

1.10.1 Tumour Spheroids

The use of tumour spheroids in cancer research is widespread. Many cancer cell populations will readily form three-dimensional aggregates or compact spheroids when cultured on non-adhesive surfaces, for example agarose or polyHEMA coated plates, or when grown in droplet suspension as per the hanging drop method. In contrast to traditional two-dimensional monolayer culture, three-dimensional spheroids can incorporate aspects of spatial architecture, biophysical environment, phenotypic heterogeneity and mechanisms of chemoresistance which are apparent in solid tumours (213). Spheroid models for ovarian cancer can be even more revealing given the mechanism by which ovarian cancer can disseminate through the peritoneum (63). Multi-cell aggregates, endogenous tumour spheroids, are abundant

in the ascites and are hypothesised to represent discrete metastatic units capable of initiating secondary metastases within the peritoneal cavity (64, 66).

A number of features of spheroid molecular physiology can have significant impact on the ability of cancer cell populations to survive intraperitoneal dissemination and adhesion, and to subsequently seed secondary metastases. In vitro, phenotypically heterogeneous populations of cells develop naturally in spheroids, driven by gradients of nutrient availability and hypoxia, and consequently viability and proliferative capacity (Figure 1.6) (213). Such intra-tumoral heterogeneity is apparent in solid tumours, for example mosaic expression of the cell surface marker E-cadherin is apparent in both primary and secondary EOC tumours, as well as endogenous tumour spheroids (65, 214). Growing evidence suggests that endogenous ovarian ascites spheroids also incorporate multiple, non-malignant cell types including mesothelial cells, fibroblasts and macrophages and heterotypic spheroid cultures have been used to explore these phenomena (66, 68, 69).

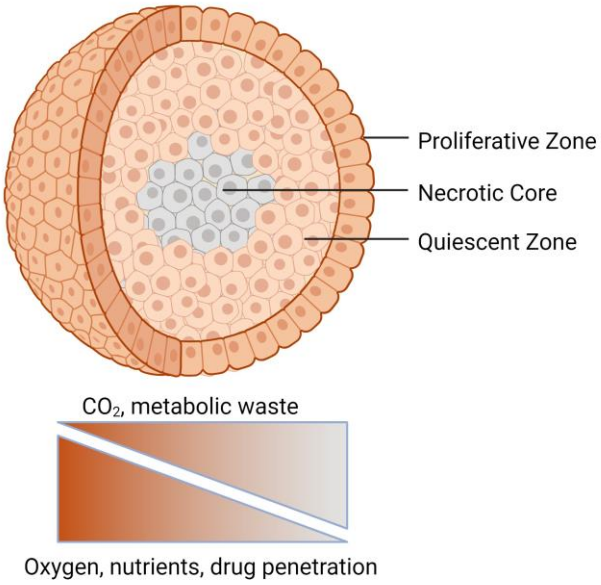

Figure 1.6 Tumour Spheroids. *Tumour spheroids generate heterotypic populations of cells including proliferative regions of cells at the periphery and a quiescent core inside the proliferative zone. Gradients of availability of oxygen and nutrients produce a necrotic core at the centre of the spheroid. Created with BioRender.com.*

1.10.2 *In Vitro* Models of Ovarian Cancer Metastasis

A wide range of tools and techniques have been utilised to generate biocompatible matrices to recreate the ovarian cancer metastatic tumour microenvironment (82). Cell-derived scaffolds, for example decellularized fibroblast-derived matrices offer a complex protein environment and structural composition (215). Similarly, Matrigel, a hydrogel derived from Engelbreth-Holm-Swarm mouse sarcoma cells, is comprised largely of collagen IV, laminin and entactin and has been widely used to generate a 3D microenvironment for ovarian cancer (118, 216). Similarly, semi-synthetic matrices have been developed, for example collagen-based hydrogels formed from purified type I collagen derived from rat tail (217, 218), the biological and mechanical

properties of which can be modified through modulation of collagen concentration and the incorporation of other collagen types and glycosaminoglycans. Adhesion assays to explore mechanisms of ovarian cancer adherence at the peritoneal mesothelium have been developed using biocompatible matrices, for example quantification of fluorescently labelled OC cell lines adhered to fibronectin or patient-derived ascites spheroids adhered to fibronectin, laminin and collagen types I and IV (219, 220).

Due to the prevalence of the omentum as a site of intra-peritoneal metastasis, a number of studies have sought to recreate specific aspects of the omental microenvironment and ECM in vitro. An organotypic model of peritoneal invasion was developed to replicate the omental metastatic niche, and incorporates primary, fibroblasts and mesothelial cells isolated from omental tissue obtained during surgery, alongside EOC(221). Fibroblasts are seeded in 3D collagen I gel, before the addition of a mesothelial monolayer at the surface. Studies incorporating primary adipocytes and EOC cells in simple transwell co-culture, alongside mouse models have revealed how reciprocal metabolic alterations in malignant and stromal components can enhance proliferation, migration and invasion of tumour cells detailed above (107, 146).

1.10.3 *In Vitro* Culture of Adipocytes

In vivo, mature adipocytes are generated from pre-adipocyte precursors, which are in turn derived from a multipotent population of stem cells within adipose tissue (222). Mature adipocytes have been generated from a number of precursor cells in culture, as well as from direct isolation from adipose tissue. Due to the presence of lipids,

adipocytes are buoyant and therefore float in cell culture. While this is a barrier to generating adherent cell populations, it also allows for separation of adipocytes from other cellular components of adipose tissue. Following digestion of tissue (e.g. with collagenase), tissue digest can be centrifuged to separate out adipocytes from the non-buoyant population of cells termed the stromal vascular fraction (SVF). The SVF contains a heterogeneous population of fibroblasts, pre-adipocytes and other adipocyte-derived stem cells, immune cells, pericytes and vascular smooth muscle cells among others (223).

Early work using subcutaneous and inguinal fat demonstrated that cells of the SVF could be differentiated using specific growth media containing insulin and triiodothyronine, and additionally stimulated with corticosteroids (224, 225). The composition and activity of adipose-derived cells within a population varies depending on the source of tissue (226), and as such protocol have been developed to isolate omental SVF and adipocytes using similar methodologies (227). Other studies use primary adipocytes isolated from the adipocyte fraction of omental tissue digest (107, 146). The proliferative capacity of these mature adipocytes is weakened and this, alongside reduced adherence due to cell buoyancy, can lead to poor cell yields. To increase yield, researchers have utilised “ceiling culture”, whereby cells adhere to the ceiling of a culture flask that is completely filled with media (228).

1.11 Research Aims

As described, numerous studies have reported an important role for adipocytes in ovarian cancer progression. An inflammatory microenvironment promotes EOC

development and metastasis, while adipocyte-derived signalling and metabolites within the peritoneal metastatic TME drive secondary tumour growth at the omentum. This study sought to develop *in vitro* models incorporating multiple aspects of the ovarian tumour metastatic TME to explore pro-cancer signalling within an adipocyte-rich niche.

The aims of the study were as follows:

- Develop heterotypic, spheroid-based models incorporating ovarian cancer cells and adipocytes.
- Explore the impact of adipocytes on ovarian cancer growth and response to therapy.
- Explore signalling mechanisms regulating ovarian cancer – adipocyte interactions.
- Explore the impact of inflammation on adipocytes and cancer cells to recapitulate the inflammatory ovarian TME.

Chapter 2. Materials and Methods

2.1 Introduction to Ovarian Cancer Cell Lines

In this work, three human cell lines were utilised to model different aspects of Epithelial Ovarian Cancer (EOC). The SKOV-3 cell line was isolated from the ascites of a 64 year old Caucasian patient with ovarian adenocarcinoma in 1973 (229). In adherent culture, SKOV-3 cells display epithelial morphology and serous histological properties (230), although tumours generated by intraperitoneal injection in mice have been shown to display a clear-cell adenocarcinoma pathology (231). Presence in the ascites indicates metastatic disease and SKOV-3 cells have been shown to have high invasive capacity, as well as omentum tropism, in mice (107, 232). As such, SKOV-3 represents a model for aggressive, metastatic disease. As the cell line was derived from a patient receiving treatment prior to the introduction of taxane and platinum-based chemotherapeutics, SKOV-3 has been demonstrated to be sensitive to such treatments relative to other ovarian cancer cell lines (230).

OVCAR-3 was derived from the ascites of a patient with progressive adenocarcinoma in 1982 and similarly these cells display epithelial morphology and high-grade serous histology (230, 233). In contrast to SKOV-3, OVCAR-3 was isolated from a patient whose disease had demonstrated resistance to cisplatin and was developed specifically to study chemoresistance in ovarian cancer. Analyses of EMT markers in SKOV-3 and OVCAR-3 show relatively high expression of the mesenchymal-related marker vimentin and the epithelial maker e-cadherin respectively (234, 235).

Additionally, OVCAR-3 cells have relatively lower invasive capacity upon intraperitoneal injection into mice, and lower migratory capacity *in vitro* (232, 236).

CAOV-3 was isolated from a 54-year old ovarian cancer patient in 1976 and displays invasive capacity lower than SKOV-3 but higher than OVCAR-3 (237). These three cell lines were chosen as they represent a range of EOC phenotypes in respect to their invasive capacity, aggressiveness and response to therapy. SKOV-3, OVCAR-3 and CAOV-3 cells were purchased from American Type Culture Collection (ATCC, Cat. Nos. HTB-77, HTB-161 and HTB-75).

2.2 Culture of Ovarian Cancer Cell Lines

All cell lines were cultured in T75 plastic culture vessels as directed by supplier as follows: SKOV-3 cells were cultured in McCoy's 5A Medium supplemented with 10% Fetal Bovine Serum (FBS) and 1% Penicillin-Streptomycin (P/S); OVCAR-3 cells were cultured in RPMI 1640 supplemented with 20% FBS, 1% P/S and 0.01mg/ml bovine insulin; CAOV-3 cells were cultured in Dulbecco's Modified Eagle's Medium supplemented with 10% FBS, 1% P/S. All cells were maintained at 37^{o}c and 5% CO^{2} in a humidified incubator and sub-cultured at 80-90% confluence as follows: cells were washed with phosphate buffered saline (PBS) and incubated for 5 minutes at 37^{o}c to maintain pH and osmotic balance and to promote cell detachment. Cells were detached via incubation with 2ml 0.25% trypsin, 1mM Ethylenediaminetetraacetic acid (EDTA) (pH 8) in Hanks' Balanced Salt Solution (HBSS) containing phenol red and excluding $CaCl_2$, $MgCl_2$ and $MgSO_4$ for ~5 minutes or until cells had completely detached. Cell detachment from the plastic vessel was confirmed via visualisation with

an inverted light microscope. Trypsin was neutralised using 4ml cell media and a pellet generated from the cell suspension via centrifugation at 300 × g for 5 minutes at room temperature. Supernatant was removed via aspiration or decanting, and the pellet re-suspended in 5-10ml of media. For routine sub-culturing, this cell suspension was split 1:5 – 1:10 in culture media in a T75 plastic culture vessel. Cell lines were cultured up to 30th passage and phenotypic stability monitored through visualisation with an inverted light microscope. Where necessary, cells were frozen in freeze media comprising 90% FBS, 10% Dimethyl sulfoxide (DMSO) in cryogenic vials. Vials were frozen at -80^{o}c in iso-propanol to ensure gradual reduction in temperature before transfer to liquid nitrogen. Cells were thawed via brief submersion in a 37^{o}c water bath before immediate transfer to fresh culture media.

Where necessary, cells were counted using TC10 Automated cell counter (Bio-Rad, UK). Cells in suspension were mixed 1:1 with Trypan blue and inserted into Cell Counting Slides (Bio-Rad, Cat. No. 1450015). Trypan blue is selectively taken up by dead cells, and cell counter software can therefore determine the proportion of living cells in a population. For seeding cells for quantitative assays, >90% living cells was deemed acceptable.

2.3 Three-dimensional Spheroid Culture

Three-dimensional (3D) cell spheroids or multi-cell aggregates were generated through two primary methods: the liquid overlay technique (LOT) and using ultra-low attachment (ULA) plates. LOT generates a non-adhesive surface through coating of culture plastic with agarose or agar. This prevents cells from adhering to a plastic

surface, instead inducing cells in culture to adhere to each other, forming multi-cellular spheroids (238). Here, 96-well plates were coated with 2% agarose prior to cell seeding. Following preparation of 2% agarose in water, agarose gel was autoclaved to ensure sterility in cell culture. Agarose forms a gel-like solid at room temperature, so was heated until liquid, avoiding bubbling, in a microwave before decanting into a 50ml sterile reservoir. 50µl of agarose was pipetted into 96-well plates using a multichannel pipette, and an even covering of the well confirmed by eye and with an inverted light microscope. Plates were left under ultraviolet (UV) for at least 1 hour following preparation to further ensure sterility and to allow agarose to cool and solidify. For seeding of spheroids, the appropriate concentration of cells in suspension (2×10^3 cells in 100µl of media for SKOV-3 and OVCAR-3 spheroids, 3×10^3 cells in 100µl of media for CAOV-3 spheroids) was prepared and pipetted directly on top of the agarose coating. Speed of formation and structure of spheroid culture depends upon the cell-type and culture conditions and was observed via light microscope.

ULA plates induce spheroid formation on the same basis: a non-adherent surface promotes cell-cell adhesion and aggregation. ULA plates incorporating black opaque sidewalls (Corning, Cat. No 3916) were utilised in all experiments involving fluorescence, luminescence and absorption (confocal microscopy, cell viability assays) as they minimize well-to-well cross talk and ensure lower inter-well heterogeneity. For RNA and protein extraction ≥48 spheroids were collected.

2.4 Adipose-Derived Stem Cell-Derived Adipocytes

Mature adipocytes were reliably generated from StemPro Human Adipocyte-Derived Stem Cells (ADSCs), (ThermoFisher Cat No. R7788). ADSCs are multipotent stem cells, isolated from adipose tissue collected during liposuction procedures, capable of differentiation into mature cell types including osteoblasts, chondrocytes and adipocytes. ADSCs were cultured as per distributor's recommendation in MesenPro RS Media (Cat No. R7788-110) supplemented with 1% P/S (henceforth Stem Cell [SC] Base Media) and sub-cultured at 80-90% confluence.

For adipocyte differentiation, ADSCs were seeded at 1 x 10^4 viable cells/cm^2 for adherent culture and 2 x 10^3 viable cells/well for spheroid culture. After 48 hours of expansion in Stem Cell Base Media, or when cells reached 80% confluency, media was replaced with StemPro Adipogenesis Media (Cat. No. A100700) supplemented with 1% P/S (henceforth Adipogenesis Media). Media was replaced every 3-4 days, and differentiation allowed 14 days to proceed for all work presented in Chapter 2, and 21 days for all work presented in Chapters 3 and 4. Differentiation of ADSCs into mature adipocytes was observed in the appearance of lipid droplets and the expression of adipocyte specific markers, as described below.

2.5 Verification of Mature Adipocytes

Mature adipocytes are identifiable visually through their distinct morphology, most significantly the present of multiple, large lipid droplets containing triacylglycerides and other lipids alongside cholesterols and other components of lipid metabolism (168). Differentiation of pre-adipocytes into mature adipocytes also coincides with increased

expression of adipocyte-specific protein markers, and the secretion of adipocyte-specific hormones (adipokines). The presence of mature adipocytes was therefore confirmed through identification of lipid droplets and adipokine secretion, described here, as well 45abelleh the expression of adipocyte-specific markers observed via immunoblotting, as described in Section 2.8.

2.5.1 Oil Red O Staining

For staining of lipid droplets in 2D cell cultures Oil Red O staining was used, a fat-soluble dye which stains neutral triglycerides and other lipids. Stock solution of 0.5% Oil Red O (Abcam, Cat. No. Ab146295) in isopropanol was kept at room temperature for up to 1 year. For staining assay, working solution of 3:2 stock solution: H_2O was diluted and maintained for no longer than 2 hours. Cells for staining were grown in 6-well culture dishes and washed twice with PBS before fixing with 10% formalin for 30 minutes. Cells were then washed twice with water before incubation with 60% isopropanol for 5 minutes. Cells were covered with Oil Red O working solution and incubated for 10 minutes, before cells were washed with water until all excess stain was removed. Staining was visualised with an inverted light microscope and images acquired with Zen Blue software (Version.3.2)

2.5.2 BODIPY Staining and Confocal Microscopy

BODIPY lipid probes are lipophilic fluorophores which can be used for tracking of lipids. In order to detect lipids in spheroid culture, BODIPY 493/503 (ThermoFisher,

Cat. No D3922) was diluted in culture media from a stock concentration of 5nM before addition to live spheroid cultures to a final concentration of 1:5000. Spheroids were co-stained with DAPI (1:500) and incubated with both fluorophores for 45 minutes at 37^{o}c. Fluorescence was visualised via confocal laser scanning microscopy (CLSM). In CLSM, light of specific wavelength is focussed onto a very small area of sample in a narrow depth of focus. Fluorophores present in the sample are excited and emit light of a higher wavelength, which is again focussed to ensure light from the sample area only is collected, before being captured by a digital camera. Therefore, for fluorophores present in the sample, criteria for specific excitation and emission wavelengths are set. The microscope will scan a specified region of the sample, detecting light from multiple small sections, which are collected by software and an image of the sample is produced. Furthermore, multiple cross sections of a sample at different focal plains can be collected and collated together to produce a 3D image of the sample in a 46abelles known as optical sectioning. In this work, z-stack images were produced from at least 10 2D cross-sections at ×20 magnification using A1 Nikon Confocal Imaging System (Nikon Corporation, Tokyo, Japan) with NIS Elements AR Software (Version 4.5) or with Zeiss LSM710 and Zen Black software (version 3.2). DAPI was excited with 402nm laser and BODIPY with 495nm laser.

2.5.3 Adiponectin Enzyme-Linked Immunoassay

The adipocyte-specific hormone adiponectin (APN) is involved in the regulation of a variety of metabolic processes, notably glucose regulation and fatty acid catabolism. Therefore, to assess adipocyte activity, levels of APN in samples were quantified via Enzyme-Linked Immunosorbant Assay (ELISA). In ELISA, the target antigen (here,

APN) in a sample binds to protein-specific antibodies, inducing downstream colour change which can be quantified. Human Adiponectin Platinum ELISA kit was purchased from Thermofisher (Catalogue no. BMS2032) and performed as per distributor's instructions. Samples were diluted 1/100 to ensure APN levels fall within the range of the assay, and a serial dilution of APN protein samples produced. The ELISA kit contains 96-well plates coated with anti-APN antibody, to which samples and standards were added, inducing binding of APN. A biotin-conjugated anti-APN antibody was then added, which binds the captured human APN. Streptavidin-horseradish peroxidase (HRP) was then added, which binds biotin conjugated anti-APN antibody. Unbound protein, biotin-conjugated antibody and streptavidin-HRP were washed off after every step. Samples were incubated with an HRP-reactive substrate, which induces a colour change correlated with the amount of streptavidin-HRP in the sample, and therefore correlated with APN volume. Absorbances at 450nm were read using BMG Fluostar Omega Microplate spectrophotometer and a standard curve was generated using BMG Labetch Mars data analysis software (version) from protein standards via 5-parameter curve fit. APN concentration of samples could then be calculated from the standard curve.

2.5.4 Expression of Adipocyte-Specific Genes

The expression of adipocyte-specific genes was assessed as a marker for mature adipocyte phenotype. *ADIPOQ* encodes for adiponectin, as noted above a hormone synthesised in adipocytes, while *LEP* encodes leptin, which is similarly produced by mature adipocytes. *LPL* encodes lipoprotein lipase which metabolizes

triacylglycerides in lipid droplets found in adipocytes. The expression of *ADIPOQ*, *LEP* and *LPL* was assessed via real-time quantitative PCR, as detailed in Section 2.9.

2.5.5 Expression of Adipocyte-Specific Protein Markers

Changes in protein markers was assessed over the course of differentiation. As noted above, adiponectin (APN) is a hormone abundantly secreted by adipocytes. Cellular APN was measured by immunoblotting, along with levels of the transcription factor Peroxisome proliferator-activated receptor gamma (PPARγ), increased expression of which is essential for adipocyte differentiation. Following heterodimerization with retinoic X receptor (RXR), PPARγ induces the downstream expression in a range of gene regulating lipid storage, glucose metabolism and adipogenesis. Protein was extracted from differentiating ADSCs at intervals during adipogenesis, and immunoblotting carried out as detailed in Section 2.8.

2.6 Transwell Co-Culture

To explore the interactions between EOC cell lines and adipocytes *in vitro* co-cultures were generated using transwell inserts (Figure 2.1). Transwell inserts allow for the establishment of monolayer adipocyte populations separate from cancer cell populations but enable the exchange of signalling molecules and other biological molecules. The two populations are then easily separated for analysis. Adipocytes were differentiated on semi-permeable transwell inserts with 5.0μm pores (Corning, Cat No. CLS3387) before insertion on top of EOC cells in monolayer or spheroids

populations. ADSCs were seeded at 1.4 x 10^3 cells/well in transwell inserts and expanded in SC Base Media for 48 hours prior to replacement with Adipogenesis Media or maintenance in SC Base Media for undifferentiated control. Cells were grown in 80µl of media in the upper chamber of the plate while 100µl of media was placed into the lower chamber to ensure submersion of the membrane in growth media. Concurrently, spheroids comprising OVCAR-3 or SKOV-3 cells were generated in ULA plates and grown for 24 hours. ADSCs formed monolayer culture in transwell inserts, and after 21 days inserts containing either differentiated adipocytes or undifferentiated ADSCs were removed placed into spheroid-containing ULA plates. Co-culture proceeded for 72 hours before the cancer compartment and adipocyte compartment were separated for analysis.

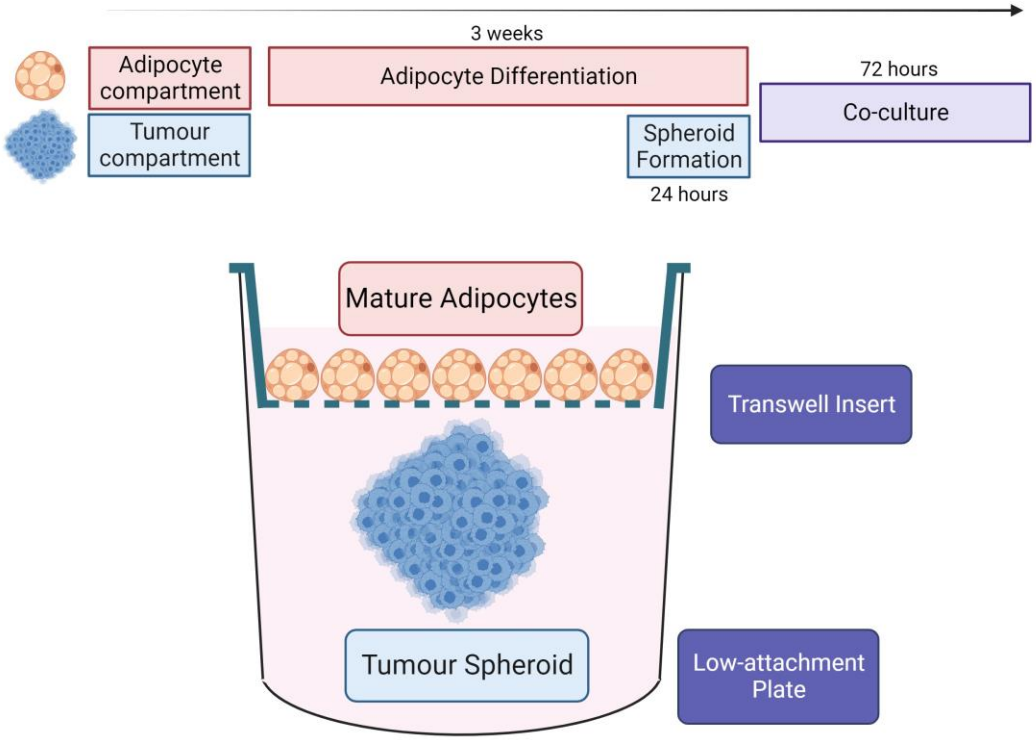

***Figure 2.1. Transwell Co-Culture of Adipocytes and EOC Cells**. ADSCs were seeded onto transwell inserts and differentiated for 3 weeks into mature adipocytes. Tumour spheroids were generated for 24 hours prior to co-culture. Transwell inserts were added on top of spheroids for co-culture for 72 hours.*

2.7 Cell Viability Assays

The impact of adipocyte co-culture, alongside other treatments detailed below, on EOC proliferation and population viability was assessed via a number of viability assays.

2.7.1 RealTime-Glo MT Cell Viability Assay

RealTime-Glo MT Cell Viability Assay (Promega, Cat. No. G9712). Measures the metabolic activity of a population of cells by introduction of a prosubstrate (MT Cell Viability Substrate), which is reduced by viable cells and can subsequently be utilized by a luciferase enzyme (NanoLuc Luciferase) to produce a luminescent signal. Reagents were added to each well at the outset, resulting in a final dilution of 1:1000 of both substrate and enzyme in primary ovarian media. Luminescence was measured with a BMG Fluostar Omega Microplate spectrophotometer, maintained at 37^{o}c, at 1 hour, 24 hours, 48 hours, 72 hours and 96 hours after seeding. Cell treatments were run in triplicate for each cell line.

2.7.2 MTT Assay

The MTT assay measures the ability of viable cells to reduce MTT (3-(4,5-Dimethylthiazol-2-yl)-2,5-Diphenyltetrazolium Bromide), a yellow tetrazolium salt, into formazan crystals with a purple colour. The amount of formazan produced is directly proportional to the metabolic activity and the number of viable cells and can be measured through its absorbance. Absorbance was read at 24 hours after cell seeding to ensure cells were proliferating and a blank containing media only was used in each experiment. Absorbance at 435nm was read in a BMG Fluostar Omega Microplate spectrophotometer.

2.7.3 CellTiter-Glo 3D Cell Viability Assay

CellTiter-Glo 3D Cell Viability Assay (Promega, G9682) quantifies the level of ATP in a population via ATP-dependent oxygenation of luciferin to luminescent oxyluciferin. The reagent also includes a potent lytic agent to ensure the disruption of spheroid structure and access of assay reagent to the whole cell population. For the end-point assay, 100µl of media was removed from well and 100µl of CellTiter-Glo 3D Cell Viability Assay reagent added for a final dilution of 1:1. Plates were shaken at 700rpm for 5 minutes before incubation at room temperature for 25 minutes. Luminescence was read in a BMG Fluostar Omega Microplate spectrophotometer as a measurement of population viability.

2.7.4 Live/Dead Fluorescence Cell Viability Assay

For visualisation of spheroid population viability, staining of cancer spheroids with stains for live and dead cells was performed. CalceinAM (Invitrogen, Cat No. C1430) is a non-fluorescent dye which only becomes fluorescent upon permeation of live cells due to the presence of intracellular esterases. Conversely, Ethidium Homodimer-1 (EthD1) (Invitrogen, Catalogue No. E1169), which fluoresces upon binding to nucleic acids, is not cell permeable and therefore will only fluoresce in cells with damaged membranes. Spheroids were incubated with CalceinAM (2µM) and EthD1 (3µM), as well as Hoechst (33µM), diluted in appropriate cell media, for 3H at 37^{o}c. Fluorescence was imaged via confocal laser scanning microscopy, as detailed in Section 2.5.2 using lasers at 402, 488 and 561nm. Z-stacks of ≥10 images were produced, and total

fluorescence for each stain was calculated using ImageJ (version 1.52a). CalceinAM and EthD1 fluorescence were both normalised to Hoechst, and a ratio of CalceinAM:EthD1 calculated as a measure of spheroid population viability.

2.8 Immunoblotting

2.8.1 Protein Isolation

For two-dimensional (2D) monolayer culture, cells were grown to 80-90% confluency in at least 2 wells of a six-well plate to ensure sufficient protein quantity. Cell were washed with PBS before covering with 60µl Radioimmunoprecipitation (RIPA) lysis buffer plus 10µl /ml protease inhibitor (Cat. Nos.). Cells were manually detached using a cell scraper and kept on ice in a 1.5ml Eppendorf tube for two hours to allow complete lysis of non-protein components. The protein lysate was then separated from lysed components via centrifugation at 10,000 × g for 10 minutes and the protein-containing supernatant removed by pipetting. Protein isolation was carried out at below 4^{o}c and lysate samples stored at -20^{o}c.

For 3D cultures, at least 48 spheroids were generated by LOT and cultured for 96 hours to ensure sufficient protein quantity. Spheroids were isolated from wells with a 1ml pipette and transferred to a 15ml falcon tube before centrifugation at 300 × g for 10 minutes. Supernatant was removed by decanting and the spheroid-containing pellet washed with PBS before re-centrifugation. PBS was replaced with 80µl lysis buffer as described above. Due to multiple, compact cell-cell adhesions present in spheroids, a freeze-thaw cycle was implemented to disrupt adhesions and rupture cells. Spheroids were placed on dry ice for 30 seconds, followed by 30 seconds

submersion in a 37^{o}c water bath and finally agitation by vortexing. This cycle was repeated at least 3 times or until spheroids were no longer visible by eye. Lysis then proceeded as for 2D cell culture above.

2.8.2 Protein Quantification

Protein quantification was carried out using Pierce™ Rapid Gold BCA Protein Assay Kit (ThermoFisher, Cat. No A53225). A serial dilution of bovine serum albumin (BSA) protein standards was produced with a range of 25-1500µg/µl and sample protein lysates were diluted 1:10 in RIPA buffer to ensure results sat within this range. Triplicates of sample or standard were incubated with assay reagents at room temperature for 15 minutes. Reaction of the assay reagents with protein induces a colour change, and absorbance was measured with a BMG Fluostar Omega Microplate spectrophotometer and a standard curve was produced by linear regression analysis using BMG Labetch Mars data analysis software (version). An R^2 value of >0.995 was considered sufficient for protein concentration of samples to be accurately calculated.

2.8.3 SDS-PAGE

Separation of proteins according to molecular weight was achieved through sodium dodecyl sulfate–polyacrylamide gel electrophoresis (SDS-PAGE). Following quantification, protein samples were diluted in RIPA buffer to achieve a final concentration of 30ug of protein in 30µl of buffer. A dilution of 10:1 4X Laemmli buffer

(BioRad, Cat. No. 1610747): beta-mercaeptoethanol was prepared, and 10µl added to each protein sample. Samples were mixed by pipetting and briefly centrifuged to remove bubbles before incubation at 95^{o}c for 5 minutes. The combined action of SDS components in Laemmli buffer, thiol activity of beta-mercaeptoethanol and heating effectively unfolds and linearizes proteins in the sample, as well as adding uniform negative charge, to ensure further separation is based on protein size only. Additionally, glycerol components in Laemmli buffer act to weigh down samples while they are in the gel so as to prevent well-to-well crossover, while a colouring agent enables tracking of proteins through the gel.

40µl of protein sample/buffer dilution were loaded into a precast 4-20% polyacrylamide gel (Biorad, Cat. No. 4561094), along with at least one well of 3.5µl protein standards (BioRad Precision Plus Protein Dual Color Standards, Cat No. 1610374) to generate a protein size reference ladder. Gels were run at 100V for approximately 1 hour, until the dye front passed the base of the gel to ensure sufficient separation of proteins. Protein was transferred to 0.2µm Polyvinylidene fluoride (PVDF) membrane (BioRad, Cat. No. 4561094) via the Biorad Trans-Blot Turbo Transfer System. Where appropriate, PVDF membranes were cut to allow efficient, simultaneous staining of multiple proteins on a single membrane.

2.8.4 Antibody Staining

Membranes were blocked in blocking buffer comprising 5% bovine serum albumin (BSA) in tris buffered saline (TBS) (BioRad, Cat. No. 1706435) containing 0.1% tween 20 (TBS/T) for one hour at room temperature or overnight at 4^{o}c. Proteins in BSA

passively bind excess binding sites on the gel, preventing non-specific binding of secondary antibody and ultimately reducing noise when imaging the gel. Following blocking, membranes were incubated with primary antibody for 2 hours or overnight at 4^{o}c. Primary antibodies were diluted in blocking buffer as per table. Primary antibodies used in each Chapter are given in Table 2.4, 2.6 and 2.8.

Following primary antibody incubation, membranes were washed twice for 5 minutes with TBS/T and once for 5 minutes with TBS to ensure removal of non-bound antibody. Membranes were then incubated with species-specific secondary antibody, diluted 1:1500 in blocking buffer, for 1 hour at room temperature or overnight at 4^{o}c before a second wash step as previously described.

2.8.5 Antibody Visualization

Multiple secondary antibodies, bound to a primary antibody at the protein of interest, are linked to the reporter enzyme horseradish peroxidase (HRP) and can therefore be visualised via application of a chemoluminescent substrate. Here, clarity Western ECL Substrate (BioRad, Cat. No. 1705061) was applied to protein-containing areas of the membrane, and chemoluminescent activity visualised with ChemiDoc™ Imaging System. Membranes were incubated with substrate for between 30 second and 2 minutes, depending on the abundance of protein and efficiency of primary antibody.

2.8.6 Band Intensity Calculation

The signal for each protein of interest was quantified using the rectangle tool function of Image lab software (version 6.0.1) with which signals are calculated from within a specified area equal for all samples. This signal, expressed as a function of volume data (intensity/mm^2) was used to calculate adjusted band intensity (ABI), whereby the signal of a protein band is adjusted relative to background noise. ABI was then normalized to an internal control (housekeeping gene protein), here Glyceraldehyde 3-phosphate dehydrogenase (GAPDH), such that normalized band intensity was calculated as follows:

$$normalized\ band\ intensity = \frac{ABI\ protein\ of\ interest}{ABI\ internal\ control}$$

2.9 Quantitative Real-Time Polymerase Chain Reaction

Relative levels of relevant gene mRNA in samples were quantified using Quantitative Real-Time Polymerase Chain Reaction (Q-RT-PCR). This process, briefly outlined below, involves isolation and purification of RNA from samples, followed by conversion to copy DNA (cDNA) for analysis by Q-RT-PCR.

2.9.1 RNA Extraction and Purification

For RNA extraction, 2D and 3D cell cultures were grown as per protein extraction for immunoblotting. RNA extraction and purification was carried out using Rneasy Mini Kit (Qiagen, Cat. No. 74106), and samples were kept on ice throughout while centrifuges

were cooled to 4^{o}c. Following washing with PBS, adherent cells were covered with 350µl Rneasy lysis buffer for 1 minute before disruption with a cell scraper and collection. For 3D culture, 350µl Rneasy lysis buffer was added to spheroids in a 15ml falcon tube and kept on ice for 15 minutes with periodic agitation by vortexing. If immediate purification was not possible, RNA lysates were stored at -80^{o}c.

RNA purification was carried out per supplier's instructions as follows. Briefly, samples were centrifuged for 2 minutes at full speed in QIAshredder to ensure complete homogenization of the lysate. The homogenized lysate was combined with equal volume 70% ethanol and centrifuged for 15 seconds at 10,000 × g in an RNAeasy spin column. The silica 58abelled contained in this column selectively binds RNA, while contaminants are washed away and discarded with flow-through. The membrane was then rinsed through with wash buffer before the membrane was incubated at room temperature for 15 minutes with Dnase 1 to degrade contaminating genomic components. The RNA-containing membrane was further washed before 30µl of Rnase free water was spun through the column for 1 minute at 10,000 × g to elute the purified RNA. Concentration and purity of RNA was measured using NanoDrop spectrophotometer (ThermoFisher, NanoDrop One^{c}). The ratio of spectrophotometric absorbance at wavelengths of 260nm and 280nm ($A_{260/280}$) and the ratio of absorbance at 260nm and 230nm ($A_{260/230}$) are used to determine the purity of RNA samples. $A_{260/280}$ and $A_{260/230}$ of pure RNA are approximately 2, and here ratios within the range 1.8-2.2 were sufficient for conversion of RNA to cDNA to be able to proceed.

2.9.2 Conversion of RNA to cDNA

Conversion of 100ng/µl of RNA produced sufficient cDNA for Q-RT-PCR to proceed effectively, therefore samples were diluted to this concentration in Rnase free water prior to cDNA conversion. cDNA master mix (BioRad, Cat. No. 1708891) was prepared for each sample.

Purified RNA sample was diluted 1:1 with master mix and reverse transcription reaction catalysed in thermocycler with the following steps: 25^{o}c for 10 minutes, 37^{o}c for 120 minutes, 85^{o}c for 5 minutes. cDNA concentration was measured using Nanodrop, with a minimum concentration of 1500ng/µl required for accurate analysis via Q-RT-PCR.

2.9.3 Quantification of RNA by Q-RT-PCR

The polymerase chain reaction (PCR) amplifies a specific nucleic acid sequence (amplicon) via the action of DNA polymerase, which is directed by sequence-specific primers to replicate the amplicon. In Q-RT-PCR, the amount of PCR product is quantified via the use of a fluorescent reporter of the polymerase reaction. Thermocyclic heating and cooling of samples induces denaturation of double stranded DNA (dsDNA), annealing of DNA with primers and subsequently binding by DNA polymerase. In this work two different fluorescent reporters were utilised.

2.9.3.1 SYBR Green Assay

SYBR Green is a fluorescent dye that binds to double-stranded DNA molecules and fluoresces at 521nm. In a SYBR Green Q-RT-PCR assay, the reaction mixture contains the DNA template, primers specific to the target sequence, and the SYBR Green dye. As DNA amplification progresses, the DNA polymerase generates double-stranded DNA products, and the SYBR Green dye binds to these products. The dye's fluorescence increases as more double-stranded DNA accumulates. Relative florescent units (RFU) is plotted against cycle number, generating a sigmoidal amplification curve as RFU increases exponentially before plateauing as reaction components are exhausted. The quantification cycle (Cq) denotes the number of cycles taken to reach a specific threshold. Thus, Cq is inversely correlated to the abundance of amplicon at the outset. SYBR Green assays were used in analysing relative gene expression in work presented in Chapter 3 and primers are shown in Table 2.5.

Samples were diluted 1:10 in Rnase free water added to reaction components in chilled clear 96 well optical reaction plates (Cat.No.) as follows: 5µl SYBR green, 1.25µl forward primer (8 µM), 1.25µl reverse primer (800 µM), 2.5µl sample cDNA. Negative controls of Rnase free water only and purified RNA from each sample (1:10 in Rnase free warer) were also prepared.

Alongside samples and negative controls, a serial dilution of cDNA (range 1:5 – 1:10000) was used to generate a calibration curve for each set of primers. Cq values of cDNA dilutions were plotted against $\log_{10}$dilution and an R^2 value of >0.98 considered sufficient for accurate interpretation of sample Cq values. Further evaluating assay optimisation, amplification efficiency I was calculated as:

$$E = 10^{\frac{-1}{m}}$$

Where m is the slope of the line. Expressed as a percentage ([E-1] x 100), this denotes the percentage increase in amplicon per cycle, and thus the efficiency of the polymerase reaction. Amplification efficiencies of 90-110% were deemed sufficient, along with standard deviation between replicates of <0.2. Cq values of samples were plotted against serial dilutions to calculate Log Starting Quantity and a power calculation (10^Log Starting Quantity) performed to ascertain Starting Quantity of cDNA in samples.

2.9.3.2 Taqman Assay

Taqman Assays use specific DNA probes 61abelled with a fluorescent dye at the 5' end and a quencher molecule at the 3' end. The probe is designed to anneal to a specific region within the target DNA sequence. During the qPCR reaction, as the DNA polymerase extends the DNA strand, it reaches the probe's binding site. The 5' to 3' exonuclease activity of the DNA polymerase cleaves the probe, separating the fluorescent dye from the quencher. This results in an increase in fluorescence intensity as the dye becomes unquenched. Taqman probes (Applied Biosystems, Cat. No. 444557) fluoresce at 517nm and fluorescence is measured, increasing with each cycle as the target sequence is progressively amplified. As in SYBR Green assays, Cq is the number of cycles required to meet a threshold of fluorescence and is inversely correlated with the number of copies of the amplicon present. Taqman Assays were used in Q-RT-PCR experiments presented in Chapters 3 and 4 and gene probes are given in tables 2.6 and 2.7.

Samples were diluted 1:10 in Rnase free water added to reaction components in chilled clear 96 well optical reaction plates as follows: 5µl Taqman Reagent, 0.5µl DNA probe, 2.5µl nuclease-free water, 2µl sample cDNA. Negative controls of Rnase free water only and purified RNA from each sample (1:10 in Rnase free warer) were also prepared.

Starting values were normalized to a reference gene, in this case 60S ribosomal protein L19 (RPL-19) or ribosomal RNA 18S to calculate normalised mRNA levels in sample cell populations:

$$Normalised\ mRNA = \frac{SQ\ Sample}{SQ\ RPL - 19}$$

For comparisons between monolayer and spheroid cell culture, fold change in 3D relative to 2D was calculated.

2.10 Materials and Methods Used in Chapter 3

2.10.1 Patient Samples Used in Chapter 3

Ovarian cancer patient samples used in this work were collected as part of the study “Identifying ovarian and blood biomarkers for ovarian pathologies” through Swansea Bay and Cwm Taf Morgannwg University Health Boards (SBUHB and CTMUHB). Ethical approval was granted from HRA NHS REC Wales 6 Research Ethics Committee (LREC15/WA/0065), and written, informed consent was obtained from each patient prior to enrolment into the study. Patient samples used in this study are detailed in Table 2.1.

Table 2.1 Patient Samples Used in Chapter 3. *HGSOC = high-grade serous ovarian carcinoma.*

Patient ID	Tissue Samples	Diagnosis
Patient A	Left Ovary	HGSOC Stage 3
	Omentum	
Patient B	Left ovary	HGSOC
	Omentum	
Patient C	Left ovary	Ovarian Mass
	Omentum	
Patient D	Omentum	Benign Mass
Patient E	Omentum	Benign Mass
Patient F	Omentum	Benign Mass
Patient G	Omentum	Ovarian Cancer
Patient H	Omentum	Ovarian Cancer
Patient I	Omentum	Ovarian Cancer
Patient J	Omentum	Ovarian Cancer
Patient K	Omentum	Ovarian Cancer

2.10.2 Omental Tissue-Conditioned Media

In order to study the effect of secreted factors from the diverse range of cells found in ovarian and omental samples, tissue-conditioned media was collected. Tissue was washed thoroughly in PBS and cut into approximately 10mm^3 pieces. In 12-well cell culture plates (surface area: 3.5cm^2), tissue pieces were bathed in 2ml primary ovarian media, prepared as follows. Powdered MCDB medium was added to 1l autoclaved water along with 13ml of sodium bicarbonate to maintain pH. This mixture was diluted 1:1 with Media 199 (also containing 13ml sodium bicarbonate per 500ml) to a total volume of 400ml and filtered. This solution was supplemented with 20% FBS and 1%

P/S. For cells and tissue used in quantitative assays, charcoal stripped FBS was used to ensure undefined and heterogeneous hormones, growth factors and cytokines were not affecting observations. Tissue was incubated in media for 24 hours at 37^{o}c and 5% CO^{2} in a humidified incubator, before media was collected and filtered through 22µm filters to remove any cells and tissue debris. Omental tissue conditioned media (OT-CM) samples were stored at -20^{o}c.

2.10.3 Primary Adipocyte Culture

In this work, mature adipocytes were isolated from the adipocyte fraction of omental tissue digests. Due to the presence of lipids, adipocytes are buoyant and therefore float in cell culture. While this is a barrier to generating adherent cell populations, it also allows for separation of adipocytes from other cellular components of adipose tissue. Following digestion of tissue (e.g. with collagenase), tissue digest can be centrifuged to separate out adipocytes from the non-bouyant population of cells termed the stromal vascular fraction (SVF), as seen in Figure 2.2. The SVF contains a heterogeneous population of fibroblasts, pre-adipocytes and other adipocyte-derived stem cells, immune cells, pericytes and vascular smooth muscle cells among others (223).

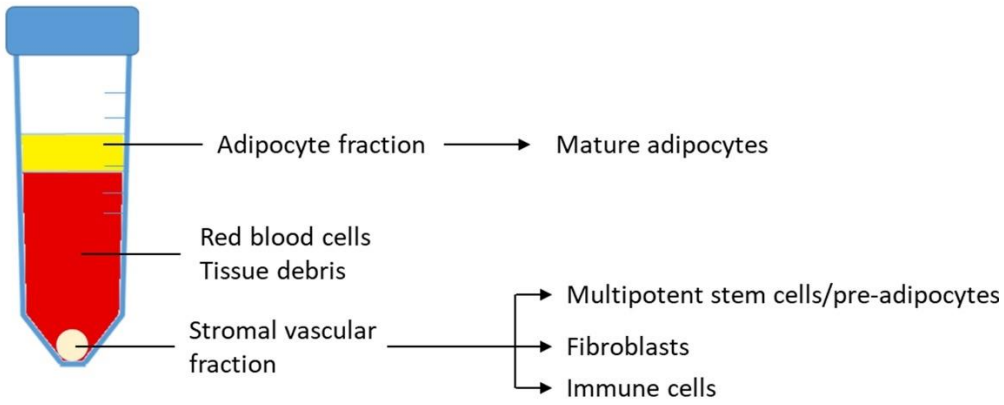

Figure 2.2 Fractionation of Adipose Tissue-Derived Cells. *Centrifugation of digested adipose tissue (e.g. omentum) produces fractions with distinct cellular populations. Adipocytes are buoyant due to high lipid content and will therefore float following mild centrifugation. A heterogeneous population of non-erythrocyte cellular components are collected in the pellet, termed the stromal vascular fraction.*

Omental tissue biopsies were obtained as per Section 2.10.2 and washed in PBS. Tissue was then cut into small pieces (~10mm^3) and digested in 15ml falcon tubes in 2mg/ml collagenase in primary ovarian media for 1-4 hours with agitation by vortexing every 15-30 minutes. Digests were then centrifuged for 1 minute at 170 × g and the adipocyte fraction was removed. The fraction was washed 1-3 times in PBS before incubation with erythrocyte lysis buffer (Table 2.2) for 15 minutes to remove any red blood cells from the sample. After each wash step, the sample was centrifuged for 1 minute at 170 × g and the adipocyte fraction collected from the top of the supernatant. Following erythrocyte lysis, the adipocyte fraction was re-suspended in adipocyte media comprising Dulbecco's Modified Eagle Medium: Nutrient Mixture F-12 (DMEM/F12) supplemented with 10% FBS, 1%P/S, 8µg/ml d-biotin, 0.5µg/ml insulin and 400ng/ml dexamethasone. T25 cell culture flasks and 24-well plates (1.9cm^2) were incubated with 100% FBS for 15 minutes before plating of adipocyte suspension to enhance cell adherence to culture plastic. To confirm the presence of mature adipocytes, cells were stained with Oil Red O and adiponectin activity confirmed via

enzyme-linked immunoassay (ELISA), detailed above, with comparison to omental stromal cell populations as negative control.

Table 2.2 Erythrocyte lysis buffer

Component	**10X Lysis Buffer**
Ammonium Chloride (NH_4Cl)	8.02g
Sodium Bicarbonate ($NaHCO_3$)	0.84g
EDTA	50ml
H_20	To 100ml

Primary adipocyte-conditioned media was generated by culturing primary adipocytes in serum-free media for 24 hours before collection and storage at -20^{o}c.

2.10.4 Treatment of Ovarian Cancer Cell Lines with Conditioned Media

In order to investigate the impact of omental and adipocyte secreted factors on ovarian cancer activity EOC cell lines SKOV-3, OVCAR-3 and CAOV-3 were treated for 72 hours with 50% conditioned media (CM) 50% serum-free media in spheroid and monolayer populations. Changes in viability were assessed via RealTime-Glo MT Cell Viability Assay, CellTiter-Glo 3D Cell Viability Assay and live/dead staining.

2.10.5 EMT Marker Characterization in Ovarian Cancer Cell Lines

The expression of markers of the Epithelial-to-Mesenchymal transition (EMT) were assessed in populations of EOC cell lines. Cells undergoing EMT go through a “cadherin switch”, whereby the expression of epithelial specific surface marker E-Cadherin is reduced and the expression of N-Cadherin, a marker for a post-EMT phenotype, is enhanced. EMT is also associated with increased expression of Vimentin. Expression of these markers was visualised via immunofluorescent microscopy. The expression of these markers, as well as the mesenchymal-specific marker vimentin, was also assessed through western blot analysis and quantitative real-time polymerase chain reaction (Q-RT-PCR), detailed above.

2.10.5.1 Immunofluorescent Confocal Microscopy

For 2D monolayer populations, cells were seeded in 8-well chambered microscope slides. At 60-80% confluency, cells were washed with PBS before being fixed and permeabilized in 4% paraformaldehyde (PFA) 0.1% Triton X-100 to allow antibody penetration. Cells were incubated with blocking buffer of PBS containing 0.1% Triton X-100 (PBST) and 3% BSA for 1 hour. Samples were incubated with antibodies for E-Cadherin, N-Cadherin and Vimentin as detailed in Table 2.4 for 2 hours prior to washing with PBST and incubation with fluorescent fluorophore-labelled anti-mouse (Alexa Fluor 488, Abcam, ab150117) and anti-rabbit (Alexa Fluor 555, Abcam, ab150086) secondary antibodies. Following further washing with PBS, cells were co-stained with DAPI and visualized using confocal microscopy as detailed in Section 2.5.2 using lasers at 405nm, 488nm, and 561nm.

For immunofluorescent analysis of tumour spheroids, immunostaining was carried out as described by Weiswald and colleagues (239). Cells were grown as spheroids via the hanging drop method for 72 hours before fixing in PBS containing 4% PFA 1% Triton for 3 hours at 4^{o}c. Following washing with PBS, spheroids were dehydrated and rehydrated via sequential incubation with 25%, 50%, 75% and 95% methanol for 30 minutes, before 5 hours in 100% methanol and reversal of the dehydration sequence to 0% methanol 100% PBS. Spheroids were blocked overnight at 4^{o}c in PBST containing 3% BSA, followed by incubation with primary and secondary antibodies as above. Prior to visualization, spheroids were co-stained with DAPI and transferred to microscope slides.

2.10.6 Transwell Invasion Assay

Transwell invasion assays use a gradient of chemoattractant across a porous membrane to assess a specific attractant's capacity to induce invasion of cell populations through the membrane. Here, the QCM ECMatrix Cell Invasion Assay (Millipore, Cat. No. ECM555) was used which uses synthetic matrix to simulate basement membrane. Conditioned media was generated from monocultures of OVCAR-3 and ADSC-derived adipocytes as well as from OVCAR-3 – adipocyte co-cultures and placed in the lower chamber. 1 x 10^3 OVCAR-3 cells were seeded in the upper chamber cultured for 24 hours. After 24 hours, cells were lysed and cellular nucleic acid activity quantified using CyQuant GR dye as an indirect indicator of the number of cells which had invaded to the bottom of the membrane. Additionally, a separate experiment included mature adipocytes in the bottom well and was performed as above. Matrix inserts were removed and washed with PBS prior to analysis to ensure adipocytes in the lower chamber did not impact results.

2.10.7 SKOV-3/Luc Cells in Co-Culture

In addition to transwell co-cultures outlined in Section 2.6, SKOV-3 cells stably expressing firefly luciferase gene and Puromycin resistance gene (SKOV-3/LUC, Cambridge Bioscience Ltd, Cat. No. AKR-232) were utilised in co-culture experiments to understand the impact of direct cell-cell contact on adipocyte-EOC interactions. SKOV-3/Luc cells were sub-cultured as per wildtype with the addition of 2mM L-glutamine and 1µg/ml Puromycin to ensure maintenance of the mutated phenotype. For co-culture, adipocyte spheroids were generated as follows: ADSCs were seeded into ULA plates at a concentration of 2 x 10^3 cells/well and differentiated for 14 days into mature adipocytes as outlined in Section 2.4. Following differentiation, 2 x 10^3 SKOV-3/LUC cells were added into wells containing mature adipocyte spheroids and co-cultured for 72 hours. To measure SKOV-3/Luc viability only, luciferase activity was measured using Pearson Firefly One-Step Glow Assay (Thermofisher, Catalogue No. 16197). Cells were equilibrated to room temperature and a 1:1 dilution of assay reagent was added to samples (to a total volume of 200µl). Samples were mixed by vigorous pipetting and also shaken at 300rpm for 3 minutes to ensure spheroids are disaggregated and assay reagent can access the whole cell population. Samples were incubated at room temperature for 10 minutes before reading of luminescence using BMG Fluostar Omega Microplate spectrophotometer.

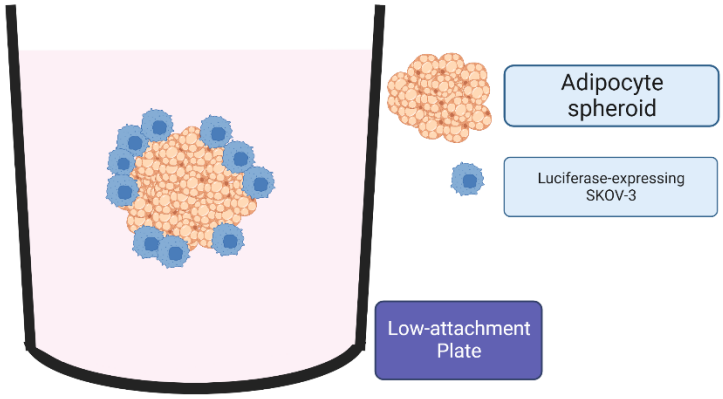

***Figure 2.3. Direct co-culture of adipocytes with SKOV-3/LUC cells**. ADSCs were seeded as spheroids and differentiated to mature adipocytes prior to the addition, in suspension, of SKOV-3/LUC cells.*

2.10.8 Paclitaxel Treatment of Ovarian Cancer Cell Lines

To understand the impact of omental and adipocyte secreted factors and signalling on EOC response to therapy, conditioned media-treated cells and cells in co-culture were treated with a range of concentrations of paclitaxel (PTX) (5nM, 50nM and 500nM). For conditioned media (CM), cells were treated with 50% CM for 72 hours as per Section 2.10.4. For co-culture experiments, co-cultures were allowed to progress for 24 hours prior to challenge with PTX for 72 hours to allow potential signalling pathways to be activated prior to the introduction of the drug. The impact of PTX on EOC cell lines was assessed via viability assays (Section 2.7).

2.10.9 Omentum-Derived Exosomes

2.10.9.1 Isolation of Exosomes from Tissue-Conditioned Media

Since their discovery in the 1980s, a number of techniques for isolating exosomes have been developed (240, 241). Sequential steps of ultracentrifugation can be performed to remove cells and other contaminants, while combination of ultracentrifugation with a sucrose density gradient can help to purify exosomes based on their density. However, high pressures generated ultracentrifugation can distort and damage exosome structure. Techniques such as ultrafiltration and size-exclusion chromatography can isolate and purify exosomes based on their size. A more highly selective approach is to capture exosomes with antibodies for exosome-specific proteins in order to select for a highly homogenous group of extracellular vesicles (EVs). However, exosomes display great diversity in their surface proteins and such techniques can therefore reduce yield omit groups of EVs.

In this work, Exosomes were isolated from 10ml OT-CM using qEV original column, according to manufacturer's instructions (Izon Science). Prior to sample loading, the OT-CM samples were concentrated using the Centriprep 10K filter device (Merck Millipore) according to manufacturer's instructions. This concentrated 10ml of OT-CM to a final volume of 500-600µl. After rinsing the column with PBS (0.02 µm filtered), 500µl of the concentrated OT-CM was added to the top of the qEV column. Subsequently, EV fractions of 500µl were collected. Purified exosomes were resuspended in 10ml primary ovarian media, while for exosome-concentrated treatments purified exosomes were resuspended in 5ml primary ovarian media. Exosome-depleted treatments were generated via ultracentrifugation. Particle size

distribution was measured by dynamic light scattering (DLS, Malvern Zetasizer nanoseries) and nanoparticle tracking analysis (NTA) (ZetaView PMX 110 V3.0, Particle Metrix, USA).

2.10.9.2 Characterization of Omental Exosomes

The size and polydispersity index (PDI, a measurement of the distribution of sizes of particle within the sample) were assessed using dynamic light scattering (DLS). 100 µl of purified exosome sample was aliquoted into disposable microcuvettes (Fisher Scientific, Cat. No. 10730445) for measurement, which was run at 25^{o}c. Material refractive index was set to 1.47 and measurements consisted of 10 individual runs.

Exosome-specific protein (CD9, CD63 and CD81) content in samples was analysed using ExoELISA-ULTRA assays (Systems Bioscience) as per supplier's instructions. Colorimetric ELISA measurements were normalized to particle number, as measured by nanoparticle tracking analysis.

2.10.9.3 Exosome Treatment of Ovarian Cancer Cell Lines

To understand whether exosomes were actively contributing to EOC cell growth, exosomes isolated from 10ml of OT-CM were resuspended in 10ml plain primary ovarian media, or 5ml for concentrated treatments. Cells were seeded at a concentration of 1 x 10^3 cells/well in 96 well plates and treated with omental exosomes for 72 hours. Treatments, including exosome depleted OT-CM were compared to

primary ovarian media as a negative control. Viability was measured via RealTime-Glo MT Assay.

2.10.10 Sequencing of Omental Exosome MicroRNAs

The miRNA sequencing of exosome content was carried out by Qiagen through a subcontracted service.

MicroRNA was isolated from 200µl purified exosome using miRNeasy Serum/Plasma Kit (QIAGEN, Cat. No. 217184) according to manufacturer's instructions with an elution volume of 14µl. Library preparation was performed using QIAseq miRNA Library Kit (QIAGEN, Cat. No. 331502). Briefly, a total of 5µl total RNA was converted into miRNA NGS libraries. After adapter ligation, UMIs were introduced in the reverse transcription step. The cDNA was amplified using PCR (22 cycles) and during the PCR indices were added. After PCR the samples were purified. Library preparation was quality controlled using capillary electrophoresis (Agilent DNA 1000 Chip). Based on quality of the inserts and the concentration measurements the libraries were pooled in equimolar ratios. The library pool(s) were quantified using qPCR. The library pool(s) were then sequenced on a NextSeq (Illumina Inc.) sequencing instrument according to the manufacturer instructions (1x75, 1x8). The raw read count data was received from Qiagen. The raw read count data was generated from mapping the short reads to miRBase version 22. Briefly, the reads are processed by trimming of the common sequence, (Unique Molecular Identifier UMI) and adapters, and filtering of reads with length < 15 nucleotides or length > 55 nucleotides. They are then deduplicated using their UMI. Reads are grouped into UMI groups when they start at the same position

based on the end of the read to which the UMI is ligated. Groups that contain only one read (singletons) are merged into non-singleton groups if the singleton's UMI can be converted to a UMI of a non-singleton group by introducing an SNP (the biggest group is chosen).

2.10.11 Transfection of Ovarian Cancer Cell Lines with MicroRNAs

Highly abundant miRNAs in OT-CM were identified from miRNA sequencing and iScript miRNA mimics were procured from Qiagen (Table 2.3) The molecular weight of these brief 22-nucleotide sequence mimics was assumed to be 7300 g/mol and a concentration of 5μM used to for cell treatments. OVCAR-3 cells were seeded at 1 x 103 cells/well and grown for 24 hours prior to transfection. Transfection was enabled using HiPerfect Transfection reagent (Qiagen Cat. No. 301704). A non-targeting siRNA cocktail (ON-TARGETplus non-targeting pool, Horizon Discovery, Cat. No. D-001810-10-05) was used as a negative control. Cells were transfected with and without the addition of 5nM PTX for 48 hours. Cell viability was measured via RealTime-Glo MT Assay.

Table 2.3 miRNA Mimics

miRNA	miRbase ID	Sequence	Product No.
Syn-has-let-7b-5p	MIMAT0000063	5'-UGAGGUAGUAGGUUGUGUGGU-3'	MSY00000063
Syn-has-miR-16-5p	MIMAT0000069	5'-UAGCAGCACGUAAAUAUUGGCG-3'	MSY00000069
Syn-has-miR-21-5p	MIMAT0000076	5'-UAGCUUAUCAGACUGAUGUUGA-3'	MSY00000076
Syn-has-miR-92a-5p	MIMAT0000092	5'-UAUUGCACUUGUCCCGGCCUGU-3'	MSY00000092

2.10.12 Antibodies Used in Chapter 3

Table 2.4 Antibodies Used in Chapter 3

Antibody Target	Type/Source	Optimised Concentration	Catalogue Number
N-Cadherin	Rabbit polyclonal	1:1000	ab1416, Abcam
E-Cadherin	Mouse monoclonal	1:1000	ab18203, Abcam
Vimentin	Mouse Monoclonal	1:1000	sc-373717, Santa Cruz Biotech
PPAR-γ	Rabbit polyclonal	1:500	ab45036, Abcam
Adiponectin	Rabbit monoclonal	1:500	11H4L4, Invitrogen
GAPDH	Mouse Monoclonal	1:1000	sc-47724, Santa Cruz Biotech
Anti-mouse IgG HRP-conjugated	Goat Polyclonal	1:1000	A28177, ThermoFisher
Anti-rabbit IgG HRP-conjugated	Goat Polyclonal	1:1000	A16110, ThermoFisher
Anti-mouse IgG Alexa Fluor 488-conjugated	Goat Polyclonal	1:500	ab150117, Abcam
Anti-rabbit IgG-Alexa Fluor 555-conjugated	Goat Polyclonal	1:500	ab150086, Abcam

2.10.13 Primers Used in Chapter 3

Table 2.5 Primers Used in Chapter 3

Target	Primer	Sequence	Ta (°c)
RPL19	Forward	CCTGTACGGTCCATTC	54.3
	Reverse	AATCCTCATTCTCCTCATCC	
N-Cadherin (*CDH2*)	Forward	CCATCATTGCCATCCTGCTC	60
	Reverse	GTTTGGCCTGGCGTTCTTTA	
E-Cadherin (*CDH1*)	Forward	ACAACAAGCCCGAATTCACC	60
	Reverse	ATCTTGGCTGAGGATGGTGT	
Vimentin (*VIM*)	Forward	GAGAACTTTGCCGTTGAAGC	60
	Reverse	TCCAGCAGCTTCCTGTAGGT	

2.11 Materials and Methods Used in Chapter 4

2.11.1 Inflammation of Adipocytes

ADSC-derived mature adipocytes were inflamed via exogenous treatment with TNFα (Peprotech, Cat. No. 300-01A) for 24 hours. The impact of a range of concentrations of TNFα (25ng/ml, 50ng/ml and 125ng/ml) on adipocytes was measured via expression of inflammatory cytokines interleukin-6 (*IL6*), CCL2 and interleukin-8 (IL-8, encoded by *CXCL8*). Gene probes used in the chapter are listed in Table 2.6. To ensure that TNFα was not having a cytotoxic effect, the impact of treatment on proliferation was also assessed via MTT assay (Section 2.7.2).

2.11.2 Lipolysis Assays

The impact of TNFα adipocyte inflammation on the rate of lipolysis was assessed. Cellular lipolysis has two major products: glycerol and free fatty acids (FFAs). As such, extracellular glycerol and FFA concentration was measured as a maker for cellular lipolysis. As above, mature adipocytes were cultured for 72 hours after treatment with 125ng/ml TNFα and supernatant media collected. Glycerol was measured using Lipolysis Colorimetric Assay Kit (Sigma-Aldrich, Cat. No. MAK211) in which a colorimetric product is produced via reaction with glycerol. A series of standards were produced and colorimetric reaction quantified via measuring absorbance at 570nm. Fatty acid release was quantified using Free Fatty Acid Quantitation Kit (Sigma-Aldrich, Cat. No. MAK044). Similarly, an enzymatic reaction with FFAs results in a colorimetric response and absorbance at 570nm is measured and plotted against palmitic acid standards.

2.11.3 Lipid Droplet Analysis

Lipolysis results in the breakdown of triacylglycerides stored in the form of large lipid droplets (LDs), organelles found abundantly in adipocytes where they form a prominent aspect of cellular morphology. The impact of inflammation on LDs in adipocytes was assessed using BODIPY staining. Mature adipocytes were treated for 72 hours with 125ng/ml TNFα prior to staining. Cells were washed with PBS and stained with 2μM BODIPY for 15 minutes at 37^{o}c while protected from light. Cells were then fixed with 4% PFA for 30 minutes at room temperature before further washing with PBS and co-staining with DAPI (1:1000) for 5 minutes. Cells were imaged using

A1 Nikon Confocal Imaging System with lasers at 402nm and 488nm. To capture the full three-dimensional shape of LDs Z-stack images were generated from >10 individual slices. Adipocytes grown in spheroid culture were also assessed as above, but a concentration of 5μM was used to ensure penetration into the spheroid.

Lipid droplet quantity was analysed using imageJ (Version 1.53). Image stacks were combined via max intensity Z projection and converted to grey scale. Threshold was adjusted until only LDs were visible and thresholds for counting were set for circularity (>0.5) and size (>20μm) to ensure only LDs were counted. The number of nuclei was also counted and used as a measure of cell number. LDs per cell was calculated as number LDs/number nuclei for >6 images/treatment.

2.11.4 Co-culture of Inflamed Adipocytes with Ovarian Cancer Cell Lines

Bi-directional effects of inflamed adipocyte-EOC cell signalling were investigated using a transwell co-culture system as described in Section 2.6. Mature adipocytes were generated on transwell inserts and inflamed with 125ng/ml TNFα for 24 hours prior to co-culture with EOC cell lines in 2D monolayer or 3D spheroid populations for 72 hours. Prior to co-culture, transwell inserts were thoroughly washed with PBS to ensure exogenous TNFα was not transferred to EOC cells. Two controls were used in all co-culture experiments: EOC cell only and EOC cells co-cultured with untreated adipocytes.

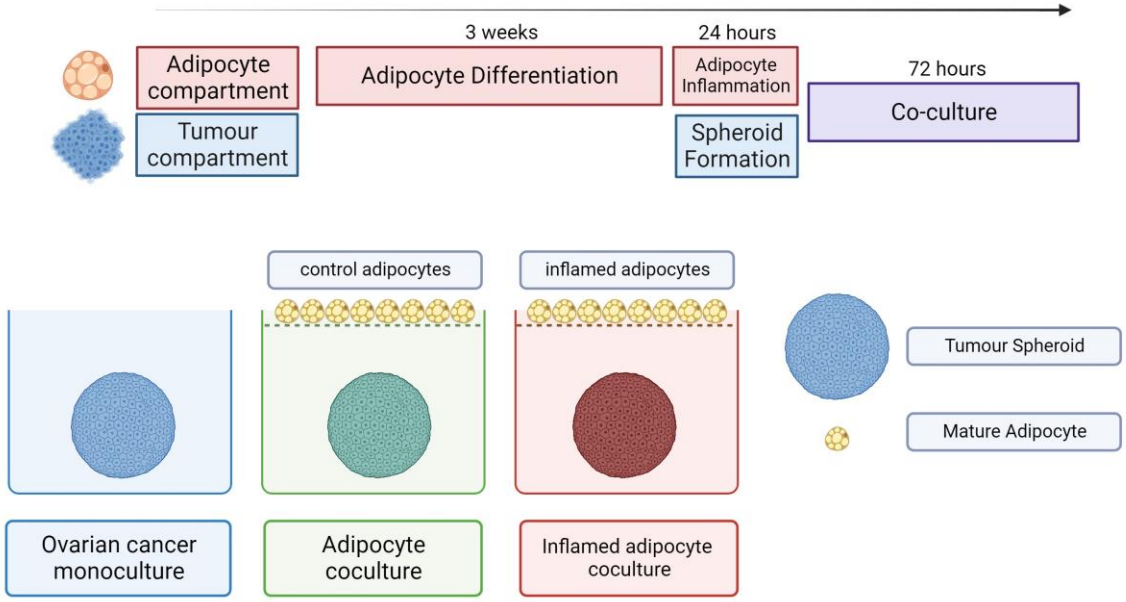

Figure 2.4 Co-Culture of Tumour Spheroids with Inflamed Adipocytes. *Adipocytes were generated from ADSCs on transwell inserts and inflamed for 24 hours with 125ng/ml TNFα before co-culture with ovarian cancer cell lines for 72 hours. 2 controls were used in all co-culture experiments: EOC cell lines in monoculture, and cell lines in co-culture with control (not inflamed) adipocytes.*

2.11.5 Fluorescent Fatty Acid Analog Transfer

The transfer of fluorescent fatty acids from adipocytes was visualised and quantified using BODIPY 500/510 C_1 C_{12} (4,4-Difluoro-5-(2-Thienyl)-4-Bora-3a,4a-Diaza-s-Indacene-3-Dodecanoic Acid), a fluorescent fatty acid analogue which incorporates the BODIPY fluorescent molecule into dodecanoic acid without affecting biological activity. As such, upon exogenous treatment it is incorporated into biological molecules for which free fatty acids are precursors, including di- and triacylglycerides as well as phospholipids. Adipocytes were treated with 5µM BODIPY 500/510 C_1 C_{12} for 4 hours and uptake of fluorescent fatty acid confirmed via confocal microscopy as detailed above. For fatty acid transfer analysis, adipocytes were inflamed with 125ng/ml TNFα for 24 hours before treatment with 5µM BODIPY 500/510 C_1 C_{12} for 4 hours followed by thorough washing with PBS before co-culture with SKOV-3 monolayer and

spheroids. Following 72 hours in co-culture Adipocytes in transwell inserts were removed and cancer cells fixed and stained as per Section 2.11.3 with the addition of a co-stain with 1.65 µM phalloidin 647 (Life Tech, Cat. No. A22287). Z-stack images were obtained and volume of fluorescence for each channel obtained using imageJ. BODIPY 500/510 C_1 C_{12} fluorescence relative to DAPI was calculated to take spheroid size into account when quantifying fluorescence.

2.11.6 Fluorescent Fatty Acid Analog Transfer Quantification via Flow Cytometry

Flow cytometry enables characterization and quantification of individual cells within a population. Briefly, flow cytometry involves the passage of cells through a fluidic system in single file, where they are illuminated by lasers. While flow cytometry can provide information on the size and granularity of cells within a population based on the scattering of light, here it was used only to quantify the number of BODIPY+ cells within SKOV-3 populations following co-culture. BODIPY 500/510 C_1 C_{12} fed co-cultures were established as above and after 72 hours SKOV-3 cells were detached (2D monolayer) or dissociated (3D spheroid) using 0.25% trypsin, 1mM Ethylenediaminetetraacetic acid (EDTA). For spheroid populations ≥48 spheroids were collected manually into a 15ml falcon tube using a pipette and incubated with PBS at 37oc for 10 minutes prior to the addition of 1ml trypsin to aid dissociation. The presence of BODIPY 500/510 C_1 C_{12} was detected using BD FACS Fortessa and laser at 488nm. Data analysis was carried out using FCS Express (Version 7) and SKOV-3 cells grown in monoculture were used as a negative control to establish a threshold for fluorescence.

2.11.7 Etomoxir Treatment of Ovarian Cancer Cell Lines

The metabolic drug etomoxir was used to block fatty acid (FA) metabolism in EOC cells to investigate the role of FAs in adipocyte-EOC interactions. Etomoxir is an irreversible inhibitor of carnitine palmitoyltransferase-1 (CPT1), which is a mitochondrial membrane-bound enzyme essential for fatty acid β oxidation. Etomoxir (MedChemExpress, Cat. No. HY-50202) was reconstituted in DMSO to a stock concentration of 10mM. Non-toxic concentrations of etomoxir were identified for SKOV-3, OVCAR-3 and CAOV-3 via titration with etomoxir between 0 - 200μM and the maximum non-toxic dose established. The maximal non-toxic dose was established as the highest dose with no significant impact on EOC cell viability, as assessed via MTT assay or CellTiter-Glo 3D Cell Viability Assay. EOC cells (monolayer and spheroid) in transwell co-culture were treated with maximal non-toxic dose of etomoxir for the duration of co-culture (72 hours) prior to end point viability assays.

2.11.8 Gene Probes Used in Chapter 4

Table 2.6 Gene Probes Used in Chapter 4

Gene Target	Catalogue Number	Assay ID
IL6	4331182	Hs00985636_m1
CXCL8	4331182	Hs00174103_m1
CCL2	4331182	Hs00234143_m1
ADIPOQ	4351370	Hs00605917_m1
LPL	4331182	Hs00173425_m1
FABP4	4351370	Hs01086177_m1
18S	4331182	Hs03003631_g1

2.12 Materials and Methods Used in Chapter 5

2.12.1 Luminex Assay

Luminex assays can be used to quantify the concentration of multiple analytes, such as signalling molecules, hormones and cytokines, in supernatant and as such were used to investigate changes in secreted molecules in co-cultures. Custom Luminex Assay (Human Luminex Discover Assay, R&D Systems) was purchased analyte specific antibodies for the following analytes: Adinponectin, CCL3, CCL5, CXCL10, IFN-γ, lL-1β, lL-2, IL-4, IL-7, IL-10, SPARC, CCL2, CCL4, CCL11, IFN-α, lL-1 α, lL-1RA, IL-3, IL-6, IL-8, IL-15, VEGF. Analyte-specific antibodies were pre-coated onto magnetic microparticles embedded with fluorophores at set ratios for each unique microparticle region on a 96-well plate. Media from transwell co-cultures, alongside analyte standards, were incubated with beads and analyte present in co-culture CM

was bound. After washing to remove any unbound analyte, a biotinylated antibody cocktail specific to the analytes of interest bound to fluorophores was introduced. Fluorescence, relative to the amount of analyte presence in the signal, was then read using Luminex LX 200 Multiplexing Assay System. The concentration of analyte in each sample was calculated based on standard curves generated from standards. For adipocyte and cancer cell only controls, cells were cultured in identical setting to those in co-culture but in the absence of other cell types.

2.12.2 Treatment of Ovarian Cancer Cells with Interleukin-6 and -8

A role for interleukin-6 (IL-6) and interleukin-8 (IL-8) in adipocyte-EOC interactions was investigated via upregulation with exogenous treatment of IL-6 and IL-8 and downregulation with anti-IL-6 receptor (IL6-R) antibody, anti-IL-8 antibody and IL-8 inhibitor reparixin. Recombinant IL-6 (Peprotech, Cat. No. 200-06) and IL-8 (Peprotech, Cat. No 200-08M) were resuspended in water before further dilution in water containing 0.1% BSA as a carrier to a final stock concentration of 20µg/ml. EOC cell lines were treated with a range of concentrations (0.4ng/ml – 100 ng/ml) for 24, 48 and 72 hours and the impact on cell proliferation (MTT and CellTiter-Glo 3D assay), STAT3 expression (Q-RT-PCR) and fatty acid uptake (fluorescent fatty acid analogue uptake) was assessed.

2.12.3 Patient Samples Used in Chapter 5

Cytokine levels in patient serum was assessed. Prior to analysis, patients were subdivided into two group: sensitive to platinum therapy and partially or wholly resistant based on clinical data. Patient biopsies were collected consecutively during interval debulking operations following three cycles of platinum therapy. Tumors were categorized as cisplatin sensitive, or cisplatin refractory on the basis of their response to a platinum-based therapy as assessed by a mid-course CT scan (computerized tomography) where tumors showing a poor, response following chemotherapy were classified as platinum-refractory and those responding well to therapy classified as platinum sensitive. In this context, patients that progressed on therapy had less than a partial response or recurred within 6 months were considered platinum-resistant, while patients who recur in 6 to 12 months as partially platinum-resistance and those who recur more than 12 months as fully platinum sensitive. 45 patients were enrolled in this study

2.12.4 Quantification of Cytokine Concentration in Patient Serum

Concentration of cytokines (L IL-6, IL-8, IL1B, IL-2, IL-4, IL-12p70, TNFα, IFNγ, IL-17A, IL10) in patient serum was assessed via ELISA as per . IL-2, IL-10, TNF, IL-4, IFNγ, IL-6 and IL17A were assessed using BD Cytometric Bead Array Human Th1/Th2/Th17 Kit (BD Biosciences, Cat. No. 560484) while IL-8, IL-1β, IL-6, IL-10 and IL-12p70 were assessed using BD Human Inflammatory Cytokine Cytometric Bead Array (BD Biosciences, Cat. No. 551811).

2.12.5 Cisplatin Treatment of Ovarian Cancer Cell Lines in Co-Culture

The impact of Transwell co-culture on EOC response to therapy was investigated through treatment of EOC cells with cisplatin. Initially, half maximal inhibitory concentration (IC_{50}), the dose of cisplatin required to kill 50% of EOC cells in culture, was established. SKOV-3, OVCAR-3 and CAOV-3 were grown in monolayer and spheroid culture and treated with a range of concentrations of cisplatin from 0 - 500μM for 72 hours. Change in viability relative to control was plotted against log_{10} cisplatin concentration. GraphPad Prism (Version 8.4.3) was used to calculate IC_{50} using a nonlinear, variable slope fit. Cells in co-culture were treated with cisplatin IC_{50} for 72 hours and cancer cell viability analysed via MTT assay (monolayer populations) or CellTiter-Glo 3D assay and live/dead staining (spheroid populations). The percentage survival was calculated by comparing viability of treatment groups following cisplatin treatment to the same group when untreated. The impact of SKOV-3 IC_{50} on adipocytes was also assessed in order to establish whether cytotoxic effect on adipocytes were impacting results.

2.12.6 Transfection of SKOV-3 Cells with STAT3 siRNA

A role for STAT3 in SKOV-3 response to cisplatin therapy was investigated through siRNA initiated knockdown of *STAT3* in SKOV-3 cells. Initially, the efficacy of STAT3 knockdown was established. SKOV-3 cells were seeded at a density of 2.8 x 10^4 cells/well in a 12 well plate and cultured for 24 hours prior to transfection. *STAT3* siRNA (QIAGEN GeneGlobe, Cat. No. SI01435287|S2|000|M0) was reconstituted to a concentration of 10μM in sterile nuclease-free water. *STAT3* siRNA was then mixed

1:1 with Lipofectamine RNAiMAX (Life Tech, Cat. No. 13778), diluted 1:20 in optiMEM media. Positively charged lipids in lipofectamine bind to negatively charged nucleic acids, forming lipid complexes (lipoplexes). This enables endocytosis into the cell and subsequent release of *STAT3* siRNA into the cell via endosomal escape. The formation of lipoplexes was achieved after 5 minutes incubation at room temperature. Cells were treated with a final concentration of STAT3 siRNA of 15nM. Downregulation of STAT3 expression was confirmed via Q-RT-PCR with probes for *STAT3*. For all experiments using STAT3 siRNA, non-specific RNA control at the same concentration was used as a negative control (Life Technologies, AM4636).

For STAT3 knockdown in co-culture, steps were taken to avoid *STAT3* knockdown in adipocytes and observe only the impact of knockdown in SKOV-3 cells. As such SKOV-3 cells were grown for 24 hours in monoculture before 3 hours treatment with STAT3 siRNA. Cells were then washed to ensure removal of reagents and co-culture progressed for 24 hours before re-treatment with STAT3 siRNA for 3 hours. This was repeated for 72 hours of co-culture.

2.12.7 Antibodies Used in Chapter 5

Table 2.7 Antibodies Used in Chapter 5

Antibody Target	Type/Source	Optimised Concentration	Catalogue Number
STAT3	Rabbit Monoclonal	1:1000	Ab68153, Abcam
Phospho-STAT3	Rabbit monoclonal	1:1000	Ab267373, Abcam
GAPDH	Rabbit monoclonal	1:1000	2118, Cell Signalling Tech
Anti-mouse IgG HRP-conjugated	Goat Polyclonal	1:1000	A28177, ThermoFisher
Anti-rabbit IgG HRP-conjugated	Goat Polyclonal	1:1000	A16110, ThermoFisher

2.12.8 Gene Probes Used in Chapter 5

Table 2.8 Gene Probes Used in Chapter 5

Gene Target	Catalogue Number	Assay ID
IL6	4331182	Hs00174131_m1
CXCL8	4331182	Hs00174103_m1
ADIPOQ	4351370	Hs00605917_m1
LPL	4331182	Hs00173425_m1
FABP4	4351370	Hs01086177_m1
STAT3	4331182	Mm01219775_m1
18S	4331182	Hs03003631_g1

2.13 Statistical Analysis

Statistical analysis and data visualisation were performed using GraphPad Prism Version 8.4.3. Generally, for experiments involving 2 treatment groups, statistical significance was tested using Student's t-test, while for experiments involving more than 2 treatment groups significance was tested using one-way ANOVA with Tukey's multiple comparisons test. Statistical significance was denoted using standard notation: *$p<0.05$, **$p<0.01$, ***$p<0.001$, and ****$p<0.0001$.

2.14 Technical and Biological Repeats in In Vitro Experiments

All in vitro experiments were performed using 3 technical replicates per plate (3 separate wells per treatment group). Replicates described in figure legends (i.e. N=3) refer to independent biological replicates performed at different times.

Chapter 3. Adipocyte-derived exosomes promote invasion and resistance to paclitaxel therapy in epithelial ovarian cancer

3.1 Introduction

Epithelial ovarian cancer (EOC) has the highest mortality rate of any gynaecological malignancy, with 5-year survival rates of less than 50% (4). This high mortality rate can be attributed to late presentation of metastatic disease, which can disseminate extensively within the peritoneal cavity before becoming symptomatic (8). A primary target of local metastasis is the omentum, an adipocyte-rich pad which covers the bowel and abdominal cavity and regulates aspects of peritoneal homeostasis including inflammation, angiogenesis, immune response and metabolism (136). The transformed omentum can therefore play an important role in generating a pro-metastatic tumour microenvironment within the peritoneal cavity (242). Furthermore, obesity is a risk factor for both incidence and prognosis of ovarian cancer (47, 50) and can lead to dysregulation and chronic inflammation of adipose tissue (45, 243).

As the basis of omentum tropism of ovarian cancer has been elucidated, the supply of energy and metabolic substrates from omental adipocytes has emerged as an important factor in the ovarian cancer metastatic niche (108). Previous work using adipocyte-ovarian cancer cell co-culture has demonstrated that reciprocal metabolic alterations in malignant and stromal components can enhance proliferation, migration and invasion of tumour cells (107, 143, 144, 146). Adipocytes are induced to favour lipolysis and the release of fatty acids, which are transferred directly to neighbouring ovarian cancer cells. Conversely, ovarian cancer cells undergo an AMP-activated protein kinase (AMPK) mediated switch from lipolysis to fatty acid β-oxidation, indicating omental adipocytes act as an important energy source for ovarian

metastases (108). Inhibition of key metabolic regulators of this process, including the fatty acid receptor CD36, fatty acid binding protein 4 (FABP4) and the AMPK-activated protein kinase salt-inducible kinase 2 (SIK2), can significantly reduce ovarian cancer metastases in mice (143, 144, 146, 244). The pro-tumorigenic effect of cancer-associated adipocytes, which provide energy and metabolites in the form of fatty acids, lactate and amino acids, has been demonstrated in a number of other malignancies including colorectal, breast and prostate cancer (45, 179, 245, 246).

Alongside late disease presentation, poor patient survival-rates can often be attributed to the high rates of development of ovarian cancer resistance to platinum- and taxane-based chemotherapy. Interactions in the omental metastatic niche can play an important role in the development of chemoresistance (45). Adipocytes and omental-derived stromal cells can enhance chemoresistance in ovarian cancer (189, 247, 248) and targeting adipocyte-derived signalling via *FABP4* knockdown can sensitize ovarian tumour cells to platinum-based therapy (144). While the mechanisms behind adipocyte-induced chemoresistance in ovarian cancer remain unclear, evidence from a variety of carcinomas suggests a role for cancer cell “stemness”, which enables cells to undergo drastic phenotypic changes such as the epithelial-mesenchymal-transition (EMT), and therefore evade treatment. Adipocyte-derived fatty acids can induce EMT in hepatocellular carcinoma and breast cancer (246, 249), while stemness in ovarian cancer cells has been linked to fatty acid metabolism (167).

Establishment of the omental metastatic niche involves complex bidirectional signalling between cancer cells and diverse omental stroma. A role for adipocyte-secreted interleukin-6 (IL-6) and interleukin-8 (IL-8) in the migration and invasion of ovarian cancer cells to omental tissue has been established in vitro (107). However, a more comprehensive understanding of signalling mechanisms acting across the

peritoneum is required to understand ovarian cancer omentum tropism, the activation of cancer-associated stroma and the development of chemoresistance. Extracellular vesicles (EVs), particularly exosomes, 30-150nm vesicles secreted by a diverse range of cells, have been implicated in signalling at a distance in the generation of metastatic microenvironments in a number of malignancies (120). Exosomes carry a cargo of bioactive molecules including proteins, lipids, metabolites, RNA and DNA, and therefore have the capacity to alter cellular activity at sites distant from their cell of origin. In ovarian cancer, tumour-derived exosomes carrying MMP1 mRNA can induce destruction of peritoneal mesothelial cells in mouse via apoptotic cell death, suggesting a role for exosomes in peritoneal dissemination (128), while exosomes derived from cancer-associated adipocytes and fibroblasts can induce chemoresistance through the transfer of microRNA-21 (250). Exosomes, therefore, represent a mechanism for bidirectional modification of a tumour and its microenvironment through the exchange of a range of bioactive molecules.

3.2 Hypotheses and Aims

As noted above, omentum tropism in metastatic ovarian cancer is widely reported. Therefore, it is suggested that omental adipocytes may generate a pro-tumour microenvironment prior to the development of metastatic disease. As such this chapter tests the following hypotheses:

1. Omentum-secreted factors have a significant impact on EOC proliferation, invasion and response to therapy regardless of disease state.

2. Omental adipocytes are the primary drivers of pro-tumorigenic activity in omental tissue.
3. Omental exosomes play a significant role in omentum-derived signalling in the development of ovarian cancer.

In order to test these hypotheses, the aims of the chapter were as follows:

1. Use three-dimensional (3D), spheroid-based in vitro models to explore the impact of omentum-secreted factors on EOC activity.
2. Use 3D co-culture models to explore cancer-adipose interactions.
3. Isolate adipose-derived exosomes and explore their impact on EOC activity.
4. Elucidate potential downstream signalling pathways acting in cancer-adipose interactions.

3.3 Materials and Methods

Materials and methods used in this chapter are descried in detail in Section 2.10. Briefly, omentum and adipocyte secreted factors were collected from primary patient omental tissue and omentum-derived adipocytes and their impact on EOC cell line (OVCAR-3 and SKOV-3) proliferation explored. The impact of adipocytes on EOC proliferation and response to paclitaxel (PTX) therapy was further explored using co-culture models. Transwell co-cultures incorporated adipose-derived stem cell-derived adipocytes and EOC spheroids, while direct spheroid co-culture of mature adipocytes and luciferase expressing SKOV-3 cells were also established. Expression of cell surface makers associated with the epithelial-to-mesenchymal transition were characterized to understand their response to therapy. Exosomes were explored as a

mechanism of adipose-derived signalling through exogenous treatment of EOC cell lines with primary omentum-derived exosomes. Omental exosome-derived microRNAs (miRNAs) were sequenced and the impact of transfection of EOC cell lines with highly abundant miRNAs on EOC response to paclitaxel therapy was explored.

3.4 Results

3.4.1 Omentum-secreted factors promote ovarian cancer proliferation

Metastasizing ovarian cancer has been shown to home to the omentum, and this organ is commonly invaded (107). Initially, therefore, the effect of omentum-secreted factors on ovarian cancer cell lines was explored. Omental tissue was collected from two patients undergoing surgery whose diagnoses were high-grade serous ovarian carcinoma (HGSOC) and a benign ovarian mass (Table 3.1). Tissue was used to generate omental tissue-conditioned media (OT-CM) containing tissue secretome. Adipocyte activity in these tissues was confirmed by adiponectin ELISA and was detected in OT-CM but not media conditioned by ovary tissue (Table. 3.1).

Table 3.1 Adiponectin Concentration in Patient Samples

Patient	**Diagnosis**	**Sample**	**Adiponectin conc. (ng/ml)**
A	HGSOC stage 3	Omental stromal cell culture	n.d
		Primary adipocyte Cell culture	15.2
B	HGSOC	Ovarian Tissue	n.d
		Omental Tissue	29.07
C	Ovarian Mass	Ovarian Tissue	n.d
		Omental Tissue	45.74

Ovarian cancer cell lines (SKOV-3, OVCAR-3) were treated with 50% OT-CM in two-dimensional (2D) monolayer and three-dimensional (3D) spheroid culture (Fig. 3.1). A significant increase in proliferation was observed in both cell lines in 2D monolayer cultures upon culture with OT-CM after 96 hours. However, striking differences in the response of two epithelial ovarian cancer (EOC) cell lines was observed in spheroid cultures. Viability was significantly increased in SKOV-3 spheroids by treatment with OT-CM from 48 hours onwards but was significantly reduced in OVCAR-3 spheroids relative to unconditioned media (UCM) control after 72 hours. Notably, similar results were obtained regardless of whether the omental sample originated from a malignant or benign ovarian mass (Fig. 3.1).

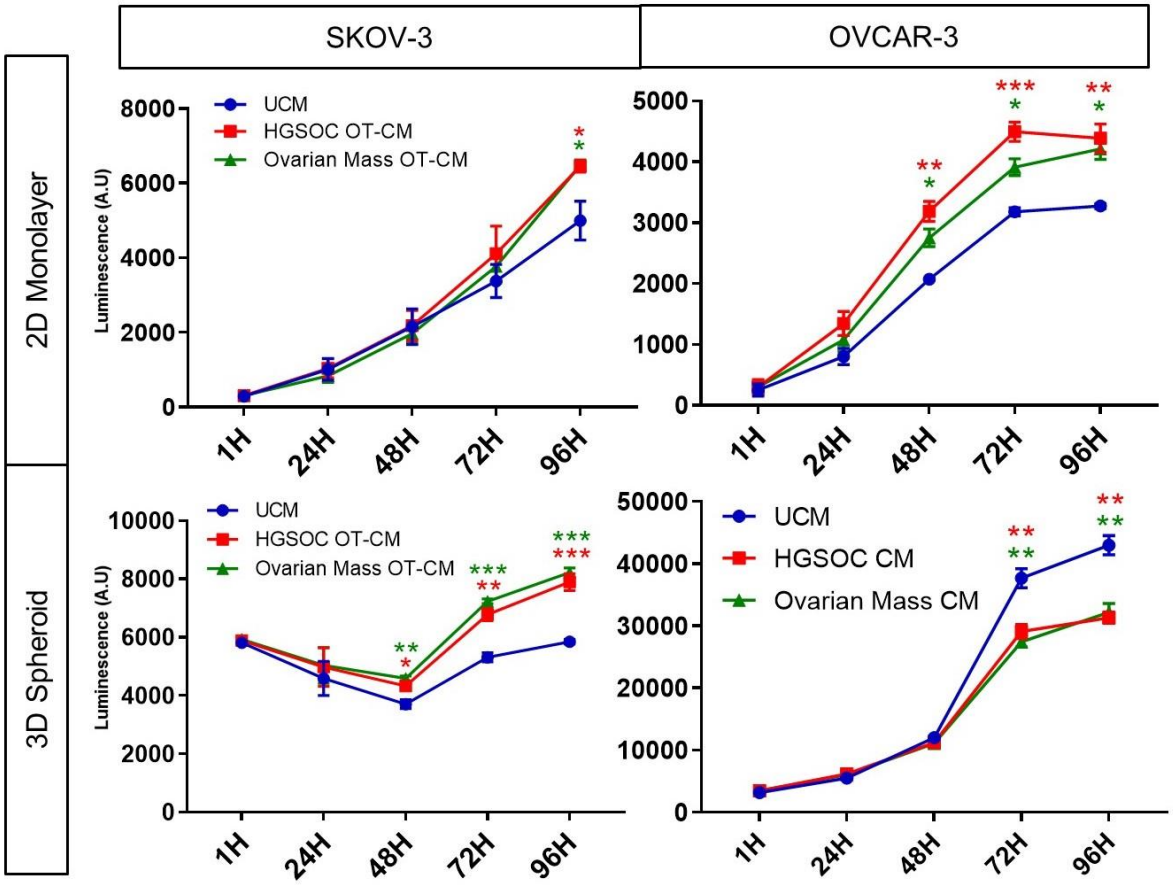

Figure 3.1 Impact of Omentum Secreted Factors on EOC Cell Line Proliferation. *Ovarian cancer cell lines (SKOV-3 and OVCAR-3) grown as 2D monolayer or 3D spheroid were treated with unconditioned media (control), or media conditioned by patient omentum samples and cell viability was measured by Realtime-Glo and 3D Glo cell viability assays respectively. Bar blots show mean +SD, n ≥3, *p<0.05, **p<0.001, ***p<0.0001, ****p<0.00001 (One-way ANOVA with Tukey's multiple comparisons test)*

To confirm the contribution of omental adipocytes to observed changes in ovarian cancer cell viability, mature adipocytes were isolated from omental tissue (Table 3.1, Patient A) and the effect of adipocyte-secreted factors assessed. The presence of mature adipocytes in culture was confirmed by Oil Red staining (Figure 3.2a) and ELISA (Table 3.1), with non-adipocyte omental stromal cells as negative control (Figure 1D), and adipocyte-conditioned media was collected. The effect of primary adipocyte-conditioned media on viability of EOC spheroids was assessed by fluorescent staining of conditioned media-treated cell populations with Calcein-AM and Ethidium Homodimer-1 (EthD1) to identify live and dead cells respectively (Figure 3.2b). As seen in omental tissue CM-treated SKOV-3 spheroids, adipocyte-conditioned media was found to significantly increase SKOV-3 viability ($p<0.001$P, while population viability decreased in OVCAR-3 spheroids ($p<0.0001$), as quantified by the ratio of Calcein-AM+:Ethd1+ cells (Figure 3.2c). OVCAR-3 spheroids treated with primary adipocyte CM also formed less effectively, with a notably less rounded morphology (Figure 3.2b).

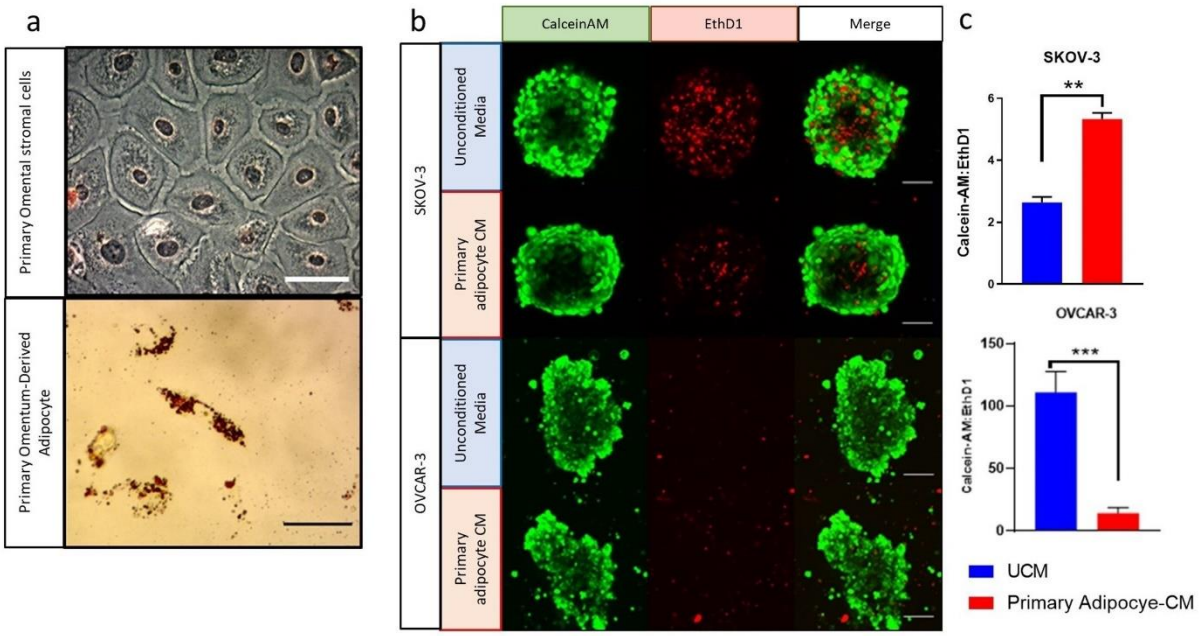

Figure 3.2 Impact of Adipocyte Secreted Factors on EOC Cell Line Proliferation. *Tumour spheroids generated from EOC cell lines were treated with media conditioned by primary adipocytes (a) derived from patient omentum samples and incubated with viability stains (b). Ratio of CalceinAM (live cells) to Ethidium homodimer (dead cells) was calculated as a measure of population viability (c). Bar blots show mean +SD, n=3, *p<0.05, **p<0.001, ***p<0.0001 (Student's t-test). Scale bar = 20 μm for a and 100μm for b.*

3.4.2 Co-culture of Adipocytes and EOC Cell Lines

To explore the effect of bidirectional signalling with adipocytes on ovarian cancer cell proliferation, ovarian cancer cell lines were co-cultured with mature adipocytes derived from adipose-derived stem cells (ADSCs) as described in Section 2.4. Differentiation of adipocytes from stem cells took place over 14 days and was confirmed by the expression of adipocyte specific markers PPAR-γ and Adiponectin, as assessed via immunoblotting (Figure 3.3a), and via BODIPY lipid staining (Figure 3.3b). Expression of PPAR-γ increased over the course of differentiation, while expression of adiponectin

was apparent after 10 days. Large lipid droplets were apparent at cell surface of mature adipocytes following BODIPY staining.

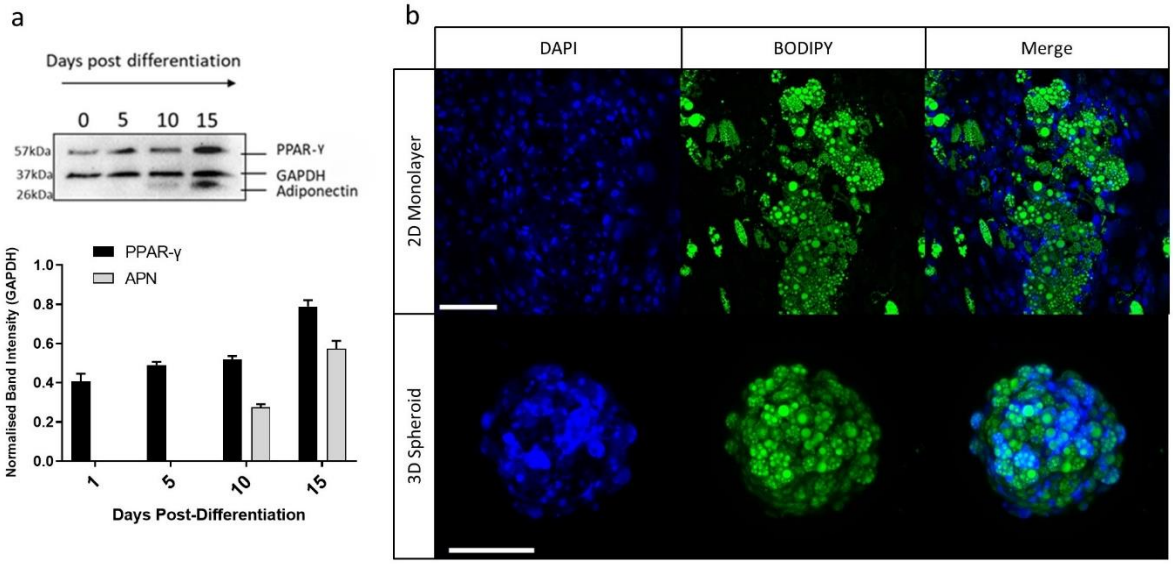

Figure 3.3 Differentiation of Adipose-Derived Stem Cells*. Differentiation of ADSCs into mature adipocytes was confirmed by immunoblotting (a) and confocal microscopy following BODIPY staining (b). a shows representative blot and quantified normalised band intensity. Scale bar = 100μm*

Transwell co-cultures were established incorporating mature adipocytes derived from ADSCs seeded onto transwell inserts alongside SKOV-3 and OVCAR-3 spheroids (Figure 2.1). Spheroid viability after 72 hours of co-culture was assessed via Celltiter-Glo 3D viability assay (Figure 3.4a). Again, SKOV-3 and OVCAR-3 cell lines demonstrated striking differences in their response to adipocyte co-culture, with significant increase ($*p<0.05$) and decrease ($p<0.001$) in population viability respectively. As ADSC-derived adipocytes constitute a heterogenous population of cells including partially differentiated or undifferentiated stem cells, the effect of undifferentiated ADSC populations on EOC growth was assessed (Figure 3.4b). Undifferentiated ADSCs were found to have no impact on EOC spheroid viability.

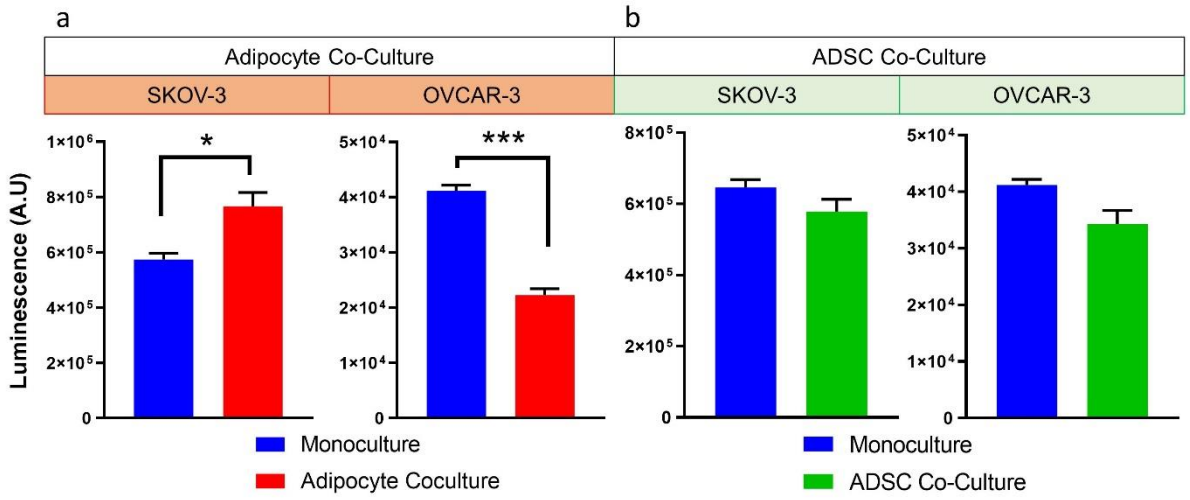

Figure 3.4 Transwell Co-Culture of Adipocytes and EOC Spheroids. *Following 72 hours in co-culture with mature adipocytes (a) and undifferentiated ADSCs (b), population viability of spheroids was measured via Celltiter-Glo 3D viability assay. Bar plots show mean + SD, n≥3. Significance assessed via Student's t-test*

An alternative co-culture system was established to assess the impact of direct contact with adipocytes on EOC growth (Fig. 2.3). Here, spheroids comprising ADSC-derived mature adipocytes were established and SKOV-3 cells stably expressing luciferase (SKOV-3/LUC) were added directly in co-culture as described in Section 2.10.7. Initially, to ensure only luciferase activity from SKOV-3/LUC cells was read by the assay, the signal from SKOV-3/LUC cells upon the addition of luciferase substrate was compared with SKOV-3 cells without luciferase expression, as well as undifferentiated ADSCs and mature adipocytes (Figure 3.5a). To ensure the readout from the luciferase assay was an accurate indicator of spheroid population viability, luminescence from SKOV-3/LUC cells treated with luciferase substrate was compared with luminescence produced by Celltiter Glo 3D viability assay for spheroids seeded at different quantities of cells/well (Figure 3.5b). Signal was only apparent in SKOV-3/LUC cells and for spheroids with cells 2 x 10^3 – 8 x 10^3 cells/spheroid relative luminescence (relative to 1 x 10^3 cells/spheroid) were comparable. For spheroids with

16 x 10^3 cells/spheroid there was a difference in relative viability between luciferase assay and Celltiter Glo 3D, however no spheroids this large were used in this work. Discrepancies between tests in larger spheroids were probably due to incomplete disassociation of the spheroid. Upon spheroid co-culture with adipocytes, luciferase activity increased by more than four-fold relative to cells grown in monoculture, indicating a striking increase in proliferation ($p<0.00001$) ((Figure 3.5c). To ensure the presence of other cells in co-culture alone was not sufficient to impact SKOV-3/LUC activity, cancer cells were also co-cultured alongside undifferentiated ADSCs, and a similar increase in luciferase activity was observed ($p<0.00001$) (Figure 35.c)

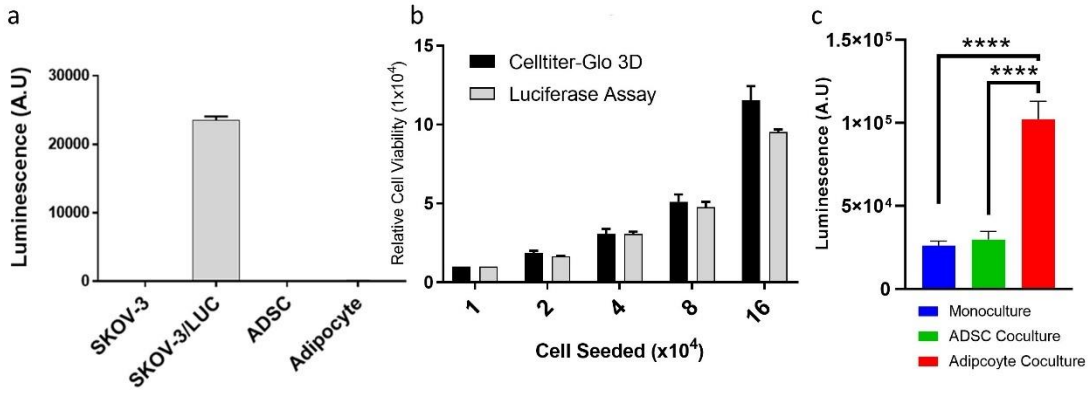

Figure 3.5 Direct 3D Co-Culture of Adipocytes with SKOV-3/LUC. *Luciferase activity (Pierce Firefly One-Step Luc Glow Assay) in SKOV-3/LUC spheroid culture was compared to SKOV-3 without luciferase gene as well as undifferentiated ADSCs and ADSC-derived adipocytes (a). Luciferase activity in spheroids generated from serial dilution of SKOV-3/LUC cells was compared with CellTiter-Glo Luminescent Cell Viability Assay to ensure luciferase activity corresponded to SKOV-3/LUC cell number. (b). The impact of direct coculture with adipocytes on SKOV-3/LUC cells was assessed via Pierce Firefly One-Step Luc Glow Assay (c).Bar blots show mean +SD, n≥3, *p<0.05, **p<0.001, ***p<0.0001, ****p<0.00001 (One-way ANOVA with Tukey's multiple comparisons test)*

3.4.3 EMT Marker Expression in EOC Cell Lines

Given the observed differences in the response of two epithelial ovarian cancer (EOC) cell lines (SKOV-3 and OVCAR-3) to adipocyte signalling and co-culture, we explored potential sources of a differential response. The epithelial-to-mesenchymal transition (EMT) plays an important role in ovarian cancer metastasis and can have profound impacts on tumour cell behaviour. To further explore a potential role of EMT in observed differences between cell lines, the expression of mesenchymal cell surface markers N-Cadherin and Vimentin, along with the epithelial marker E-Cadherin, in EOC cell lines was profiled.

The expression of N-Cadherin, E-Cadherin and Vimentin in 2D and 3D EOC cell populations was assessed via immunoblotting (Figure 3.6a), quantified through normalisation to GAPDH (Figure 3.6b). N-Cadherin expression was high in SKOV-3 populations compared to OVCAR3 populations, where N-cadherin expression was not apparent ($p<0.05$) (Figure 3.6b). E-Cadherin was detected in OVCAR-3 in 2D monolayer and spheroid populations at significantly higher levels than SKOV-3 ($p<0.05$). Vimentin was only detected in SKOV-3 populations ($p<0.05$).

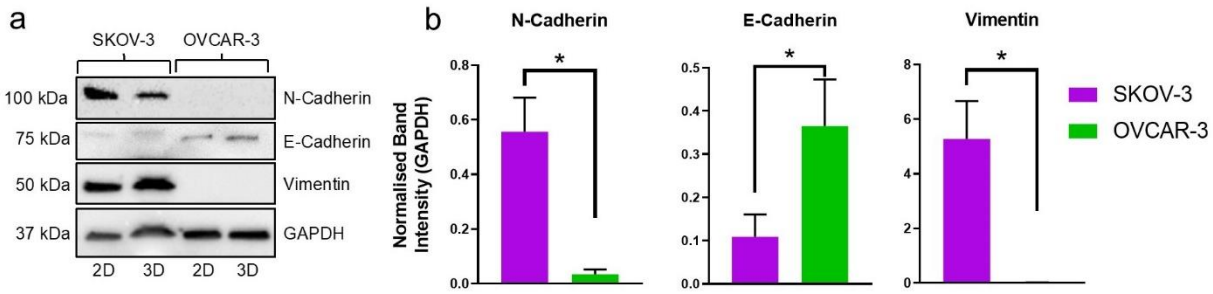

Figure 3.6 EMT Marker Characterization of EOC Populations by Immunoblotting. *Representative blot for expression of EMT markers N-Cadherin, E-Cadherin and Vimentin in SKOV-3 and OVCAR-3 cell lines (a) and quantification of band intensity for 2D populations (b). Bar blots show mean +SD, n=3, *p<0.05 (Student's t-test)*

Similarly, immunofluorescent staining of SKOV-3 and OVCAR-3 in monolayer populations showed N-Cadherin^{+} E-Cadherin^{-} Vimentin^{+} phenotype for SKOV-3, and N-Cadherin^{+} E-Cadherin^{-} Vimentin^{+} phenotype for OVCAR-3 (Figure 3.7).

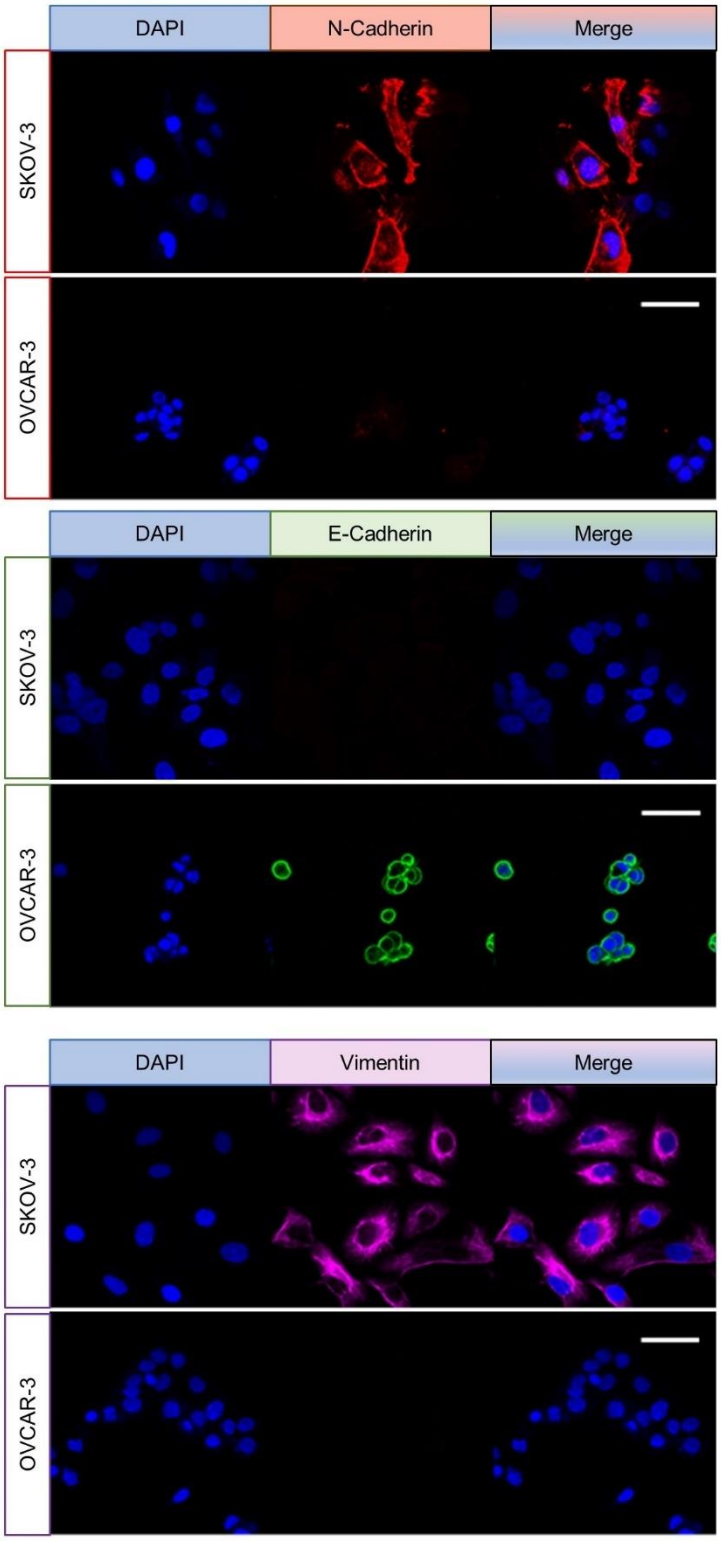

Figure 3.7 EMT Marker Characterization of EOC Populations by Immunofluorescent microscopy. SKOV-3 and OVCAR-3 cells in monolayer culture were stained for expression of EMT markers N-Cadherin, E-Cadherin and Vimentin by immunofluorescent staining and images with confocal microscope at 40 x magnification *Representative images, n≥3. Scale bar = 50μm*

As significant differences in the response of OVCAR-3 to OT-CM and adipocyte co-culture had been observed between cells grown in monolayer and spheroid populations, the expression of EMT markers in these different culture settings was assessed by Q-RT-PCR (Figure 3.8). SKOV-3 expression of N-Cadherin and Vimentin significantly decreased in 3D culture ($p<0.0001$, $p<0.00001$ respectively), while E-Cadherin expression significantly increased ($p<0.0001$). N-Cadherin and Vimentin expression increased in OVCAR-3 spheroids relative to 2D monolayer populations ($p<0.0001$). Figure 3.8 displays a logarithmic scale, therefore suggesting a 100 fold increase in N-Cadherin expression. These changes in EMT marker expression in spheroid culture indicate changes in phenotype across the population and may indicate a switch to a more hybrid expression profile across different regions of the spheroid.

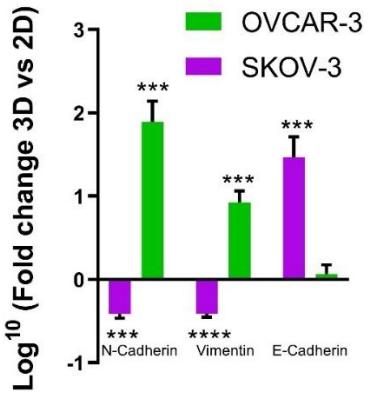

Figure 3.8 EMT Marker Characterization of EOC Populations by Q-RT-PCR. *Bar plots display log 10 fold change relative to 2D, significance indicates significant differences in 3D populations compared to 2D. n=3, ***p<0.0001, ****p<0.00001 (Student's t-test).*

The presence of more hybrid expression of EMT markers in 3D populations was demonstrated through immunofluorescent staining of SKOV-3 and OVCAR-3

multicellular aggregates (Figure 3.9). Contrary to expression visualised in 2D (Figure 3.7), both cell lines displayed expression of all EMT markers in spheroid culture.

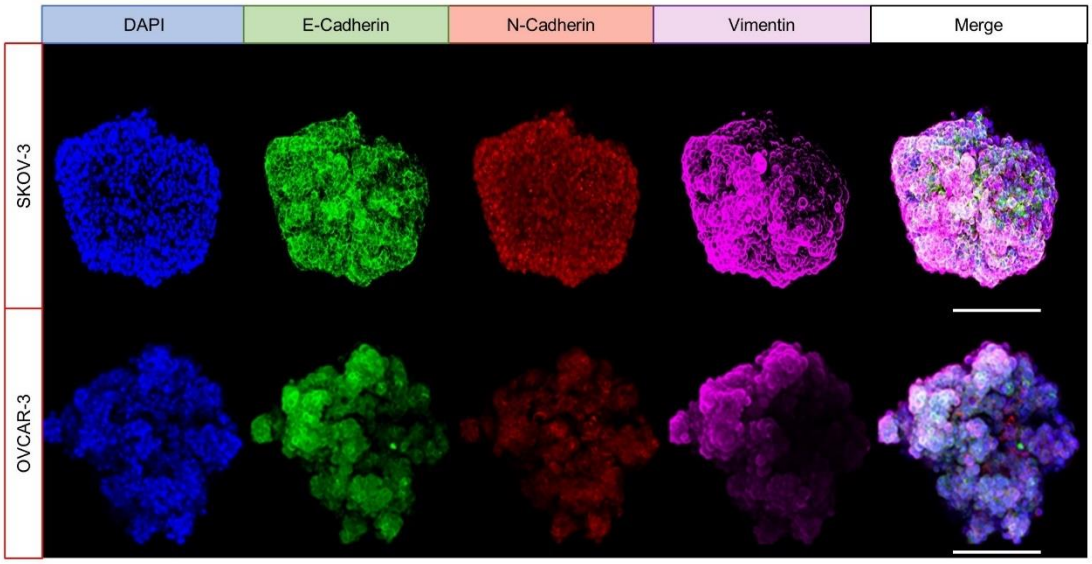

Figure 3.9 EMT Marker Characterization of EOC Spheroids by Immunofluorescent Microscopy. *Representative images, n≥3. Scale bar = 100μm*

3.4.4 Impact of Adipocyte Co-Culture on EMT Marker Expression in OVCAR-3

Given the observed difference in EMT marker expression in 2D monolayer and 3D spheroid populations, it was hypothesized that increased plasticity and phenotypic heterogeneity expression in OVCAR-3 aggregates may enable adipocyte-induced EMT, thus explaining differences in response to OT-CM observed between 2D and 3D OVCAR-3 populations (Figure 3.1). We explored the impact of adipocyte co-culture on the EMT marker expression in OVCAR-3 spheroids (Figure 3.10). Transwell adipocyte co-culture drastically increased the expression of vimentin in OVCAR-3 spheroids (Figure 3.10a), indicating a switch to a post-EMT, invasive phenotype. The change in vimentin expression was only apparent in OVCAR-3 spheroids, and not seen in monolayer or SKOV-3 populations (Figure 3.10b,c).

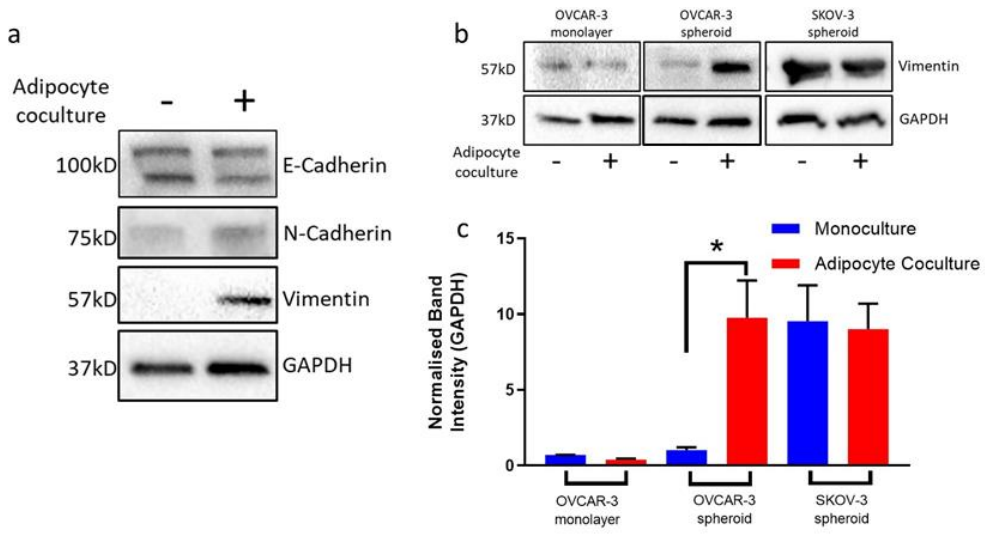

Figure 3.10 Impact of Transwell Adipocyte Co-Culture on EMT marker expression. *Impact of adipocyte co-culture on EMT marker expression in OVCAR-3 spheroids is displayed in a (representative blot). Changes in vimentin expression in OVCAR-3 spheroids in co-culture compared to OVCAR-3 in monolayer and SKOV-3 spheroids are shown in representative blots (a) and quantified (b Bar blots show mean +SD, n=3, *p<0.05 (Student's t-test).*

Increased vimentin expression indicated a switch to a post-EMT, invasive phenotype. To further investigate this switch, the impact of co-culture on OVCAR-3 invasiveness was investigated. Conditioned media (CM) from OVCAR-3 – adipocyte co-culture was collected and its effect on OVCAR-3 invasiveness, relative to CM from OVCAR-3 and adipocyte monocultures, was assessed via transwell invasion assay (Figure 3.11a). Co-culture CM significantly increased invasiveness relative to adipocyte CM ($p<0.05$), indicating that bi-directional signalling between the two cell compartments results in the release of pro-invasion signalling factors. Furthermore, the presence of mature adipocytes in the lower chamber of the Transwell invasion assay also increased OVCAR-3 invasiveness ($p<0.05$) (Figure 3.11b), further indicating that adipocyte signalling can act to increase the capacity for OVCAR-3 to migrate and invade through basement membrane.

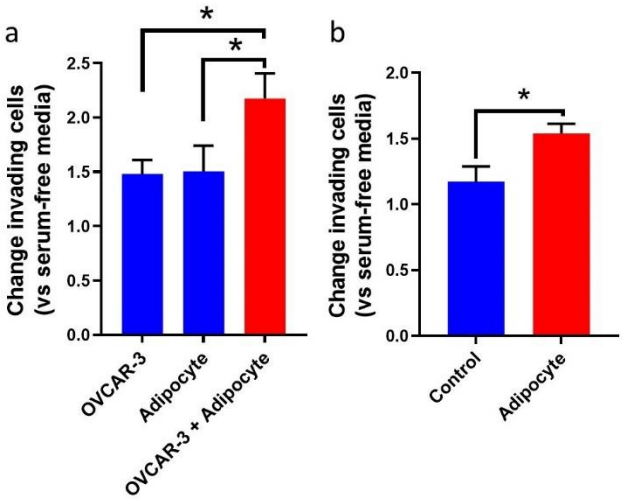

Figure 3.11 Impact of Transwell Adipocyte Co-Culture on OVCAR-3 Invasiveness. *The impact of conditioned media (CM) from co-culture on OVCAR-3 invasiveness, relative to OVCAR-3 or adipocyte monoculture CM was assessed (a) as well as the impact of adipocytes in the lower chamber (b). Bar blots show mean +SD, n=3, *p<0.05, **p<0.001, ***p<0.0001, ****p<0.00001 (One-way ANOVA with Tukey's multiple comparisons test)*

.

3.4.5 Transwell Co-culture Reduces EOC Response to Paclitaxel Therapy

A major problem facing ovarian cancer patients in the clinic is the common development of resistance to therapy. Furthermore, EMT has been shown to play an important role in the response of tumour cells to therapy in a number of cancers, including ovarian cancer. As such, a role for adipocytes in EOC response to paclitaxel (PTX) therapy was explored. SKOV-3 spheroids were treated with primary adipocyte CM and 50nM PTX and viability was assessed via live/dead staining (Figure 3.12). SKOV-3 spheroids treated with primary adipocyte CM displayed a significantly higher ratio of CalceinAM: Ethidium Homodimer ($p<0.05$), indicating a chemoprotective effect for primary adipocyte-secreted factors.

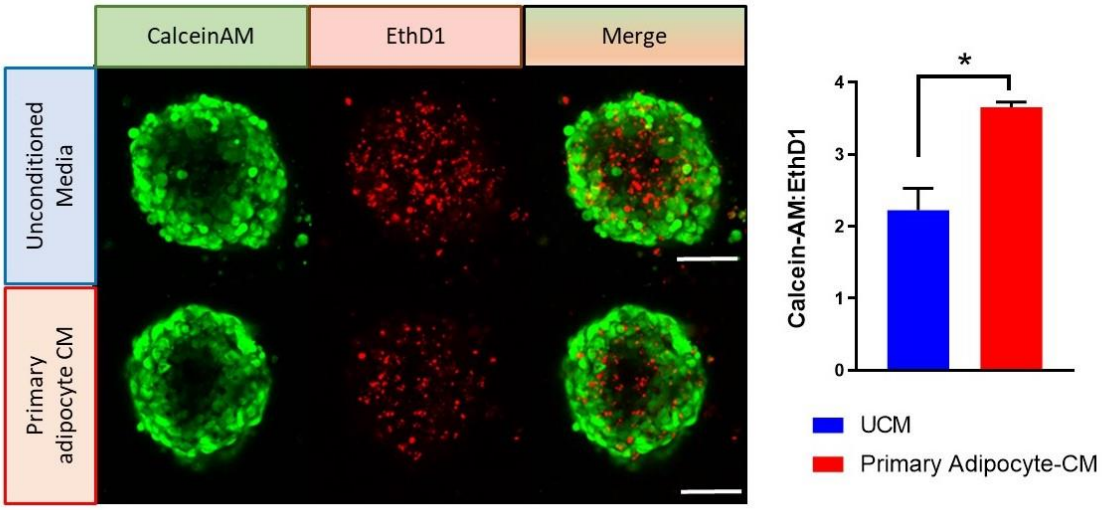

Figure 3.12 Response to Paclitaxel Therapy in Primary Adipocyte CM-Treated SKOV-3 spheroids
*Representative images at 20 x magnification and quantification of the ratio of CalceinAM to Ethidium Homodimer (EthD1). Bar blots show mean +SD, n≥5, *p<0.05 (Student's t-test)*

The impact of adipocyte co-culture on EOC cell line response to therapy was investigated in a Transwell model. Following 24 hours of co-culture, EOC spheroids were treated with a range of concentrations of PTX (5nM, 50nM, 500nM) (Figure 3.13). Response to therapy was calculated as % survival compared to untreated spheroids. At all concentrations, with the exception of 5nM treatment in SKOV-3 where no cytotoxic effect was observed, response to PTX therapy was significantly reduced by adipocyte co-culture.

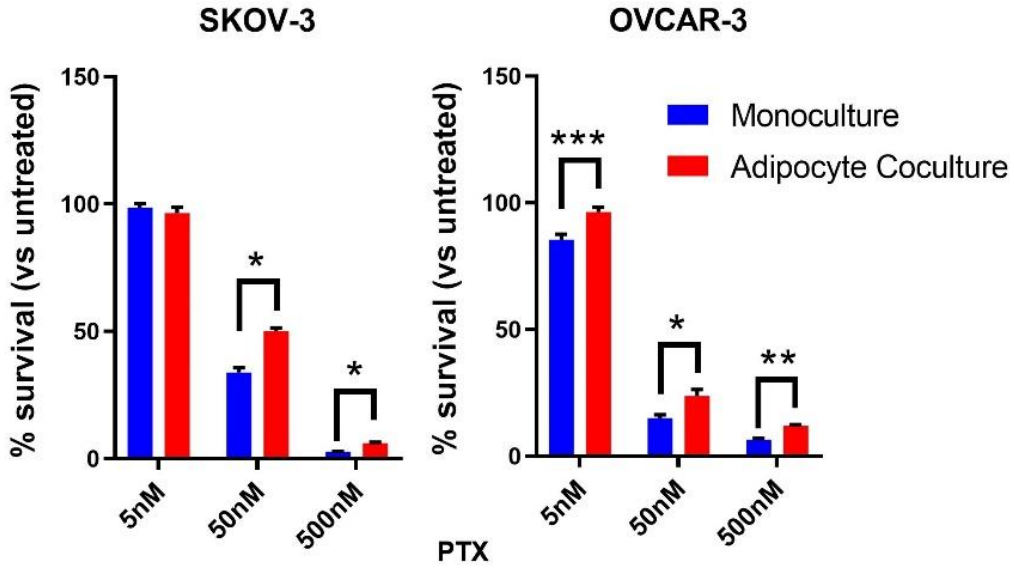

Figure 3.13 EOC Response to Paclitaxel Therapy in Transwell Co-Culture *% survival was calculated relative to untreated spheroids under the same culture conditions. Bar blots show mean +SD, n=5, *p<0.05, **p<0.001, ***p<0.0001, (One-way ANOVA with Tukey's multiple comparisons test)*

The impact of adipocyte co-culture on SKOV-3/LUC response to therapy was also investigated in a direct co-culture model (Figure 3.14). As above, SKOV-3/LUC cells were also co-cultured with undifferentiated ADSCs to ensure any effect observed was not the result of the presence of another cell type alone. Adipocytes exhibited a statistically significant chemoprotective effect when compared to SKOV-3/LUC spheroids in monoculture and in co-culture with ADSCs (Figure 3.14; $p \leq 0.05$).

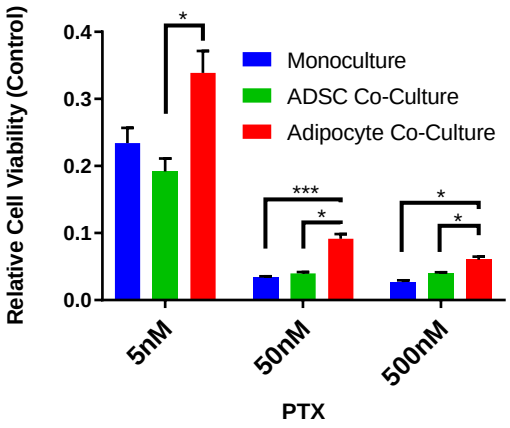

Figure 3.14 SKOV-3/LUC Response to Paclitaxel Therapy in Direct Co-Culture *Relative cell viability was calculated relative to untreated controls. .Bar blots show mean +SD, n=5, *p<0.05, ***p<0.0001 (One-way ANOVA with Tukey's multiple comparisons test)*

3.4.6 The Role of Omental Exosomes in EOC Development

Exosomes have been implicated in tumour-stroma interactions in several malignancies, including ovarian cancer (120). A role for exosomes in omental tissue-induced ovarian cancer cell proliferation was therefore tested. Exosomes were extracted from OT-CM from patients with HGSOC and benign ovarian mass (Table 3.1) using qEV original columns, while OT-CM was exosome depleted by ultracentrifugation. These omental exosomes were characterized based on their size distribution as well as the presence of exosome-specific protein markers. Exosome size was analysed by dynamic light scattering (DLS) which demonstrated a characteristic peak at ~80nm (Figure 3.15) while in exosome depleted samples this peak was absent.

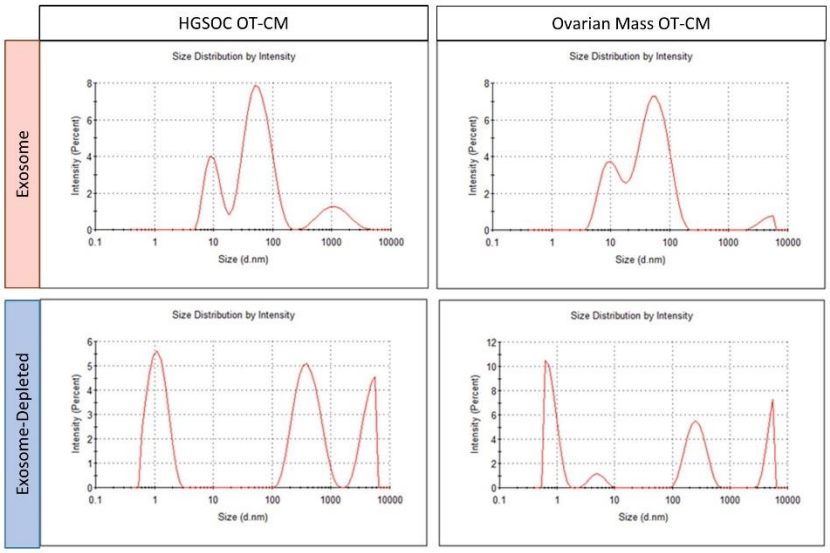

Figure 3.15 Size Distribution of Omental exosomes.

The presence of exosome-specific markers (CD63, CD9, CD81) was confirmed by ExoELISA-ULTRA assays and protein levels normalized to particle number (Figure 3.16). Exosome specific markers were present in extracellular vesicles isolated from patient samples, again indicating the presence of exosomes in samples.

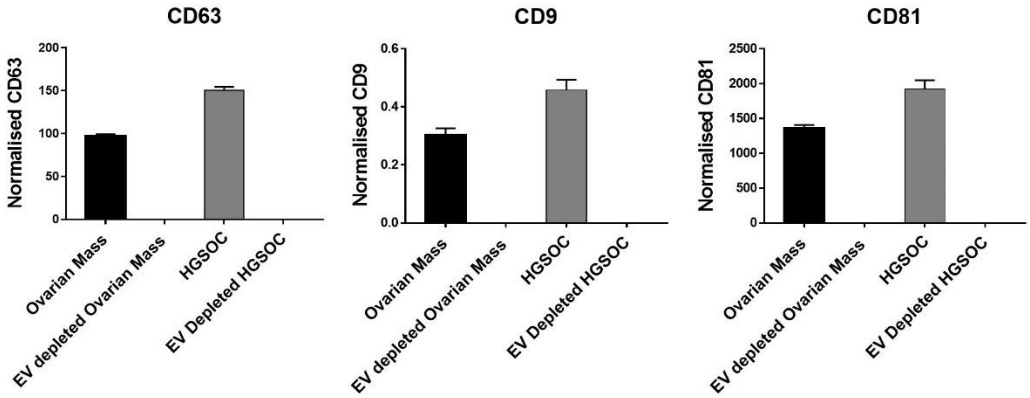

Figure 3.16 Expression of Exosome-Specific Markers in Omental Exosomes . *Exosome-specific markers CD63, CD9 and CD81 were present in extracellular vesicles isolated from OT-CM. Bar blots show mean +SD, n=3.*

OT-CM had been demonstrated to have a pro-proliferative effect on OVCAR-3 cells (Figure 3.1). To test whether exosomes played an important role as omental secreted factors, exosomes isolated from OT-CM were resuspended in an equal amount of media from that which they had been extracted. The impact of omental exosomes on OVCAR-3 proliferation was assessed by exogenous treatment of OVCAR-3 cells for 72 hours with omental exosomes and exosome depleted samples which were compared to OT-CM and plain media (Figure 3.17). Exosome treated samples displayed significantly increased proliferation relative to plain media for both patient samples (**p<0.001), in line with increases induced by OT-CM. Exosome depletion of OT-CM samples significantly reversed pro-cancer effects (**p<0.001). Taken together these data indicate a significant role for exosomes in observed pro-proliferative effects of omentum-secreted factors.

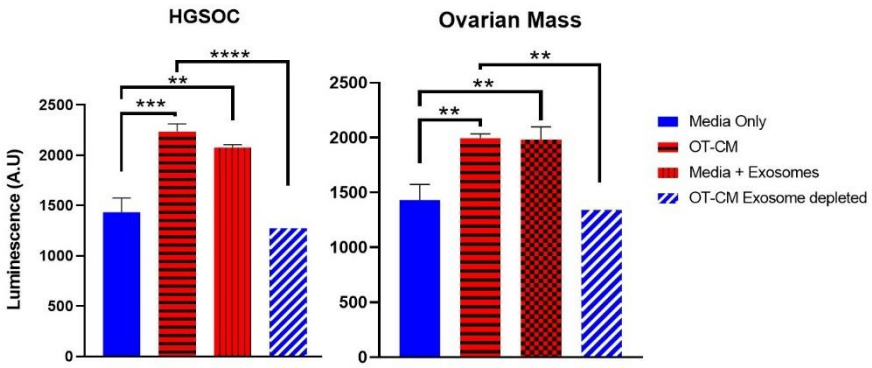

Figure 3.17 Impact of Omental Exosomes on OVCAR-3 proliferation. *OVCAR-3 cells were treated with omental exosomes and changes in cell proliferation compared to plain media, OT-CM and exosome-depleted treatment. Bar blots show mean +SD, n=3, *p<0.05, **p<0.001, ***p<0.0001, ****p<0.00001 (One-way ANOVA with Tukey's multiple comparisons test)*

A role for omental exosomes in OVCAR-3 response to therapy was also investigated. OVCAR-3 spheroids were treated with omental exosomes as above with and without 50nM PTX for 72 hours. Percentage survival was calculated relative to untreated cells. Compared to plain media control, exosome treated spheroids were significantly protected from PTX treatment ($p<0.05$) (Figure 3.18)

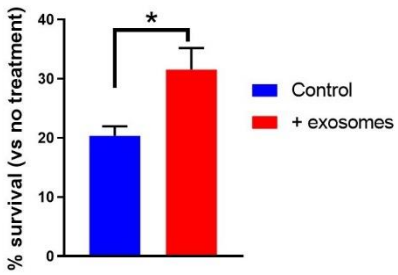

Figure 3.18 Impact of Omental Exosomes on OVCAR-3 Response to Therapy. *OVCAR-3 cells were treated with omental exosomes with and without 50nM PTX and cell viability at 72 hours compared with plain media control. % survival relative to untreated cells was calculated. Bar blots show mean +SD, n=3, *p<0.05 (Student's t-test).*

A role for adipocytes in the invasive capacity of OVCAR-3 cells had been demonstrated (Figures 3.10, 3.11), therefore the role of omental exosomes in this mechanism was also explored. Omental exosomes were used as a chemoattractant in a Transwell invasion assay and the impact on invasion compared to OT-CM and exosome depleted samples assessed, with serum free media used as negative control (Figure 3.19a). Exosomes displayed a similar impact on OVCAR-3 invasion as that seen in OT-CM and significantly higher than exosome-depleted OT-CM (Figure 3.19a, $p\leq0.05$). Changes in EMT marker expression, indicative of a switch to a more invasive phenotype, were assessed by immunoblotting. OVCAR-3 spheroids were treated with omental exosomes and EMT marker expression compared to OVCAR-3 spheroids

grown in plain media. Expression of N-Cadherin was significantly increased (p≤0.001) while E-Cadherin was significantly decreased (p≤0.01), indicating a switch to a post-EMT, invasive phenotype (Figure 3.19b,c). No change was observed in the expression of vimentin, indicating different molecular pathways may be activated by omental exosomes than those apparent in OVCAR-3 – adipocyte co-cultures.

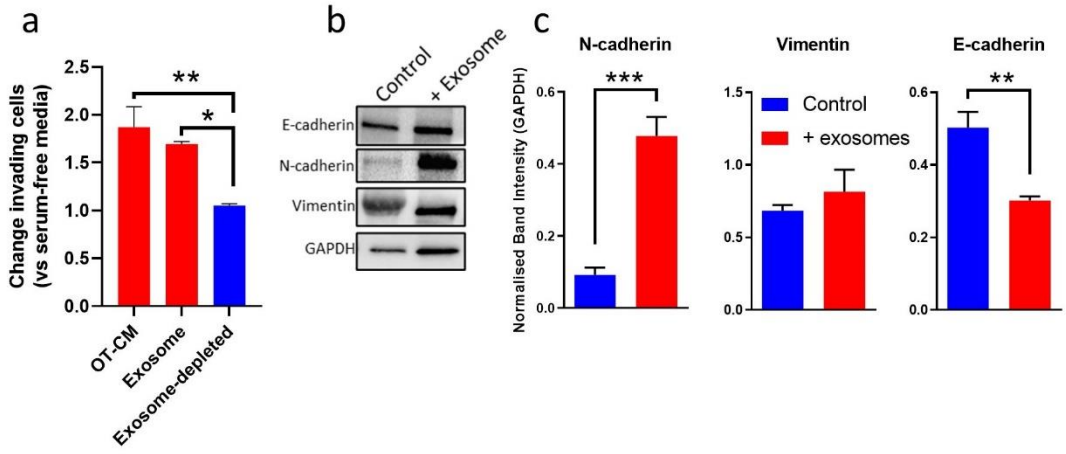

Figure 3.19 Impact of Omental Exosomes on OVCAR-3 Invasion. *The impact of omental exosomes on OVCAR-3 invasion was observed in Transwell invasion assay (a) and number of invaded cells calculated relative to serum-free media controls. The impact of omental exosomes on EMT markers was assessed by immunoblotting, (b) displays representative blot, quantified relative to GAPDH (c). Bar blots show mean +SD, n=3, *p<0.05, **p<0.001, ***p<0.0001 (One-way ANOVA with Tukey's multiple comparisons test)*

3.4.7 Omental Exosome miRNAs in EOC Development

Exosome-derived microRNAs (miRNAs) have been shown to play a substantial role in exosome signalling at a distance in various cancers, including EOC (251). As a pro-cancer effect had been demonstrated by omental secreted factors regardless of the presence of malignancy (Figure 3.1), exosomes were isolated from OT-CM of patients with both benign ovarian neoplasms and malignant tumours (Table 3.1). miRNA next

generation sequencing revealed 30 miRNAs highly abundant in exosomes derived from omental tissues (Fig. 3.20a). Pathway analysis of target genes using KEGG 2021 HUMAN (Figure 3.20b) and DisGeNET (3.20c) revealed top pathways including cancer and EOC-related regulation, as well as prolactin signalling pathways.

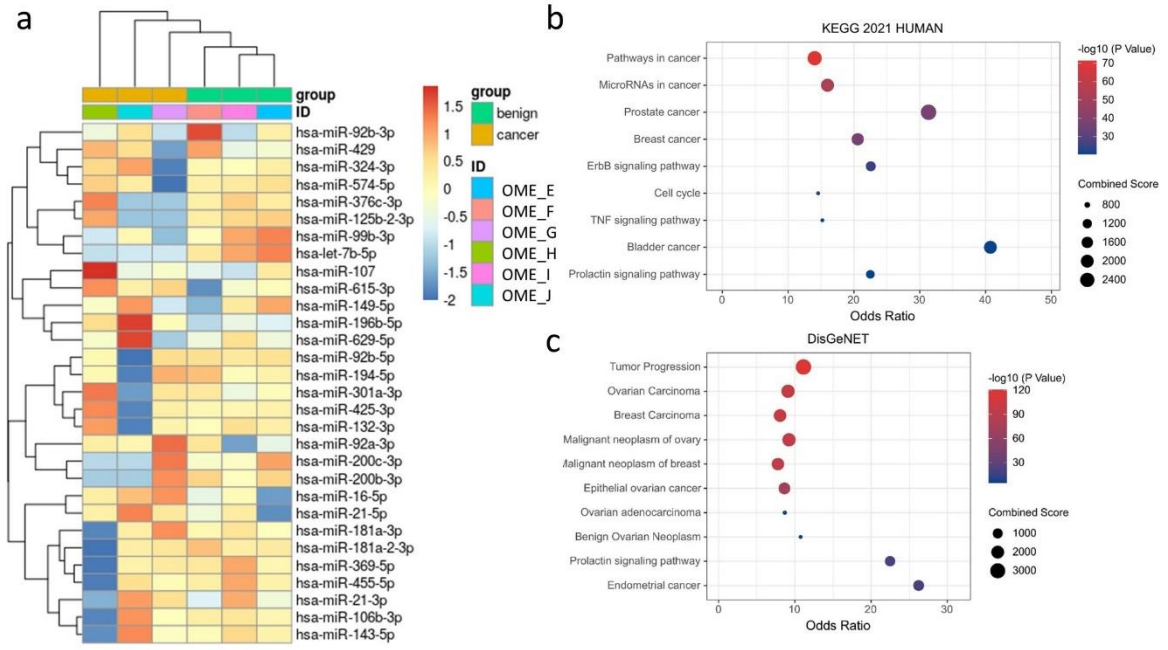

Figure 3.20 miRNA Sequencing of Omental Exosomes *miRNA sequencing of microRNAs isolated from omental exosomes. miRNAs abundant in benign and malignant were identified (a) and pathway analysis performed with KEGG 2021 HUMAN (b) and DisGeNET (c)*

To validate the significance of exosomal miRNAs in EOC progression and decreased response to PTX treatment, 4 miRNAs abundant in exosomes isolated from the omental secretome (let-7b, miR-16, miR-21, miR-92a) were selected and transfected into OVCAR-3 cells. Transfected cells were grown for 72 hours with and without 50nM PTX. With the exception of miR-16, exosomal miRNAs significantly increased proliferation in OVCAR-3 cells (Figure 3.21a; p≤0.001) while all miRNAs protected EOC cells from PTX treatment (Figure 3.21b) (p≤0.001).

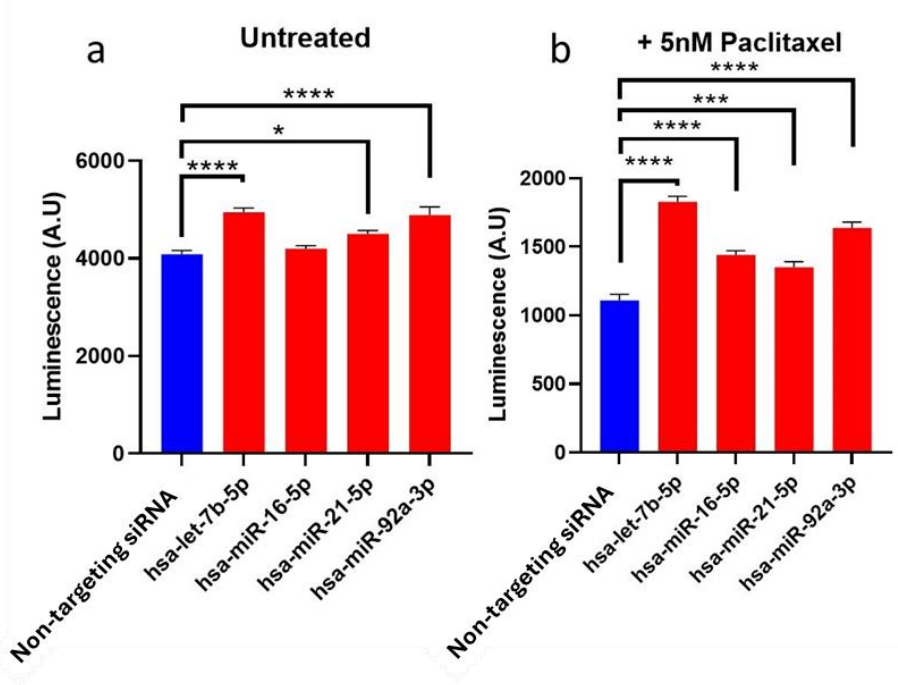

Figure 3.21 Transfection of Exosome miRNAs in OVCAR-3 *miRNAs abundant in omental exosomes were transfected into OVCAR-3 cells, which were grown without treatment (a) and with 50nM PTX (b) for 72 hours. Bar blots show mean +SD, n=3, *p<0.05, **p<0.001, ***p<0.0001, ****p<0.00001 (One-way ANOVA with Tukey's multiple comparisons test)*

3.5 Discussion

Epithelial ovarian cancer (EOC) metastasis is a complex, multistep process involving shedding of cells from the primary tumour, intra-peritoneal dissemination, and attachment and invasion at a secondary site within the peritoneal cavity (8). Previous work has demonstrated omentum tropism in ovarian cancer cells in a mouse model (107), while omentum-derived adipocytes and adipose stem cells can regulate gene expression in EOC cell lines in favor of survival, proliferation and chemoresistance (143, 146, 247, 252). Omental adipocytes have been shown to provide energy for proliferating EOC via the direct transfer of fatty acids to neighbouring cancer cells (108), while suppression of this process through inhibition of CD36 or FABP4 can sensitize EOC to chemotherapy (144, 244). Here, an important role for omental adipocytes in clinically relevant aspects of EOC biology was further demonstrated. Omentum-derived secreted factors significantly impacted EOC cell line proliferation (Fig. 1). Notably, this effect was apparent in omental tissue obtained from patients with both malignant and non-malignant ovarian neoplasms. The presence of pro-cancer signalling within the peritoneum in absence of malignant disease highlights the importance of this microenvironment in the establishment and development of EOC. Intra-peritoneal ovarian cancer metastasis requires multiple cell types interacting in a dynamic three-dimensional environment and multicellular 3D models can, therefore, provide insights into mechanisms of disease progression (66, 68, 69, 253). A heterotypic spheroid model for adipocyte-EOC interactions incorporating adipose-derived stem cell (ADSC)-derived adipocytes and EOC cell lines was developed. Tumour spheroids incorporate aspects of a localised tumour microenvironment such as gradients of nutrient availability and cellular necrosis and can recapitulate phenotypic heterogeneity and mechanisms of chemoresistance which are apparent in

solid tumours (213). Furthermore, ovarian cancer metastasis has been shown to progress through the dissemination of multicellular aggregates, endogenous tumour spheroids, throughout the peritoneum (64, 66). Omentum-derived factors and adipocyte co-culture had significant impact on the proliferative capacity of EOC spheroids, as well as populations grown in monolayer culture (Fig. 1,2).

Notably, omental tissue and adipocyte-derived paracrine signalling decreased proliferation in OVCAR-3 spheroids, in contrast to monolayer populations and SKOV-3. To understand differences observed in response of EOC populations to adipocyte signalling, the phenotypic characteristics of cell lines was explored, specifically in relation to epithelial-to-mesenchymal transition (EMT), whereby epithelial cells undergo widespread changes in gene expression and phenotype and which has been shown to promote invasion and protect metastasizing cancer cells from therapy, while reducing proliferation (59, 61, 254). SKOV-3 represents a post-EMT phenotype (Vimentin^{+}, N-Cadherin^{+} E-Cadherin^{low}) with an invasive pathology, while OVCAR-3 displayed an epithelial profile (Vimentin^{-} N-Cadherin^{-} E-Cadherin^{high}) typical of a less invasive, epithelial phenotype (60, 62, 219).

Tumour spheroids have been shown to generate a heterogenous population of cells whose activity and response to therapy is determined by their position in three-dimensional space relative to spheroid architecture and by differential penetration of nutrients and other bioactive molecules, including therapeutic agents (63, 213). OC cell lines grown in spheroid culture demonstrated significantly more heterogeneous expression of EMT markers than those grown in monolayer culture (Figure 3.9). Similarly, spheroid culture has been shown to upregulate population ‘stemness’, the capacity for phenotypic change in response to signalling factors and other external stimuli (255). In response to adipocyte signalling, OVCAR-3 cells transition to a more

invasive, vimentin^{+} phenotype (Figure 3.19) suggesting that phenotypic heterogeneity within spheroid populations potentiates this phenotypic switch. Vimentin has previously been shown to play a central role in EMT-mediated metastasis and targeting vimentin can increase susceptibility to chemotherapy in ovarian cancer cells (62, 256, 257). Epithelial cancer cell transition to a mesenchymal-like phenotype via EMT has been associated with poor response to chemotherapy in ovarian cancer, a major obstacle in effective treatment of advanced stage disease (258). The impact of bi-directional signalling between EOC and adipocytes on response to paclitaxel (PTX) therapy was explored and it was found that adipocytes acted to protect EOC cell lines from chemotherapy (Fig. 5).

Extracellular vesicles (EVs), including exosomes, have been implicated in response to chemotherapy in a wide range of cancers (259, 260), and play a significant role in signalling between malignant and non-malignant cell types (120). Adipocytes secrete exosomes in abundance, and adipose-derived exosomes play a role in the regulation of angiogenesis, proliferation, immunity and metabolism (261). In the tumour microenvironment, adipocyte-derived exosomes promote cancer cell proliferation and migration in breast cancer via activation of the Hippo pathway (262). Similarly, adipocyte-derived exosomes can reprogram tumour cell metabolism in melanoma through upregulation of fatty acid oxidation (263). Omentum-derived exosomes provide chemoprotection in EOC cells and drive EMT and invasion in OVCAR-3 via the downregulation of E-Cadherin and overexpression of N-Cadherin (Figures 3.17, 3.18, 3.19). These data further demonstrate the capacity of adipocyte-derived exosomes to generate a pro-tumorigenic microenvironment. In this context, obesity, characterized by adipose hypertrophy, is a risk factor for many cancers, including EOC (47, 50, 264) and the cargo of exosomes secreted by hypertrophic adipocytes has

been shown to be drastically altered (265, 266, 267). Obesity-induced changes in exosome content may, therefore, be a contributing factor in observed obesity and adiposity-related cancer risk.

To better understand the pro-cancer components of adipocyte-derived exosome cargo, miRNA next generation sequencing on exosomes secreted by primary omental tissue was performed. Exosome-derived microRNAs have an impact on cancer development, progression, mortality, and resistance to therapy (251, 259, 268, 269). Highly abundant miRNAs in patients with both benign and malignant neoplasms were idenified (Figure 3.20). Pathway analysis revealed signalling networks related to ovarian cancer as well as breast, prostate, bladder, and endometrial cancers (Figure 3.21). Adipocytes have been shown to promote cancer development in breast (179, 246, 270) and prostate cancer (271, 272), while obesity is a risk factor for endometrial cancer (189, 273, 274). The exosome miRNA-regulated signalling networks identified here may therefore play a wider-reaching role in the development of the metastatic adipose niche and cancer development, especially those cancers where increased adiposity is a known risk factor. Furthermore, prolactin (PRL) signalling, identified here through pathway analysis, is upregulated in numerous hormone-dependent cancers including ovarian, breast, prostate and endometrial cancer and is linked to cancer via activation of JAK/STAT, AKT and MAPK pathways (275, 276, 277, 278, 279, 280). In EOC, PRL-JAK-STAT pathway signalling can lead to phosphorylation of STAT3 and STAT5 (277), connecting PRL signalling to EMT, EOC cancer stemness and resistance to therapy (64, 281, 282, 283).

To validate the role of adipocyte-derived exosome miRNAs in EOC the impact of miR-21, let-7b, miR-16 and miR-92a on OVCAR-3 proliferation and response to therapy was assessed and found a chemoprotective effect for each miRNA. Previous work has

demonstrated the transfer of miR-21 from adipocytes to EOC cell lines and shown that miR-21 can lower sensitivity to PTX in cancer cells in *in vitro* and *in vivo* models (250). This previous study suggested miR-21 exerts its chemoprotective effects via downregulation of APAF1, while miR-21 can also promote cisplatin resistance in EOC by negatively targeting the tumour suppressor PTEN (284). Exosomal miR-21, derived from cancer associated fibroblasts, was shown also to activate STAT3 and promote cisplatin resistance in oesophageal squamous cell carcinoma (285). miR-92a is part of the oncogenic miR-72-92 cluster and is highly expressed in a number of cancers, including in EOC patient serum (286, 287), and its targets include E-Cadherin (288). The role of Let-7b in reducing PTX cytotoxicity is less clear as the Let-7 family of miRNAs have previously been shown to act as tumour suppressors in ovarian cancer (289, 290, 291) and let-7b is relatively less abundant in exosomes derived from patients with ovarian malignancies (Fig. 7A) as seen elsewhere (291, 292). However, transfection of OVCAR-3 with let-7b miRNA increased proliferation and protection from PTX therapy (Fig. 7C,D). Alongside the data presented here, a meta-analysis of transcriptomes of 1,170 patients with high grade ovarian cancer showed let-7b was associated with poor survival rates, implicating let-7b in resistance to therapy (293), further substantiating these findings. Previous work has elucidated the role in the tumour-derived exosomes in the formation of the pre-metastatic niche (294) while here the capacity for adipocyte-derived exosomes to generate a pro-tumorigenic, chemoprotective environment via miRNA signalling was demonstrated. More importantly, adipocytes from non-cancer patients also contain key pro-oncogenic mediators of cancer proliferation, invasion and response to treatment, highlighting the importance of increased adiposity as known cancer risk factor. Therapies which aim to target cells within adipose tissue in order to suppress cancer have shown promise

in animal models may provide a means to modulate and inhibit cancer-specific signalling and metabolism (295, 296). Currently, obese and non-obese patients receive the same cancer treatment, despite apparent differences in risk and outcome (45). A more comprehensive understanding of the mechanisms through which the adipose microenvironment drives pathogenesis and chemoresistance will enable tailored therapies which target specific pro-cancer signalling in healthy and obese or dysregulated adipose tissue.

Chapter 4. An Inflammatory Adipose Environment Promotes Ovarian Cancer Growth

4.1 Introduction

Metastatic epithelial ovarian cancer (EOC) displays consistent omentum tropism (8). The omentum, which has functions in fat storage as well as a regulatory role in immunity and tissue regeneration, is invaded in >60% of cases of metastatic ovarian cancer (8, 297, 298) and omental metastases are often the largest tumour in size (299). In a mouse model of EOC, human cancer cells have been shown to home to the omentum following intraperitoneal injection and tumour cells at the interface with adipose tissue have increased levels of intracellular lipids (107). In Chapter 3 it was demonstrated that co-culture of ovarian cancer cells with adipocytes can increase cancer proliferation and reduce response to therapy. Elsewhere, co-culture models have shown increased lipolysis in adipocytes, which results in the release of fatty acids, as well as an increase in fatty acid β oxidation in ovarian cancer cells (107), suggesting a role for omental adipocytes in altering EOC metabolism and providing nutrients for increased cancer cell proliferation. Furthermore, co-culture of EOC cells with adipocytes drastically changes global cancer cell metabolism, including increases in intracellular lipids and reactive oxygen species (144).

An important role for fatty acid chaperone proteins in EOC development has also been explored. Small molecule inhibition of Fatty Acid Binding Protein 4 (FABP4) can reverse pro-cancer effects of adipocytes in co-culture (107) while short hairpin RNA (shRNA) knockdown of FABP4 expression can reduce or negate adipocyte-induced alteration of cancer metabolism (144). CD36 has been found to be upregulated in omental metastases, and knockdown of CD36 can drastically reduce tumour size in

xenograft mouse model of EOC (143). The evidence, therefore, suggests that cancer activated adipocytes release free fatty acids as a result of increased lipolysis, which are then sequestered by proliferating tumour cells to drive rapid growth and expansion.

The metastatic peritoneal environment, in which omentum invasion takes place, is highly inflamed (83, 300). The development of metastatic disease is often coupled with the development of ascites, an inflammatory condition caused by an imbalance in fluid production and reabsorption (70). Malignant ascites is characterized by an abundance of pro-inflammatory cytokines which act to drive tumour growth and suppress immune response (83, 301). In particular, interleukin-6 (IL-6) has been associated with poor survival (71) and may promote tumour angiogenesis through matrix metalloproteinase-9 (MMP-9) induction (104) and cancer cell proliferation by downstream activation of the JAK/STAT pathway (302). Tumour Necrosis Factor alpha (TNFα) is produced by innate immune cells and tumour cells during ovarian cancer development and autocrine and paracrine TNFα signalling can promote cancer cell proliferation and angiogenesis and suppress anti-cancer immunity (83). Inhibition of TNF signalling via neutralizing antibodies or silencing RNA (siRNA) can inhibit pro-cancer NOTCH signalling and angiogenesis (92). Furthermore, patients who use anti-inflammatory drugs such as acetaminophen and aspirin have a reduced risk of EOC (303, 304, 305).

Obesity, which is characterized by chronic inflammation of adipose tissue, is a risk factor for numerous cancers (45). In obesity, hypertrophy of white adipose tissue (WAT) results in metabolic dysregulation and cell death, triggering tissue remodelling and the recruitment of innate and adaptive immune cells leading to a state of chronic, low-grade inflammation (168, 193). Although there is some contradictory evidence within the literature, meta-analyses have demonstrated a relationship between obesity

or adiposity and the risk of ovarian cancer (47) and patient survival (50). The presence of chronic inflammation, a hallmark of cancer (148), in adipose tissue has been proposed as a potential link between obesity and cancer (45).

Furthermore, obesity is associated with hyperlipidaemia, elevated lipid levels in blood (195, 306). Inflammation of adipose tissue can increase lipolysis and fatty acid release (307), while pro-inflammatory cytokines IL-6 and TNFα, abundant in the ovarian cancer metastatic microenvironment, have been shown to directly stimulate lipolysis (308, 309). It was demonstrated in Chapter 3 that adipocytes can drive ovarian cancer growth and it has been shown elsehwere that adipocyte-derived fatty acids can drive tumour growth, and inflammation of adipose tissue can lead to increased lipolysis and fatty acid release. This chapter, therefore, investigates whether inflammation can enhance pro-cancer activity in adipocytes.

4.2 Hypotheses and Aims

The hypotheses tested in this chapter were:

1. Inflammation of adipocytes leads to increased release of free fatty acids via increased cellular lipolysis.
2. Release of free fatty acids by inflamed adipocytes promotes ovarian cancer proliferation.

As such, the aims of this chapter were as follows:

1. Develop an *in vitro* model of adipocyte inflammation.
2. Investigate inflammation induced changes in rates of lipolysis in adipocytes.

3. Investigate the impact of co-culture with inflamed adipocytes on ovarian cancer cell lines.
4. Quantify the transfer of free fatty acids from inflamed adipocytes to ovarian cancer cell lines.

4.3 Materials and Methods

Materials and methods used in this chapter are descried in detail in Section 2.11. Briefly, an in vitro model of adipocyte inflammation was developed through exogenous treatment of adipose-derived stem cell (ADSC)-derived adipocytes with TNFα. The impact of TNFα treatment on the expression and release of inflammatory cytokines was investigated, as well as the expression of adipocyte-specific markers as an indicator of inflammation-induced de-differentiation. Changes in lipolysis and fatty acid release were assessed alongside morphology of adipocyte lipid droplets as a marker of lipolysis and de-differentiation. Transwell co-cultures were established incorporating inflamed adipocytes and ovarian cancer cell lines and the impact on EOC proliferation was evaluated. The transfer of free fatty acids from adipocytes to EOC cell lines was visualized and quantified using a fluorescent fatty acid analogue. Finally, the role of fatty acid metabolism in EOC response to adipocytes was investigated using etomoxir an irreversible a carnitine palmitoyltransferase 1 (CPT1)-specific inhibitor that prevents the transport from fatty acids into the mitochondrial matrix, to inhibit fatty acid metabolism in cancer cells.

4.4 An *In Vitro* Model of Adipocyte Inflammation

TNFα is abundant in the ovarian cancer metastatic tumour microenvironment (TME) and has been associated with ovarian cancer progression and metastasis (83, 101, 113, 310, 311). An *in vitro* model of inflammation of ADSC-derived adipocytes was established using exogenous treatment with recombinant TNFα. Initially, adipocytes were treated with 25ng/ml, 75ng/ml and 125ng/ml for 72 hours and the expression of pro-inflammatory cytokines was quantified by quantitative real-time PCR (Q-RT-PCR) as an indicator of the establishment of an inflammatory phenotype. Expression of genes encoding the pro-inflammatory cytokines *IL6* (encoding interleukin-6, IL-6), *CCL2* (encoding chemokine ligand 2, CCL2) and *CXCL8* (encoding interleukin-8, IL-8) increased in a dose-dependent fashion upon TNFα treatment (Figure 4.1)

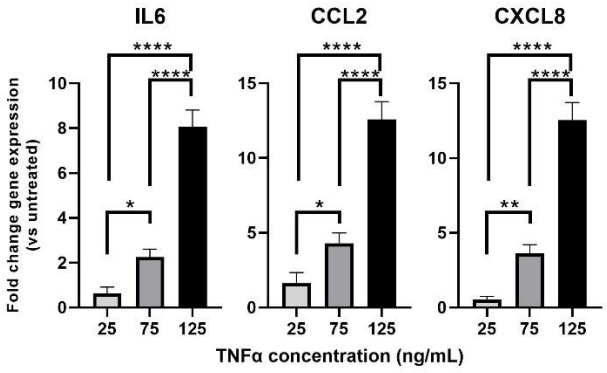

Figure 4.1 Expression of Inflammatory Cytokines in TNFα-Treated Adipocytes. *Adipocytes were treated with TNFα for 72 hours and expression of IL6, CCL2 and CXCL8 assessed by Q-RT-PCR. Gene expression normalised to RPL19 and fold change given relative to untreated adipocytes. Bar blots show mean +SD, n=3, *p>0.05, **p>0.005, ****p>0.00005 (One-way ANOVA with Tukey's multiple comparisons test).*

As stated above, the aim of this study was to understand the impact of inflamed adipocytes on ovarian cancer cells in co-culture. As such, the duration of cytokine

expression was assessed to understand if an inflammatory phenotype in TNFα-treated adipocytes would persist during co-culture given the short half-life of TNFα in suspension (<24 hours). Mature adipocytes were treated with 125ng/ml TNFα and cytokine expression assessed 4, 24, 48, 72 and 96 hours after treatment (Figure 4.2). *IL6* and *CXLC8* expression persisted after 96 hours, while *CCL2* expression decreased after 24 hours, while remaining 50-fold higher than untreated samples. Therefore, it was established that an inflammatory phenotype persisted following TNFα treatment. Henceforth adipocytes treated with and without 125ng/ml TNFα are referred to as inflamed adipocytes and control adipocytes respectively.

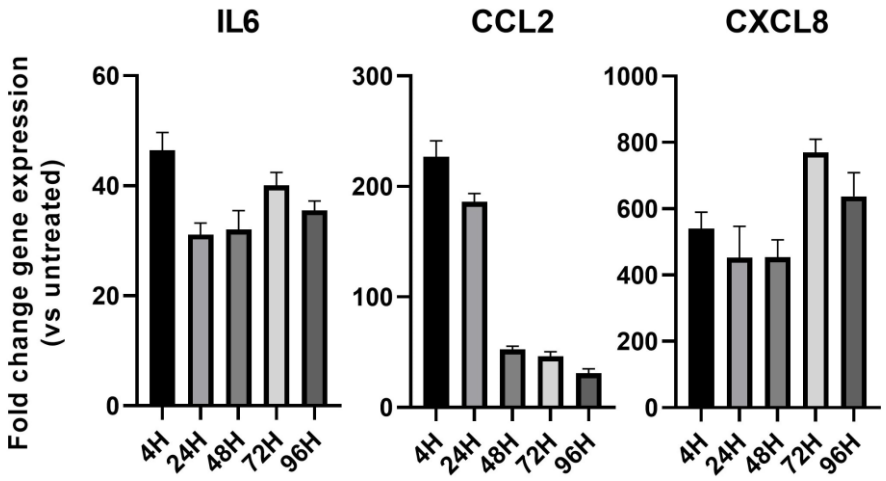

Figure 4.2 Duration of Expression of Inflammatory Cytokines in TNFα-Treated Adipocytes. *Adipocytes were treated with 125ng/ml TNFα and expression of IL6, CCL2 and CXCL8 assessed by Q-RT-PCR at time points Gene expression normalised to RPL19 and fold change given relative to untreated adipocytes. Bar blots show mean +SD.*

In order to explore a broader spectrum of cytokine secretion in inflamed adipocytes, Luminex assay was performed to compare concentration of secreted cytokines in media conditioned by control and inflamed adipocytes. A panel of cytokines and

signalling factors were assessed as displayed in Figure 4.3a and summarized in Figure 4.3b. With the exception of CCL3, IL-2, interferon- α (IFN- α) and IL-1 α, the release of all analytes was significantly upregulated in inflamed adipocytes, further indicating a strong inflammatory phenotype for TNFα treated adipocytes.

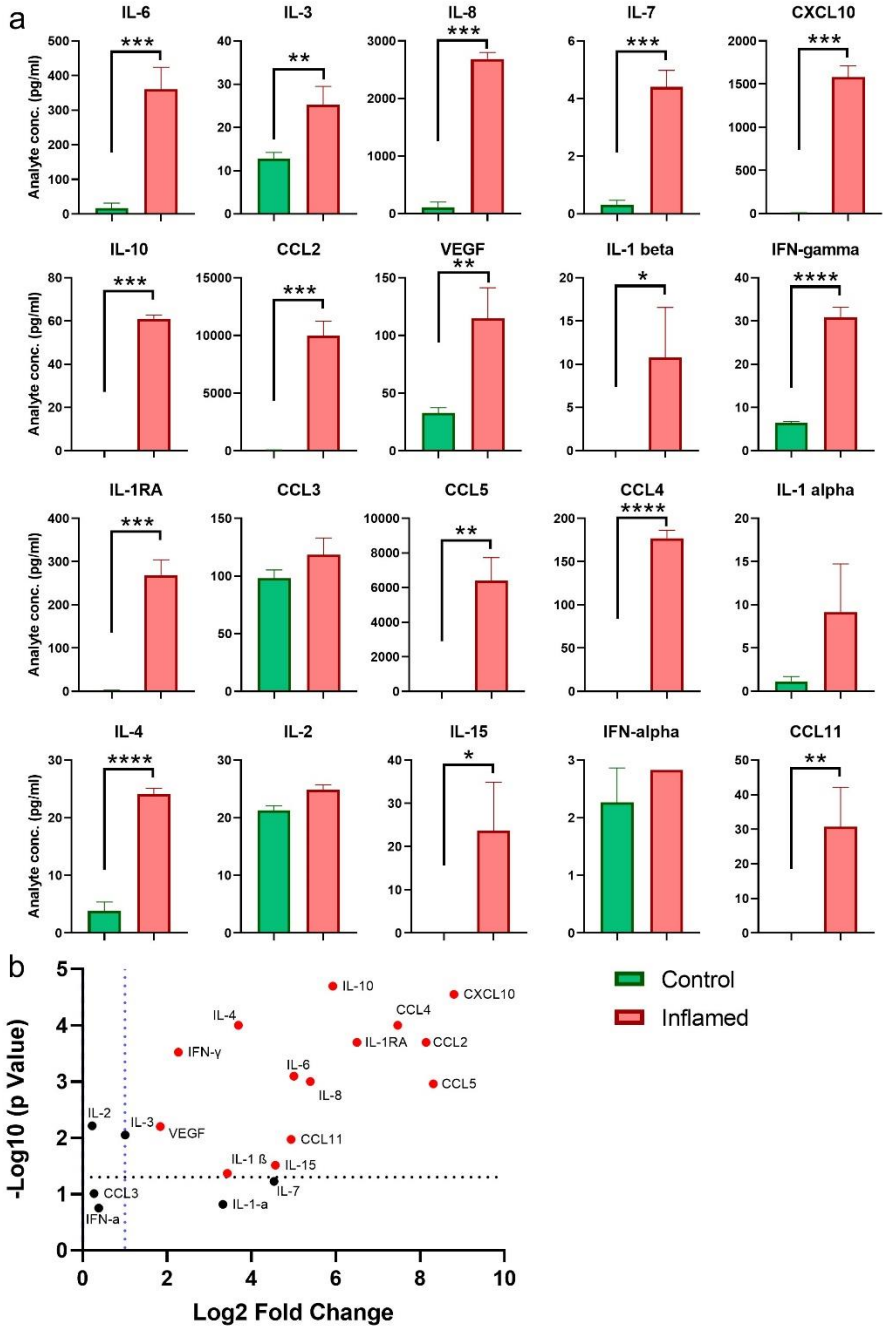

Figure 4.3 Secretion of Cytokines and Signalling Factors by Inflamed Adipocytes. *Adipocytes were treated with 125ng/ml TNFα for 72 hours and release of analytes investigated by Luminex assay (a), summarized in (b). Bar blots show mean +SD, n=3, *p>0.05, **p>0.001, ***p>0.0001 ****p>0.00001 (Student's t-test).*

The inflamed adipocyte phenotype was further investigated by flow cytometry (Figure 4.5). Inflamed adipocytes displayed significantly increased forward scatter (**p<0.001), characteristic of increased cell size which may indicate hypertrophy, indicative of adipocytes found in obese adipose tissue. Inflamed adipocytes also displayed increased side scatter, indicating higher granularity which may be a result of smaller lipid droplet size as observed in brown adipose tissue (312), discussed below.

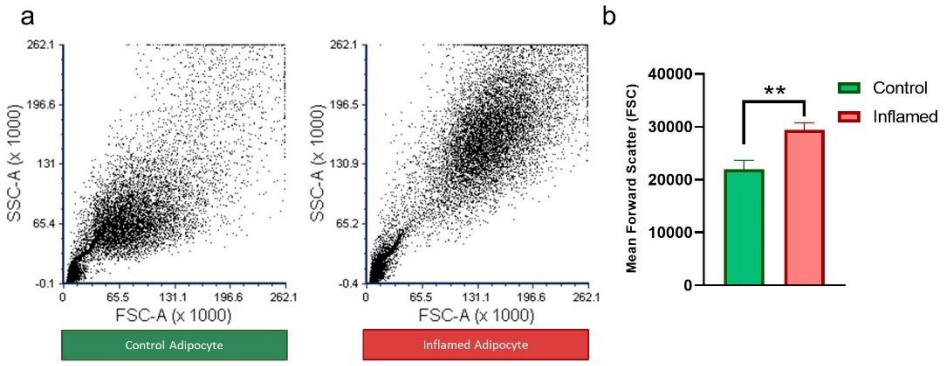

Figure 4.4 Characterization of Inflamed Adipocytes by Flow Cytometry. *Plot (a) displays forward scatter (FSC) and side scatter (SSC). Relative cell size was quantified by forward scatter. Bar blots show mean +SD, n=3, **p>0.001 (Student's t-test).*

4.5 Inflammation of Adipocytes Induces Lipolysis and Promotes De-Differentiation

To explore the hypothesis that inflammation of adipocytes leads to increased release of free fatty acids via increased cellular lipolysis, assays were performed to quantify extracellular fatty acid concentration (Figure 4.4a) and glycerol (Figure 4.4b). Free fatty acids and glycerol are the two major products of lipolysis of triacylglycerides, such

as that found in adipocytes lipid droplets. Both fatty acid concentration (****p<0.00001) and glycerol concentration (**p<0.001) were significantly increased in inflamed adipocyte media, indicating an increase in lipolysis leading to increased release of free fatty acids.

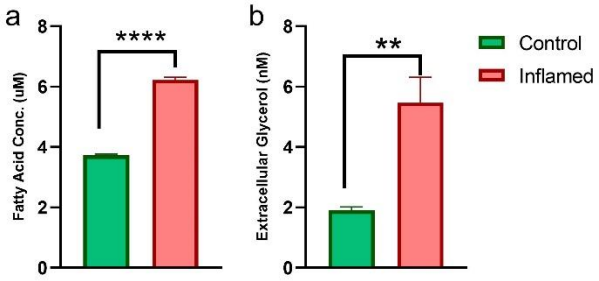

Figure 4.5 Lipolysis Assays in Inflamed Adipocytes. *Fatty acid (a) and glycerol (b) concentration in inflamed adipocyte media was compared to control adipocyte media. Bar blots show mean +SD, n=3, **p>0.001, ****p>0.00001 (Student's t-test).*

Adipocyte-derived fatty acids are the product of lipolysis of triacylglycerides stored in large, morphologically distinct lipid droplets (LDs), a characteristic feature of adipocyte morphology. To further investigate the impact of inflammation on adipocyte metabolism, changes in lipid droplet morphology were observed via BODIPY staining of neutral lipids (Figure 4.6). Adipocytes were grown in 2D monolayer (Figure 4.6a) and 3D spheroid (Figure 4.6c) cultures and inflamed with 125ng/ml TNFα for 72 hours prior to fixing and staining. In both culture systems, changes in LD size and number was observed, with inflamed adipocytes displaying fewer, smaller LDs. Images were analysed to identify lipid droplets (Figure 4.6a,c, right-hand panel) based on their size and morphology (circularity), with lipid droplets being defined as >2μm in diameter and having circularity higher than 0.5. LD number was counted and normalised to cell number in monolayer populations (Figure 4.6b), as defined by number of nuclei (DAPI stain). For spheroid populations the 3D nature of Z-stack images obtained meant

counting overlapping nuclei was not possible, therefore lipid droplet number was normalised to approximate spheroid volume instead. In both culture systems, inflammation of adipocytes resulted in significantly fewer LDs ($p<0.05$, $p<0.0001$). Notably, total BODIPY fluorescence was not decreased, rather it was not present in the form of mature LDs, indicating fatty acids were being released from LDs in intra- and extracellular spaces, further supporting the hypothesis that inflammation of adipocytes increases lipolysis and fatty acid secretion.

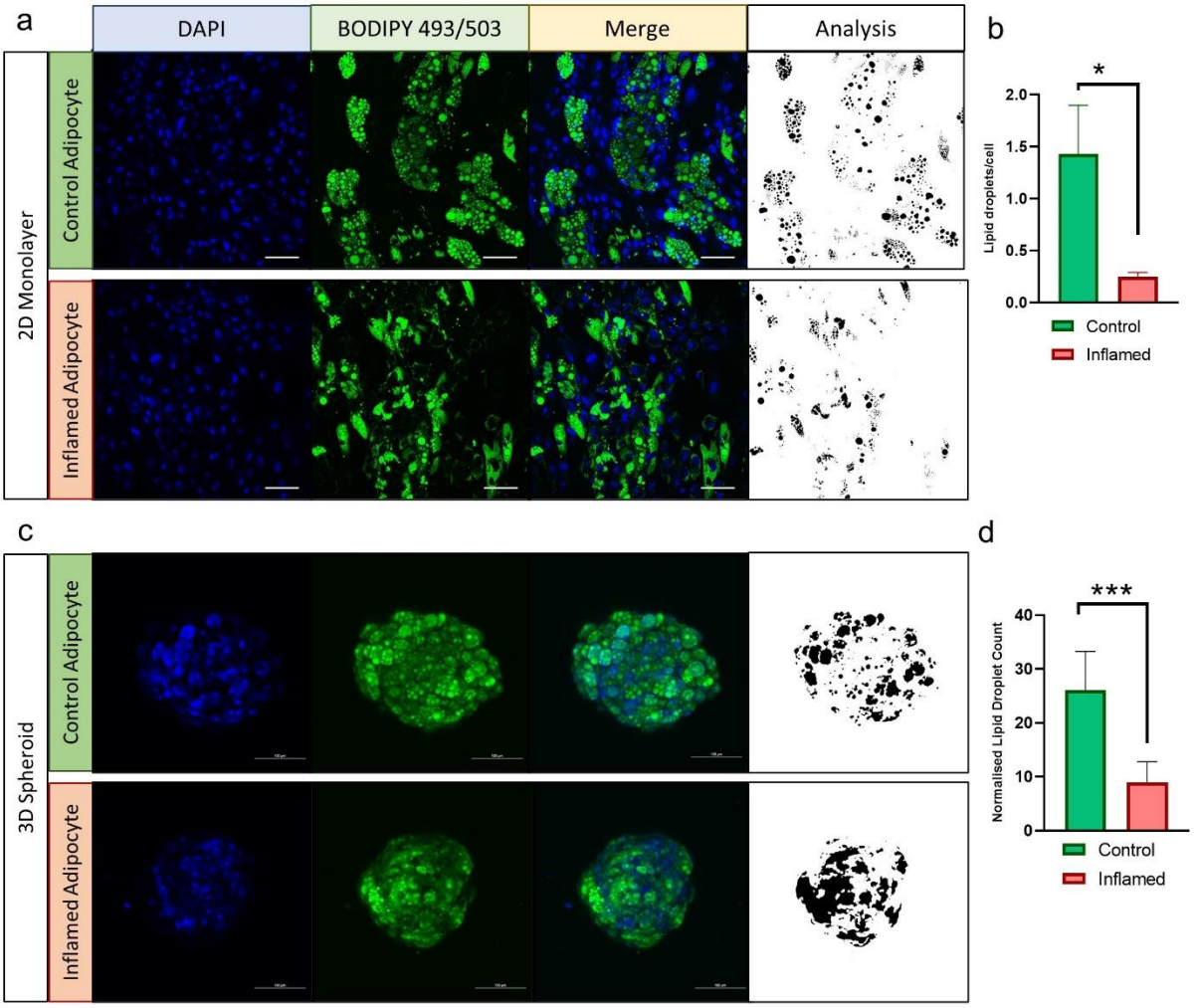

Figure 4.6 Lipid Droplet Analysis in Inflamed Adipocytes. *Inflamed adipocytes were fixed and stained with BODPIY 493/503 and DAPI. Lipid droplets were identified via analysis with imageJ. For adipocytes grown in monolayer culture (a), lipid droplet number was normalised to DAPI stained nuclei number (b), while for adipocytes grown in spheroid culture (c), lipid droplet number was normalised to spheroid volume (d). Scale bar in a = 50μm, b= 100μm Bar blots show mean +SD, n=5, *p>0.05, ***p>0.0001 (Student's t-test).*

Release of fatty acids by inflamed adipocytes was further tested using fluorescent fatty acid analogue BODIPY 500/510 C_1 C_{12} which incorporates a fluorescent BODIPY molecule into the fatty acid dodecanoic acid. Following 3 hours treatment, uptake of fluorescent probe was observed with fluorescent microscopy (Figure 4.7a). Following 72 hours inflammation, cells were lysed and the percentage of BODIPY$^+$ cells was calculated following flow cytometry (Figure. 4.7b,c). Inflamed adipocyte populations had significantly lower % BODIPY$^+$ cells ($p<0.05$), indicating again that fatty acids were being secreted.

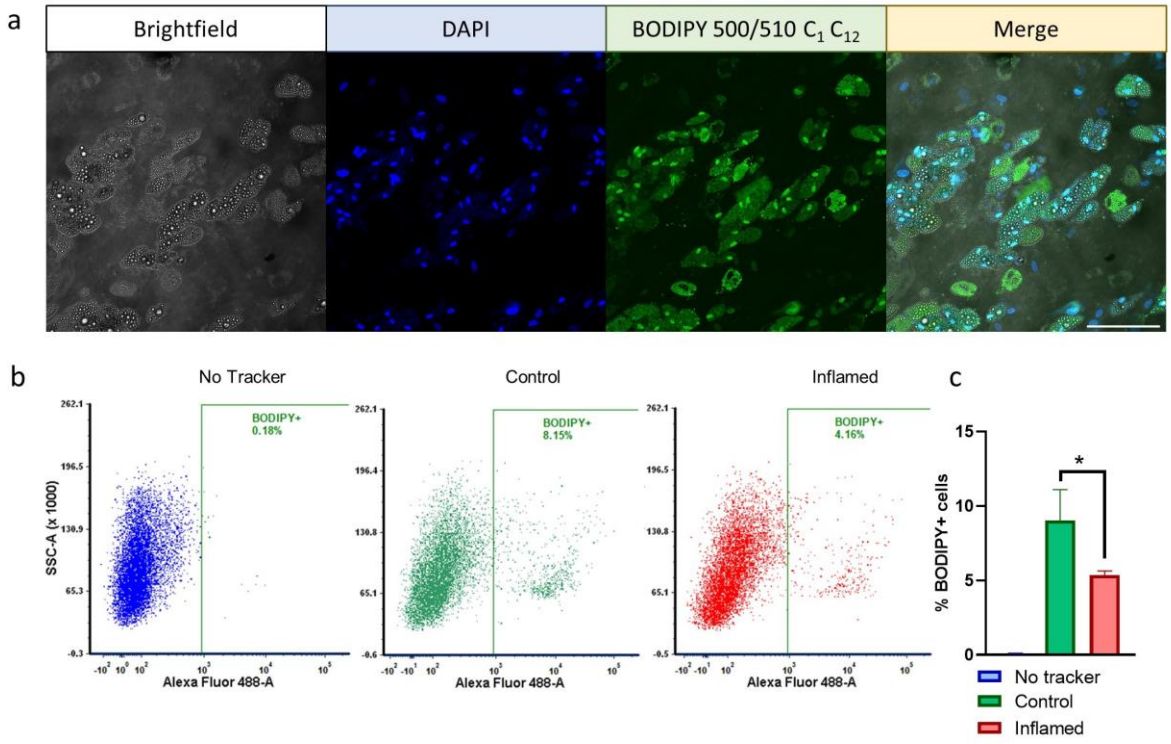

Figure 4.7 Secretion of Fatty Acid Analogue in Inflamed Adipocytes. *Uptake of fluorescent fatty acid analogue BODIPY 500/510 C1 C12 was confirmed by fluorescent microscopy (a). Following 72 hours inflammation, number of BODIPY$^+$ cells was assessed by flow cytometry (b) and quantified (c). Bar blots show mean +SD, n ≥5, *p>0.05 (Student's t-test). Scale bar = 100μm.*

Loss of LDs in inflamed adipocytes suggested that inflammation may cause some degree of de-differentiation, as indicated by loss of characteristic adipocyte morphology. Expression of adipocyte specific markers adiponectin (encoded by ADIPOQ) and lipoprotein lipase (encoded by LPL) was assessed Q-RT-PCR (Figure 4.8a), while secretion of adiponectin was also assessed by Luminex assay (Figure 4.8b). Expression and release of adiponectin was significantly reduced, and expression of LPL was significantly reduced.

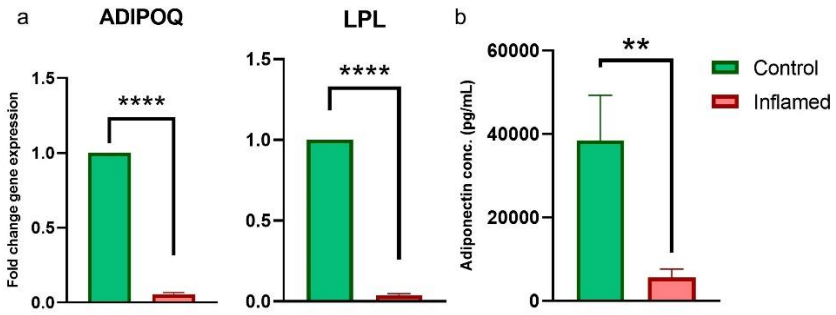

Figure 4.8 Expression of Adipocyte-Specific Markers in Inflamed Adipocytes. *Expression of ADIPOQ and LPL was assessed by Q-RT-PCR (b) and fold change relative to control adipocytes calculated. Concentration of adiponectin in adipocyte media was quantified by Luminex assay (b). Bar blots show mean +SD, n=3, **p>0.001, ****p>0.00001 (Student's t-test).*

Changes in morphology and loss of adipocyte-specific markers suggested a possibly cytotoxic effect of TNFα on adipocytes. Therefore, viability of adipocyte populations following inflammation was assessed by MTT assay (Figure 4.9). No change in viability was observed.

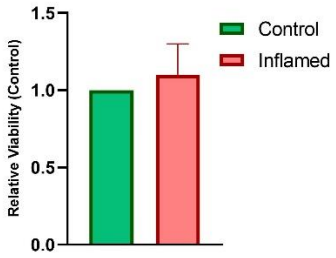

Figure 4.9 Cytotoxic Impact of TNFα Treatment on Adipocytes. *Cell viability 72 hours following 125ng/ml TNFα treatment was assessed by MTT assay. Viability is given relative to untreated (control) adipocytes. Significance assessed by Student's t-test.*

4.6 Co-Culture with Inflamed Adipocytes Increased Ovarian Cancer Cell Proliferation

To explore the hypothesis that increased fatty acid release in inflamed adipocytes would promote ovarian cancer proliferation, Transwell co-cultures were established in which mature adipocytes, seeded onto Transwell inserts, were inflamed for 24 hours prior to co-culture with EOC cell lines in monolayer and spheroid culture. Inserts were washed thoroughly prior to co-culture to ensure there was no direct treatment of cancer cells with TNFα. Cell viability of cell lines (SKOV-3, OVCAR-3, CAOV-3) in monolayer culture (measured by MTT assay) and spheroid culture (measured by CellTiter-Glo 3D assay) upon 72 hours co-culture with inflamed adipocytes was compared to cancer cells in monoculture and cancer cells co-cultured with control adipocytes (Figure 4.11). Cancer cell population viability was significantly increased in inflamed adipocyte co-culture for all cell lines in 2D and 3D models. SKOV-3 and CAOV-3 spheroid displayed a striking ~2- and ~3- fold increase in viability in inflamed adipocyte co-culture respectively.

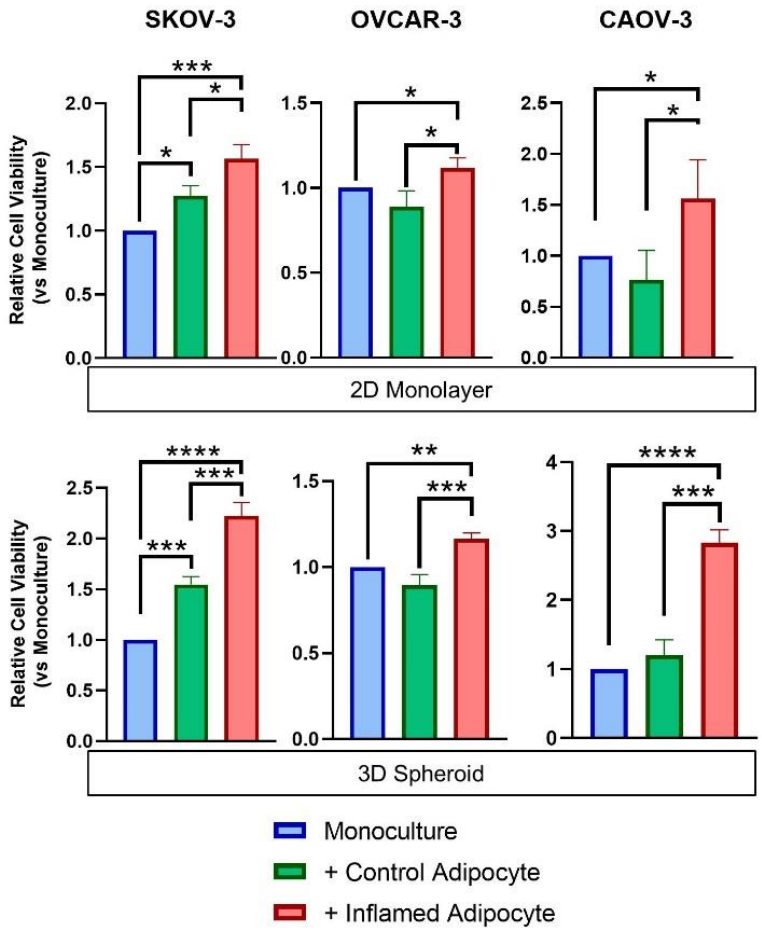

Figure 4.10 Co-Culture of Ovarian Cancer Cell Lines with Inflamed Adipocytes. *Cell viability in EOC cell populations in 2D and 3D culture following Transwell co-culture with inflamed adipocytes was quantified and compared to cells grown in monoculture and co-culture with control adipocytes. Viability is given relative to EOC cells in monoculture. Bar blots show mean +SD, n=4, *p>0.05, **p>0.001, ***p>0.0001, ****p>0.00001 (One-way ANOVA with Tukey's multiple comparisons test).*

Spheroids grown in co-culture with inflamed adipocytes were visibly larger, indicating increased proliferation. SKOV-3 spheroids were imaged (Figure 4.12a) and approximate volume calculated from height and width (Figure 4.12b). SKOV-3 spheroids co-cultured with inflamed adipocytes significantly greater volume than other cultures analysed ($p<0.05$).

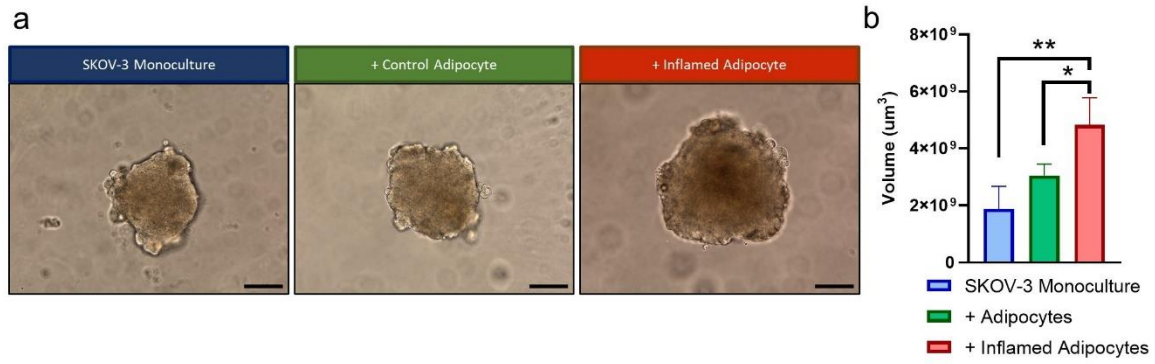

Figure 4.11 SKOV-3 Spheroid Size Following Co-Culture with Inflamed Adipocytes. *SKOV-3 spheroids in mono- and co-culture were imaged (a) and volume calculated (b). Scaled bar = 100µm. Bar blots show mean +SD, n=4, *p>0.05, **p>0.005, (One-way ANOVA with Tukey's multiple comparisons test).*

Given that inflamed adipocytes release fatty acids upon inflammation, it was hypothesised that inflamed adipocyte conditioned media would promote ovarian cancer cell growth, as seen in co-culture models. EOC cell line spheroids were treated with inflamed adipocyte conditioned media and viability compared to control adipocyte conditioned media and untreated spheroids. To investigate whether bi-directional signalling was required to induce pro-tumour effects, EOC spheroids were also treated with media conditioned in co-culture experiments, as detailed above. Spheroids were treated with conditioned media from co-cultures using the same cell line for 72 hours (Figure 4.13). Treatment with control adipocyte and inflamed adipocyte conditioned media had no impact on EOC spheroid viability. However, treatment with conditioned

media collected from co-cultures of EOC cell lines with inflamed adipocytes significantly increased viability relative to conditioned media from monocultures and control adipocyte co-cultures. This indicates that bi-directional signalling between cancer and adipocyte compartments are required to induce increased cancer cell proliferation.

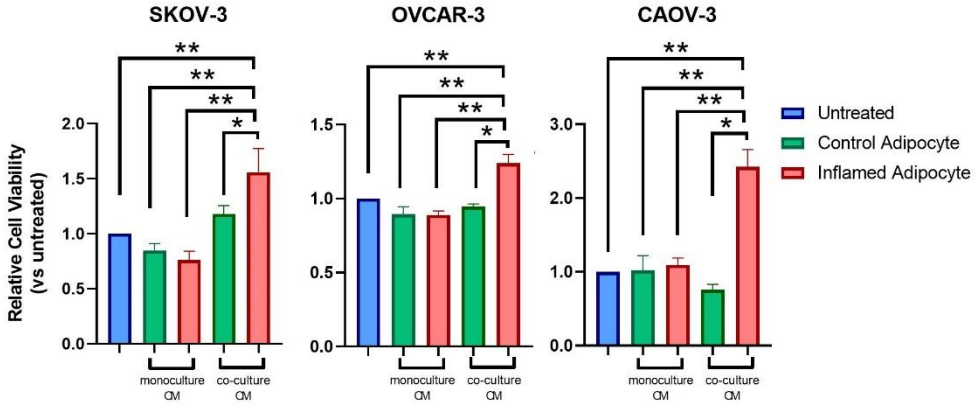

Figure 4.12 Treatment of EOC Spheroids with Mono- and Co-Culture Conditioned Media. *Conditioned media was collected from control and inflamed adipocyte monocultures as well as co-cultures with EOC cell lines. EOC spheroids were treated with conditioned media for 72 hours and viability measured by CellTiter-Glo 3D assay. Bar blots show mean +SD, n=4, *p>0.05, **p>0.001, (One-way ANOVA with Tukey's multiple comparisons test).*

To test the hypothesis that increased cancer cell proliferation in co-culture was the result of direct transfer of fatty acids from adipocytes, the fluorescent fatty acid analogue BODIPY 500/510 C_1 C_{12} was used. As in Figure 4.8, adipocytes were 'fed' with BODIPY 500/510 C_1 C_{12} for 3 hours and uptake confirmed by fluorescent microscopy. Adipocytes were then inflamed for 24 hours prior to co-culture with SKOV-3 cells for 72 hours. The transfer of fatty acids was visualised by fluorescent confocal microscopy and BODIPY 500/510 C_1 C_{12} fluorescence quantified, normalised to DAPI

(Figure 4.13). Cells grown in monoculture in the absence of BODIPY 500/510 C_1 C_{12} were used as negative control. SKOV-3 cells in 2D and 3D co-culture models displayed significantly higher BODIPY fluorescence than those grown with control adipocytes ($p<0.00001$), suggesting inflammation of adipocytes increases uptake of adipocyte-derived fatty acids in EOC cells.

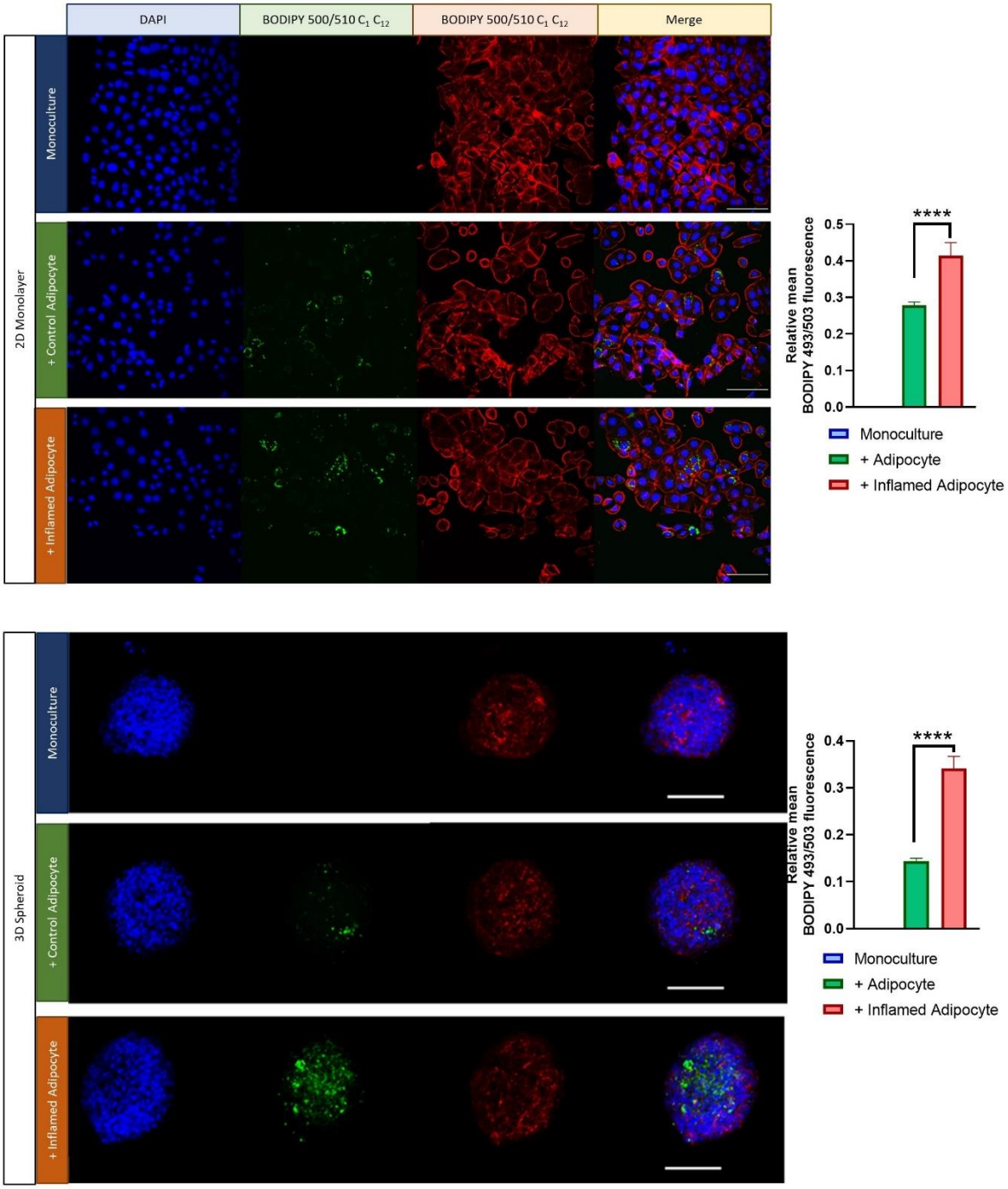

Figure 4.13 Fluorescent Microscopy Analysis of Transfer of Fluorescent Fatty Acid Analogue from Adipocytes to SKOV-3 Cells. *SKOV-3 cells in monolayer and spheroid culture were co-cultured alongside BODIPY 500/510 C1 C12-fed adipocytes prior to co-staining with DAPI (blue) and phalloidin (red). Mean fluorescence intensity was normalised to DAPI and quantified. Scale bar for 2D monolayer = 50μm, 3D spheroid= 100μm Bar blots show mean +SD, n=s****p>0.00001, (One-way ANOVA with Tukey's multiple comparisons test).*

The transfer of fatty acids from inflamed adipocytes to 2D cultured SKOV-3 cells was further quantified by flow cytometry following co-culture as detailed above (Figure 4.15). SKOV-3 cells in monoculture, adipocyte co-culture and inflamed adipocyte co-culture displayed similar profiles in size (Figure4.15a) and a significant shift in the level of BODIPY+ was apparent in SKOV-3 cells co-cultured with inflamed adipocytes ($p<0.05$) (Figure 4.15c,d quantified in e). Again, this indicates a significantly increased uptake of fatty acids into SKOV-3 cells of adipocyte-derived fatty acids. Dissociation of spheroid required for flow cytometry was highly damaging to cells, and therefore cytometric analysis of cells from 3D co-cultured was not possible.

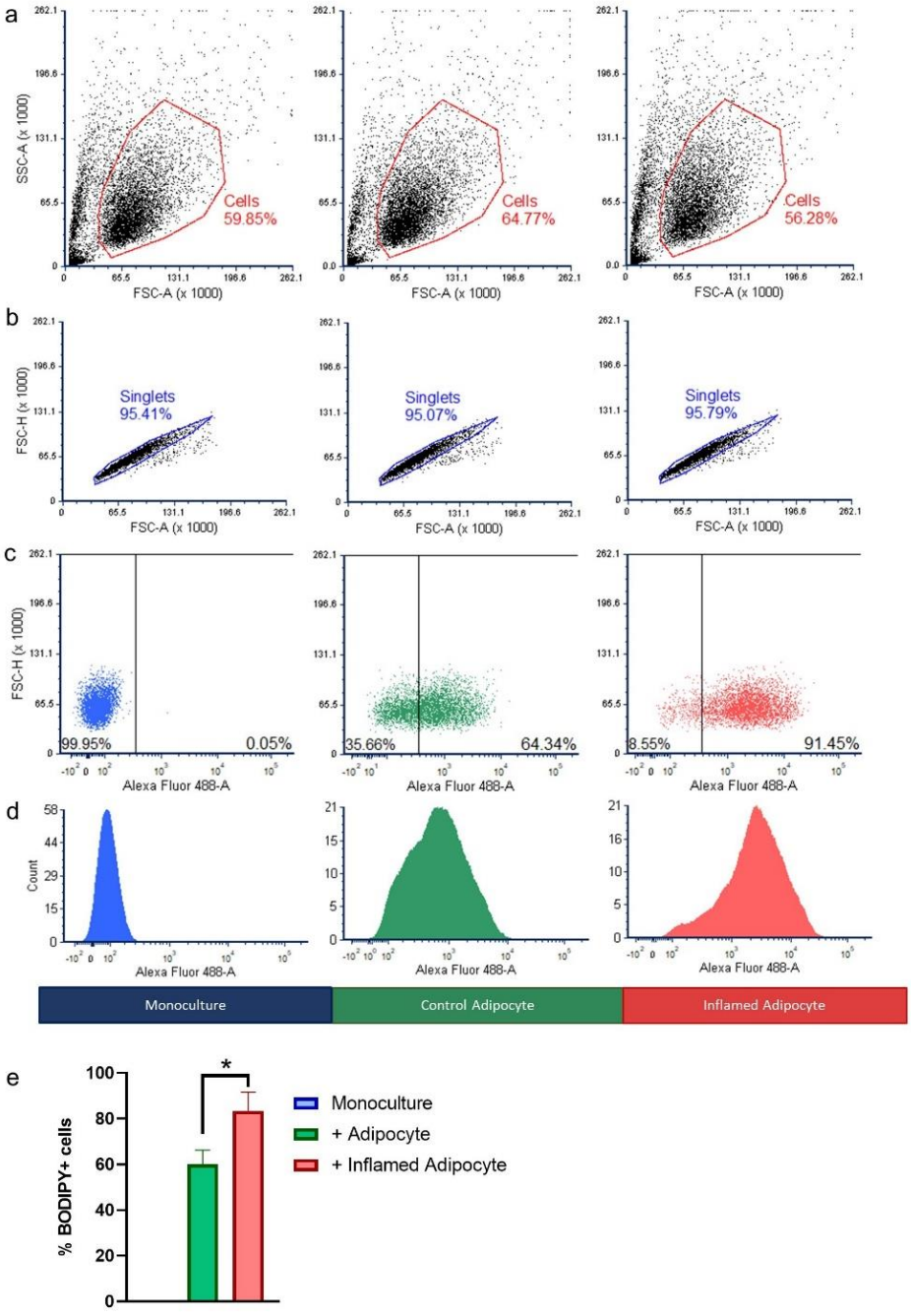

Figure 4.14 Flow Cytometry Transfer of Fluorescent Fatty Acid Analogue from Adipocytes to SKOV-3 Cells. *SKOV-3 cells in monolayer were co-cultured alongside BODIPY 500/510 C1 C12-fed adipocytes prior to analysis by flow cytometry. Cells (a) and single cells (b) were identified based on forward (FSC) and side scatter (SSC). BODIPY+ cells were characterised using monocultured SKOV-3 cells as negative control (scatter plot c and histogram d). Number of BODIPY+ cells was quantified (e). Bar blots show mean +SD, n=3 *p>0.05, (One-way ANOVA with Tukey's multiple comparisons test).*

The impact of co-culture on the adipocyte compartment of co-cultures was also investigated. Figure 4.15a shows whole well images of adipocytes in Transwell culture following 72 hours co-culture for BODIPY 500/510 C_1 C_{12}-fed inflamed and control adipocytes. Inflamed adipocytes, following SKOV-3 co-culture, displayed significantly less BODIPY fluorescence than control adipocytes ($p<0.001$) (Figure 4.15b), further suggesting increased release of fatty acid from inflamed adipocytes and sequester by SKOV-3 cells.

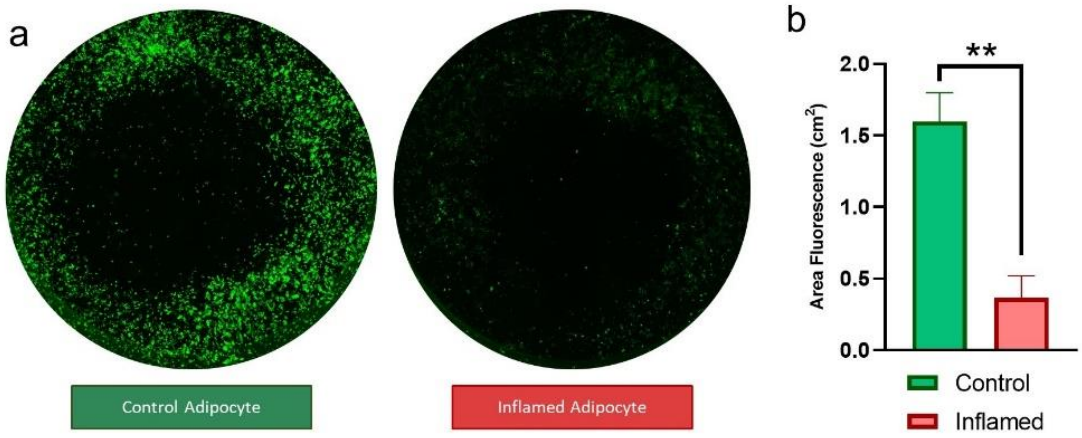

Figure 4.15 Release of Fluorescent Fatty Acids by Adipocytes in Co-Culture. *BODIPY 500/510 C1 C12-fed adipocytes were imaged following co-culture with SKOV-3 cells (whole well, a) and total area of BODIPY fluorescence calculated (b). Bar blots show mean +SD, n=3 **p>0.005, (One-way ANOVA with Tukey's multiple comparisons test).*

Potential mechanisms of fatty acid uptake into ovarian cancer cells were explored through Q-RT-PCR for genes encoding fatty acid chaperone proteins. No expression in EOC cell lines in any culture model of CD36 was found (negative data, not shown). However, expression of Fatty Acid Binding Protein 4 (*FABP4*) was significantly

increased in all EOC cell lines co-cultured with inflamed adipocytes (Figure 4.16), suggesting increased availability of fatty acids increased *FABP4* expression or inflamed adipocyte-derived signalling induced expression of *FABP4*.

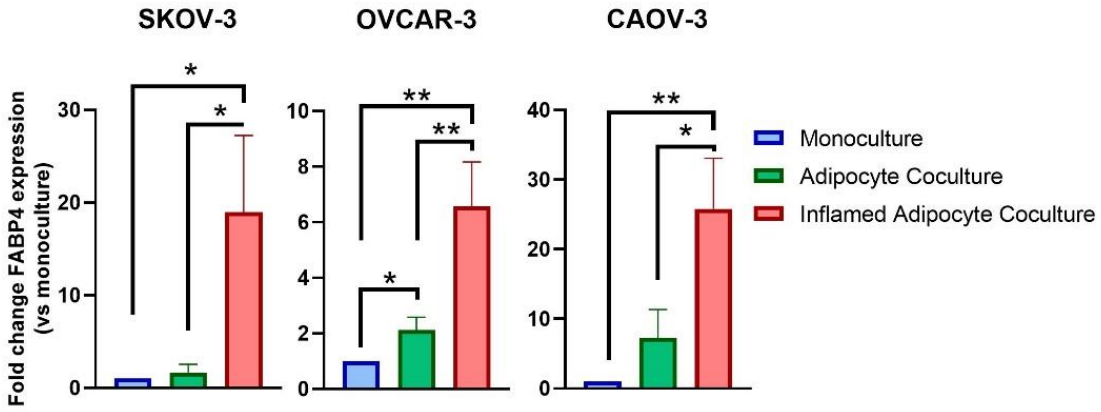

Figure 4.16 FABP4 Expression in EOC Cells in Co-Culture. *Fold change relative to cancer cells in monoculture. Bar plots show mean +SD, n=3, *p<0.05, **p<0.001, (One-way ANOVA with Tukey's multiple comparisons test).*

In order to investigate the hypothesis that increased sequester of fatty acids by ovarian cancer cells in inflamed adipocyte co-culture leads directly to increased cancer cell proliferation, the metabolic drug etomoxir was used to block fatty acid metabolism in EOC cell lines. Etomoxir inhibits carnitine palmitoyltransferase-1 (CPT1), blocking uptake of fatty acids into the mitochondria thereby inhibiting fatty acid β oxidation. Initially, non-toxic dosage of etomoxir in EOC spheroids was established by 72 hours treatment of SKOV-3, OVCAR and CAOV-3 in monoculture. Spheroid viability was assessed by CellTiter-Glo 3D assay and significant decrease was displayed at 20μM and 15μM for SKOV-3 and OVCAR-3 respectively (Figure 4.17). Non-toxic dose was

established to ensure etomoxir did not interrupt normal fatty acid metabolism but would inhibit increased fatty acid β oxidation if it was apparent in co-culture. CAOV-3 response to etomoxir treatment was unusual and cell viability increased following treatment (Figure 4.17). The underlying mechanisms behind this phenomenon were not clear, and etomoxir treatment of CAOV-3 was not included in future experiments.

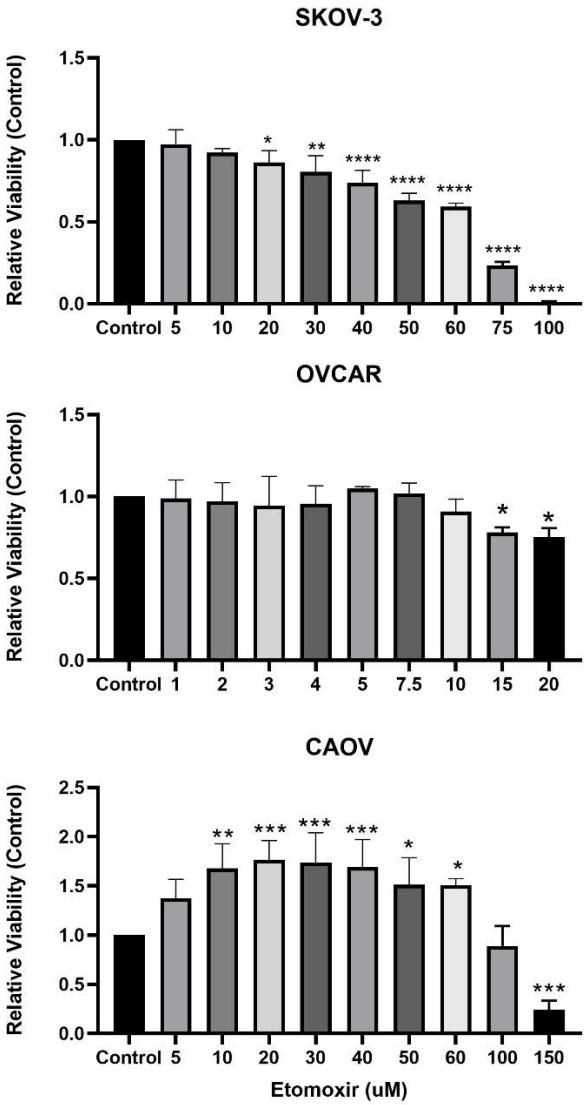

Figure 4.17 Establishment of Non-Toxic Dose of Etomoxir in Ovarian Cancer Cell Lines. *EOC spheroids were treated with etomoxir for 72 hours and cell viability measured by CellTiter-Glo 3D assay, displayed relative to untreated spheroid control. Bar blots show mean +SD, n=5 *p>0.05, **p>0.001, ***p>0.0001, ****p>0.00001, (One-way ANOVA with Tukey's multiple comparisons test).*

SKOV-3 and OVCAR-3 spheroids in co-culture with control and inflamed adipocytes, as well as spheroids in monoculture, were cultured for 72 hours with and without treatment with etomoxir (20μM for SKOV-3 and 15μM OVCAR-3). Etomoxir treatment had no impact on viability in monoculture and adipocyte co-cultures but significantly reduced proliferation in spheroids co-cultured with inflamed adipocytes (Figure 4.18). Etomoxir, through inhibition of increased fatty acid β oxidation, reverses adipocyte induced increases in cancer cell proliferation, supporting the hypothesis that such increases in proliferation are a result of fatty acid oxidation. However, off target effects of etomoxir on cellular respiration have been observed, notably inhibition of complex I of the electron transport chain (313), and effects may therefore not be directly related to fatty acid oxidation.

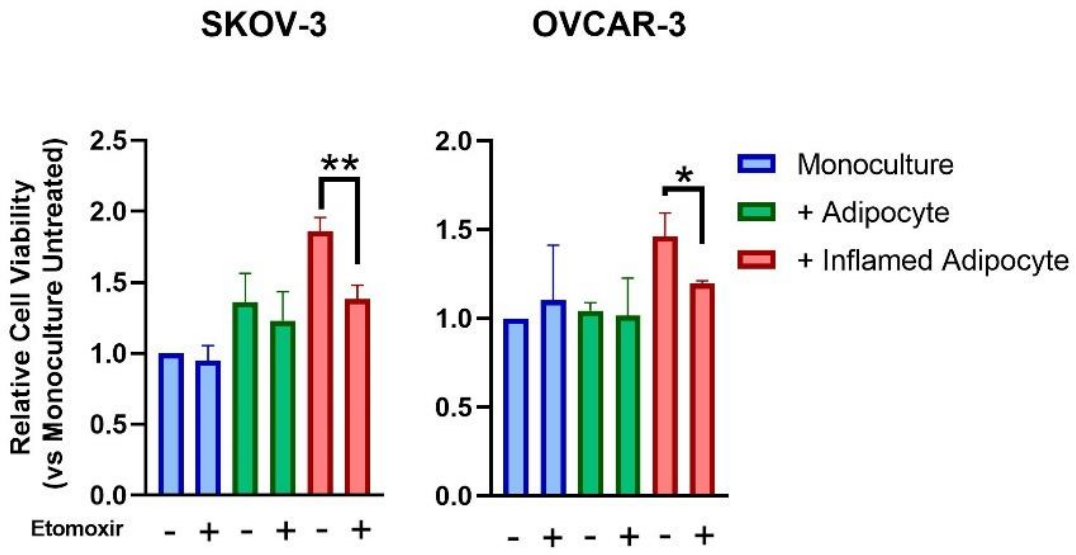

Figure 4.18 Etomoxir Treatment of EOC Spheroids in Co-Culture. *EOC spheroids were treated with etomoxir for 72 hours during co-culture and cell viability measured by CellTiter-Glo 3D assay, displayed relative to untreated spheroid control. Bar blots show mean +SD, n=5 *p>0.05, **p>0.001, (One-way ANOVA with Tukey's multiple comparisons test).*

4.7 Discussion

TNFα plays an important role in ovarian cancer progression (83) and increased levels of TNFα in serum, ascites and tumour tissue have been associated with poor patient outcomes (101, 113, 310, 311, 314). A number of sources of TNFα in the ovarian TME have been proposed. Bulk mRNA sequencing of ovarian tumours has revealed overexpression of TNFα (114, 314), however ovarian tumours comprise a heterogeneous mixture of cells including tumour cells, fibroblasts and immune cells. RNA in situ hybridization analysis of ovarian tumour microarray slides showed localization of TNFα expression in tumour compartments and TNFα expression was present in high-grade serous tissue samples but not low-grade (113). Autocrine activity of tumour-produced TNFα can induce tumour progression via activation of a tumour promoting cytokine network (315), though the impact of TNFα on stromal cells, outside of immune components, has not been thoroughly explored.

TNFα is also secreted by a number of immune cells with known roles in ovarian cancer progression (301, 316). The role of macrophages in ovarian cancer development is complex and diverse. Macrophages are typically polarised to an inflammatory M1-like state or an anti-inflammatory M2-like state, which is classically characterized as pro-tumoral due to the capacity for M2 macrophages to suppress anti-cancer immunity (115). Indeed, a high M1/M2 ratio within tumour tissue is correlated with extended survival (116, 317). However, as previously noted, the ovarian cancer metastatic TME is characterized by abundant pro-inflammatory cytokines and TNFα-secreting M1 macrophages are recruited to inflamed adipose tissue, such as that seen in obesity (194), and may promote metastasis (89, 117).

TNFα was also investigated as a source of adipocyte inflammation due its role in adipose inflammation, obesity and metabolism. In obesity, expansion and hypertrophy of white adipose tissue (WAT) results in cell death, immune infiltration and the development of chronic low-grade inflammation (168, 193). In obesity, adipose tissue macrophages switch from an M1 phenotype to a pro-inflammatory M2 phenotype, demonstrating increased release of TNFα, alongside other inflammatory cytokines (318, 319). Serum TNFα concentration is increased in obese subjects (320) and inhibition of TNFα signalling by neutralizing antibody can inhibit adipocyte inflammation in an adipocyte – macrophage co-culture model (321). Furthermore, TNFα levels have been shown to decrease in obese patients upon sustained weight loss (322). Inflammation and TNFα promote lipolysis in human adipocytes (307, 309), resulting in the release of free fatty acids, which in turn can further promote adipose inflammation (323, 324). Evidence for a role for TNFα in ovarian cancer progression and adipose inflammation, which couples TNFα to adipocyte lipolysis, informed the approach of this study to generate an inflamed adipocyte model to study ovarian cancer – adipocyte interactions.

In this chapter, treatment of ADSC-derived adipocytes with TNFα resulted in the expression and release of a suite of inflammatory cytokines (Figure 4.1, 4.3). The capacity of adipocytes to generate an inflammatory environment in ovarian cancer has not previously been thoroughly investigated. Previous seminal work has demonstrated an inflammatory cytokine network induced by TNFα signalling incorporating IL-6, CCL2, CXCL12, Vascular endothelial growth factor (VEGF) and macrophage migration inhibitory factor (MIF) can drive ovarian cancer proliferation and metastasis, and while this network is hypothesized to be regulated by autocrine signalling within tumour cells (92, 315), paracrine signalling within the TME would likely have similar

downstream effect. In this study, TNFα induced expression and release of IL-6 and CCL2 both major regulators of EOC development, as well as VEGF (8, 83). IL-6 in particular is involved in major aspects of ovarian cancer development including carcinogenesis, migration, invasion and chemoresistance as well as regulating adipocyte – cancer interaction (71, 99, 107, 325). Similarly, IL-8 is shown to be dramatically upregulated in TNFα inflamed adipocytes (Figure 4.3) and may regulate adipocyte – cancer crosstalk in the EOC metastatic microenvironment (107, 108). Also of note, high circulating levels of IL-1β have been associated with poor prognosis. Global changes in cytokine expression demonstrate the capacity for adipocytes to generate a pro-inflammatory environment in response to TNFα signalling. This study further explored the impact of adipocyte inflammation on adipocyte activity in monoculture and co-culture with EOC cell lines.

Inflamed adipocytes increased in size (Figure 4.4), which may suggest hypertrophy, as associated with dysfunctional adipocytes in obesity (168). Inflamed adipocytes also demonstrated increased granularity (Figure 4.4), which may be a result of decreased lipid droplet (LD) size. Lipid droplet number was decreased in inflamed adipocytes (Figure 4.5) and these data suggest increased lipolysis results in the breakdown of LD triacylglycerides into fatty acids which are then released into intra- and extracellular space (Figure 4.5, 4.6, 4.7). Omental white adipocytes are unilocular, while ADSC-derived adipocytes used in this study are multilocular and therefore may not recapitulate in vivo conditions. Adipocytes in different tissues have been demonstrated to have significant differences in their metabolism and signalling (172) and future work should aim to investigate the impact of inflammation on primary omental adipocytes.

Pearce and colleagues (80) explored changes in tissues of the TME during ovarian cancer development and showed a loss of adipose tissue in line with tumour

progression. This study demonstrates adipocyte de-differentiation following inflammation through loss of adipocyte phenotype (Figure 4.5) and adipocyte markers (Figure 4.6). This de-differentiation may represent early stages of fibrosis, whereby adipose tissue function is dysregulated, ECM production is increased leading tissue to become thickened and fibroblast number increases (326). Adipose fibrosis is associated with recruitment of inflammatory macrophages and has been associated with breast cancer development (45). Importantly, loss of adipose tissue is observed in cachexia, a metabolic syndrome associated with ovarian cancer which results in weight loss and muscle wasting and can be the cause of death for ovarian cancer patients (327, 328, 329). Dysregulated energy metabolism and poor nutritional status are associated with circulating pro-inflammatory cytokines (330) and may be a direct result of chronic inflammation (83).

Previous work has shown that adipocytes provide nutrients for ovarian cancer growth via provision of free fatty acids, resulting in upregulation of fatty acid chaperone proteins and increased fatty acid β oxidation in ovarian cancer cells (107, 108, 143, 144). Co-culture experiments with SKOV-3 cells demonstrated a pro-cancer effect for control adipocytes, in line with previous studies. This effect was more pronounced in spheroid culture than 2D monolayer, which may be a result of increased fatty acid uptake under hypoxic conditions, such as those found at the centre of tumour spheroids (161). Importantly, this study demonstrates inflammation of adipocytes results in increased adipocyte lipolysis and fatty acid release, exacerbating pro-cancer effects of adipocytes in co-culture with all cancer cell lines (Figure 4.11, 4.12). Bidirectional signalling is required for these effects to be seen, as inflamed adipocyte secreted factors from monocultures are not sufficient to increase ovarian cancer proliferation (Figure 4.13). The nature and downstream effects of this signalling are

explored in Chapter 5. Direct transfer of fatty acids from adipocytes to EOC cells is demonstrated and is significantly increased in inflamed adipocytes (Figures 4.15, 4.16, 4.17). The effect of inflammation on the pro-tumour effects of adipocyte suggest that previous *in vitro* models may lack important elements of the tumour microenvironment, most notably the presence of a pro-inflammatory microenvironment that promotes adipocyte de-differentiation and fatty acid transfer.

Meta-analyses of clinical data have demonstrated a link between obesity and ovarian cancer (47, 50), and this study proposes a mechanism by which obesity can enhance ovarian cancer growth and promote proliferation in the omental metastatic niche. Obesity is associated with chronic inflammation of adipose tissue, including recruitment and polarization of M1 macrophages (319), as well as adipose fibrosis and metabolic dysregulation including increased fatty acid release (306, 307, 331). Therefore, while the generation of an inflamed microenvironment may occur as a result of metastasizing tumour cells in ascites and the peritoneal TME, the pre-existence of obesity-induced inflammation may promote or exacerbate these mechanisms.

Chapter 5. An Inflammatory Adipose Environment Reduces Ovarian Cancer Response to Cisplatin Therapy

5.1 Introduction

Development of resistance to chemotherapy is a major challenge facing the treatment of ovarian cancer in the clinic. The majority of patients (~70-80%) respond well to standard treatment with platinum- and taxane-based therapy, alongside cytoreductive surgery (332). However, ~50-70% of ovarian cancer patients experience recurrence associated with the development of resistance to chemotherapy (333). Adipocytes have been implicated in regulating epithelial ovarian cancer (EOC) response to therapy and it has been previously been shown that inhibition of fatty acid uptake by fatty acid binding protein 4 (FABP4) in ovarian cancer cells can increase sensitivity to carboplatin therapy (144). It was demonstrated in Chapter 3 that adipocytes can reduce EOC response to paclitaxel therapy by promoting the epithelial-to-mesenchymal transition (EMT), inducing a more aggressive and less chemosensitive phenotype in OVCAR-3 cells.

Mechanisms of bi-directional signalling by which adipocytes might promote resistance to therapy in ovarian cancer have not been thoroughly elucidated. Previous work has shown that interleukin-6 (IL-6) and interleukin 8 (IL-8) can promote EOC homing to the adipocyte-rich omentum (107) and it was demonstrated in Chapter 4 that inflammation of adipocytes, which promotes EOC growth, induced the release of IL-6 and IL-8. The IL-6/IL-6R pathway has been implicated in therapeutic resistance in ovarian cancer and inhibition of IL-6 signalling with anti-IL6R antibody can sensitize EOC cell lines to carboplatin treatment (334). IL-6 secretion has been also shown to be higher in ovarian cancer cells following the development of chemoresistance (335). Similarly, IL-8 has

been associated with EOC response to therapy and immunohistochemical analysis of ovarian metastatic tumours demonstrated IL-8 is associated with poor survival following treatment (336). Knockdown of IL-8 can increase sensitivity to platinum therapy while overexpression of IL-8 can confer therapeutic resistance in EOC cells *in vitro* (109, 337). IL-6 and IL-8 have also been shown to upregulate JAK/STAT signalling, a pathway with well described rolls in cancer cell proliferation and survival (103), as well as lipid metabolism (338).

EOC cells can sequester fatty acids from adipocytes, as shown in Chapter 4. Adipocyte-derived lipids and tumour fatty acid metabolism have been associated with resistance to chemotherapy in a number of cancers (339). In pancreatic cancer, for example, increased fatty acid synthesis in tumour cells is associated with poor response to gemcitabine therapy, which can be improved by inhibition of fatty acid synthase activity (340). In ovarian cancer, cisplatin-resistant cells demonstrate increased fatty acid uptake which may act to overcome therapy-induced oxidative stress (163, 341). As noted above, inhibition of fatty acid uptake into EOC cells can increase sensitivity to platinum therapy (144, 163).

A role for lipid metabolism in chemoresistance links response to therapy to metabolic diseases such as obesity (342). As explored in Chapter 4, obesity increases adipose secretion of free fatty acids and leads to widespread dysregulation of adipose metabolism. Obesity is associated with a poor response to therapy in breast cancer (46, 343) and it has been suggested that obesity-induced hypoxia can prevent drug distribution with adipose-associated tumours (339). It has been hypothesized that reduced membrane fluidity, a result of an increase of saturated fatty acids chains in membrane lipids, can reduce uptake of cytotoxic drugs into cancer cells as a result of altered lipid metabolism in obesity (342).

Observations in Chapter 4 suggest that adipocytes can promote ovarian cancer growth via provision of free fatty acids and an inflamed adipose microenvironment can exacerbate these effects. As such, this study sought to elucidate adipose-derived signalling regulating this phenomenon and identify downstream effects which could regulate adipose – tumour interactions. Given the association previously described between fatty acid metabolism and cancer cell response to therapy, this study explored the impact of adipocyte inflammation on EOC response to therapy.

5.2 Hypotheses and Aims

Hypotheses tested in this chapter were as follows:

- Pro-cancer effects of inflamed adipocytes are the result of bi-directional signalling between cancer cell and adipocyte compartments in co-culture.
- Adipocyte-derived IL-6 and IL-8 regulate ovarian cancer response to an inflamed adipose microenvironment.
- Inflamed adipocytes protect ovarian cancer cells from cisplatin therapy in co-culture.
- STAT3 regulates ovarian cancer response to cisplatin therapy in co-culture with adipocytes.

As such, the aims of this chapter were as follows:

- Explore changes in the secretion and expression of signalling molecules in cancer and adipocyte compartments in co-culture.
- Investigate the role IL-6 and IL-8 in adipocyte-induced changes in cancer activity including changes in proliferation and fatty acid uptake.
- Validate *in vitro* findings using patient samples.

- Explore the impact of adipocyte co-culture on ovarian cancer response to cisplatin therapy.
- Explore the role of STAT3 in adipocyte – EOC interactions via *STAT3* knockdown.

5.3 Materials and Methods

The materials and methods used in this Chapter are described in detail in Section 2.12. Briefly, co-cultures incorporating EOC cell line spheroids with control (untreated) adipocytes and inflamed (125ng/ml TNFα treated) adipocytes. Changes in cell-cell signalling were explored with Luminex assay and Q-RT-PCR and analytes were identified which were upregulated in control and inflamed adipocyte co-cultures. The impact of IL-6 and IL-8 on EOC activity was investigated using exogenous treatment with recombinant IL-6 and IL-8, as well as inhibitory antibodies for IL-6 receptor (IL-6R) and IL-8. Interplay between IL-6 and IL-8 signalling and fatty acid uptake in SKOV-3 cells was investigated using combination treatment with recombinant cytokines and the fatty acid oleic acid or fluorescent fatty acid BODIPY 500/510 C_1 C_{12}. Levels of IL-6 and IL-8 in patient serum were evaluated via ELISA. In order to study the impact of adipocyte co-culture on EOC response to chemotherapy, SKOV-3 cells in co-culture were treated with IC50 for cisplatin. The role of STAT3 in EOC response to therapy was investigated via transfection with silencing RNA (siRNA) for STAT3.

5.4 Cytokine Signalling in Adipocyte – Ovarian Cancer Co-Culture

As demonstrated in Chapter 4, signalling between adipocyte and cancer compartments in co-culture is required to evoke a pro-cancer response in adipocytes (Figure 4.13). To explore the nature of this signalling, changes in cytokines and other signalling molecules in co-cultures were assessed via Luminex assay (Figure. 5.1). Ovarian cancer cell line spheroids were co-cultured with adipocytes for 72 hours, as previously described, and media collected. Concentration of signalling molecules in ovarian cancer cell lines in co-culture with control and inflamed adipocytes was quantified and compared to EOC and adipocyte monocultures. Of note were analytes which were significantly more and less abundant in co-cultures than monocultures. Adiponectin was substantially decreased in co-cultures with EOC cell lines compared to control and inflamed adipocyte monocultures, suggesting further de-differentiation as noted in Chapter 4. CXCL10 was increased in co-culture with inflamed adipocytes relative to inflamed adipocytes alone, but no expression was apparent in control adipocyte co-cultures. IL-2 was significantly down-regulated in co-culture with control adipocytes, but no difference was found in inflamed co-cultures. VEGF was downregulated in co-cultures relative to their adipocyte monoculture counterparts. Most notably, IL-6 and IL-8 were upregulated in co-cultures with both control and inflamed adipocytes, suggesting they may be important regulators of adipocyte – ovarian cancer interactions in both healthy and inflamed adipose microenvironment.

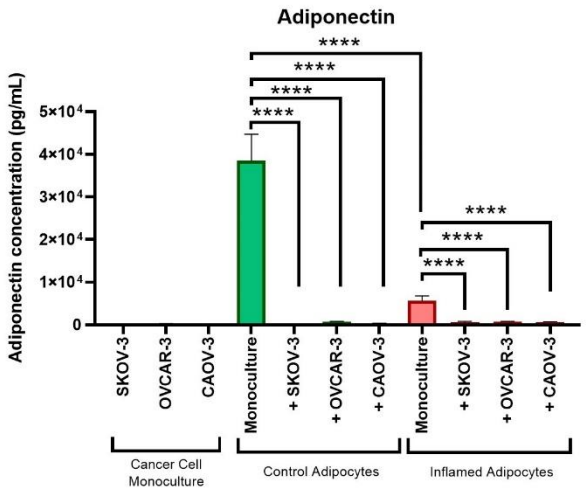
Adiponectin
Adiponectin concentration (pg/mL)
5×10⁴
4×10⁴
3×10⁴
2×10⁴
1×10⁴
0
****
****
****
****
****
****
****
SKOV-3
OVCAR-3
CAOV-3
Monoculture
+ SKOV-3
+ OVCAR-3
+ CAOV-3
Monoculture
+ SKOV-3
+ OVCAR-3
+ CAOV-3
Cancer Cell Monoculture
Control Adipocytes
Inflamed Adipocytes

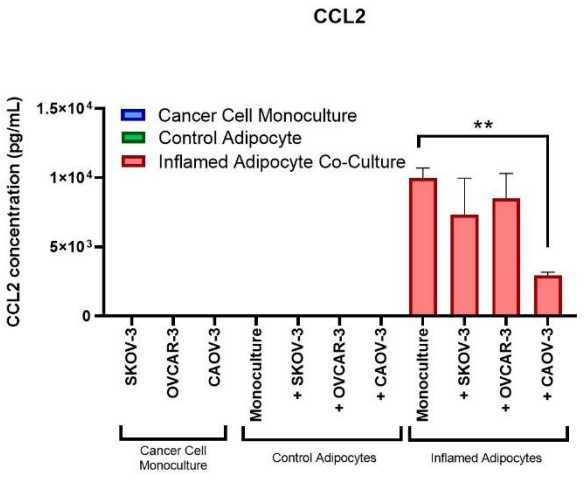
CCL2
CCL2 concentration (pg/mL)
1.5×10⁴
1×10⁴
5×10³
0
Cancer Cell Monoculture
Control Adipocyte
Inflamed Adipocyte Co-Culture
**
SKOV-3
OVCAR-3
CAOV-3
Monoculture
+ SKOV-3
+ OVCAR-3
+ CAOV-3
Monoculture
+ SKOV-3
+ OVCAR-3
+ CAOV-3
Cancer Cell Monoculture
Control Adipocytes
Inflamed Adipocytes

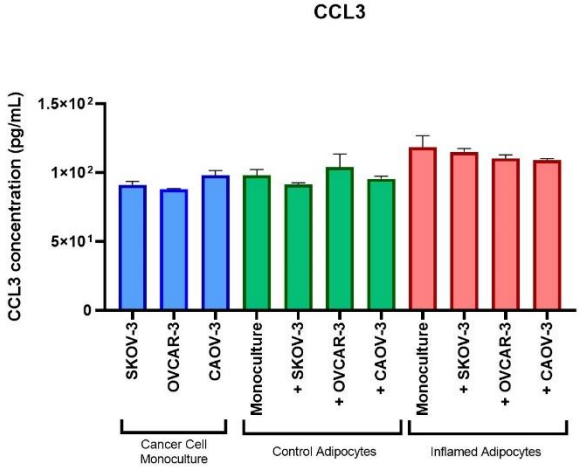
CCL3
CCL3 concentration (pg/mL)
1.5×10²
1×10²
5×10¹
0
SKOV-3
OVCAR-3
CAOV-3
Monoculture
+ SKOV-3
+ OVCAR-3
+ CAOV-3
Monoculture
+ SKOV-3
+ OVCAR-3
+ CAOV-3
Cancer Cell Monoculture
Control Adipocytes
Inflamed Adipocytes

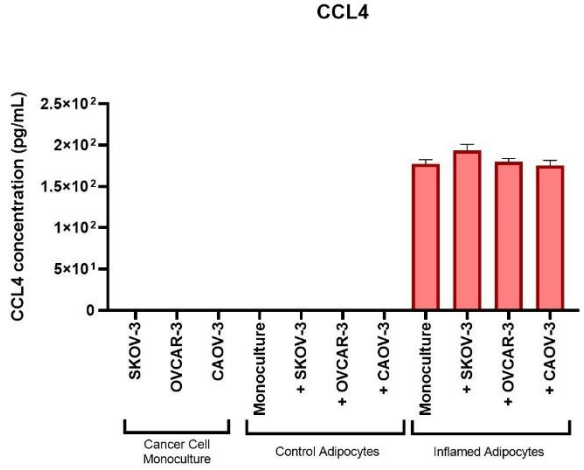
CCL4
CCL4 concentration (pg/mL)
2.5×10²
2×10²
1.5×10²
1×10²
5×10¹
0
SKOV-3
OVCAR-3
CAOV-3
Monoculture
+ SKOV-3
+ OVCAR-3
+ CAOV-3
Monoculture
+ SKOV-3
+ OVCAR-3
+ CAOV-3
Cancer Cell Monoculture
Control Adipocytes
Inflamed Adipocytes

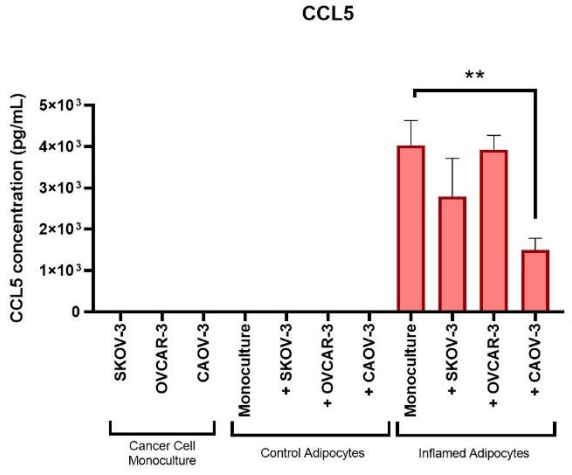
CCL5
CCL5 concentration (pg/mL)
5×10³
4×10³
3×10³
2×10³
1×10³
0
**
SKOV-3
OVCAR-3
CAOV-3
Monoculture
+ SKOV-3
+ OVCAR-3
+ CAOV-3
Monoculture
+ SKOV-3
+ OVCAR-3
+ CAOV-3
Cancer Cell Monoculture
Control Adipocytes
Inflamed Adipocytes

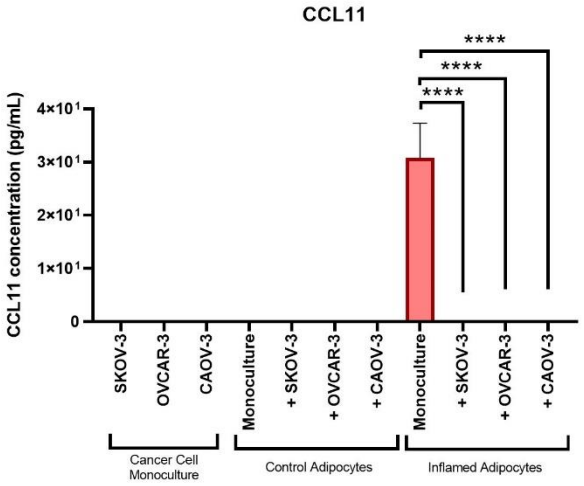
CCL11
CCL11 concentration (pg/mL)
4×10¹
3×10¹
2×10¹
1×10¹
0
****
****
****
SKOV-3
OVCAR-3
CAOV-3
Monoculture
+ SKOV-3
+ OVCAR-3
+ CAOV-3
Monoculture
+ SKOV-3
+ OVCAR-3
+ CAOV-3
Cancer Cell Monoculture
Control Adipocytes
Inflamed Adipocytes

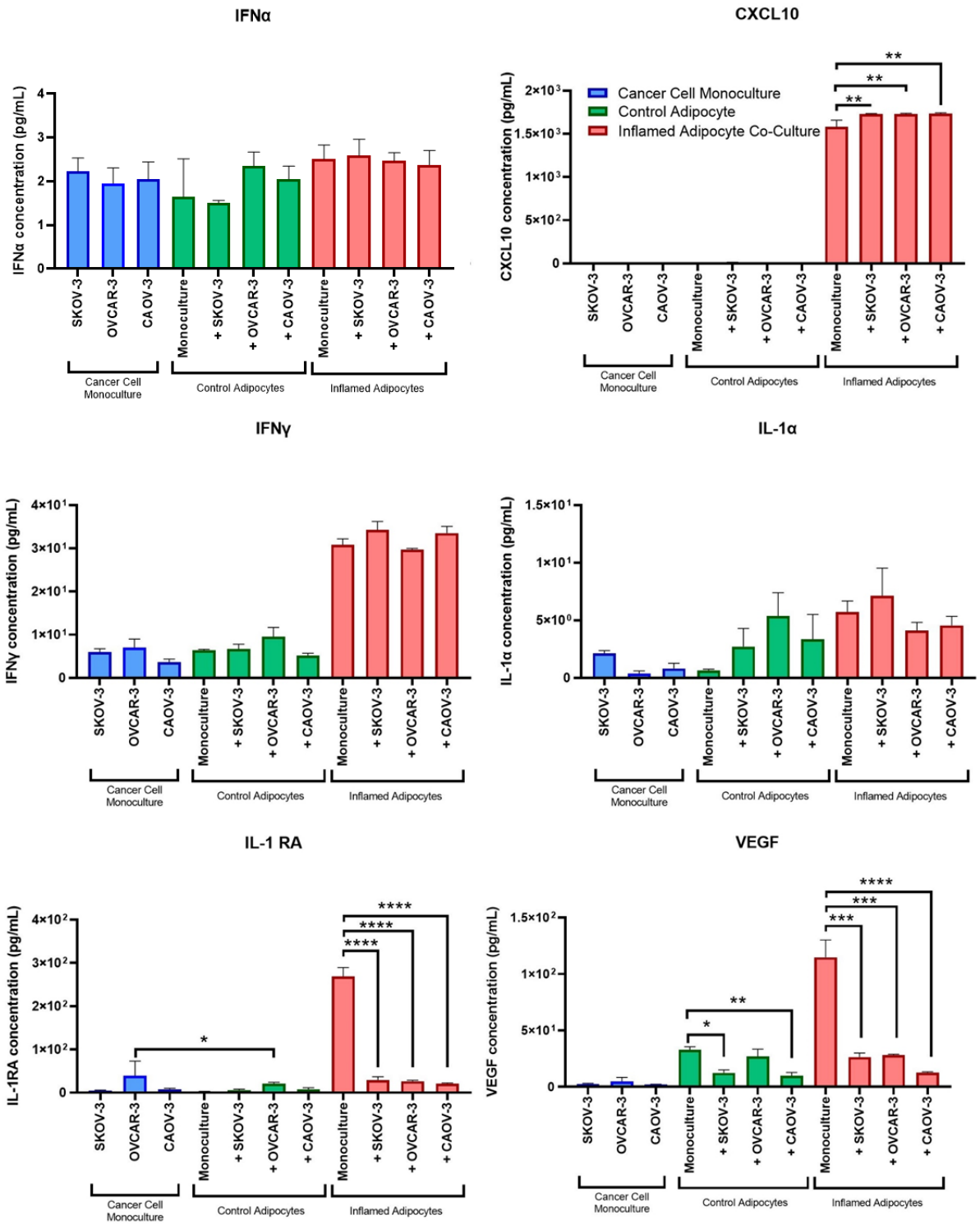
IFNα
IFNα concentration (pg/mL)
CXCL10
CXCL10 concentration (pg/mL)
Cancer Cell Monoculture
Control Adipocyte
Inflamed Adipocyte Co-Culture
IFNγ
IFNγ concentration (pg/mL)
IL-1α
IL-1α concentration (pg/mL)
IL-1 RA
IL-1RA concentration (pg/mL)
VEGF
VEGF concentration (pg/mL)
SKOV-3
OVCAR-3
CAOV-3
Monoculture
+ SKOV-3
+ OVCAR-3
+ CAOV-3
Cancer Cell Monoculture
Control Adipocytes
Inflamed Adipocytes

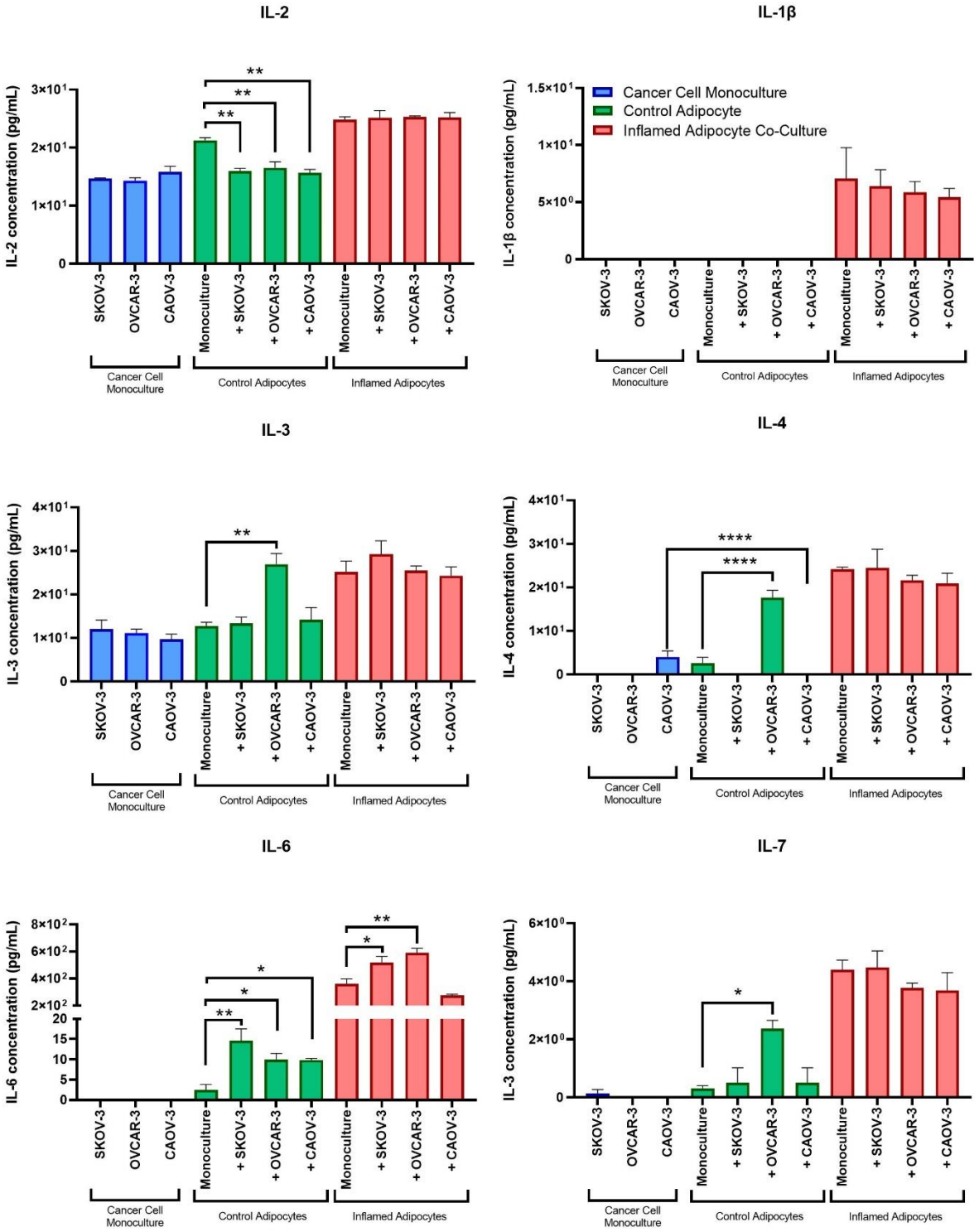
IL-2
IL-2 concentration (pg/mL)
IL-1β
IL-1β concentration (pg/mL)
Cancer Cell Monoculture
Control Adipocyte
Inflamed Adipocyte Co-Culture
IL-3
IL-3 concentration (pg/mL)
IL-4
IL-4 concentration (pg/mL)
IL-6
IL-6 concentration (pg/mL)
IL-7
IL-3 concentration (pg/mL)
SKOV-3
OVCAR-3
CAOV-3
Monoculture
+ SKOV-3
+ OVCAR-3
+ CAOV-3
Cancer Cell Monoculture
Control Adipocytes
Inflamed Adipocytes

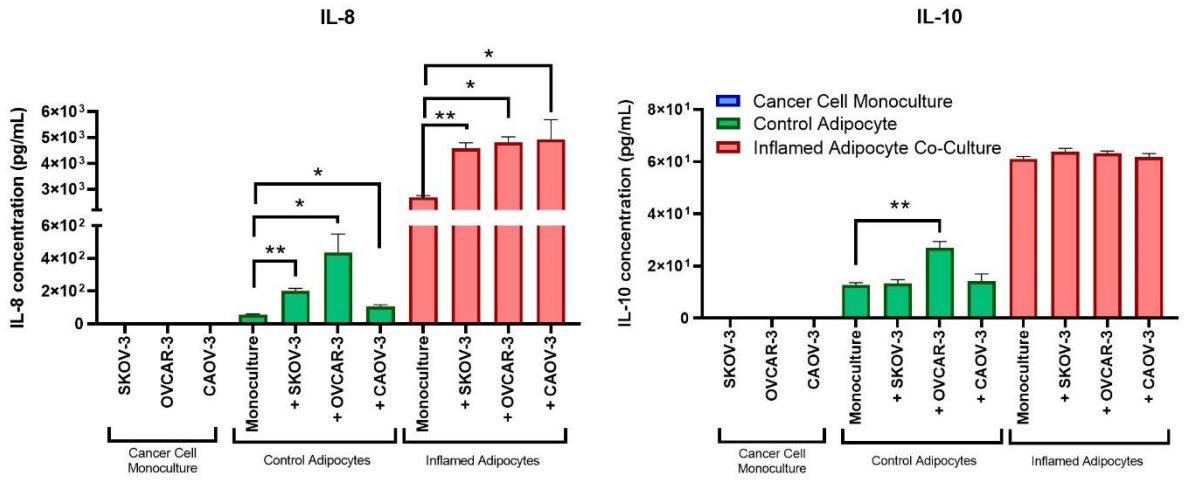

Figure 5.1 Concentration of Signalling Molecules in Co-Culture. *Concentration of Analytes in Media in Adipocyte – EOC co-cultures was quantified by Luminex Assay and compared to monoculture counterparts. Significance noted where appropriate. Bar blots show mean +SD, n=3, *p<0.05, **p<0.001, ***p<0.0001, ****p<0.00001 (One-way ANOVA with Tukey's multiple comparisons test).*

Fold change in analyte concentration was calculated in co-cultures relative to monocultures (co-cultures of EOC cell lines with control adipocytes were compared to control adipocyte monoculture and co-cultures of EOC with inflamed adipocytes compared to inflamed adipocytes) (Figure 5.1) and heat maps were generated (Figure 5.2). As noted previously, IL-6 concentration was significantly increased in media from control and inflamed co-cultures, with the exception of inflamed adipocytes co-cultured with CAOV-3 spheroids. IL-8 concentration was significantly increased in all co-cultures. No secreted IL-6 or IL-8 was found in media from EOC cell line monocultures.

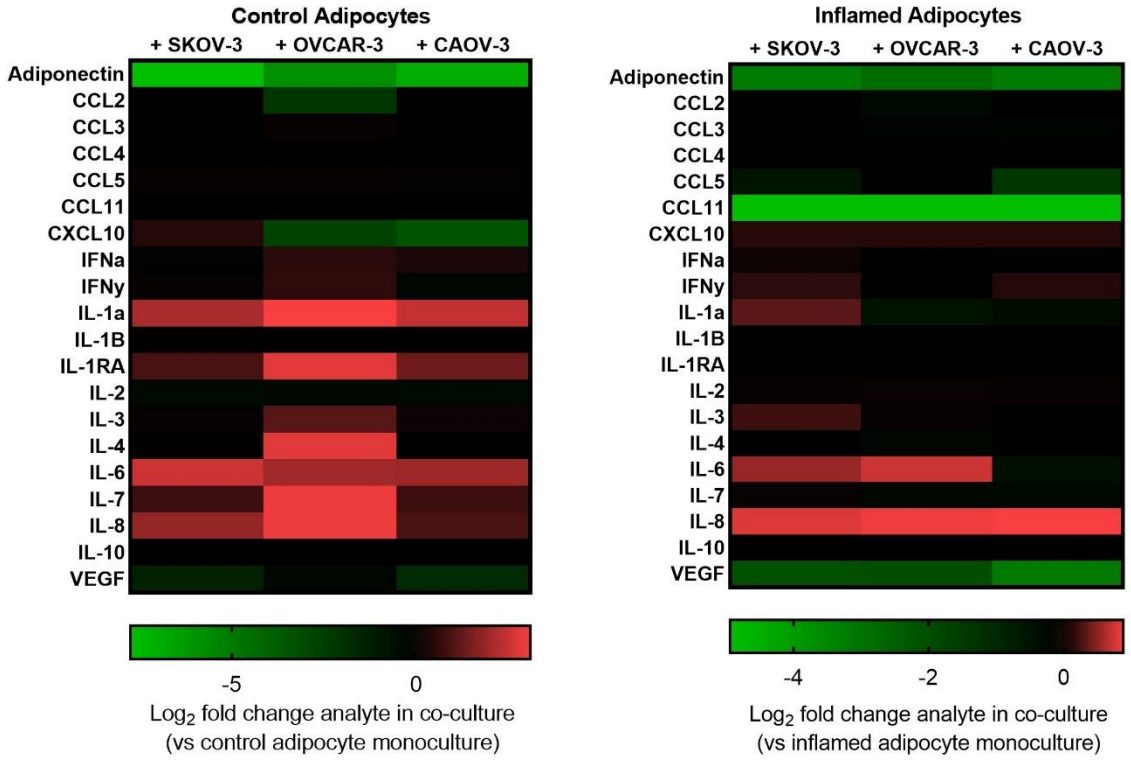

Figure 5.2 Fold Change of Signalling Molecules in Co-Culture. *Summary of data in Figure 5.1. Log_2 fold change in analyte concentration in co-culture media was calculated for EOC cell line spheroids in co-culture with control adipocyte relative to control adipocytes only (left), and for EOC spheroids in co-culture with inflamed adipocyte relative to inflamed adipocytes only (right).*

In order to establish which cells in co-culture were responsible for increases in IL-6 and IL-8, Q-RT-PCR was performed on EOC spheroids and adipocytes following 72 hours of co-culture. *IL-6* expression was significantly increased in control adipocytes and inflamed adipocytes following co-culture with EOC spheroids, excluding inflamed adipocytes in co-culture with CAOV-3 (Figure 5.3). No expression of *IL-6* was detected in EOC spheroids in any culture system.

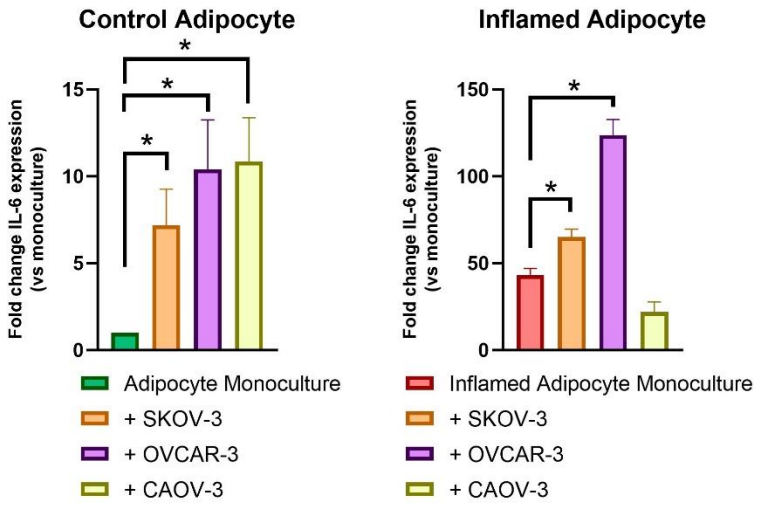

Figure 5.3 IL-6 Expression in Adipocytes in Co-Culture. *Expression of IL-6 in adipocytes in co-culture was explored via Q-RT-PCR. Fold change in gene expression is shown relative to control adipocytes in monoculture. Bar blots show mean +SD, n=3, *p<0.05 (One-way ANOVA with Tukey's multiple comparisons test).*

Similarly, IL-8 (encoded by *CXCL8*) expression was significantly increased in control adipocytes and inflamed adipocytes following co-culture with EOC spheroids. (Figure 5.4). No expression of CXCL8 was detected in EOC spheroids.

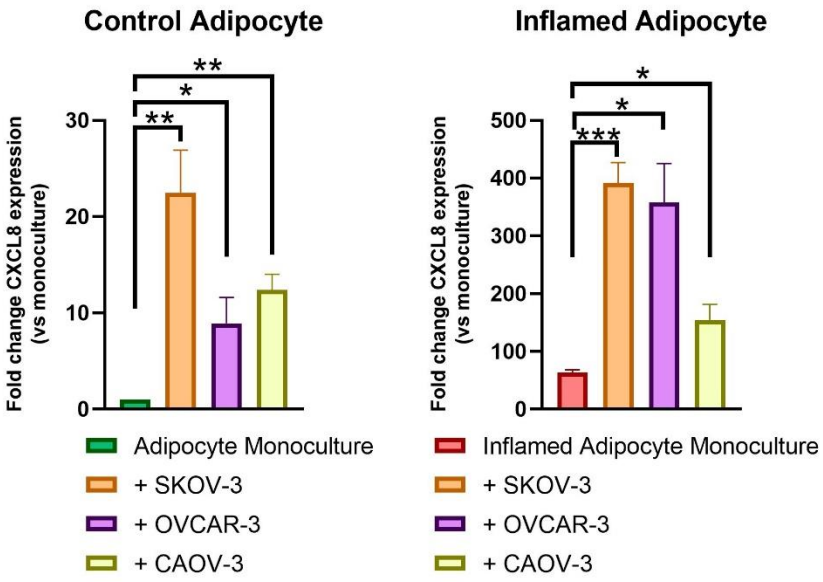

Figure 5.4 IL-8 Expression in Adipocytes Co-Culture. *Expression of CXCL8 (encoding IL-8) in adipocytes in co-culture was explored via Q-RT-PCR. Fold change in gene expression is shown relative to control adipocytes in monoculture. Bar blots show mean +SD, n=3, *p<0.05, **p<0.001, ***p<0.0001 (One-way ANOVA with Tukey's multiple comparisons test).*

It was demonstrated in Chapter 4 that adipocyte or inflamed adipocyte conditioned media (CM) alone was not sufficient to induce an increase in cancer cell proliferation (Figure 4.2). Therefore, it was hypothesized that cancer-secreted factors are required to induce a pro-cancer effect in adipocytes. To test this hypothesis, CM was collected from EOC spheroids and used to treat adipocytes in monolayer culture for 24 hours. A shorter treatment time was chosen relative to co-culture as the half-life of cytokines such as TNFα is short (<24 hours) and therefore changes in gene expression in adipocytes may be transient compared to that seen in co-culture, where signalling between cell types is persistent. The expression of *IL6* and *IL8* in adipocytes following treatment with EOC cell line CM was assessed via Q-RT-PCR and found to be

significantly increased (Figure 5.5). This suggests that EOC cells are able to induce a pro-cancer, inflammatory phenotype in adipocytes.

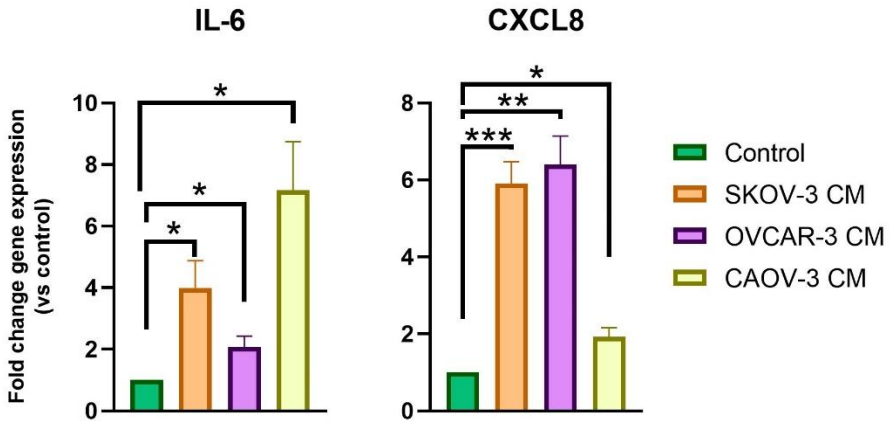

Figure 5.5 IL6 and CXCL8 Expression Adipocytes Following EOC Conditioned Media Treatment. *Expression of IL6 and CXCL8 (encoding IL-8) in adipocytes following 24 hours treatment with ovarian cancer cell line spheroid CM was assessed by Q-RT-PCR. Fold change in gene expression is shown relative to untreated adipocytes. Bar blots show mean +SD, n=3, *p<0.05, **p<0.001, ***p<0.0001 (One-way ANOVA with Tukey's multiple comparisons test).*

It was noted that adiponectin concentration decreased in co-cultures with EOC cell lines relative to adipocyte monocultures (Figures 5.1, 5.2). It was therefore hypothesized that ovarian cancer cells can induce de-differentiation similar to that seen in inflamed adipocytes (Figure 4.9). To test this hypothesis, expression of *ADIPOQ* (encoding adiponectin) and *LPL* (lipoprotein lipase), markers for a mature adipocyte phenotype, was assessed in adipocytes following co-culture via Q-RT-PCR (Figure 5.6). Adiponectin and LPL were both significantly decreased in adipocytes following co-culture with SKOV-3 and CAOV-3 spheroids, indicating that ovarian cancer cells induce significant changes in adipocyte phenotype.

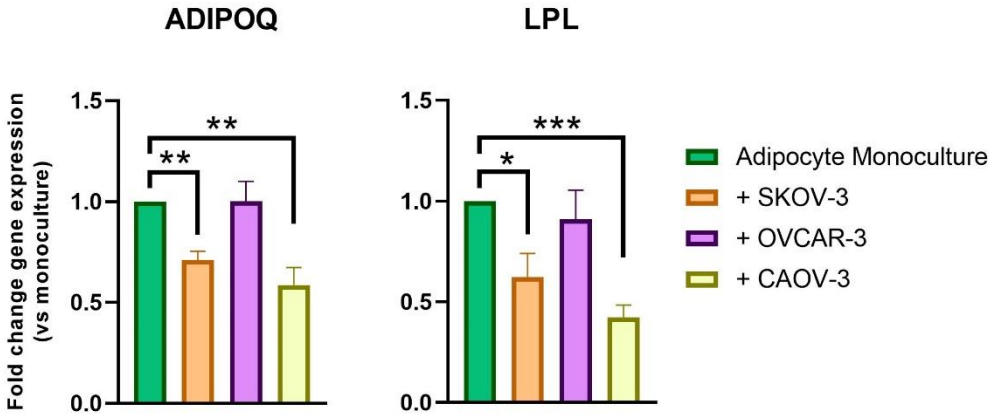

Figure 5.6 Adiponectin and LPL Expression Adipocytes Following Co-Culture. *Expression of ADIPOQ and LPL adipocytes following co-culture with ovarian cancer cell line spheroid. Fold change in gene expression is shown relative to adipocytes in monoculture. Bar blots show mean +SD, n=3, *p<0.05, **p<0.001, ***p<0.0001 (One-way ANOVA with Tukey's multiple comparisons test).*

5.5 Adipocyte-Derived IL-6 Signalling Promotes Ovarian Cancer Proliferation

It had been demonstrated that IL-6 and IL-8 are upregulated in adipocytes in response to ovarian cancer cell signalling (Figures 5.1 – 5.5). To further explore a causal role for IL-6 and IL-8 in adipocyte- and inflamed adipocyte-induced promotion of ovarian cancer proliferation, IL-6 and IL-8 signalling were inhibited in co-culture using antibodies for IL-6 receptor (anti-IL-6R) and IL-8 (anti-IL8). SKOV-3 spheroids were treated with 100ng/ml and 2µg/ml of anti-IL-6R and anti-IL-8 respectively for 72 hours, concurrently with co-culture with adipocytes and inflamed adipocytes, and viability assessed via CellTiter-Glo 3D assay (Figure 5.7). Adipocyte and inflamed adipocyte induced increase in cancer spheroid viability was observed, as previously, with the impact of inflamed adipocytes being greater. IL-6 and IL-8 inhibition had no impact on spheroid viability in monoculture. However, anti-IL-6R treatment of control adipocyte co-culture significantly reduced SKOV-3 spheroid viability compared to control adipocyte co-culture ($p<0.0001$), effectively negating the impact of adipocytes on

SKOV-3 growth. Similarly, anti-IL-6R treatment reversed pro-cancer effects of inflamed adipocytes. No effect of anti-IL-8 treatment was seen in SKOV-3 spheroids, while combination treatment demonstrated similar impact on cancer cell viability to anti-IL6R alone. These data suggest a role for IL-6 signalling in pro-tumour effect seen in adipocyte – EOC co-cultures.

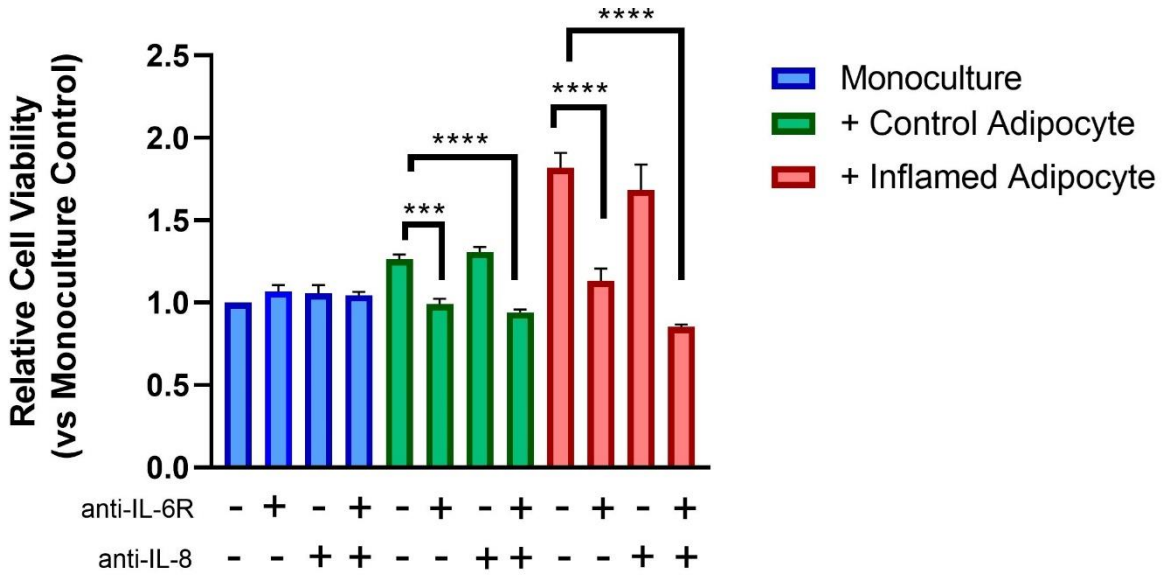

Figure 5.7 Inhibition of IL-6 and IL-8 in Adipocyte – EOC Co-Culture. *SKOV-3 spheroids were treated with single inhibitor and combination anti-IL-6R and anti-IL-8 for 72 hours, concurrently with co-culture with control or inflamed adipocytes. Viability after 72 hours measured by CellTiter-Glo 3D assay. Viability given relative to untreated monoculture. Bar blots show mean +SD, n=5, ***p<0.0001, ****p<0.00005 (One-way ANOVA with Tukey's multiple comparisons test).*

To explore a direct role of IL-6 and IL-8 in ovarian cancer proliferation, EOC cell lines were treated with recombinant IL-6 and IL-8 at concentrations of 1ng/ml, 10ng/ml and 100ng/ml for 72 hours. While higher concentrations are above the highest quantified in co-cultures (Figure 4.1) (~0.6ng/ml for IL-6 and ~4ng/ml for IL-8), cells in co-culture will receive continual signalling over the period of co-culture and therefore higher bulk concentrations were hypothesized to be required for one-off treatment. Treatment with

recombinant IL-6 and IL-8 alone had no impact on EOC cell line spheroid viability (Figure 5.7).

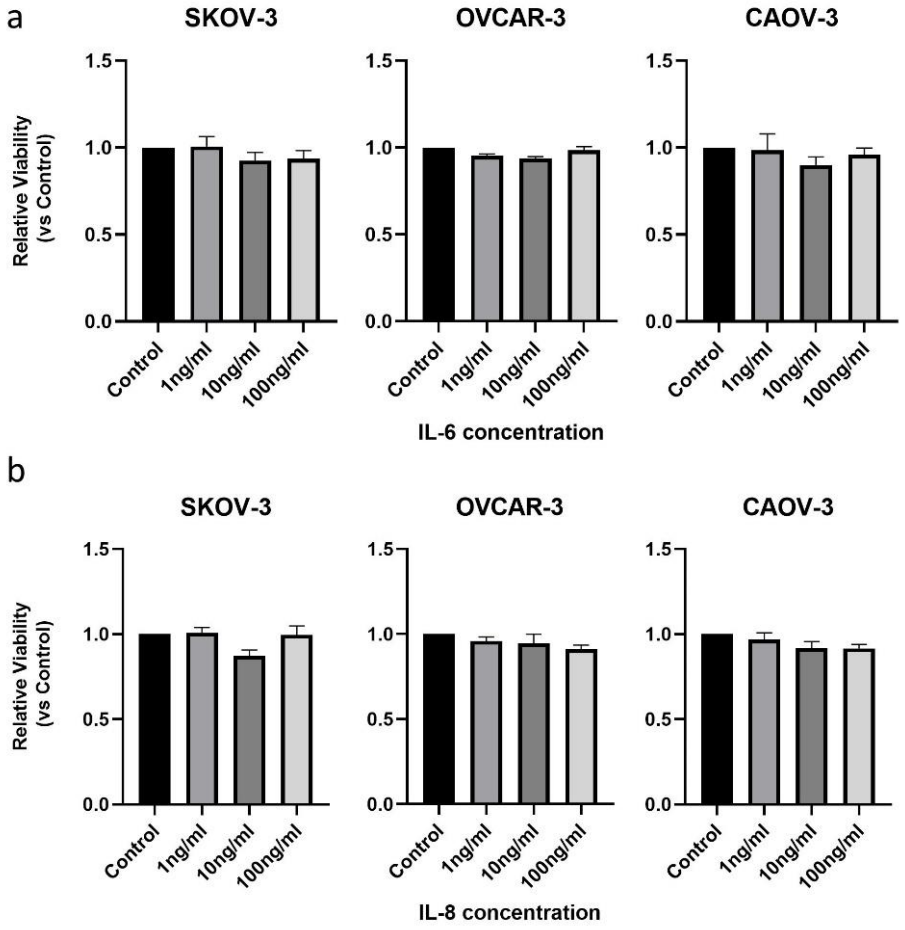

Figure 5.8 Impact of IL-6 and IL-8 on EOC Spheroid Growth. *EOC Spheroids were treated with recombinant IL-6 and IL-8 for 72 hours, viability after 72 hours measured by CellTiter-Glo 3D assay. Viability given relative to untreated control, significance between treatments assessed by One-way ANOVA.*

As previous experiments had shown both IL-6 and IL-8 expression had increased in adipocyte co-culture, it was hypothesized that both IL-6 and IL-8 signalling was required to induce increased cancer spheroid viability in the presence of adipocytes. Therefore, SKOV-3 spheroids were treated with a combination of 100ng/ml recombinant IL-6 and IL-8, as described above. Combination treatment had no impact

on SKOV-3 spheroid growth and was not significantly different to IL-6 and IL-8 treatment alone (Figure 5.8).

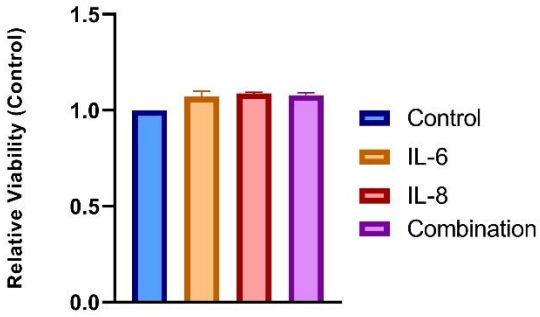

Figure 5.9 Impact of combination IL-6 and IL-8 treatment on EOC Spheroid Growth. *EOC Spheroids were treated with single and combination recombinant IL-6 and IL-8 for 72 hours, viability after 72 hours measured by CellTiter-Glo 3D assay. Viability given relative to untreated control, significance between treatments assessed by One-way ANOVA.*

Inhibition of IL-6 negated pro-cancer effect of control and inflamed adipocytes in co-culture, while IL-6 treatment alone was not sufficient to induce a proliferative effect. These findings suggested that other adipocyte-derived factors were required to increase ovarian cancer growth. Given the established role of free fatty acids in pro-tumour impact of adipocytes, it was hypothesized that increased uptake of fatty acids may play a role in observed phenomena. Therefore, the impact of the fatty acid oleic acid on EOC proliferation was explored. Initially, the effect of oleic acid alone on SKOV-3 spheroid growth was explored. SKOV-3 spheroids were grown for 72 hours following treatment with a range of concentrations of oleic acid (Figure 5.10). SKOV-3 spheroids demonstrated a dose-dependent response to oleic acid treatment, indicating that increased availability and uptake of oleic acid can induce a proliferative effect in EOC cells.

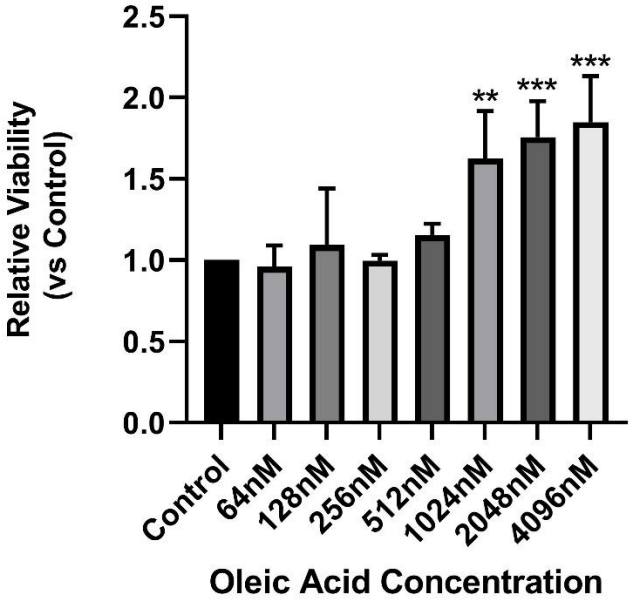

Figure 5.10 Oleic Acid Treatment of SKOV-3 Spheroids. *SKOV-3 spheroids were treated with oleic for 72 hours at concentrations indicated. Viability after 72 hours measured by CellTiter-Glo 3D assay. Viability given relative to untreated monoculture. Bar blots show mean +SD, n=5, **p<0.001, ***p<0.0001 (One-way ANOVA with Tukey's multiple comparisons test).*

To further explore the impact of IL-6 and IL-8 treatment on fatty acid uptake in ovarian cancer cells, the effect of anti-IL-6R and anti-IL-8 antibodies on FABP4 expression in SKOV-3 cells in co-culture was explored. It had previously been demonstrated that co-culture with inflamed adipocytes significantly increases expression of the fatty acid chaperone protein FABP4 in EOC cell lines (Figure 4.17). Therefore, the impact of interleukin inhibition on *FABP4* expression in SKOV-3 spheroids in co-culture with inflamed adipocytes was investigated. SKOV-3 spheroids were co-cultured with inflamed adipocytes for 72 hours and concurrently treated with anti-IL6R and anti-IL8, as well as a combination of both inhibitory antibodies, and the effect on *FABP4* expression assessed via Q-RT-PCR (Figure 5.11). Anti-IL-6R and combination treatment reduced *FABP4* expression relative to untreated SKOV-3 cells in inflamed adipocyte co-culture, while anti-IL8 had no significant impact relative to untreated inflamed adipocyte co-culture.

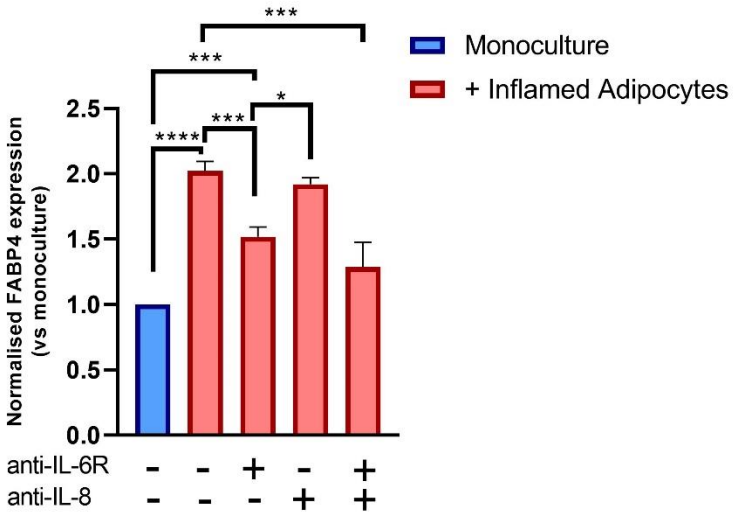

Figure 5.11 Impact of Inhibition of IL-6 and IL-8 on FABP4 Expression in SKOV-3 cells. *SKOV-3 spheroids were treated with anti-IL-6R and anti-IL-8 concurrently with co-culture with inflamed*

*adipocytes for 72 hours before gene expression was assessed via Q-RT-PCR. Bar blots show mean +SD, n=5, ***p<0.0001, ****p<0.00001 (One-way ANOVA with Tukey's multiple comparisons test).*

As both IL-6 and IL-8 promote fatty acid uptake in ovarian cancer cells, it was hypothesized that adipocyte-derived interleukin signalling, and fatty acid release may be responsible for pro-cancer effects observed. To test this hypothesis, SKOV-3 spheroids were treated with combination 1μM oleic acid alongside 100ng/ml recombinant IL-6 and IL-8 for 72 and viability assessed (Figure 5.12). Oleic acid treatment increased SKOV-3 spheroid growth, as previously seen (Figure 5.10). However, combination of oleic acid and IL-6 further increased spheroid growth relative to oleic acid or IL-6 only ($p<0.001$ and $p<0.00001$), indicating that increased fatty acid uptake, resulting from IL-6 signalling, can increase cancer cell proliferation. Combination treatment of IL-8 and oleic acid had no impact on SKOV-3 growth relative to oleic acid only.

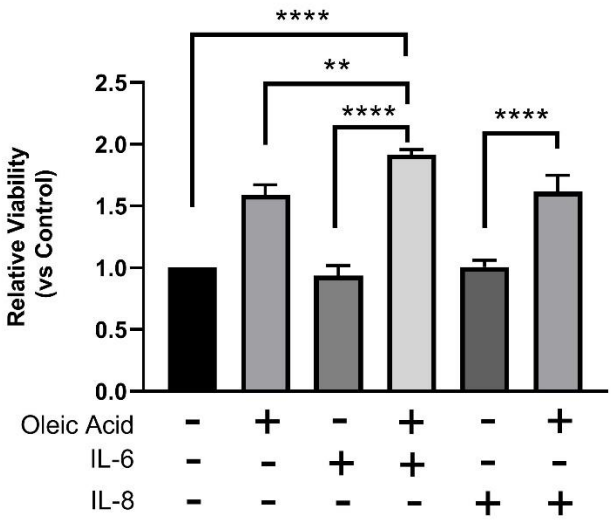

Figure 5.12 Treatment of SKOV-3 Spheroids with Oleic Acid, IL-6 and IL-8. *SKOV-3 spheroids were treated with combinations of IL-6 and IL-8 for 72 hours Viability assessed via CellTiter-Glo 3D assay. Bar blots show mean +SD, n=3, **p<0.001, ****p<0.00001 (One-way ANOVA with Tukey's multiple comparisons test).*

5.6 Inflamed Adipocytes Reduce Ovarian Cancer Cell Response to Cisplatin Therapy

In order to validate observations made in *in vitro* models, levels of cytokines in ovarian cancer patient serum were assessed. Patient samples used in this study are detailed in Chapter 2 (n=45). No differences in cytokine levels were detected between patients diagnosed with different stages of ovarian cancer (Figure 5.13).

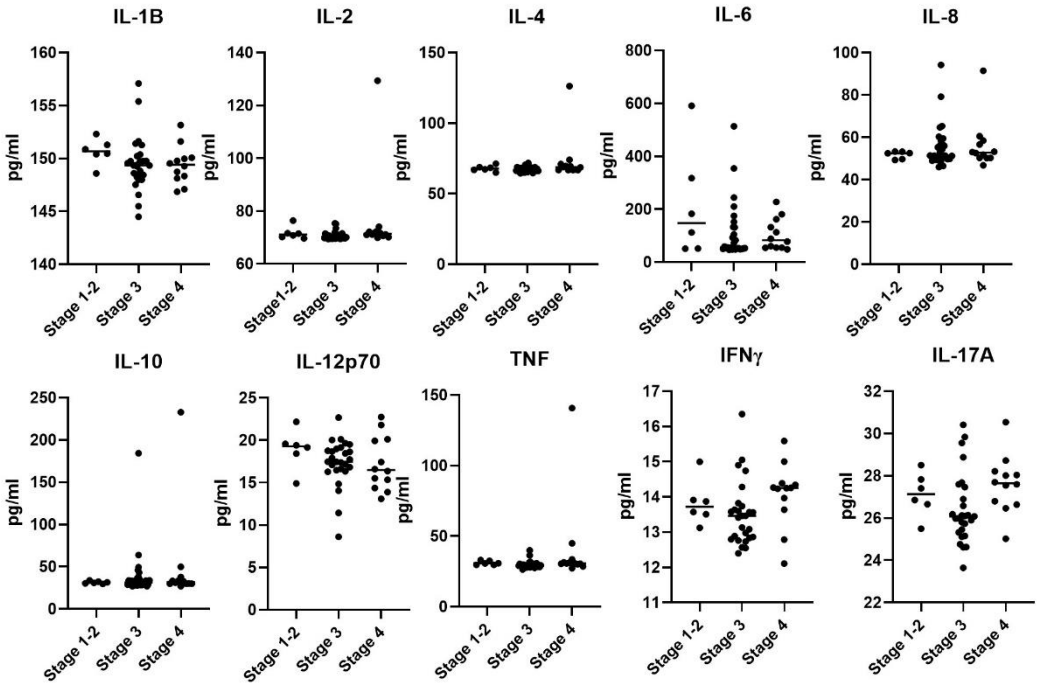

Figure 5.13 Cytokine Concentration in Ovarian Cancer Patient Serum by Stage. *Ovarian cancer patients were grouped by stage of disease and serum levels of cytokines were assessed by ELISA Data points indicate cytokine levels for individual patients, significance assessed by One-way ANOVA. n=45*

While no difference in cytokine levels were observed in patients with different stages of disease, patients were also grouped based on their sensitivity to platinum therapy (n=43). Adipocytes have been previously been shown to play a role in EOC response to therapy (144), a major clinical challenge in the treatment of ovarian cancer and

therefore a role for interleukin signalling was explored. IL-6 and IL-8 were not found to be significantly increased in patients demonstrating partial or complete resistance to therapy, however some resistant patients displayed high levels of IL-6 and IL-8 (Figure 5.14).

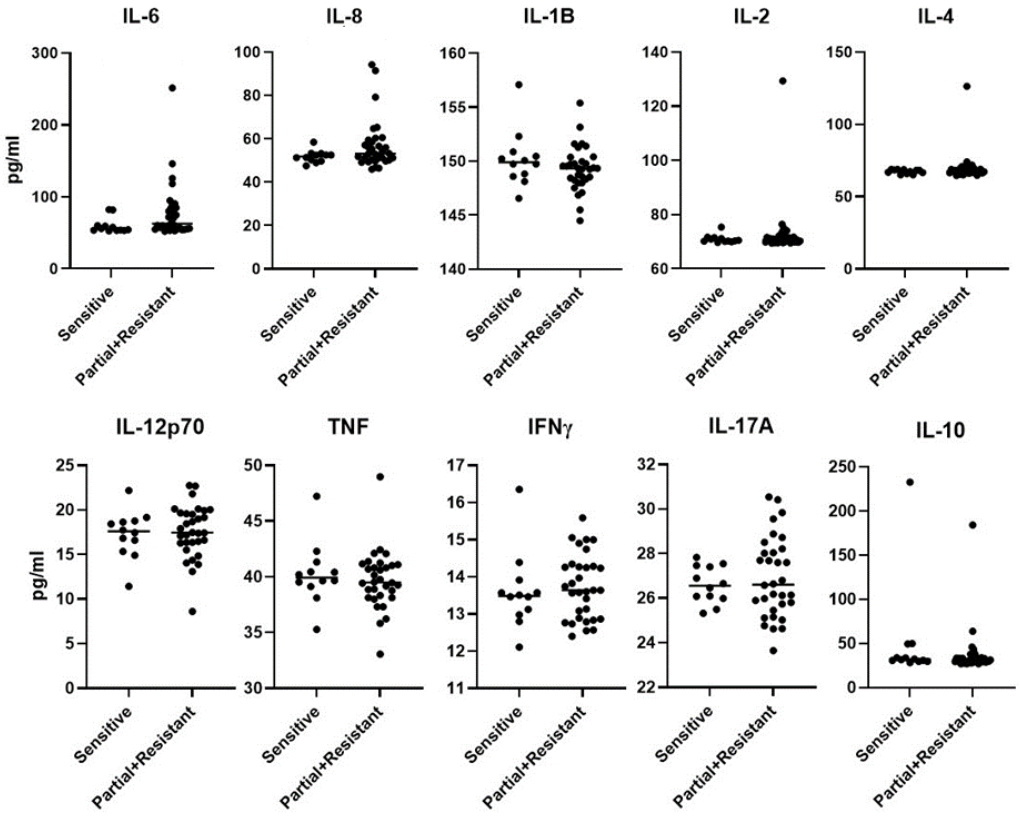

Figure 5.14 Cytokine Concentration in Ovarian Cancer Patient Serum by Platinum Sensitivity. *Ovarian cancer patients were grouped by sensitivity to platinum therapy and serum levels of cytokines were assessed by ELISA. Data points indicate cytokine levels for individual patients. Differences between means assessed via Mann-Whitney test, n=43).*

A role for adipocyte inflammation in EOC response to cisplatin therapy was then explored. Initially, half maximal inhibitory concentration (IC_{50}) of Cisplatin for SKOV-3 cells in monolayer and spheroid culture was established by treatment with a range of concentrations of cisplatin for 72 hours (Figure 5.15a). IC_{50}s were calculated by nonlinear regression fit (Figure 5.15b). Cisplatin IC_{50} for SKOV-3 cells in 2D monolayer and 3D spheroid culture were calculated to be 1.266μM and 19.57μM respectively.

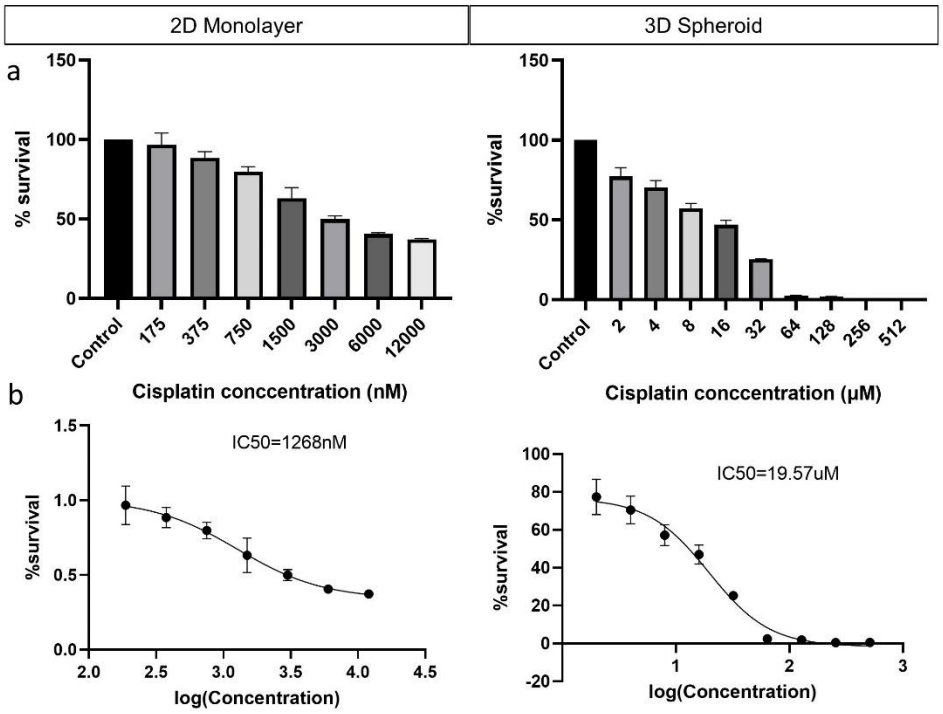

Figure 5.15 Calculation of Cisplatin IC_{50} for SKOV-3 Cells. *SKOV-3 cells in 2D monolayer and 3D spheroid culture were treated with a range of concentrations of Cisplatin for 72 hours (a). IC_{50} was calculated by nonlinear regression (b).*

SKOV-3 cells were then co-cultured with adipocytes and inflamed adipocytes, as well as in monoculture, for 24 hours, prior to treatment with cisplatin IC_{50} for 48 hours with co-culture ongoing. Viability after 72 hours of co-culture (48 hours of cisplatin treatment) was measured (Figure 5.16a, b). SKOV-3 cells in co-culture with inflamed adipocytes displayed significantly higher viability compared to both monoculture and control adipocyte co-culture. Changes in cell survival in cisplatin treated cultures relative to untreated cultures were calculated as % survival to establish the chemoprotective effect of adipocyte co-culture (Figure 5.16c, d). In monolayer and spheroid culture, inflamed adipocytes demonstrated a significant chemoprotective effect when compared to control adipocyte co-culture and monoculture. In SKOV-3 spheroids, control adipocytes also induced a significant chemoprotective effect when compared to monoculture.

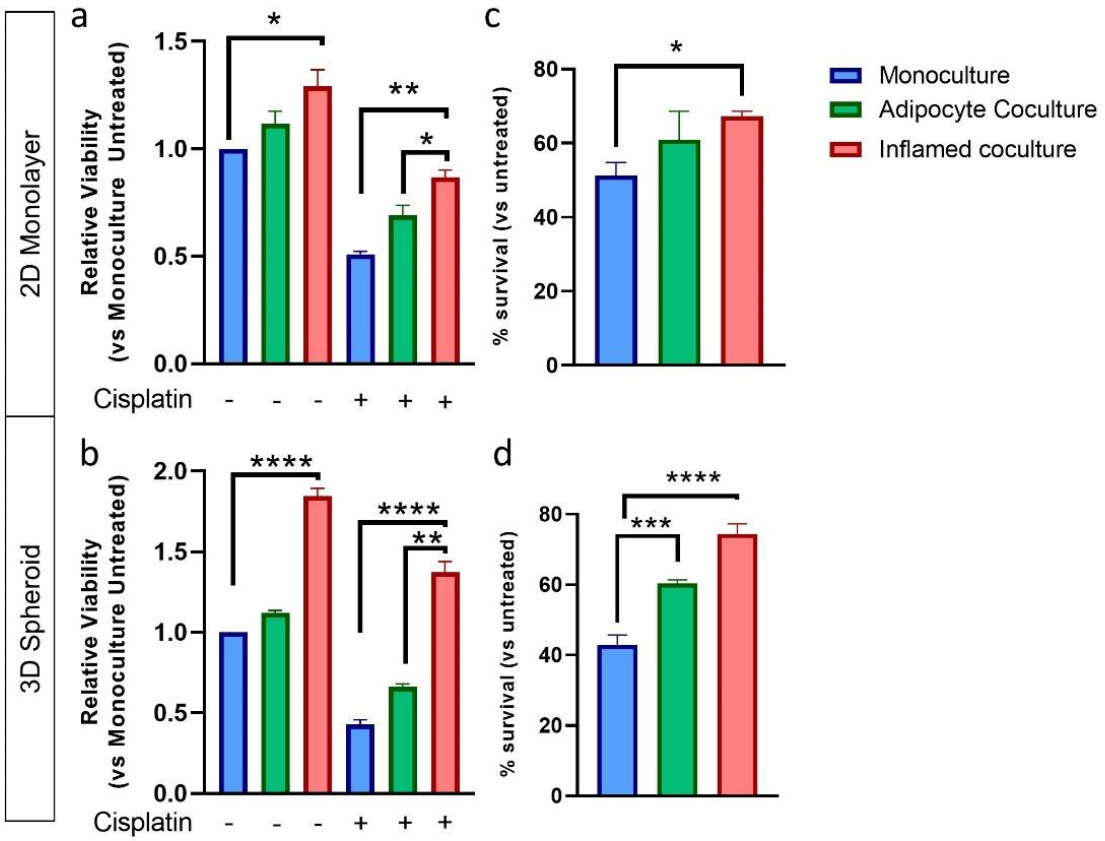

Figure 5.16 Cisplatin Treatment of SKOV-3 Cells in Co-Culture. *SKOV-3 cells in 2D monolayer (a) and 3D spheroid culture (b) in adipocyte co-culture were treated with IC50 Cisplatin for 48 hours. % survival in cisplatin treated cultures was calculated relative to untreated cultures (c,d). Bar blots show mean +SD, n=5, *p<0.05, **p<0.001, ***p<0.0001, ****p<0.00001 (One-way ANOVA with Tukey's multiple comparisons test).*

5.7 STAT3 Regulates Ovarian Cancer Response to Cisplatin Therapy

Given the observed chemoprotective effect of inflamed adipocytes on EOC cells and the potential role of IL-6 and IL-8 in pro-cancer signalling from inflamed adipocytes, potential downstream effects of IL-6 and IL-8 signalling were explored. IL-6 and IL-8 have both been shown to promote the expression of *STAT3*, a transcription factor with

roles in regulating cancer cell proliferation, fatty acid metabolism and response to therapy (338). Initially the impact of treatment of SKOV-3 cells with IL-6 and IL-8 for 24 hours on STAT3 expression was assessed by Q-RT-PCR (Figure 5.17). *STAT3* expression in SKOV-3 cells demonstrated dose-dependent increases upon treatment with both IL-6 and IL-8.

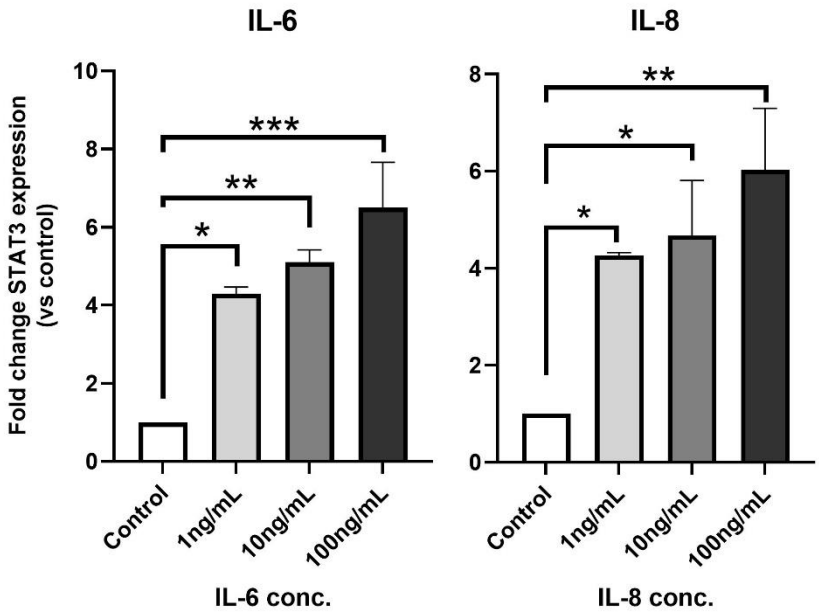

Figure 5.17 STAT3 Expression in IL-6 and IL-8-Treated SKOV-3. *SKOV-3 cells were treated with IL-6 and IL-8 24 hours before gene expression was assessed via Q-RT-PCR. Bar blots show mean +SD, n=3, *p<0.05, **p<0.001, ***p<0.0001 (One-way ANOVA with Tukey's multiple comparisons test).*

Next, the expression of *STAT3* in EOC spheroids in adipocyte co-culture was investigated. EOC cells and adipocytes were co-cultured for 72 hours as described above, and STAT3 expression assessed by Q-RT-PCR (Figure 5.18). Both control and inflamed adipocytes significantly increased *STAT3* expression in EOC cell lines, while in OVCAR-3 *STAT3* expression was significantly increased in inflamed adipocyte co-culture relative to culture with control adipocytes.

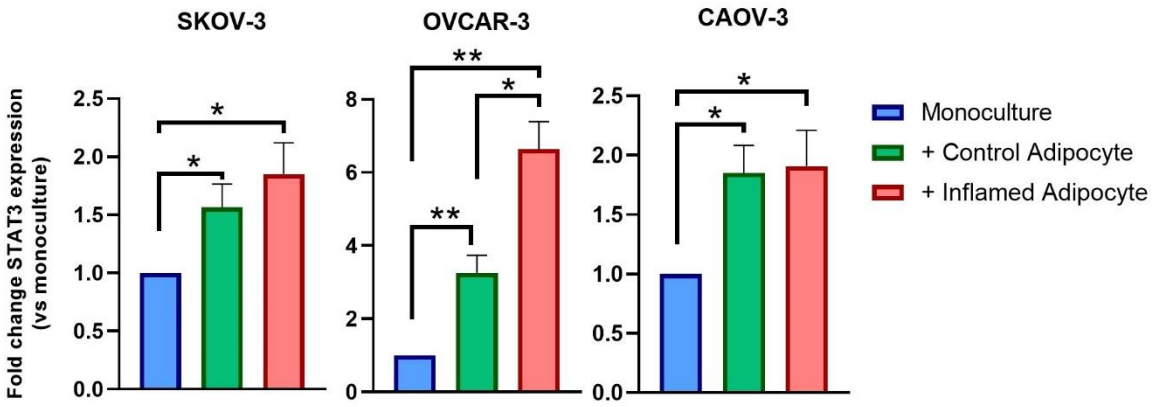

Figure 5.18 STAT3 Expression in EOC Spheroids in Co-Culture. *EOC cell lines were co-cultured with control and inflamed adipocytes before gene expression was assessed via Q-RT-PCR. Bar blots show mean +SD, n=3, *p<0.01, **p<0.001, ***p<0.0001 (One-way ANOVA with Tukey's multiple comparisons test).*

STAT3 is a transcription factor and is activated by phosphorylation, typically at tyrosine residue 705 (Tyr 705). As such, activation of STAT3 by Tyr 705 phosphorylation following co-culture was investigated by immunoblotting (Figure 5.19). Levels of phosphorylated STAT3 were significantly increased in SKOV-3 following co-culture with inflamed adipocytes relative to control adipocytes ($p<0.05$) and SKOV-3 spheroids in monoculture ($p<0.001$). Levels of total STAT3 remained the same in SKOV-3 cells in all culture systems.

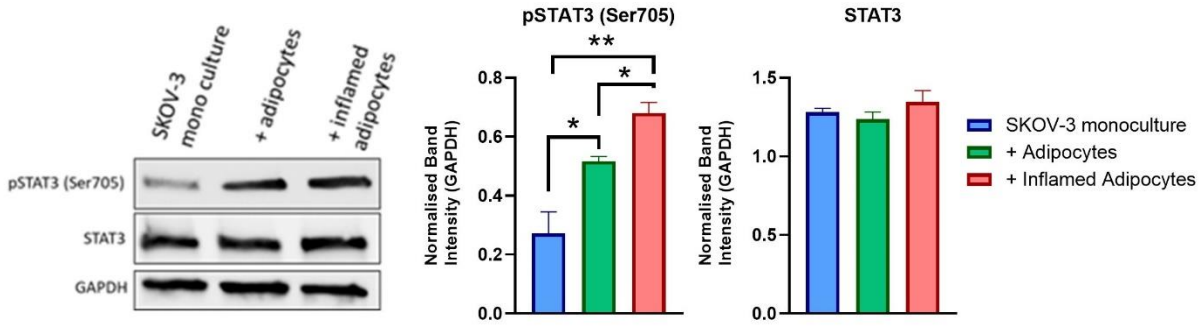

Figure 5.19 Phosphorylation of STAT3 in EOC Spheroids in Co-Culture. *EOC cell lines were co-cultured with control and inflamed adipocytes and phosphorylation of STAT3 was assessed via immunoblotting (Representative blot, left and quantification normalised to GAPDH, right). Bar blots show mean +SD, n=3, *p<0.05, **p<0.001, (One-way ANOVA with Tukey's multiple comparisons test).*

A dramatic difference in IC_{50} between SKOV-3 cells grown in monolayer and spheroid culture had previously been observed (Figure 5.14). STAT3 expression in 2D and 3D cultures was therefore explored as a possible factor in this different response. SKOV-3 cells grown in spheroid culture showed a significantly higher expression of STAT3 than those grown in monolayer ($p<0.05$) (Figure 5.20).

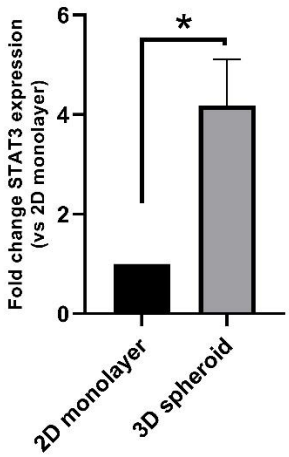

Figure 5.20 STAT3 expression in SKOV-3 Cells in 2D and 3D Culture. *SKOV-3 cells were grown in 2D monolayer and 3D spheroid culture for 72 hours before assessment of STAT3 expression by Q-RT-PCR. STAT3 expression calculated relative to 2D monolayer Bar blots show mean +SD, n=3, *p<0.05, (Student's t-test).*

The role of IL-6 and IL-8 in inflamed adipocyte-induced changes in STAT3 expression were then explored via inhibition of IL-6 and IL-8 signalling by neutralizing antibodies. SKOV-3 spheroids in co-culture with inflamed adipocytes were treated with anti-IL-6R and anti-IL8 as described above and STAT3 expression assessed by Q-RT-PCR (Figure 5.21). Inhibition of IL-6 signalling significantly reduced STAT3 expression in SKOV-3 cells in co-culture with inflamed adipocytes relative to untreated cells in co-culture ($p<0.05$). Anti-IL-8 had no impact on STAT3 expression in SKOV-3 cells in co-culture with inflamed adipocytes, while combination treatment with both antibodies produced similar effects to those seen with IL-6 only. These data suggest that adipocyte-derived IL-6 signalling plays an important role in regulating STAT3 expression in ovarian cancer cells.

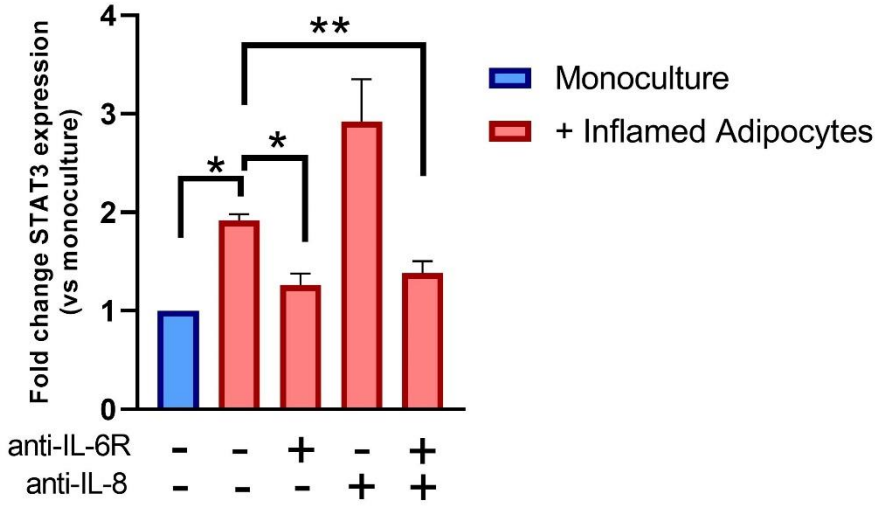

Figure 5.21 STAT3 expression in SKOV-3 Cells Following IL-6 and IL-8 Inhibition. *SKOV-3 cells were grown co-culture with inflamed adipocytes and treated with anti-IL-6R and anti-IL8 antibodies before assessment of STAT3 expression by Q-RT-PCR. Relative STAT3 expression calculated relative to untreated monoculture. Bar blots show mean +SD, n=3, *p<0.05, **p<0.005, One-way ANOVA with Tukey's multiple comparisons test).*

Finally, the role of STAT3 in regulating EOC response to cisplatin therapy was investigated by silencing STAT3 expression in co-culture with siRNA. Initially, STAT3 silencing by siRNA was validated by Q-RT-PCR (Figure 5.22). SKOV-3 cells in monolayer and spheroid culture were treated with STAT3 siRNA for 24 hours and displayed significant reduction in STAT3 expression, approximately 25% of cells treated with control siRNA. This was deemed to be sufficient reduction in STAT3 expression to invoke a significant reduction in STAT3 activity in SKOV-3 cells.

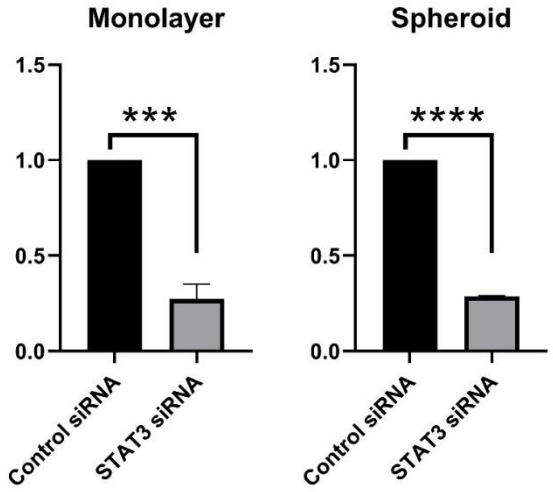

Figure 5.22 STAT3 Knockdown in SKOV-3 by siRNA. *SKOV-3 cells were treated for 24 hours with control siRNA and STAT3 siRNA and STAT3 expression assessed by Q-RT-PCR. Relative STAT3 expression calculated relative to control siRNA. Bar blots show mean +SD, n=3, ***p<0.0001, ****p<0.00001, (Student's t-test).*

STAT3 expression was then knocked down in SKOV-3 cells in co-culture with control and inflamed adipocytes and in monoculture. STAT3 expression was knocked down 24 hours prior to the start of co-culture, and cells were re-treated with siRNA every 24 hours to ensure knockdown was persistent. As described above, SKOV-3 cells were co-cultured for 24 hours before treatment for 48 hours with cisplatin alongside co-

culture. Survival following was calculated relative to untreated cultures (% survival, Figure. 5.23). STAT3 knockdown had no impact on cancer cell survival in monoculture. However, in co-culture with control adipocytes and inflamed adipocytes, STAT3 knockdown significantly reduced survival from cisplatin treatment in 2D and 3D cultures, suggesting STAT3 plays a vital role in adipocyte-induced protection from platinum therapy.

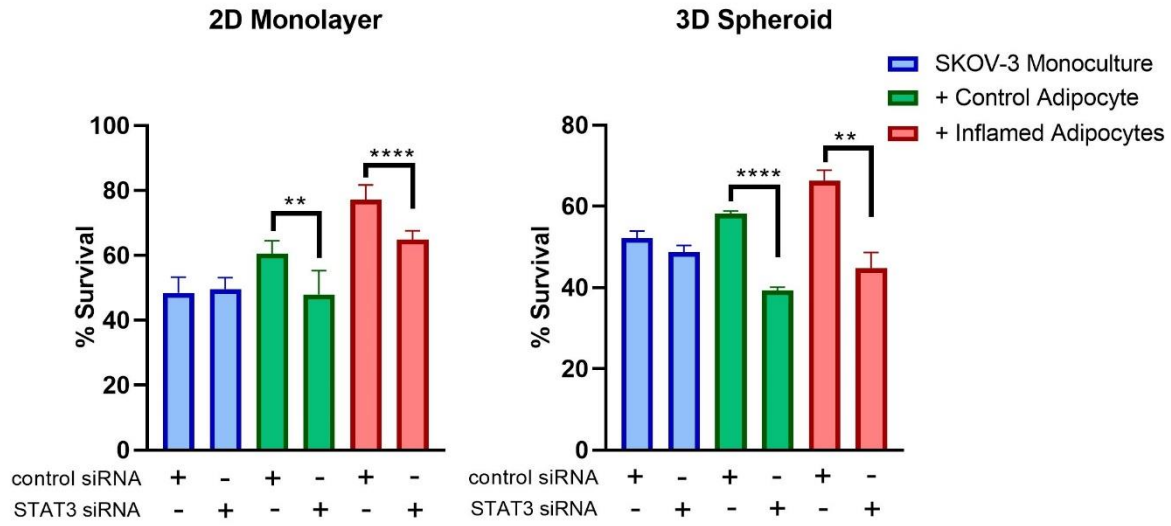

Figure 5.23 STAT3 Knockdown in SKOV-3 in Co-Culture. *SKOV-3 cells were treated for 24 hours with control siRNA and STAT3 siRNA and STAT3 expression assessed by Q-RT-PCR. Relative STAT3 expression calculated relative to control siRNA. Bar blots show mean +SD, n=3, **p<0.001, ****p<0.00015, (Student's t-test).*

5.8 Discussion

Previous work has shown that IL-6 and IL-8 are increased in ovarian cancer co-culture with adipocytes and inhibition of IL-6 and IL-8 signalling can prevent ovarian cancer homing to the omentum in a mouse model (107). Here, Luminex assay revealed significant increases in IL-6 and IL-8 in culture media in adipocyte – EOC co-culture compared to adipocytes alone (Figures 5.1, 5.2). No IL-6 or IL-8 secretion was apparent in EOC cell line monoculture, while Q-RT-PCR assessment revealed increased expression of IL-6 and IL-8 in co-cultured adipocytes but no detectable levels of expression in EOC spheroids. Taken together these data suggest that increases in IL-6 and IL-8 expression is increased in adipocytes in response to ovarian cancer.

IL-6 and IL-8 can both act via autocrine and paracrine signalling and multiple sources for these cytokines in the TME have been identified including tumour cells, macrophages, fibroblasts and adipocytes (337, 344, 345, 346). Wang et al (344) demonstrated IL-6 secretion in SKOV-3 and CAOV-3 via ELISA at concentrations of $2 \times 10^3 – 16 \times 10^3$pg/ml, while here no cytokine was detected. No clear explanation for disparities in results is apparent, however, as IL-6 levels were very high in inflamed adipocytes (5×10^4 pg/ml), samples were heavily diluted prior to assessment by Luminex in order for concentrations to fit within the range of standards, which may have masked lower levels of IL-6 levels in EOC monoculture. In light of previous work, autocrine IL-6 signalling by tumour cannot be excluded as a contributor to cytokine signalling between EOC cells and adipocytes, however these data suggest that contribution of adipocytes is substantially greater. Similarly, the same authors (337) demonstrated IL-8 secretion by SKOV-3 and CAOV-3, which is also reported here but

at negligible levels compared to that of adipocytes. These data support a model in which paracrine signalling from adipocytes, rather than autocrine signalling between tumour cells, is the major component of IL-6 and IL-8 concentration in the ovarian TME.

Secretion of IL-6 and IL-8 was significantly higher in inflamed adipocytes than control adipocytes, with inflamed adipocytes releasing ~100-fold greater concentration. Both IL-6 and IL-8 concentration was significantly increased upon co-culture with EOC cell lines compared to inflamed adipocytes only, and expression of cytokine encoding genes was also increased. It can be concluded that any downstream impact of adipocyte-derived IL-6 and IL-8 signalling will be increased and exacerbated by an inflamed adipose microenvironment.

In Chapter 4, adiponectin concentration was shown to be decreased in inflamed adipocytes, and inflamed adipocytes demonstrated multiple signs of loss of mature adipocyte phenotype (de-differentiation). In this study, adiponectin was significantly decreased in control adipocyte co-culture with cancer cells (Figures 5.1, 5.2 5.6). This suggests that cancer cells alone are sufficient to induce changes in adipocytes similar to those seen upon inflammation, including loss of adipocyte phenotype. Furthermore, co-culture with EOC cells, and treatment with ovarian cancer cell conditioned media, invoked an inflammatory response similar to that seen by treatment with TNFα including increased expression and release of IL-6 and IL-8. These data further suggest that ovarian cancer cells can promote an inflammatory adipose environment with significant pro-cancer metabolic and cytokine secretion profile. Obesity, which is characterized by a state of chronic, low-grade inflammation of adipose tissue, may therefore act to promote ovarian cancer growth and metastasis by ‘pre-treatment’ of

adipose metastatic niche with inflammatory cytokines to pre-empt and compound cancer induced inflammation.

A role for IL-6 signalling pathway as a causal factor in adipocyte – EOC interactions was demonstrated using inhibitory anti-IL6R antibody in co-culture, while exogenous treatment of EOC cell lines with IL-6 alone had no impact on cancer cell proliferation. Associations between IL-6 and ovarian cancer prognosis in patients have been previously described (99, 336, 345), while a role for IL-6 in direct upregulation of EOC proliferation *in vitro* is less well described. One study demonstrated that inhibition of IL-6 expression in SKOV-3 cells can reduce proliferation (105), while others have demonstrated changes in transcription downstream of IL-6 receptor binding activates pro-proliferation pathways (282, 347). In this study it was found that further metabolites are required for IL-6 signalling-induced changes in cancer cell proliferation as co-treatment with IL-6 and the fatty acid oleic acid promoted EOC proliferation where IL-6 alone did not. IL-6 also increased uptake of fatty acids in ovarian cancer cells (Figures 5.12) and expression of fatty acid chaperone protein FABP4. These data support a model in which adipocyte-derived IL-6 signalling, alongside adipocyte-derived fatty acids, drive ovarian cancer growth. While this may seem to contradict a previous study which showed that inhibition of IL-6 expression in SKOV-3 cells can reduce proliferation (105), this study used transfection of SKOV-3 with antisense IL-6, drastically impacting cellular IL-6 pathway and inhibiting autocrine signalling, rather than simulating endogenous paracrine signalling.

The role of IL-8 in adipocyte – EOC interactions based on these data is less clear. Inhibition of IL-8 had no impact on adipocyte-induced changes in EOC proliferation (Figure 5.9) or FABP4 expression (Figure 5.11) and co-treatment of SKOV-3 spheroids with IL-8 and oleic acid had no impact on spheroid viability compared to

oleic acid only. Therefore, these data suggest the role of IL-8 in adipocyte-induced changes in EOC activity are less significant than those of IL-6.

Analysis of patient serum revealed no association between stage of disease and IL-6 concentration (Figure 5.13). Previous studies have shown a correlation between IL-6 and ovarian cancer prognosis (71, 100, 345, 348). However, these studies have either assessed IL-6 levels in ascites fluid as a prognostic factor rather than serum (71, 100) or compared IL-6 expression at the ovarian epithelium between patients with malignant or healthy tissue (345). Scambia and colleagues (348) did investigate serum levels of IL-6, however they found that low levels of IL-6 predicted an improved outcome, rather than a direct correlation between IL-6 concentration and disease stage.

Given the association between IL-6 serum concentration and platinum sensitivity, and the observed increase in IL-6 expression and release in inflamed adipocytes, a role for inflamed adipose microenvironment in EOC response to cisplatin was explored. Co-culture with adipocytes decreased EOC response to therapy, an effect further aggravated by inflammation of adipocytes (Figure 5.16). Lipid metabolism has been linked to drug resistance in number of malignancies (339) and it has been hypothesized that changes in lipid content in cell membrane can inhibit drug uptake into cancer cells (342, 349). Targeting fatty acid uptake (144) and synthesis (350) in ovarian cancer cells can sensitize them to therapy. As such, increased fatty acid uptake of cancer cells as a result of co-culture with inflamed adipocytes (Figure 4.15) may impact response to therapy.

To understand mechanisms by which inflamed adipocytes and adipocyte-derived IL-6 can, potential regulatory factors downstream of IL-6 were explored. A role for IL-6 in

regulating the JAK/STAT pathway in ovarian and other cancer is well established (103). IL-6 binds its receptor (IL-6R), initiating intracellular signalling resulting in the recruitment of Janus kinase (JAK) proteins via gp130. JAK proteins mediate the activation of STAT3 via phosphorylation, resulting in STA3 translocation to the nucleus where it induces the transcription of a broad range of genes, including those involved in proliferation, survival and invasion (351). Here, expression of STAT3 was increased in SKOV-3 cells in co-culture (Figure 5.18) and, importantly, phosphorylation of STAT3 was increased, indicating greater activation (Figure 5.19). Furthermore, inhibition of IL-6 reversed inflamed adipocyte-induced upregulation of STAT3, directly implicating adipocyte-derived IL-6 signalling in STAT3 activity in EOC. Interestingly, STAT3 expression was significantly higher in spheroid culture than monolayer culture and increased levels of STAT3 may play a role in decreased chemosensitivity observed in 3D culture (Figure. 5.15). Knockdown of STAT3 expression in EOC cell lines reversed pro-cancer effects of inflamed adipocytes (Figure 5.23), indicating a regulatory role for STAT3 in adipocyte-induced response to cisplatin therapy. Previous work suggested that knockdown of STAT3 in SKOV-3, with similar efficiency to that seen here, can sensitize cells to cisplatin treatment (352). However, in this work knockdown of STAT3 in untreated cells also caused increased apoptosis and therefore data suggesting cells were sensitized may be the result of a general cytotoxic effect of siRNA transfection. Notably, in EOC cell lines where there was no apoptotic effect for STAT3 siRNA transfection in untreated cells, there was also no difference in groups after cisplatin treatment.

Notably, in addition to well described roles in cancer cell proliferation and survival, STAT3 has also been implicated in regulation of lipid metabolism (338). STAT3 activation can upregulate expression of fatty acid transport proteins FABP4 and CD36

(353, 354) and can increase fatty acid oxidation via upregulation of CPT1 (355). Fatty acid oxidation can, in turn, enhance phospholipid synthesis, leading to changes in mitochondrial membrane potential which inhibits apoptosis (356). In breast cancer, white adipose tissue-derived IL-6 signalling has been shown to upregulate STAT3 activity in tumour cells, promoting metastasis, cancer cell stemness and reducing response to therapy (179, 356). IL-6/STAT3 signalling may, therefore, play a central role in regulating ovarian cancer response to adipocytes. Both IL-6 signalling and STAT3 expression are significantly upregulated in co-culture with inflamed adipocytes, suggesting an explanation for reduced response to therapy and further highlighting a potential mechanism for poor outcomes observed for obese patients. Further work should investigate molecular mechanisms potentially linking STAT3 regulation of fatty acid metabolism to ovarian cancer cell survival and explore therapies which seek to disrupt this signalling mechanism. These data suggest that anti-IL-6 or anti-STAT3 therapies may be more effective in patients with obesity or high adiposity.

Chapter 6. Discussion and Conclusions

No cell is an island, and cancer cells grow and develop in the context of their microenvironment. Non-malignant cells play an important role in all aspects of cancer biology and targeting elements of the tumour stroma has led to the development of novel therapies, including immunotherapy and anti-angiogenic drugs. *In vitro* models which seek to recreate multiple aspects of the TME are important tools in understanding cancer biology and developing new, effective, targeted therapies. In this study, three-dimensional, multicellular models were devised and generated to study interactions between ovarian cancer cells and adipocytes and elucidate the role of adipose tissue in the development of epithelial ovarian cancer (EOC). This study highlights the advantages and limitations of *in vitro* models of the tumour microenvironment (TME). Three-dimensional tumour spheroids can provide insights into the *in vivo* environment and enable aspects of cancer biology not recreated in two-dimensional models. For example, adipocytes induced epithelial-to-mesenchymal transition in OVCAR-3 spheroids but not monolayer populations, potentially due to increased cellular heterogeneity and plasticity in spheroid populations (Section 3.6). Transwell co-culture enables cell compartments to be individually manipulated, for example inflammation of adipocytes prior to co-culture enabled the development of an inflamed phenotype (Section 4.6). The separation of cellular compartments in transwell co-culture also allows for separate analysis to pinpoint, for example, sources of cytokine secretion by gene expression analysis (Section 5.5). Conversely, in vitro co-cultures cannot recapitulate systemic phenomena. Obesity, for example, impacts adipose tissue including adipocytes, fibroblasts, macrophages and other immune cells, and also impacts organism-wide hormone signalling, cytokine levels,

metabolism (168). Obesity is also associated with multiple co-morbidities including insulin resistance, high blood pressure, hyperlipidaemia and high blood sugar levels (195). Such systemic effects will have important implications for the development of cancer and rates of cancer mortality.

Adipose tissue plays an important role in the development of multiple cancers (45). A major role of adipose tissue is a deposit and source of cellular energy, typically in the form of triacylglycerides. Fat, therefore, is a potential source of energy and metabolites required by cancer cells to power rapid proliferation and enable phenotypic changes to drive metastasis and resistance to therapy. In this study, omentum-derived exosomes were shown to promote ovarian cancer proliferation and reduce response to therapy (Section 3.8) and next generation sequencing of exosomal miRNAs revealed high overlap in miRNAs in exosomes derived from omental tissue of patients with ovarian cancer and patients without malignant disease (Section 3.9). Pathways analysis revealed omentum-derived exosomes regulate signalling networks related not only to ovarian cancer but also breast cancer, endometrial cancer, bladder cancer and prostate cancer. This work may, therefore, have implications outside of the ovarian metastatic TME and suggests a role for adipose tissue in generating a pro-cancer environment prior to tumorigenesis or metastasis via secretion of exosomes. A role for adipocyte-derived exosomes in generating a pro-metastatic niche has been suggested in breast cancer (261, 357) and prostate cancer (358) and this study supports such hypotheses. These data are particularly relevant to cancers which metastasize to the omentum, such as colorectal, pancreatic and endometrial, as omentum adipose tissue produced pro-tumorigenic exosomes in the absence of ovarian cancer.

Similarly, risk and mortality for numerous cancers is associated with obesity (191). Characterized by a state of chronic, low-grade inflammation, obesity may contribute to cancer in part by dysregulation of adipocyte lipid metabolism. In this study, inflammation of adipocytes induced lipolysis, resulting in the release of fatty acids and loss of mature adipocyte phenotype (Section 4.4). Cancer cells in multiple malignancies are metabolically reprogrammed to favour, and rely on, fatty acid β oxidation for energy production (159). These data, therefore, suggest a link between obesity and onset of pro-cancer metabolism in adipocytes. Here, co-culture with inflamed adipocytes induced ovarian cancer cell proliferation, however future work incorporating cells from other obesity-related cancers may reveal a more general pro-cancer role for adipocyte inflammation.

This study demonstrates multiple mechanisms by which adipose tissue and adipocytes might impact ovarian cancer development (Figure 6.1). Omental adipose-derived exosomes can induce EMT in EOC cells, increasing their invasive capacity and reducing response to paclitaxel (Section 3.8). Transfection with miRNAs abundant in exosomes can similarly reduce response to chemotherapy (Section 3.9). Given the broad range of roles for exosomes, targeting exosome signalling as a form of therapeutic intervention has received little attention. However, given that cancer cells readily take up exosomes from the TME, exosome-facilitated drug delivery has been proposed as a mechanism for targeting EOC (359, 360). Understanding targeting mechanisms and lipid composition of adipose-derived exosomes could aid in generating exosome-loaded cancer targeted therapies. Given the lack of reliable markers for ovarian cancer, exosomes, and profiles of exosome miRNAs, have also been proposed as markers for ovarian cancer development (360).

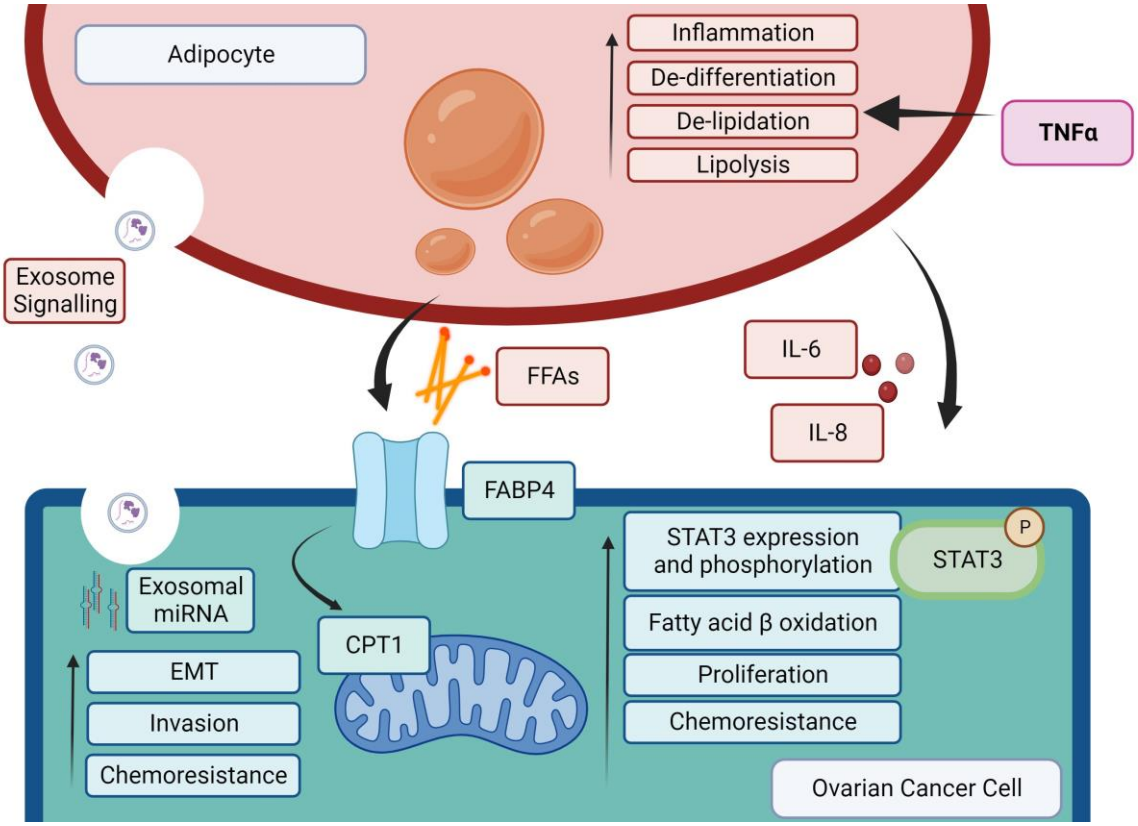

Figure 6.1 Study Summary. *Adipocytes promote ovarian cancer growth and progression. Adipocyte-derived exosome signalling induces EMT, invasion and resistance to therapy in ovarian cancer cells through miRNA transfer. Inflammation of adipocytes with TNFα induces lipolysis and de-differentiation, resulting in secretion of free fatty acids and IL-6 and IL-8. Fatty acid uptake via FABP4 is increased in ovarian cancer cells and promoted by IL-6 signalling, resulting in increased cancer cell proliferation. Inflamed adipocytes increase EOC proliferation by increased fatty acid β oxidation via CPT1. Adipocyte-derived IL-6 signalling induced STAT3 activation, resulting in reduced response to cisplatin therapy. Created with BioRender.com.*

Inflamed adipocytes were shown to promote EOC proliferation through increased transfer of free fatty acids and downstream effects of IL-6 signalling (Sections 4.6, 5.6). In line with previous studies, a pro-cancer effect of adipocytes was demonstrated (107, 143), however this effect was increased upon adipocyte inflammation. This suggests an important role for the inflammatory microenvironment in adipocyte-cancer interactions and demonstrates the importance of incorporating multiple elements of the TME into in *vitro* models of cancer. Multiple strategies have been proposed to

target fatty acid metabolism for anti-cancer drugs (159). Many such drugs target *de novo* fatty acid synthesis, which was not shown to be increased in cancer cells here. Inhibition of acetyl-CoA synthesis has been suggested as a mechanism to target bladder cancer cells over reliance on fatty acid oxidation for energy production, and may also act to overcome cisplatin resistance (361). Etomoxir, used here to inhibit fatty acid oxidation through CPT1, is not FDA approved due to severe off target effects, but increased prominence of tools for targeted therapy may overcome such limitations (313). Drugs targeting dysregulated metabolism may work in concert with established chemotherapy to inhibit tumour-stroma interactions, particularly the impact of adipocytes, and increase sensitization to therapy.

IL-6 signalling has long been recognised as a crucial element of EOC biology and has been proposed as a prognostic factor (345). In line with previous studies, it was shown that adipocyte-derived IL-6 impacts EOC activity (107). IL-6 was shown to induce expression and activation of STAT3, which regulates EOC response to therapy. STAT3 activity is particularly notable in this case as the wide-acting transcription factor may play a role in cancer cell proliferation and chemoresistance but can also regulate lipid metabolism and fatty acid uptake (338). STAT3 may therefore act as a central regulator in EOC response to adipocytes via adipocyte-derived IL-6 signalling. Due to its almost ubiquitous action as a transcription factor, STAT3 has been considered undruggable due to inevitable off target effects. Targeting upstream signalling, in this case IL-6, may therefore enable suppression of STAT3 activity and multiple drugs targeting IL-6, its receptor and downstream JAK activity have been developed (351), while targeting STAT3 modulation of lipid metabolism with plant-derived phytochemicals may inhibit therapeutic resistance (362).

6.1 Study Limitations

There are a number of limitations to this study which could be addressed in future work. Transwell co-cultures used here incorporated adipose-derived stem cell (ADSC)-derived adipocytes, which were morphologically and phenotypically distinct from omental adipocytes. Even between white adipose tissues there exists substantial diversity in gene expression (173), and the characterisation of adipocytes generated in this study is not clear. Phenotypic profiling of ADSC-derived adipocytes would provide important information regarding the applicability of findings to different adipocytes, particularly expression of mitochondrial uncoupling protein 1 (UCP1), associated with brown adipocytes which are, similar to ADSC-derived adipocytes, multilocular (169). In vitro models using omental adipocytes would provide tissue-specific information regarding the response of adipocytes to inflammation and EOC activity. Furthermore, the contribution of immune cells in the adipose microenvironment to inflammation and response to cancer cell signalling is considerable (83, 108, 115) and multicellular models incorporating further cell types would better recapitulate the *in vivo* environment.

6.2 Future Research

This study identifies adipocyte-derived IL-6 signalling as driving EOC response to therapy via STAT3 activation and upregulation. However, downstream mechanisms and signalling are not elucidated. RNA sequencing could provide insights into networks upregulated in cancer cells in co-culture and reveal mechanisms through

which STAT3 modulation might impact proliferation and cisplatin resistance, for example via regulation of lipid metabolism and apoptosis inhibition. Similarly, a wider understanding of changes in gene expression in adipocytes following inflammation and in co-culture would provide information regarding changes in phenotype and metabolic reprogramming, as would lipidomic analysis of lipid species secreted. Technologies which assess changes in cellular metabolism, for example Seahorse metabolic analysis, would better elucidate bi-directional changes in metabolism in adipocyte and cancer cells in co-culture.

The hypotheses tested in *in vitro* models in this study require further testing and validation in *in vivo* models and with patient data. The role of obesity in the impact of adipocytes on ovarian cancer could be explored using diet-induced mouse models of obesity, as has been demonstrated elsewhere (363, 364). Xenograft models using siRNA-induced knockdown of STAT3 in EOC cells would provide further evidence for the role of STAT3 in response to therapy. Similarly, assessment of STAT3 expression and activation in patient tumour samples, particularly in a cohort of patients grouped by response to therapy as seen here, would further test the hypothesis that STAT3 regulates chemoresistance in EOC. Comparisons of samples from primary tumours with those from adipose metastases could test the hypothesis that STAT3 and IL-6 signalling is upregulated in response to adipocytes.

6.3 Conclusions

In summary, this study provides further evidence that adipocytes are important regulators in ovarian cancer progression. Adipose tissue generates a pro-cancer

environment through secretion of exosomes and exosome-derived miRNAs. Inflammation of adipocytes further promotes a pro-cancer phenotype through increased secretion of free fatty acids. These data provide a link between observed associations between multiple malignancies and adiposity and obesity and provide a basis for observed omentum and adipose tropism of EOC and other cancers. This study highlights a novel mechanism by which adipocyte-derived IL-6 signalling can increase fatty acid uptake in ovarian cancer cells and data from primary patient samples suggests an association between IL-6 concentration in serum and cisplatin resistance. Adipocytes can reduce response to cisplatin therapy by IL-6-induced activation of STAT3. These data elucidate novel mechanisms playing a role in EOC disease progression and provide potential novel targets for therapies which seek to overcome chemoresistance in ovarian cancer patients.

Chapter 7. Bibliography

1. Ferlay J, Colombet M, Soerjomataram I, Parkin DM, Piñeros M, Znaor A, et al. Cancer statistics for the year 2020: An overview. International journal of cancer. 2021;149(4):778-89.
2. Siegel RL, Miller KD, Fuchs HE, Jemal A. Cancer statistics, 2021. Ca Cancer J Clin. 2021;71(1):7-33.
3. Dalmartello M, La Vecchia C, Bertuccio P, Boffetta P, Levi F, Negri E, et al. European cancer mortality predictions for the year 2022 with focus on ovarian cancer. Annals of Oncology. 2022;33(3):330-9.
4. Matulonis UA, Sood AK, Fallowfield L, Howitt BE, Sehouli J, Karlan BY. Ovarian cancer. Nature reviews Disease primers. 2016;2(1):1-22.
5. Nogales FF, Dulcey I, Preda O. Germ cell tumors of the ovary: an update. Archives of Pathology and Laboratory Medicine. 2014;138(3):351-62.
6. Schultz KAP, Harris AK, Schneider DT, Young RH, Brown J, Gershenson DM, et al. Ovarian sex cord-stromal tumors. Journal of oncology practice. 2016;12(10):940-6.
7. Cheung A, Shah S, Parker J, Soor P, Limbu A, Sheriff M, et al. Non-epithelial ovarian cancers: how much do we really know? International Journal of Environmental Research and Public Health. 2022;19(3):1106.
8. Lengyel E. Ovarian cancer development and metastasis. The American journal of pathology. 2010;177(3):1053-64.
9. Bowtell DD, Böhm S, Ahmed AA, Aspuria P-J, Bast Jr RC, Beral V, et al. Rethinking ovarian cancer II: reducing mortality from high-grade serous ovarian cancer. Nature reviews Cancer. 2015;15(11):668-79.
10. Torre LA, Trabert B, DeSantis CE, Miller KD, Samimi G, Runowicz CD, et al. Ovarian cancer statistics, 2018. CA: a cancer journal for clinicians. 2018;68(4):284-96.
11. Kurman RJ, Carcangiu ML, Herrington CS. World Health Organisation classification of tumours of the female reproductive organs: International agency for research on cancer; 2014.
12. Shih I-M, Kurman RJ. Ovarian tumorigenesis: a proposed model based on morphological and molecular genetic analysis. The American journal of pathology. 2004;164(5):1511-8.
13. Koshiyama M, Matsumura N, Konishi I. Recent concepts of ovarian carcinogenesis: type I and type II. BioMed research international. 2014;2014.
14. Javadi S, Ganeshan DM, Qayyum A, Iyer RB, Bhosale P. Ovarian cancer, the revised FIGO staging system, and the role of imaging. American Journal of Roentgenology. 2016;206(6):1351-60.
15. Bast R, Feeney M, Lazarus H, Nadler LM, Colvin RB, Knapp RC. Reactivity of a monoclonal antibody with human ovarian carcinoma. The Journal of clinical investigation. 1981;68(5):1331-7.
16. Gupta KK, Gupta VK, Naumann RW. Ovarian cancer: screening and future directions. International Journal of Gynecologic Cancer. 2019;29(1).
17. Buys SS, Partridge E, Black A, Johnson CC, Lamerato L, Isaacs C, et al. Effect of screening on ovarian cancer mortality: the Prostate, Lung, Colorectal and Ovarian (PLCO) cancer screening randomized controlled trial. Jama. 2011;305(22):2295-303.
18. Charkhchi P, Cybulski C, Gronwald J, Wong FO, Narod SA, Akbari MR. CA125 and ovarian cancer: a comprehensive review. Cancers. 2020;12(12):3730.
19. Yurkovetsky ZR, Linkov FY, E Malehorn D, Lokshin AE. Multiple biomarker panels for early detection of ovarian cancer. 2006.
20. Bandiera E, Zanotti L, Fabricio AS, Bucca E, Squarcina E, Romani C, et al. Cancer antigen 125, human epididymis 4, kallikrein 6, osteopontin and soluble mesothelin-related peptide immunocomplexed with immunoglobulin M in epithelial ovarian cancer diagnosis. Clinical chemistry and laboratory medicine. 2013;51(9):1815-24.

21. Goff BA, Mandel LS, Melancon CH, Muntz HG. Frequency of symptoms of ovarian cancer in women presenting to primary care clinics. Jama. 2004;291(22):2705-12.
22. Society AC. Treatment of Invasive Epithelial Ovarian Cancers, by Stage 2022 [Available from: https://www.cancer.org/cancer/types/ovarian-cancer/treating/by-stage.html.
23. Tewari D, Java JJ, Salani R, Armstrong DK, Markman M, Herzog T, et al. Long-term survival advantage and prognostic factors associated with intraperitoneal chemotherapy treatment in advanced ovarian cancer: a gynecologic oncology group study. Journal of Clinical Oncology. 2015;33(13):1460.
24. Wright AA, Cronin A, Milne DE, Bookman MA, Burger RA, Cohn DE, et al. Use and effectiveness of intraperitoneal chemotherapy for treatment of ovarian cancer. Journal of Clinical Oncology. 2015;33(26):2841.
25. Jaaback K, Johnson N, Lawrie TA. Intraperitoneal chemotherapy for the initial management of primary epithelial ovarian cancer. Cochrane database of systematic reviews. 2016(1).
26. Franzese E, Centonze S, Diana A, Carlino F, Guerrera LP, Di Napoli M, et al. PARP inhibitors in ovarian cancer. Cancer Treatment Reviews. 2019;73:1-9.
27. Moore K, Colombo N, Scambia G, Kim B-G, Oaknin A, Friedlander M, et al. Maintenance olaparib in patients with newly diagnosed advanced ovarian cancer. New England Journal of Medicine. 2018;379(26):2495-505.
28. Pujade-Lauraine E, Ledermann JA, Selle F, Gebski V, Penson RT, Oza AM, et al. Olaparib tablets as maintenance therapy in patients with platinum-sensitive, relapsed ovarian cancer and a BRCA1/2 mutation (SOLO2/ENGOT-Ov21): a double-blind, randomised, placebo-controlled, phase 3 trial. The lancet oncology. 2017;18(9):1274-84.
29. Mirza MR, Monk BJ, Herrstedt J, Oza AM, Mahner S, Redondo A, et al. Niraparib maintenance therapy in platinum-sensitive, recurrent ovarian cancer. New England Journal of Medicine. 2016;375(22):2154-64.
30. Coleman RL, Oza AM, Lorusso D, Aghajanian C, Oaknin A, Dean A, et al. Rucaparib maintenance treatment for recurrent ovarian carcinoma after response to platinum therapy (ARIEL3): a randomised, double-blind, placebo-controlled, phase 3 trial. The Lancet. 2017;390(10106):1949-61.
31. Burger RA, Brady MF, Bookman MA, Fleming GF, Monk BJ, Huang H, et al. Incorporation of bevacizumab in the primary treatment of ovarian cancer. New England Journal of Medicine. 2011;365(26):2473-83.
32. Haunschild CE, Tewari KS. Bevacizumab use in the frontline, maintenance and recurrent settings for ovarian cancer. Future Oncology. 2020;16(7):225-46.
33. Rafiyath SM, Rasul M, Lee B, Wei G, Lamba G, Liu D. Comparison of safety and toxicity of liposomal doxorubicin vs. conventional anthracyclines: a meta-analysis. Experimental hematology & oncology. 2012;1:1-9.
34. Enomoto T, Aoki D, Hattori K, Jinushi M, Kigawa J, Takeshima N, et al. The first Japanese nationwide multicenter study of BRCA mutation testing in ovarian cancer: CHARacterizing the cross-sectionaL approach to Ovarian cancer geneTic TEsting of BRCA (CHARLOTTE). International Journal of Gynecologic Cancer. 2019;29(6).
35. Zhang S, Royer R, Li S, McLaughlin JR, Rosen B, Risch HA, et al. Frequencies of BRCA1 and BRCA2 mutations among 1,342 unselected patients with invasive ovarian cancer. Gynecologic oncology. 2011;121(2):353-7.
36. Alsop K, Fereday S, Meldrum C, DeFazio A, Emmanuel C, George J, et al. BRCA mutation frequency and patterns of treatment response in BRCA mutation–positive women with ovarian cancer: a report from the Australian Ovarian Cancer Study Group. Journal of Clinical Oncology. 2012;30(21):2654.
37. Norquist BM, Harrell MI, Brady MF, Walsh T, Lee MK, Gulsuner S, et al. Inherited mutations in women with ovarian carcinoma. JAMA oncology. 2016;2(4):482-90.

38. Reid BM, Permuth JB, Sellers TA. Epidemiology of ovarian cancer: a review. Cancer biology & medicine. 2017;14(1):9.
39. Riman T, Nilsson S, Persson IR. Review of epidemiological evidence for reproductive and hormonal factors in relation to the risk of epithelial ovarian malignancies. Acta obstetricia et gynecologica Scandinavica. 2004;83(9):783-95.
40. Moorman PG, Schildkraut JM, Calingaert B, Halabi S, Vine MF, Berchuck A. Ovulation and ovarian cancer: a comparison of two methods for calculating lifetime ovulatory cycles (United States). Cancer Causes & Control. 2002;13:807-11.
41. Tung K-H, Wilkens LR, Wu AH, McDuffie K, Nomura AM, Kolonel LN, et al. Effect of anovulation factors on pre-and postmenopausal ovarian cancer risk: revisiting the incessant ovulation hypothesis. American journal of epidemiology. 2005;161(4):321-9.
42. Cramer DW, Welch WR. Determinants of ovarian cancer risk. II. Inferences regarding pathogenesis. Journal of the National Cancer Institute. 1983;71(4):717-21.
43. Coughlin SS, Giustozzi A, Smith SJ, Lee NC. A meta-analysis of estrogen replacement therapy and risk of epithelial ovarian cancer. Journal of clinical epidemiology. 2000;53(4):367-75.
44. Garg PP, Kerlikowske K, Subak L, Grady D. Hormone replacement therapy and the risk of epithelial ovarian carcinoma: a meta-analysis. Obstetrics & Gynecology. 1998;92(3):472-9.
45. Lengyel E, Makowski L, DiGiovanni J, Kolonin MG. Cancer as a matter of fat: the crosstalk between adipose tissue and tumors. Trends in cancer. 2018;4(5):374-84.
46. Calle EE, Kaaks R. Overweight, obesity and cancer: epidemiological evidence and proposed mechanisms. Nature Reviews Cancer. 2004;4(8):579-91.
47. Olsen CM, Green AC, Whiteman DC, Sadeghi S, Kolahdooz F, Webb PM. Obesity and the risk of epithelial ovarian cancer: a systematic review and meta-analysis. European journal of cancer. 2007;43(4):690-709.
48. Olsen CM, Nagle CM, Whiteman DC, Ness R, Pearce CL, Pike MC, et al. Obesity and risk of ovarian cancer subtypes: evidence from the Ovarian Cancer Association Consortium. Endocrine-related cancer. 2013;20(2):251-62.
49. Protani MM, Nagle CM, Webb PM. Obesity and ovarian cancer survival: a systematic review and meta-analysis. Cancer prevention research. 2012;5(7):901-10.
50. Nagle C, Dixon S, Jensen A, Kjaer S, Modugno F, DeFazio A, et al. Obesity and survival among women with ovarian cancer: results from the Ovarian Cancer Association Consortium. British journal of cancer. 2015;113(5):817-26.
51. Piek JM, Van Diest PJ, Zweemer RP, Jansen JW, Poort-Keesom RJ, Menko FH, et al. Dysplastic changes in prophylactically removed Fallopian tubes of women predisposed to developing ovarian cancer. The Journal of Pathology: A Journal of the Pathological Society of Great Britain and Ireland. 2001;195(4):451-6.
52. Perets R, Wyant GA, Muto KW, Bijron JG, Poole BB, Chin KT, et al. Transformation of the fallopian tube secretory epithelium leads to high-grade serous ovarian cancer in Brca; Tp53; Pten models. Cancer cell. 2013;24(6):751-65.
53. Clark-Knowles KV, Senterman MK, Collins O, Vanderhyden BC. Conditional inactivation of Brca1, p53 and Rb in mouse ovaries results in the development of leiomyosarcomas. PloS one. 2009;4(12):e8534.
54. Tone AA, Virtanen C, Shaw P, Brown TJ. Prolonged postovulatory proinflammatory signaling in the fallopian tube epithelium may be mediated through a BRCA1/DAB2 axis. Clinical cancer research. 2012;18(16):4334-44.
55. Network CGAR. Integrated genomic analyses of ovarian carcinoma. Nature. 2011;474(7353):609.
56. Bashashati A, Ha G, Tone A, Ding J, Prentice LM, Roth A, et al. Distinct evolutionary trajectories of primary high-grade serous ovarian cancers revealed through spatial mutational profiling. The Journal of pathology. 2013;231(1):21-34.

57. Milner BJ, Allan LA, Eccles DM, Kitchener HC, Leonard RC, Kelly KF, et al. p53 mutation is a common genetic event in ovarian carcinoma. Cancer Research. 1993;53(9):2128-32.
58. Haverty PM, Hon LS, Kaminker JS, Chant J, Zhang Z. High-resolution analysis of copy number alterations and associated expression changes in ovarian tumors. BMC medical genomics. 2009;2:1-15.
59. Iwatsuki M, Mimori K, Yokobori T, Ishi H, Beppu T, Nakamori S, et al. Epithelial–mesenchymal transition in cancer development and its clinical significance. Cancer science. 2010;101(2):293-9.
60. Moreno-Bueno G, Peinado H, Molina P, Olmeda D, Cubillo E, Santos V, et al. The morphological and molecular features of the epithelial-to-mesenchymal transition. Nature protocols. 2009;4(11):1591-613.
61. Haslehurst AM, Koti M, Dharsee M, Nuin P, Evans K, Geraci J, et al. EMT transcription factors snail and slug directly contribute to cisplatin resistance in ovarian cancer. BMC cancer. 2012;12:1-10.
62. Li X, Yang J, Wang X, Liang J, Xing H. Role of TWIST2, E-cadherin and Vimentin in epithelial ovarian carcinogenesis and prognosis and their interaction in cancer progression. European journal of gynaecological oncology. 2016;37(1):100-8.
63. Shield K, Ackland ML, Ahmed N, Rice GE. Multicellular spheroids in ovarian cancer metastases: Biology and pathology. Gynecologic oncology. 2009;113(1):143-8.
64. Latifi A, Luwor RB, Bilandzic M, Nazaretian S, Stenvers K, Pyman J, et al. Isolation and characterization of tumor cells from the ascites of ovarian cancer patients: molecular phenotype of chemoresistant ovarian tumors. 2012.
65. Al Habyan S, Kalos C, Szymborski J, McCaffrey L. Multicellular detachment generates metastatic spheroids during intra-abdominal dissemination in epithelial ovarian cancer. Oncogene. 2018;37(37):5127-35.
66. Gao Q, Yang Z, Xu S, Li X, Yang X, Jin P, et al. Heterotypic CAF-tumor spheroids promote early peritoneal metastasis of ovarian cancer. Journal of Experimental Medicine. 2019;216(3):688-703.
67. Sodek KL, Ringuette MJ, Brown TJ. Compact spheroid formation by ovarian cancer cells is associated with contractile behavior and an invasive phenotype. International journal of cancer. 2009;124(9):2060-70.
68. Matte I, Legault CM, Garde-Granger P, Laplante C, Bessette P, Rancourt C, et al. Mesothelial cells interact with tumor cells for the formation of ovarian cancer multicellular spheroids in peritoneal effusions. Clinical & experimental metastasis. 2016;33:839-52.
69. Yin M, Li X, Tan S, Zhou HJ, Ji W, Bellone S, et al. Tumor-associated macrophages drive spheroid formation during early transcoelomic metastasis of ovarian cancer. The Journal of clinical investigation. 2016;126(11):4157-73.
70. Kipps E, Tan DS, Kaye SB. Meeting the challenge of ascites in ovarian cancer: new avenues for therapy and research. Nature Reviews Cancer. 2013;13(4):273-82.
71. Lane D, Matte I, Rancourt C, Piché A. Prognostic significance of IL-6 and IL-8 ascites levels in ovarian cancer patients. BMC cancer. 2011;11(1):1-6.
72. Ayantunde A, Parsons S. Pattern and prognostic factors in patients with malignant ascites: a retrospective study. Annals of oncology. 2007;18(5):945-9.
73. Ip CK, Li S-S, Tang MY, Sy SK, Ren Y, Shum HC, et al. Stemness and chemoresistance in epithelial ovarian carcinoma cells under shear stress. Scientific reports. 2016;6(1):26788.
74. Hyler AR, Baudoin NC, Brown MS, Stremler MA, Cimini D, Davalos RV, et al. Fluid shear stress impacts ovarian cancer cell viability, subcellular organization, and promotes genomic instability. PloS one. 2018;13(3):e0194170.
75. Rizvi I, Gurkan UA, Tasoglu S, Alagic N, Celli JP, Mensah LB, et al. Flow induces epithelial-mesenchymal transition, cellular heterogeneity and biomarker modulation in 3D ovarian cancer nodules. Proceedings of the National Academy of Sciences. 2013;110(22):E1974-E83.
76. Paget S. The distribution of secondary growths in cancer of the breast. The Lancet. 1889;133(3421):571-3.

77. Fidler IJ. The pathogenesis of cancer metastasis: the'seed and soil'hypothesis revisited. Nature reviews cancer. 2003;3(6):453-8.
78. Strobel T, Cannistra SA. β1-integrins partly mediate binding of ovarian cancer cells to peritoneal mesothelium in vitro. Gynecologic oncology. 1999;73(3):362-7.
79. Slack-Davis JK, Atkins KA, Harrer C, Hershey ED, Conaway M. Vascular cell adhesion molecule-1 is a regulator of ovarian cancer peritoneal metastasis. Cancer research. 2009;69(4):1469-76.
80. Pearce OM, Delaine-Smith RM, Maniati E, Nichols S, Wang J, Böhm S, et al. Deconstruction of a metastatic tumor microenvironment reveals a common matrix response in human cancers. Cancer discovery. 2018;8(3):304-19.
81. Kenny HA, Chiang C-Y, White EA, Schryver EM, Habis M, Romero IL, et al. Mesothelial cells promote early ovarian cancer metastasis through fibronectin secretion. The Journal of clinical investigation. 2014;124(10):4614-28.
82. Loessner D, Rizzi SC, Stok KS, Fuehrmann T, Hollier B, Magdolen V, et al. A bioengineered 3D ovarian cancer model for the assessment of peptidase–mediated enhancement of spheroid growth and intraperitoneal spread. Biomaterials. 2013;34(30):7389-400.
83. Macciò A, Madeddu C. Inflammation and ovarian cancer. Cytokine. 2012;58(2):133-47.
84. Radke J, Schmidt D, Böhme M, Schmidt U, Weise W, Morenz J. -Cytokine level in malignant ascites and peripheral blood of patients with advanced ovarian carcinoma. Geburtshilfe und Frauenheilkunde. 1996;56(2):83-7.
85. Savant SS, Sriramkumar S, O'Hagan HM. The role of inflammation and inflammatory mediators in the development, progression, metastasis, and chemoresistance of epithelial ovarian cancer. Cancers. 2018;10(8):251.
86. Lee L-F, Hellendall RP, Wang Y, Haskill JS, Mukaida N, Matsushima K, et al. IL-8 reduced tumorigenicity of human ovarian cancer in vivo due to neutrophil infiltration. The Journal of Immunology. 2000;164(5):2769-75.
87. Haskill S, Becker S, Fowler W, Walton L. Mononuclear-cell infiltration in ovarian cancer. I. Inflammatory-cell infiltrates from tumour and ascites material. British Journal of Cancer. 1982;45(5):728-36.
88. Ramakrishnan S, Xu F, Brandt S, Niedel J, Bast R, Brown E. Constitutive production of macrophage colony-stimulating factor by human ovarian and breast cancer cell lines. The Journal of clinical investigation. 1989;83(3):921-6.
89. Robinson-Smith TM, Isaacsohn I, Mercer CA, Zhou M, Van Rooijen N, Husseinzadeh N, et al. Macrophages mediate inflammation-enhanced metastasis of ovarian tumors in mice. Cancer research. 2007;67(12):5708-16.
90. Gerber SA, Rybalko VY, Bigelow CE, Lugade AA, Foster TH, Frelinger JG, et al. Preferential attachment of peritoneal tumor metastases to omental immune aggregates and possible role of a unique vascular microenvironment in metastatic survival and growth. The American journal of pathology. 2006;169(5):1739-52.
91. Clark R, Krishnan V, Schoof M, Rodriguez I, Theriault B, Chekmareva M, et al. Milky spots promote ovarian cancer metastatic colonization of peritoneal adipose in experimental models. The American journal of pathology. 2013;183(2):576-91.
92. Kulbe H, Chakravarty P, Leinster DA, Charles KA, Kwong J, Thompson RG, et al. A dynamic inflammatory cytokine network in the human ovarian cancer microenvironment. Cancer research. 2012;72(1):66-75.
93. Oh K, Moon H-G, Lee D-S, Yoo Y-B. Tissue transglutaminase-interleukin-6 axis facilitates peritoneal tumor spreading and metastasis of human ovarian cancer cells. Laboratory Animal Research. 2015;31:188-97.
94. Takaishi K, Komohara Y, Tashiro H, Ohtake H, Nakagawa T, Katabuchi H, et al. Involvement of M2-polarized macrophages in the ascites from advanced epithelial ovarian carcinoma in tumor progression via Stat3 activation. Cancer science. 2010;101(10):2128-36.

95. Yeung T-L, Leung CS, Wong K-K, Samimi G, Thompson MS, Liu J, et al. TGF-β modulates ovarian cancer invasion by upregulating CAF-derived versican in the tumor microenvironment. Cancer research. 2013;73(16):5016-28.
96. Devreotes P, Horwitz AR. Signaling networks that regulate cell migration. Cold Spring Harbor perspectives in biology. 2015;7(8):a005959.
97. Zhang M, Chen Z, Wang Y, Zhao H, Du Y. The role of cancer-associated fibroblasts in ovarian cancer. Cancers. 2022;14(11):2637.
98. Givel A-M, Kieffer Y, Scholer-Dahirel A, Sirven P, Cardon M, Pelon F, et al. miR200-regulated CXCL12β promotes fibroblast heterogeneity and immunosuppression in ovarian cancers. Nature communications. 2018;9(1):1056.
99. Browning L, Patel MR, Horvath EB, Tawara K, Jorcyk CL. IL-6 and ovarian cancer: Inflammatory cytokines in promotion of metastasis. Cancer management and research. 2018:6685-93.
100. Sanguinete MMM, Oliveira PHD, Martins-Filho A, Micheli DC, Tavares-Murta BM, Murta EFC, et al. Serum IL-6 and IL-8 correlate with prognostic factors in ovarian cancer. Immunological investigations. 2017;46(7):677-88.
101. Kolomeyevskaya N, Eng KH, Khan ANH, Grzankowski KS, Singel KL, Moysich K, et al. Cytokine profiling of ascites at primary surgery identifies an interaction of tumor necrosis factor-α and interleukin-6 in predicting reduced progression-free survival in epithelial ovarian cancer. Gynecologic oncology. 2015;138(2):352-7.
102. Lo C-W, Chen M-W, Hsiao M, Wang S, Chen C-A, Hsiao S-M, et al. IL-6 trans-signaling in formation and progression of malignant ascites in ovarian cancer. Cancer research. 2011;71(2):424-34.
103. Liang R, Chen X, Chen L, Wan F, Chen K, Sun Y, et al. STAT3 signaling in ovarian cancer: a potential therapeutic target. Journal of Cancer. 2020;11(4):837.
104. Rabinovich A, Medina L, Piura B, Segal S, Huleihel M. Regulation of ovarian carcinoma SKOV-3 cell proliferation and secretion of MMPs by autocrine IL-6. Anticancer research. 2007;27(1A):267-72.
105. Wang Y, Li L, Guo X, Jin X, Sun W, Zhang X, et al. Interleukin-6 signaling regulates anchorage-independent growth, proliferation, adhesion and invasion in human ovarian cancer cells. Cytokine. 2012;59(2):228-36.
106. Kim S, Gwak H, Kim HS, Kim B, Dhanasekaran DN, Song YS. Malignant ascites enhances migratory and invasive properties of ovarian cancer cells with membrane bound IL-6R in vitro. Oncotarget. 2016;7(50):83148.
107. Nieman KM, Kenny HA, Penicka CV, Ladanyi A, Buell-Gutbrod R, Zillhardt MR, et al. Adipocytes promote ovarian cancer metastasis and provide energy for rapid tumor growth. Nature medicine. 2011;17(11):1498-503.
108. Nieman KM, Romero IL, Van Houten B, Lengyel E. Adipose tissue and adipocytes support tumorigenesis and metastasis. Biochimica et Biophysica Acta (BBA)-Molecular and Cell Biology of Lipids. 2013;1831(10):1533-41.
109. Stronach EA, Cunnea P, Turner C, Guney T, Aiyappa R, Jeyapalan S, et al. The role of interleukin-8 (IL-8) and IL-8 receptors in platinum response in high grade serous ovarian carcinoma. Oncotarget. 2015;6(31):31593.
110. Wang Y, Xu RC, Zhang XL, Niu XL, Qu Y, Li LZ, et al. Interleukin-8 secretion by ovarian cancer cells increases anchorage-independent growth, proliferation, angiogenic potential, adhesion and invasion. Cytokine. 2012;59(1):145-55.
111. Hirose K, Hakozaki M, Nyunoya Y, Kobayashi Y, Matsushita K, Takenouchi T, et al. Chemokine gene transfection into tumour cells reduced tumorigenicity in nude mice in association with neutrophilic infiltration. British journal of cancer. 1995;72(3):708-14.

112. Yung MM-H, Tang HW-M, Cai PC-H, Leung TH-Y, Ngu S-F, Chan KK-L, et al. GRO-α and IL-8 enhance ovarian cancer metastatic potential via the CXCR2-mediated TAK1/NFκB signaling cascade. Theranostics. 2018;8(5):1270.
113. Gupta M, Babic A, Beck AH, Terry K. TNF-α expression, risk factors, and inflammatory exposures in ovarian cancer: evidence for an inflammatory pathway of ovarian carcinogenesis? Human pathology. 2016;54:82-91.
114. Szlosarek PW, Grimshaw MJ, Kulbe H, Wilson JL, Wilbanks GD, Burke F, et al. Expression and regulation of tumor necrosis factor α in normal and malignant ovarian epithelium. Molecular cancer therapeutics. 2006;5(2):382-90.
115. Cheng H, Wang Z, Fu L, Xu T. Macrophage polarization in the development and progression of ovarian cancers: an overview. Frontiers in oncology. 2019;9:421.
116. Zhang M, He Y, Sun X, Li Q, Wang W, Zhao A, et al. A high M1/M2 ratio of tumor-associated macrophages is associated with extended survival in ovarian cancer patients. Journal of ovarian research. 2014;7(1):1-16.
117. Cho U, Kim B, Kim S, Han Y, Song YS. Pro-inflammatory M1 Macrophage enhances metastatic potential of ovarian cancer cells through NF-κB activation. Molecular carcinogenesis. 2018;57(2):235-42.
118. Lau T, Chan LK, Wong EC, Hui CW, Sneddon K, Cheung T, et al. A loop of cancer-stroma-cancer interaction promotes peritoneal metastasis of ovarian cancer via TNFα-TGFα-EGFR. Oncogene. 2017;36(25):3576-87.
119. Wang Y, Ma J, Shen H, Wang C, Sun Y, Howell SB, et al. Reactive oxygen species promote ovarian cancer progression via the HIF-1α/LOX/E-cadherin pathway. Oncology reports. 2014;32(5):2150-8.
120. Wortzel I, Dror S, Kenific CM, Lyden D. Exosome-mediated metastasis: communication from a distance. Developmental cell. 2019;49(3):347-60.
121. D'Souza-Schorey C, Schorey JS. Regulation and mechanisms of extracellular vesicle biogenesis and secretion. Essays in Biochemistry. 2018;62(2):125-33.
122. Mathieu M, Martin-Jaular L, Lavieu G, Théry C. Specificities of secretion and uptake of exosomes and other extracellular vesicles for cell-to-cell communication. Nature cell biology. 2019;21(1):9-17.
123. Zhang Y, Liu Y, Liu H, Tang WH. Exosomes: biogenesis, biologic function and clinical potential. Cell & bioscience. 2019;9(1):1-18.
124. Costa-Silva B, Aiello NM, Ocean AJ, Singh S, Zhang H, Thakur BK, et al. Pancreatic cancer exosomes initiate pre-metastatic niche formation in the liver. Nature cell biology. 2015;17(6):816-26.
125. Bobrie A, Krumeich S, Reyal F, Recchi C, Moita LF, Seabra MC, et al. Rab27a supports exosome-dependent and-independent mechanisms that modify the tumor microenvironment and can promote tumor progression. Cancer research. 2012;72(19):4920-30.
126. Peinado H, Alečković M, Lavotshkin S, Matei I, Costa-Silva B, Moreno-Bueno G, et al. Melanoma exosomes educate bone marrow progenitor cells toward a pro-metastatic phenotype through MET. Nature medicine. 2012;18(6):883-91.
127. Nakamura K, Sawada K, Kinose Y, Yoshimura A, Toda A, Nakatsuka E, et al. Exosomes promote ovarian cancer cell invasion through transfer of CD44 to peritoneal mesothelial cells. Molecular Cancer Research. 2017;15(1):78-92.
128. Yokoi A, Yoshioka Y, Yamamoto Y, Ishikawa M, Ikeda S-i, Kato T, et al. Malignant extracellular vesicles carrying MMP1 mRNA facilitate peritoneal dissemination in ovarian cancer. Nature communications. 2017;8(1):14470.
129. Cho JA, Park H, Lim EH, Kim KH, Choi JS, Lee JH, et al. Exosomes from ovarian cancer cells induce adipose tissue-derived mesenchymal stem cells to acquire the physical and functional characteristics of tumor-supporting myofibroblasts. Gynecologic oncology. 2011;123(2):379-86.

130. Giusti I, Di Francesco M, D'Ascenzo S, Palmerini MG, Macchiarelli G, Carta G, et al. Ovarian cancer-derived extracellular vesicles affect normal human fibroblast behavior. Cancer biology & therapy. 2018;19(8):722-34.
131. Nakamura K, Sawada K, Kobayashi M, Miyamoto M, Shimizu A, Yamamoto M, et al. Role of the exosome in ovarian cancer progression and its potential as a therapeutic target. Cancers. 2019;11(8):1147.
132. Chen X, Zhou J, Li X, Wang X, Lin Y, Wang X. Exosomes derived from hypoxic epithelial ovarian cancer cells deliver microRNAs to macrophages and elicit a tumor-promoted phenotype. Cancer letters. 2018;435:80-91.
133. Chen X, Ying X, Wang X, Wu X, Zhu Q, Wang X. Exosomes derived from hypoxic epithelial ovarian cancer deliver microRNA-940 to induce macrophage M2 polarization. Oncology reports. 2017;38(1):522-8.
134. Iwagoi Y, Motohara T, Hwang S, Fujimoto K, Ikeda T, Katabuchi H. Omental metastasis as a predictive risk factor for unfavorable prognosis in patients with stage III–IV epithelial ovarian cancer. International journal of clinical oncology. 2021;26:995-1004.
135. Steinberg J, Demopoulos RI, Bigelow B. The evaluation of the omentum in ovarian cancer. Gynecologic oncology. 1986;24(3):327-30.
136. Meza-Perez S, Randall TD. Immunological functions of the omentum. Trends in immunology. 2017;38(7):526-36.
137. Morison R. Remarks ON SOME FUNCTIONS OF THE OMENTUM. Br Med J. 1906;1(2350):76-8.
138. Bergman RN, Van Citters GW, Mittelman SD, Dea MK, Hamilton-Wessler M, Kim SP, et al. Central role of the adipocyte in the metabolic syndrome. Journal of Investigative Medicine. 2001;49(1):119-26.
139. O'Connell J, Lynch L, Cawood TJ, Kwasnik A, Nolan N, Geoghegan J, et al. The relationship of omental and subcutaneous adipocyte size to metabolic disease in severe obesity. PloS one. 2010;5(4):e9997.
140. Kanai H, Matsuzawa Y, Kotani K, Keno Y, Kobatake T, Nagai Y, et al. Close correlation of intra-abdominal fat accumulation to hypertension in obese women. Hypertension. 1990;16(5):484-90.
141. Maury E, Ehala-Aleksejev K, Guiot Y, Detry R, Vandenhooft A, Brichard SM. Adipokines oversecreted by omental adipose tissue in human obesity. American Journal of Physiology-Endocrinology and Metabolism. 2007;293(3):E656-E65.
142. Harman-Boehm I, Blüher M, Redel H, Sion-Vardy N, Ovadia S, Avinoach E, et al. Macrophage infiltration into omental versus subcutaneous fat across different populations: effect of regional adiposity and the comorbidities of obesity. The Journal of Clinical Endocrinology & Metabolism. 2007;92(6):2240-7.
143. Ladanyi A, Mukherjee A, Kenny HA, Johnson A, Mitra AK, Sundaresan S, et al. Adipocyte-induced CD36 expression drives ovarian cancer progression and metastasis. Oncogene. 2018;37(17):2285-301.
144. Mukherjee A, Chiang C-Y, Daifotis HA, Nieman KM, Fahrmann JF, Lastra RR, et al. Adipocyte-induced FABP4 expression in ovarian cancer cells promotes metastasis and mediates carboplatin resistance. Cancer research. 2020;80(8):1748-61.
145. Mukherjee A, Bezwada D, Greco F, Zandbergen M, Shen T, Chiang C-Y, et al. Adipocytes reprogram cancer cell metabolism by diverting glucose towards glycerol-3-phosphate thereby promoting metastasis. Nature Metabolism. 2023:1-15.
146. Miranda F, Mannion D, Liu S, Zheng Y, Mangala LS, Redondo C, et al. Salt-inducible kinase 2 couples ovarian cancer cell metabolism with survival at the adipocyte-rich metastatic niche. Cancer cell. 2016;30(2):273-89.
147. Warburg O. The metabolism of carcinoma cells. The Journal of Cancer Research. 1925;9(1):148-63.
148. Fouad YA, Aanei C. Revisiting the hallmarks of cancer. American journal of cancer research. 2017;7(5):1016.

149. Stine ZE, Schug ZT, Salvino JM, Dang CV. Targeting cancer metabolism in the era of precision oncology. Nature reviews Drug discovery. 2022;21(2):141-62.
150. DeBerardinis RJ, Chandel NS. Fundamentals of cancer metabolism. Science advances. 2016;2(5):e1600200.
151. Dibble CC, Manning BD. Signal integration by mTORC1 coordinates nutrient input with biosynthetic output. Nature cell biology. 2013;15(6):555-64.
152. Yuan T, Cantley L. PI3K pathway alterations in cancer: variations on a theme. Oncogene. 2008;27(41):5497-510.
153. Ediriweera MK, Tennekoon KH, Samarakoon SR, editors. Role of the PI3K/AKT/mTOR signaling pathway in ovarian cancer: Biological and therapeutic significance. Seminars in cancer biology; 2019: Elsevier.
154. Mabuchi S, Kuroda H, Takahashi R, Sasano T. The PI3K/AKT/mTOR pathway as a therapeutic target in ovarian cancer. Gynecologic oncology. 2015;137(1):173-9.
155. Ai Z, Lu Y, Qiu S, Fan Z. Overcoming cisplatin resistance of ovarian cancer cells by targeting HIF-1-regulated cancer metabolism. Cancer letters. 2016;373(1):36-44.
156. Tania M, Khan M, Song Y. Association of lipid metabolism with ovarian cancer. Current oncology. 2010;17(5):6-11.
157. Ji Z, Shen Y, Feng X, Kong Y, Shao Y, Meng J, et al. Deregulation of lipid metabolism: The critical factors in ovarian cancer. Frontiers in oncology. 2020;10:593017.
158. Nagarajan SR, Butler LM, Hoy AJ. The diversity and breadth of cancer cell fatty acid metabolism. Cancer & Metabolism. 2021;9:1-28.
159. Koundouros N, Poulogiannis G. Reprogramming of fatty acid metabolism in cancer. British journal of cancer. 2020;122(1):4-22.
160. Su X, Abumrad NA. Cellular fatty acid uptake: a pathway under construction. Trends in Endocrinology & Metabolism. 2009;20(2):72-7.
161. Bensaad K, Favaro E, Lewis CA, Peck B, Lord S, Collins JM, et al. Fatty acid uptake and lipid storage induced by HIF-1α contribute to cell growth and survival after hypoxia-reoxygenation. Cell reports. 2014;9(1):349-65.
162. Gharpure KM, Pradeep S, Sans M, Rupaimoole R, Ivan C, Wu SY, et al. FABP4 as a key determinant of metastatic potential of ovarian cancer. Nature communications. 2018;9(1):2923.
163. Papaevangelou E, Almeida GS, Box C, deSouza NM, Chung YL. The effect of FASN inhibition on the growth and metabolism of a cisplatin-resistant ovarian carcinoma model. International journal of cancer. 2018;143(4):992-1002.
164. Cai Y, Wang J, Zhang L, Wu D, Yu D, Tian X, et al. Expressions of fatty acid synthase and HER2 are correlated with poor prognosis of ovarian cancer. Medical oncology. 2015;32:1-6.
165. Grunt TW, Wagner R, Grusch M, Berger W, Singer CF, Marian B, et al. Interaction between fatty acid synthase-and ErbB-systems in ovarian cancer cells. Biochemical and biophysical research communications. 2009;385(3):454-9.
166. Wagner R, Stübiger G, Veigel D, Wuczkowski M, Lanzerstorfer P, Weghuber J, et al. Multi-level suppression of receptor-PI3K-mTORC1 by fatty acid synthase inhibitors is crucial for their efficacy against ovarian cancer cells. Oncotarget. 2017;8(7):11600.
167. Li J, Condello S, Thomes-Pepin J, Ma X, Xia Y, Hurley TD, et al. Lipid desaturation is a metabolic marker and therapeutic target of ovarian cancer stem cells. Cell stem cell. 2017;20(3):303-14. e5.
168. Sun K, Kusminski CM, Scherer PE. Adipose tissue remodeling and obesity. The Journal of clinical investigation. 2011;121(6):2094-101.
169. Ikeda K, Maretich P, Kajimura S. The common and distinct features of brown and beige adipocytes. Trends in Endocrinology & Metabolism. 2018;29(3):191-200.
170. Cedikova M, Kripnerová M, Dvorakova J, Pitule P, Grundmanova M, Babuska V, et al. Mitochondria in white, brown, and beige adipocytes. Stem cells international. 2016;2016.

171. Wu J, Boström P, Sparks LM, Ye L, Choi JH, Giang A-H, et al. Beige adipocytes are a distinct type of thermogenic fat cell in mouse and human. Cell. 2012;150(2):366-76.
172. Lee M-J, Wu Y, Fried SK. Adipose tissue heterogeneity: implication of depot differences in adipose tissue for obesity complications. Molecular aspects of medicine. 2013;34(1):1-11.
173. Pérez-Pérez R, Ortega-Delgado FJ, García-Santos E, López JA, Camafeita E, Ricart W, et al. Differential proteomics of omental and subcutaneous adipose tissue reflects their unalike biochemical and metabolic properties. Journal of proteome research. 2009;8(4):1682-93.
174. Yang A, Mottillo EP. Adipocyte lipolysis: from molecular mechanisms of regulation to disease and therapeutics. Biochemical Journal. 2020;477(5):985-1008.
175. Duncan RE, Ahmadian M, Jaworski K, Sarkadi-Nagy E, Sul HS. Regulation of lipolysis in adipocytes. Annu Rev Nutr. 2007;27:79-101.
176. Motohara T, Masuda K, Morotti M, Zheng Y, El-Sahhar S, Chong KY, et al. An evolving story of the metastatic voyage of ovarian cancer cells: cellular and molecular orchestration of the adipose-rich metastatic microenvironment. Oncogene. 2019;38(16):2885-98.
177. Gazi E, Gardner P, Lockyer NP, Hart CA, Brown MD, Clarke NW. Direct evidence of lipid translocation between adipocytes and prostate cancer cells with imaging FTIR microspectroscopy. Journal of lipid research. 2007;48(8):1846-56.
178. Liu Y. Fatty acid oxidation is a dominant bioenergetic pathway in prostate cancer. Prostate cancer and prostatic diseases. 2006;9(3):230-4.
179. Dirat B, Bochet L, Dabek M, Daviaud D, Dauvillier S, Majed B, et al. Cancer-associated adipocytes exhibit an activated phenotype and contribute to breast cancer invasion. Cancer research. 2011;71(7):2455-65.
180. Guerrero J, Tobar N, Cáceres M, Espinoza L, Escobar P, Dotor J, et al. Soluble factors derived from tumor mammary cell lines induce a stromal mammary adipose reversion in human and mice adipose cells. Possible role of TGF-β1 and TNF-α. Breast cancer research and treatment. 2010;119:497-508.
181. Harjes U, Bridges E, Gharpure K, Roxanis I, Sheldon H, Miranda F, et al. Antiangiogenic and tumour inhibitory effects of downregulating tumour endothelial FABP4. Oncogene. 2017;36(7):912-21.
182. Sawyer BT, Qamar L, Yamamoto TM, McMellen A, Watson ZL, Richer JK, et al. Targeting fatty acid oxidation to promote anoikis and inhibit ovarian cancer progression. Molecular Cancer Research. 2020;18(7):1088-98.
183. John B, Naczki C, Patel C, Ghoneum A, Qasem S, Salih Z, et al. Regulation of the bi-directional cross-talk between ovarian cancer cells and adipocytes by SPARC. Oncogene. 2019;38(22):4366-83.
184. Tebbe C, Chhina J, Dar SA, Sarigiannis K, Giri S, Munkarah AR, et al. Metformin limits the adipocyte tumor-promoting effect on ovarian cancer. Oncotarget. 2014;5(13):4746.
185. Sun Z, Jiang Q, Li J, Guo J. The potent roles of salt-inducible kinases (SIKs) in metabolic homeostasis and tumorigenesis. Signal transduction and targeted therapy. 2020;5(1):150.
186. Ghanemi A, Yoshioka M, St-Amand J. Secreted protein acidic and rich in cysteine as a molecular physiological and pathological biomarker. Biomolecules. 2021;11(11):1689.
187. Said N, Socha MJ, Olearczyk JJ, Elmarakby AA, Imig JD, Motamed K. Normalization of the ovarian cancer microenvironment by SPARC. Molecular cancer research. 2007;5(10):1015-30.
188. Klopp AH, Zhang Y, Solley T, Amaya-Manzanares F, Marini F, Andreeff M, et al. Omental adipose tissue–derived stromal cells promote vascularization and growth of endometrial tumors. Clinical cancer research. 2012;18(3):771-82.
189. Salimian Rizi B, Caneba C, Nowicka A, Nabiyar AW, Liu X, Chen K, et al. Nitric oxide mediates metabolic coupling of omentum-derived adipose stroma to ovarian and endometrial cancer cells. Cancer Research. 2015;75(2):456-71.
190. Chu Y, Tang H, Guo Y, Guo J, Huang B, Fang F, et al. Adipose-derived mesenchymal stem cells promote cell proliferation and invasion of epithelial ovarian cancer. Experimental cell research. 2015;337(1):16-27.

191. Pati S, Irfan W, Jameel A, Ahmed S, Shahid RK. Obesity and cancer: A current overview of epidemiology, pathogenesis, outcomes, and management. Cancers. 2023;15(2):485.
192. Park J, Morley TS, Kim M, Clegg DJ, Scherer PE. Obesity and cancer—mechanisms underlying tumour progression and recurrence. Nature Reviews Endocrinology. 2014;10(8):455-65.
193. Johnson AR, Justin Milner J, Makowski L. The inflammation highway: metabolism accelerates inflammatory traffic in obesity. Immunological reviews. 2012;249(1):218-38.
194. Weisberg SP, McCann D, Desai M, Rosenbaum M, Leibel RL, Ferrante AW. Obesity is associated with macrophage accumulation in adipose tissue. The Journal of clinical investigation. 2003;112(12):1796-808.
195. Charlton M. Obesity, hyperlipidemia, and metabolic syndrome. Liver transplantation. 2009;15(S2):S83-S9.
196. Khasawneh J, Schulz M, Walch A, Rozman J, De Angelis MH, Klingenspor M, et al. Inflammation and mitochondrial fatty acid β-oxidation link obesity to early tumor promotion. Proceedings of the National Academy of Sciences. 2009;106(9):3354-9.
197. Park EJ, Lee JH, Yu G-Y, He G, Ali SR, Holzer RG, et al. Dietary and genetic obesity promote liver inflammation and tumorigenesis by enhancing IL-6 and TNF expression. Cell. 2010;140(2):197-208.
198. Ogunwobi OO, Beales IL. The anti-apoptotic and growth stimulatory actions of leptin in human colon cancer cells involves activation of JNK mitogen activated protein kinase, JAK2 and PI3 kinase/Akt. International journal of colorectal disease. 2007;22:401-9.
199. Cirillo D, Rachiglio AM, La Montagna R, Giordano A, Normanno N. Leptin signaling in breast cancer: an overview. Journal of cellular biochemistry. 2008;105(4):956-64.
200. Uddin S, Bu R, Ahmed M, Abubaker J, Al-Dayel F, Bavi P, et al. Overexpression of leptin receptor predicts an unfavorable outcome in Middle Eastern ovarian cancer. Molecular cancer. 2009;8:1-12.
201. Chen C, Chang Y-C, Lan MS, Breslin M. Leptin stimulates ovarian cancer cell growth and inhibits apoptosis by increasing cyclin D1 and Mcl-1 expression via the activation of the MEK/ERK1/2 and PI3K/Akt signaling pathways Corrigendum in/10.3892/ijo. 2016.3564. International journal of oncology. 2013;42(3):1113-9.
202. Dasari S, Tchounwou PB. Cisplatin in cancer therapy: molecular mechanisms of action. European journal of pharmacology. 2014;740:364-78.
203. Parness J, Horwitz SB. Taxol binds to polymerized tubulin in vitro. The Journal of cell biology. 1981;91(2):479-87.
204. Cooke SL, Brenton JD. Evolution of platinum resistance in high-grade serous ovarian cancer. The lancet oncology. 2011;12(12):1169-74.
205. Martincuks A, Li P-C, Zhao Q, Zhang C, Li Y-J, Yu H, et al. CD44 in ovarian cancer progression and therapy resistance—a critical role for STAT3. Frontiers in oncology. 2020;10:589601.
206. Ji T, Gong D, Han Z, Wei X, Yan Y, Ye F, et al. Abrogation of constitutive Stat3 activity circumvents cisplatin resistant ovarian cancer. Cancer letters. 2013;341(2):231-9.
207. Cornelison R, Llaneza DC, Landen CN. Emerging therapeutics to overcome chemoresistance in epithelial ovarian cancer: a mini-review. International journal of molecular sciences. 2017;18(10):2171.
208. Davidson B, Trope CG, Reich R. Epithelial–mesenchymal transition in ovarian carcinoma. Frontiers in oncology. 2012;2:21912.
209. Marchini S, Fruscio R, Clivio L, Beltrame L, Porcu L, Nerini IF, et al. Resistance to platinum-based chemotherapy is associated with epithelial to mesenchymal transition in epithelial ovarian cancer. European journal of cancer. 2013;49(2):520-30.
210. Rosanò L, Cianfrocca R, Spinella F, Di Castro V, Nicotra MR, Lucidi A, et al. Acquisition of chemoresistance and EMT phenotype is linked with activation of the endothelin A receptor pathway in ovarian carcinoma cells. Clinical cancer research. 2011;17(8):2350-60.

211. Caponigro G, Sellers WR. Advances in the preclinical testing of cancer therapeutic hypotheses. Nature reviews Drug discovery. 2011;10(3):179-87.
212. Baker BM, Chen CS. Deconstructing the third dimension–how 3D culture microenvironments alter cellular cues. Journal of cell science. 2012;125(13):3015-24.
213. Costa EC, Moreira AF, de Melo-Diogo D, Gaspar VM, Carvalho MP, Correia IJ. 3D tumor spheroids: an overview on the tools and techniques used for their analysis. Biotechnology advances. 2016;34(8):1427-41.
214. Klymenko Y, Kim O, Loughran E, Yang J, Lombard R, Alber M, et al. Cadherin composition and multicellular aggregate invasion in organotypic models of epithelial ovarian cancer intraperitoneal metastasis. Oncogene. 2017;36(42):5840-51.
215. Serebriiskii I, Castelló-Cros R, Lamb A, Golemis EA, Cukierman E. Fibroblast-derived 3D matrix differentially regulates the growth and drug-responsiveness of human cancer cells. Matrix Biology. 2008;27(6):573-85.
216. Xu F, Celli J, Rizvi I, Moon S, Hasan T, Demirci U. A three-dimensional in vitro ovarian cancer coculture model using a high-throughput cell patterning platform. Biotechnology journal. 2011;6(2):204-12.
217. Barbolina MV, Adley BP, Ariztia EV, Liu Y, Stack MS. Microenvironmental regulation of membrane type 1 matrix metalloproteinase activity in ovarian carcinoma cells via collagen-induced EGR1 expression. Journal of Biological Chemistry. 2007;282(7):4924-31.
218. Liu M, Zhang X, Long C, Xu H, Cheng X, Chang J, et al. Collagen-based three-dimensional culture microenvironment promotes epithelial to mesenchymal transition and drug resistance of human ovarian cancer in vitro. RSC advances. 2018;8(16):8910-9.
219. Sawada K, Mitra AK, Radjabi AR, Bhaskar V, Kistner EO, Tretiakova M, et al. Loss of E-cadherin promotes ovarian cancer metastasis via α5-integrin, which is a therapeutic target. Cancer research. 2008;68(7):2329-39.
220. Mitra A, Sawada K, Tiwari P, Mui K, Gwin K, Lengyel E. Ligand-independent activation of c-Met by fibronectin and α5β1-integrin regulates ovarian cancer invasion and metastasis. Oncogene. 2011;30(13):1566-76.
221. Krausz T, Lengyel E. Organotypic Models of Metastasis: A 3 Dimensional Culture Mimicking the Human Peritoneum and Omentum for the Study of the Early Steps of Ovarian Cancer Metastasis. Cancer Treat Res. 2013;149:335-51.
222. Ghaben AL, Scherer PE. Adipogenesis and metabolic health. Nature reviews Molecular cell biology. 2019;20(4):242-58.
223. Dykstra JA, Facile T, Patrick RJ, Francis KR, Milanovich S, Weimer JM, et al. Concise review: fat and furious: harnessing the full potential of adipose-derived stromal vascular fraction. Stem cells translational medicine. 2017;6(4):1096-108.
224. Deslex S, Negrel R, Vannier C, Etienne J, Ailhaud G. Differentiation of human adipocyte precursors in a chemically defined serum-free medium. International journal of obesity. 1987;11(1):19-27.
225. Hauner H, Entenmann G, Wabitsch M, Gaillard D, Ailhaud G, Negrel R, et al. Promoting effect of glucocorticoids on the differentiation of human adipocyte precursor cells cultured in a chemically defined medium. The Journal of clinical investigation. 1989;84(5):1663-70.
226. Tchkonia T, Giorgadze N, Pirtskhalava T, Tchoukalova Y, Karagiannides I, Forse RA, et al. Fat depot origin affects adipogenesis in primary cultured and cloned human preadipocytes. American Journal of Physiology-Regulatory, Integrative and Comparative Physiology. 2002;282(5):R1286-R96.
227. Bakker AH, Van Dielen FM, Greve JWM, Adam JA, Buurman WA. Preadipocyte number in omental and subcutaneous adipose tissue of obese individuals. Obesity research. 2004;12(3):488-98.
228. Sugihara H, Yonemitsu N, Miyabara S, Yun K. Primary cultures of unilocular fat cells: characteristics of growth in vitro and changes in differentiation properties. Differentiation. 1986;31(1):42-9.

229. Fogh J, Trempe G. New human tumor cell lines. Human tumor cells in vitro: Springer; 1975. p. 115-59.
230. Beaufort CM, Helmijr JC, Piskorz AM, Hoogstraat M, Ruigrok-Ritstier K, Besselink N, et al. Ovarian cancer cell line panel (OCCP): clinical importance of in vitro morphological subtypes. PloS one. 2014;9(9):e103988.
231. Shaw TJ, Senterman MK, Dawson K, Crane CA, Vanderhyden BC. Characterization of intraperitoneal, orthotopic, and metastatic xenograft models of human ovarian cancer. Molecular therapy. 2004;10(6):1032-42.
232. Hernandez L, Kim MK, Lyle LT, Bunch KP, House CD, Ning F, et al. Characterization of ovarian cancer cell lines as in vivo models for preclinical studies. Gynecologic oncology. 2016;142(2):332-40.
233. Hamilton TC, Winker MA, Louie KG, Batist G, Behrens BC, Tsuruo T, et al. Augmentation of adriamycin, melphalan, and cisplatin cytotoxicity in drug-resistant and-sensitive human ovarian carcinoma cell lines by buthionine sulfoximine mediated glutathione depletion. Biochemical pharmacology. 1985;34(14):2583-6.
234. Fang D, Chen H, Zhu JY, Wang W, Teng Y, Ding H-F, et al. Epithelial–mesenchymal transition of ovarian cancer cells is sustained by Rac1 through simultaneous activation of MEK1/2 and Src signaling pathways. Oncogene. 2017;36(11):1546-58.
235. Yi B-R, Kim T-H, Kim Y-S, Choi K-C. Alteration of epithelial-mesenchymal transition markers in human normal ovaries and neoplastic ovarian cancers. International journal of oncology. 2015;46(1):272-80.
236. Bourgeois DL, Kabarowski KA, Porubsky VL, Kreeger PK. High-grade serous ovarian cancer cell lines exhibit heterogeneous responses to growth factor stimulation. Cancer cell international. 2015;15(1):1-11.
237. Al Ameri W, Ahmed I, Al-Dasim FM, Ali Mohamoud Y, Al-Azwani IK, Malek JA, et al. Cell type-specific TGF-β mediated EMT in 3D and 2D models and its reversal by TGF-β receptor kinase inhibitor in ovarian cancer cell lines. International journal of molecular sciences. 2019;20(14):3568.
238. Lin RZ, Chang HY. Recent advances in three-dimensional multicellular spheroid culture for biomedical research. Biotechnology Journal: Healthcare Nutrition Technology. 2008;3(9-10):1172-84.
239. Weiswald L-B, Guinebretière J-M, Richon S, Bellet D, Saubaméa B, Dangles-Marie V. In situ protein expression in tumour spheres: development of an immunostaining protocol for confocal microscopy. BMC cancer. 2010;10(1):1-11.
240. Zeringer E, Barta T, Li M, Vlassov AV. Strategies for isolation of exosomes. Cold Spring Harbor Protocols. 2015;2015(4):pdb. top074476.
241. Li P, Kaslan M, Lee SH, Yao J, Gao Z. Progress in exosome isolation techniques. Theranostics. 2017;7(3):789.
242. Yeung T-L, Leung CS, Yip K-P, Yeung CLA, Wong ST, Mok SC. Cellular and molecular processes in ovarian cancer metastasis. A review in the theme: cell and molecular processes in cancer metastasis. American Journal of Physiology-Cell Physiology. 2015.
243. Gunderson CC, Ding K, Dvorak J, Moore KN, McMeekin DS, Benbrook DM. The pro-inflammatory effect of obesity on high grade serous ovarian cancer. Gynecologic Oncology. 2016;143(1):40-5.
244. Chen RR, Yung MM, Xuan Y, Zhan S, Leung LL, Liang RR, et al. Targeting of lipid metabolism with a metabolic inhibitor cocktail eradicates peritoneal metastases in ovarian cancer cells. Communications biology. 2019;2(1):281.
245. Amemori S, Ootani A, Aoki S, Fujise T, Shimoda R, Kakimoto T, et al. Adipocytes and preadipocytes promote the proliferation of colon cancer cells in vitro. American Journal of Physiology-Gastrointestinal and Liver Physiology. 2007;292(3):G923-G9.
246. Wang YY, Attané C, Milhas D, Dirat B, Dauvillier S, Guerard A, et al. Mammary adipocytes stimulate breast cancer invasion through metabolic remodeling of tumor cells. JCI insight. 2017;2(4).

247. Nowicka A, Marini FC, Solley TN, Elizondo PB, Zhang Y, Sharp HJ, et al. Human omental-derived adipose stem cells increase ovarian cancer proliferation, migration, and chemoresistance. PloS one. 2013;8(12):e81859.
248. Yang J, Zaman MM, Vlasakov I, Roy R, Huang L, Martin CR, et al. Adipocytes promote ovarian cancer chemoresistance. Scientific reports. 2019;9(1):13316.
249. Nath S, Pigula M, Khan AP, Hanna W, Ruhi MK, Dehkordy FM, et al. Flow-induced shear stress confers resistance to carboplatin in an adherent three-dimensional model for ovarian cancer: A role for EGFR-targeted photoimmunotherapy informed by physical stress. Journal of clinical medicine. 2020;9(4):924.
250. Au Yeung CL, Co N-N, Tsuruga T, Yeung T-L, Kwan S-Y, Leung CS, et al. Exosomal transfer of stroma-derived miR21 confers paclitaxel resistance in ovarian cancer cells through targeting APAF1. Nature communications. 2016;7(1):11150.
251. Saburi A, Kahrizi MS, Naghsh N, Etemadi H, İlhan A, Adili A, et al. A comprehensive survey into the role of microRNAs in ovarian cancer chemoresistance; an updated overview. Journal of Ovarian Research. 2022;15(1):1-14.
252. Zhang Y, Dong W, Wang J, Cai J, Wang Z. Human omental adipose-derived mesenchymal stem cell-conditioned medium alters the proteomic profile of epithelial ovarian cancer cell lines in vitro. OncoTargets and therapy. 2017;10:1655.
253. Shishido A, Mori S, Yokoyama Y, Hamada Y, Minami K, Qian Y, et al. Mesothelial cells facilitate cancer stem-like properties in spheroids of ovarian cancer cells. Oncology reports. 2018;40(4):2105-14.
254. Ahmed N, Abubaker K, Findlay J, Quinn M. Epithelial mesenchymal transition and cancer stem cell-like phenotypes facilitate chemoresistance in recurrent ovarian cancer. Current cancer drug targets. 2010;10(3):268-78.
255. Liao J, Qian F, Tchabo N, Mhawech-Fauceglia P, Beck A, Qian Z, et al. Ovarian cancer spheroid cells with stem cell-like properties contribute to tumor generation, metastasis and chemotherapy resistance through hypoxia-resistant metabolism. PloS one. 2014;9(1):e84941.
256. Usman S, Waseem NH, Nguyen TKN, Mohsin S, Jamal A, Teh M-T, et al. Vimentin is at the heart of epithelial mesenchymal transition (EMT) mediated metastasis. Cancers. 2021;13(19):4985.
257. Han X, Zhou Y, You Y, Lu J, Wang L, Hou H, et al. TET1 promotes cisplatin-resistance via demethylating the vimentin promoter in ovarian cancer. Cell Biology International. 2017;41(4):405-14.
258. Pujade-Lauraine E, Banerjee S, Pignata S. Management of platinum-resistant, relapsed epithelial ovarian cancer and new drug perspectives. Journal of Clinical Oncology. 2019;37(27):2437-48.
259. Bach DH, Hong JY, Park HJ, Lee SK. The role of exosomes and miRNAs in drug-resistance of cancer cells. International journal of cancer. 2017;141(2):220-30.
260. Tian W, Lei N, Zhou J, Chen M, Guo R, Qin B, et al. Extracellular vesicles in ovarian cancer chemoresistance, metastasis, and immune evasion. Cell Death & Disease. 2022;13(1):64.
261. Jafari N, Kolla M, Meshulam T, Shafran JS, Qiu Y, Casey AN, et al. Adipocyte-derived exosomes may promote breast cancer progression in type 2 diabetes. Science signaling. 2021;14(710):eabj2807.
262. Wang S, Su X, Xu M, Xiao X, Li X, Li H, et al. Exosomes secreted by mesenchymal stromal/stem cell-derived adipocytes promote breast cancer cell growth via activation of Hippo signaling pathway. Stem Cell Research & Therapy. 2019;10:1-12.
263. Lazar I, Clement E, Dauvillier S, Milhas D, Ducoux-Petit M, LeGonidec S, et al. Adipocyte Exosomes Promote Melanoma Aggressiveness through Fatty Acid Oxidation: A Novel Mechanism Linking Obesity and CancerAdipocyte Exosomes: A New Link between Obesity and Cancer. Cancer research. 2016;76(14):4051-7.
264. Wolin KY, Carson K, Colditz GA. Obesity and cancer. The oncologist. 2010;15(6):556-65.

265. Zhang B, Yang Y, Xiang L, Zhao Z, Ye R. Adipose-derived exosomes: a novel adipokine in obesity-associated diabetes. Journal of Cellular Physiology. 2019;234(10):16692-702.
266. Sano S, Izumi Y, Yamaguchi T, Yamazaki T, Tanaka M, Shiota M, et al. Lipid synthesis is promoted by hypoxic adipocyte-derived exosomes in 3T3-L1 cells. Biochemical and biophysical research communications. 2014;445(2):327-33.
267. Wen Z, Li J, Fu Y, Zheng Y, Ma M, Wang C. Hypertrophic Adipocyte–Derived Exosomal miR-802-5p Contributes to Insulin Resistance in Cardiac Myocytes Through Targeting HSP60. Obesity. 2020;28(10):1932-40.
268. Yang H, Kong W, He L, Zhao J-J, O'Donnell JD, Wang J, et al. MicroRNA expression profiling in human ovarian cancer: miR-214 induces cell survival and cisplatin resistance by targeting PTEN. Cancer research. 2008;68(2):425-33.
269. Koutsaki M, Spandidos DA, Zaravinos A. Epithelial–mesenchymal transition-associated miRNAs in ovarian carcinoma, with highlight on the miR-200 family: Prognostic value and prospective role in ovarian cancer therapeutics. Cancer letters. 2014;351(2):173-81.
270. Wu Q, Li B, Li Z, Li J, Sun S, Sun S. Cancer-associated adipocytes: key players in breast cancer progression. Journal of hematology & oncology. 2019;12:1-15.
271. Laurent V, Guérard A, Mazerolles C, Le Gonidec S, Toulet A, Nieto L, et al. Periprostatic adipocytes act as a driving force for prostate cancer progression in obesity. Nature communications. 2016;7(1):10230.
272. Fujita K, Hayashi T, Matsushita M, Uemura M, Nonomura N. Obesity, inflammation, and prostate cancer. Journal of clinical medicine. 2019;8(2):201.
273. Nakamura K, Hongo A, Kodama J, Hiramatsu Y. Fat accumulation in adipose tissues as a risk factor for the development of endometrial cancer. Oncology reports. 2011;26(1):65-71.
274. Moukarzel LA, Ferrando L, Stylianou A, Lobaugh S, Wu M, Nobre SP, et al. Impact of obesity and white adipose tissue inflammation on the omental microenvironment in endometrial cancer. Cancer. 2022;128(18):3297-309.
275. Ben-Jonathan N, Liby K, McFarland M, Zinger M. Prolactin as an autocrine/paracrine growth factor in human cancer. Trends in Endocrinology & Metabolism. 2002;13(6):245-50.
276. Vonderhaar B. Prolactin involvement in breast cancer. Endocrine-related cancer. 1999;6(3):389-404.
277. Alkharusi A, AlMuslahi A, AlBalushi N, AlAjmi R, AlRawahi S, AlFarqani A, et al. Connections between prolactin and ovarian cancer. PLoS One. 2021;16(8):e0255701.
278. Yurkovetsky Z, Ta'asan S, Skates S, Rand A, Lomakin A, Linkov F, et al. Development of multimarker panel for early detection of endometrial cancer. High diagnostic power of prolactin. Gynecologic oncology. 2007;107(1):58-65.
279. Levina VV, Nolen B, Su Y, Godwin AK, Fishman D, Liu J, et al. Biological significance of prolactin in gynecologic cancers. Cancer research. 2009;69(12):5226-33.
280. Jacobson EM, Hugo ER, Borcherding DC, Ben-Jonathan N. Prolactin in breast and prostate cancer: molecular and genetic perspectives. Discovery medicine. 2011;11(59):315-24.
281. Yue P, Zhang X, Paladino D, Sengupta B, Ahmad S, Holloway RW, et al. Hyperactive EGF receptor, Jaks and Stat3 signaling promote enhanced colony-forming ability, motility and migration of cisplatin-resistant ovarian cancer cells. Oncogene. 2012;31(18):2309-22.
282. Colomiere M, Ward AC, Riley C, Trenerry MK, Cameron-Smith D, Findlay J, et al. Cross talk of signals between EGFR and IL-6R through JAK2/STAT3 mediate epithelial–mesenchymal transition in ovarian carcinomas. British journal of cancer. 2009;100(1):134-44.
283. Abubaker K, Luwor RB, Escalona R, McNally O, Quinn MA, Thompson EW, et al. Targeted disruption of the JAK2/STAT3 pathway in combination with systemic administration of paclitaxel inhibits the priming of ovarian cancer stem cells leading to a reduced tumor burden. Frontiers in oncology. 2014;4:75.
284. Yu X, Chen Y, Tian R, Li J, Li H, Lv T, et al. miRNA-21 enhances chemoresistance to cisplatin in epithelial ovarian cancer by negatively regulating PTEN. Oncology letters. 2017;14(2):1807-10.

285. Zhao Q, Huang L, Qin G, Qiao Y, Ren F, Shen C, et al. Cancer-associated fibroblasts induce monocytic myeloid-derived suppressor cell generation via IL-6/exosomal miR-21-activated STAT3 signaling to promote cisplatin resistance in esophageal squamous cell carcinoma. Cancer letters. 2021;518:35-48.
286. Guo F, Tian J, Lin Y, Jin Y, Wang L, Cui M. Serum microRNA-92 expression in patients with ovarian epithelial carcinoma. Journal of international medical research. 2013;41(5):1456-61.
287. Olive V, Jiang I, He L. mir-17-92, a cluster of miRNAs in the midst of the cancer network. The international journal of biochemistry & cell biology. 2010;42(8):1348-54.
288. Chen Z-l, Zhao X-h, Wang J-w, Li B-z, Wang Z, Sun J, et al. microRNA-92a promotes lymph node metastasis of human esophageal squamous cell carcinoma via E-cadherin. Journal of Biological Chemistry. 2011;286(12):10725-34.
289. Busch B, Bley N, Müller S, Glaß M, Misiak D, Lederer M, et al. The oncogenic triangle of HMGA2, LIN28B and IGF2BP1 antagonizes tumor-suppressive actions of the let-7 family. Nucleic acids research. 2016;44(8):3845-64.
290. Nam EJ, Yoon H, Kim SW, Kim H, Kim YT, Kim JH, et al. MicroRNA expression profiles in serous ovarian carcinoma. Clinical cancer research. 2008;14(9):2690-5.
291. Yu Z, Kim J, He L, Creighton CJ, Gunaratne PH, Hawkins SM, et al. Functional analysis of miR-34c as a putative tumor suppressor in high-grade serous ovarian cancer. Biology of Reproduction. 2014;91(5):113, 1-12.
292. Yamamoto CM, Oakes ML, Murakami T, Muto MG, Berkowitz RS, Ng S-W. Comparison of benign peritoneal fluid-and ovarian cancer ascites-derived extracellular vesicle RNA biomarkers. Journal of ovarian research. 2018;11:1-9.
293. Tang Z, Ow GS, Thiery JP, Ivshina AV, Kuznetsov VA. Meta-analysis of transcriptome reveals let-7b as an unfavorable prognostic biomarker and predicts molecular and clinical subclasses in high-grade serous ovarian carcinoma. International journal of cancer. 2014;134(2):306-18.
294. Feng W, Dean DC, Hornicek FJ, Shi H, Duan Z. Exosomes promote pre-metastatic niche formation in ovarian cancer. Molecular cancer. 2019;18:1-11.
295. Daquinag AC, Dadbin A, Snyder B, Wang X, Sahin AA, Ueno NT, et al. Non-glycanated decorin is a drug target on human adipose stromal cells. Molecular Therapy-Oncolytics. 2017;6:1-9.
296. Daquinag AC, Tseng C, Zhang Y, Amaya-Manzanares F, Florez F, Dadbin A, et al. Targeted proapoptotic peptides depleting adipose stromal cells inhibit tumor growth. Molecular Therapy. 2016;24(1):34-40.
297. Cho KR, Shih I-M. Ovarian cancer. Annual review of pathology: mechanisms of disease. 2009;4:287-313.
298. Landen Jr CN, Birrer MJ, Sood AK. Early events in the pathogenesis of epithelial ovarian cancer. Journal of Clinical Oncology. 2008;26(6):995-1005.
299. Sehouli J, Senyuva F, Fotopoulou C, Neumann U, Denkert C, Werner L, et al. Intra-abdominal tumor dissemination pattern and surgical outcome in 214 patients with primary ovarian cancer. Journal of surgical oncology. 2009;99(7):424-7.
300. Jia D, Nagaoka Y, Katsumata M, Orsulic S. Inflammation is a key contributor to ovarian cancer cell seeding. Scientific reports. 2018;8(1):12394.
301. Almeida-Nunes DL, Mendes-Frias A, Silvestre R, Dinis-Oliveira RJ, Ricardo S. Immune tumor microenvironment in ovarian cancer ascites. International Journal of Molecular Sciences. 2022;23(18):10692.
302. Min H, Wei-hong Z. Constitutive activation of signal transducer and activator of transcription 3 in epithelial ovarian carcinoma. Journal of Obstetrics and Gynaecology Research. 2009;35(5):918-25.
303. Akhmedkhanov A, Toniolo P, Zeleniuch-Jacquotte A, Kato I, Koenig KL, Shore RE. Aspirin and epithelial ovarian cancer. Preventive medicine. 2001;33(6):682-7.
304. Fairfield KM, Hunter DJ, Fuchs CS, Colditz GA, Hankinson SE. Aspirin, other NSAIDs, and ovarian cancer risk (United States). Cancer Causes & Control. 2002;13:535-42.

305. Altinoz M, Korkmaz R. NF-kB, macrophage migration inhibitory factor and cyclooxygenase-inhibitions as likely mechanisms behind the acetaminophen-and NSAID-prevention of the ovarian cancer. Neoplasma. 2004;51(4):239-47.
306. Sullivan PW, Ghushchyan VH, Ben-Joseph R. The impact of obesity on diabetes, hyperlipidemia and hypertension in the United States. Quality of Life Research. 2008;17:1063-71.
307. Foley KP, Chen Y, Barra NG, Heal M, Kwok K, Tamrakar AK, et al. Inflammation promotes adipocyte lipolysis via IRE1 kinase. Journal of Biological Chemistry. 2021;296.
308. Van Hall G, Steensberg A, Sacchetti M, Fischer C, Keller C, Schjerling P, et al. Interleukin-6 stimulates lipolysis and fat oxidation in humans. The Journal of Clinical Endocrinology & Metabolism. 2003;88(7):3005-10.
309. Zhang HH, Halbleib M, Ahmad F, Manganiello VC, Greenberg AS. Tumor necrosis factor-α stimulates lipolysis in differentiated human adipocytes through activation of extracellular signal-related kinase and elevation of intracellular cAMP. Diabetes. 2002;51(10):2929-35.
310. Macciò A, Lai P, Santona MC, Pagliara L, Melis GB, Mantovani G. High serum levels of soluble IL-2 receptor, cytokines, and C reactive protein correlate with impairment of T cell response in patients with advanced epithelial ovarian cancer. Gynecologic oncology. 1998;69(3):248-52.
311. Trabert B, Pinto L, Hartge P, Kemp T, Black A, Sherman ME, et al. Pre-diagnostic serum levels of inflammation markers and risk of ovarian cancer in the prostate, lung, colorectal and ovarian cancer (PLCO) screening trial. Gynecologic oncology. 2014;135(2):297-304.
312. Hagberg CE, Li Q, Kutschke M, Bhowmick D, Kiss E, Shabalina IG, et al. Flow cytometry of mouse and human adipocytes for the analysis of browning and cellular heterogeneity. Cell reports. 2018;24(10):2746-56. e5.
313. Yao C-H, Liu G-Y, Wang R, Moon SH, Gross RW, Patti GJ. Identifying off-target effects of etomoxir reveals that carnitine palmitoyltransferase I is essential for cancer cell proliferation independent of β-oxidation. PLoS biology. 2018;16(3):e2003782.
314. Piura B, Medina L, Rabinovich A, Dyomin V, Levy RS, Huleihel M. Distinct expression and localization of TNF system in ovarian carcinoma tissues: Possible involvement of TNF-α in morphological changes of ovarian cancerous cells. Anticancer research. 2014;34(2):745-52.
315. Kulbe H, Thompson R, Wilson JL, Robinson S, Hagemann T, Fatah R, et al. The inflammatory cytokine tumor necrosis factor-α generates an autocrine tumor-promoting network in epithelial ovarian cancer cells. Cancer research. 2007;67(2):585-92.
316. Preston CC, Goode EL, Hartmann LC, Kalli KR, Knutson KL. Immunity and immune suppression in human ovarian cancer. Immunotherapy. 2011;3(4):539-56.
317. Macciò A, Gramignano G, Cherchi MC, Tanca L, Melis L, Madeddu C. Role of M1-polarized tumor-associated macrophages in the prognosis of advanced ovarian cancer patients. Scientific reports. 2020;10(1):6096.
318. Lumeng CN, DeYoung SM, Bodzin JL, Saltiel AR. Increased inflammatory properties of adipose tissue macrophages recruited during diet-induced obesity. Diabetes. 2007;56(1):16-23.
319. Lumeng CN, Bodzin JL, Saltiel AR. Obesity induces a phenotypic switch in adipose tissue macrophage polarization. The Journal of clinical investigation. 2007;117(1):175-84.
320. Popko K, Gorska E, Stelmaszczyk-Emmel A, Plywaczewski R, Stoklosa A, Gorecka D, et al. Proinflammatory cytokines Il-6 and TNF-α and the development of inflammation in obese subjects. European journal of medical research. 2010;15:1-3.
321. Suganami T, Nishida J, Ogawa Y. A paracrine loop between adipocytes and macrophages aggravates inflammatory changes: role of free fatty acids and tumor necrosis factor α. Arteriosclerosis, thrombosis, and vascular biology. 2005;25(10):2062-8.
322. Jung SH, Park HS, Kim K-S, Choi WH, Ahn CW, Kim BT, et al. Effect of weight loss on some serum cytokines in human obesity: increase in IL-10 after weight loss. The Journal of nutritional biochemistry. 2008;19(6):371-5.
323. Savage DB, Petersen KF, Shulman GI. Disordered lipid metabolism and the pathogenesis of insulin resistance. Physiological reviews. 2007;87(2):507-20.

324. Mordier S, Iynedjian PB. Activation of mammalian target of rapamycin complex 1 and insulin resistance induced by palmitate in hepatocytes. Biochemical and biophysical research communications. 2007;362(1):206-11.
325. Wang Y, Zong X, Mitra S, Mitra AK, Matei D, Nephew KP. IL-6 mediates platinum-induced enrichment of ovarian cancer stem cells. JCI insight. 2018;3(23).
326. Buechler C, Krautbauer S, Eisinger K. Adipose tissue fibrosis. World journal of diabetes. 2015;6(4):548.
327. Gadducci A, Cosio S, Fanucchi A, Genazzani AR. Malnutrition and cachexia in ovarian cancer patients: pathophysiology and management. Anticancer research. 2001;21(4B):2941-7.
328. Aust S, Knogler T, Pils D, Obermayr E, Reinthaller A, Zahn L, et al. Skeletal muscle depletion and markers for cancer cachexia are strong prognostic factors in epithelial ovarian cancer. PloS one. 2015;10(10):e0140403.
329. Pin F, Barreto R, Kitase Y, Mitra S, Erne CE, Novinger LJ, et al. Growth of ovarian cancer xenografts causes loss of muscle and bone mass: a new model for the study of cancer cachexia. Journal of cachexia, sarcopenia and muscle. 2018;9(4):685-700.
330. Mantovani G, Macciò A, Mura L, Massa E, Mudu MC, Mulas C, et al. Serum levels of leptin and proinflammatory cytokines in patients with advanced-stage cancer at different sites. Journal of Molecular Medicine. 2000;78:554-61.
331. Marcelin G, Gautier EL, Clément K. Adipose tissue fibrosis in obesity: etiology and challenges. Annual Review of Physiology. 2022;84:135-55.
332. Thibault B, Castells M, Delord J-P, Couderc B. Ovarian cancer microenvironment: implications for cancer dissemination and chemoresistance acquisition. Cancer and Metastasis Reviews. 2014;33:17-39.
333. Kim S, Han Y, Kim SI, Kim H-S, Kim SJ, Song YS. Tumor evolution and chemoresistance in ovarian cancer. NPJ precision oncology. 2018;2(1):20.
334. Yousefi H, Momeny M, Ghaffari SH, Parsanejad N, Poursheikhani A, Javadikooshesh S, et al. IL-6/IL-6R pathway is a therapeutic target in chemoresistant ovarian cancer. Tumori journal. 2019;105(1):84-91.
335. De Marco M, Falco A, Festa M, Raffone A, Sandullo L, Rosati A, et al. Different mechanisms underlie IL-6 release in chemosensitive and chemoresistant ovarian carcinoma cells. American Journal of Cancer Research. 2020;10(8):2596.
336. Bonneau C, Rouzier R, Geyl C, Cortez A, Castela M, Lis R, et al. Predictive markers of chemoresistance in advanced stages epithelial ovarian carcinoma. Gynecologic oncology. 2015;136(1):112-20.
337. Wang Y, Qu Y, Niu XL, Sun WJ, Zhang XL, Li LZ. Autocrine production of interleukin-8 confers cisplatin and paclitaxel resistance in ovarian cancer cells. Cytokine. 2011;56(2):365-75.
338. Li Y-J, Zhang C, Martincuks A, Herrmann A, Yu H. STAT proteins in cancer: orchestration of metabolism. Nature Reviews Cancer. 2023;23(3):115-34.
339. Cao Y. Adipocyte and lipid metabolism in cancer drug resistance. The Journal of clinical investigation. 2019;129(8):3006-17.
340. Tadros S, Shukla SK, King RJ, Gunda V, Vernucci E, Abrego J, et al. De novo lipid synthesis facilitates gemcitabine resistance through endoplasmic reticulum stress in pancreatic cancer. Cancer research. 2017;77(20):5503-17.
341. Tan Y, Li J, Zhao G, Huang K-C, Cardenas H, Wang Y, et al. Metabolic reprogramming from glycolysis to fatty acid uptake and beta-oxidation in platinum-resistant cancer cells. Nature communications. 2022;13(1):4554.
342. Hoy AJ, Nagarajan SR, Butler LM. Tumour fatty acid metabolism in the context of therapy resistance and obesity. Nature Reviews Cancer. 2021;21(12):753-66.
343. Incio J, Ligibel JA, McManus DT, Suboj P, Jung K, Kawaguchi K, et al. Obesity promotes resistance to anti-VEGF therapy in breast cancer by up-regulating IL-6 and potentially FGF-2. Science translational medicine. 2018;10(432):eaag0945.

344. Wang Y, Niu XL, Qu Y, Wu J, Zhu YQ, Sun WJ, et al. Autocrine production of interleukin-6 confers cisplatin and paclitaxel resistance in ovarian cancer cells. Cancer letters. 2010;295(1):110-23.
345. Isobe A, Sawada K, Kinose Y, Ohyagi-Hara C, Nakatsuka E, Makino H, et al. Interleukin 6 receptor is an independent prognostic factor and a potential therapeutic target of ovarian cancer. PloS one. 2015;10(2):e0118080.
346. Wang L, Zhang F, Cui JY, Chen L, Chen YT, Liu BW. CAFs enhance paclitaxel resistance by inducing EMT through the IL-6/JAK2/STAT3 pathway. Oncology reports. 2018;39(5):2081-90.
347. Obata NH, Tamakoshi K, Shibata K, Kikkawa F, Tomoda Y. Effects of interleukin-6 on in vitro cell attachment, migration and invasion of human ovarian carcinoma. Anticancer research. 1997;17(1A):337-42.
348. Scambia G, Testa U, Benedetti Panici P, Foti E, Martucci R, Gadducci A, et al. Prognostic significance of interleukin 6 serum levels in patients with ovarian cancer. British journal of cancer. 1995;71(2):354-6.
349. Callaghan R, Van Gorkom L, Epand R. A comparison of membrane properties and composition between cell lines selected and transfected for multi-drug resistance. British journal of cancer. 1992;66(5):781-6.
350. Bauerschlag DO, Maass N, Leonhardt P, Verburg FA, Pecks U, Zeppernick F, et al. Fatty acid synthase overexpression: target for therapy and reversal of chemoresistance in ovarian cancer. Journal of translational medicine. 2015;13:1-12.
351. Johnson DE, O'Keefe RA, Grandis JR. Targeting the IL-6/JAK/STAT3 signalling axis in cancer. Nature reviews Clinical oncology. 2018;15(4):234-48.
352. Han Z, Feng J, Hong Z, Chen L, Li W, Liao S, et al. Silencing of the STAT3 signaling pathway reverses the inherent and induced chemoresistance of human ovarian cancer cells. Biochemical and biophysical research communications. 2013;435(2):188-94.
353. Yu C, Niu X, Du Y, Chen Y, Liu X, Xu L, et al. IL-17A promotes fatty acid uptake through the IL-17A/IL-17RA/p-STAT3/FABP4 axis to fuel ovarian cancer growth in an adipocyte-rich microenvironment. Cancer Immunology, Immunotherapy. 2020;69:115-26.
354. Sp N, Kang DY, Kim DH, Park JH, Lee HG, Kim HJ, et al. Nobiletin inhibits CD36-dependent tumor angiogenesis, migration, invasion, and sphere formation through the Cd36/Stat3/Nf-Kb signaling axis. Nutrients. 2018;10(6):772.
355. Wang T, Fahrmann JF, Lee H, Li Y-J, Tripathi SC, Yue C, et al. JAK/STAT3-regulated fatty acid β-oxidation is critical for breast cancer stem cell self-renewal and chemoresistance. Cell metabolism. 2018;27(1):136-50. e5.
356. Li Y-J, Fahrmann JF, Aftabizadeh M, Zhao Q, Tripathi SC, Zhang C, et al. Fatty acid oxidation protects cancer cells from apoptosis by increasing mitochondrial membrane lipids. Cell reports. 2022;39(9).
357. Lin R, Wang S, Zhao RC. Exosomes from human adipose-derived mesenchymal stem cells promote migration through Wnt signaling pathway in a breast cancer cell model. Molecular and cellular biochemistry. 2013;383:13-20.
358. Feng S, Lou K, Luo C, Zou J, Zou X, Zhang G. Obesity-related cross-talk between prostate cancer and peripheral fat: potential role of exosomes. Cancers. 2022;14(20):5077.
359. Hadla M, Palazzolo S, Corona G, Caligiuri I, Canzonieri V, Toffoli G, et al. Exosomes increase the therapeutic index of doxorubicin in breast and ovarian cancer mouse models. Nanomedicine. 2016;11(18):2431-41.
360. Cheng L, Wu S, Zhang K, Qing Ya, Xu T. A comprehensive overview of exosomes in ovarian cancer: Emerging biomarkers and therapeutic strategies. Journal of ovarian research. 2017;10(1):1-9.
361. Wen H, Lee S, Zhu W-G, Lee O-J, Yun SJ, Kim J, et al. Glucose-derived acetate and ACSS2 as key players in cisplatin resistance in bladder cancer. Biochimica et Biophysica Acta (BBA)-Molecular and Cell Biology of Lipids. 2019;1864(3):413-21.
362. Tse C, Warner A, Farook R, Cronin JG. Phytochemical targeting of STAT3 orchestrated lipid metabolism in therapy-resistant cancers. Biomolecules. 2020;10(8):1118.

363. Li Z, Liu H, He J, Wang Z, Yin Z, You G, et al. Acetyl-CoA synthetase 2: a critical linkage in obesity-induced tumorigenesis in myeloma. Cell metabolism. 2021;33(1):78-93. e7.
364. Rossi EL, Khatib SA, Doerstling SS, Bowers LW, Pruski M, Ford NA, et al. Resveratrol inhibits obesity-associated adipose tissue dysfunction and tumor growth in a mouse model of postmenopausal claudin-low breast cancer. Molecular carcinogenesis. 2018;57(3):393-407.